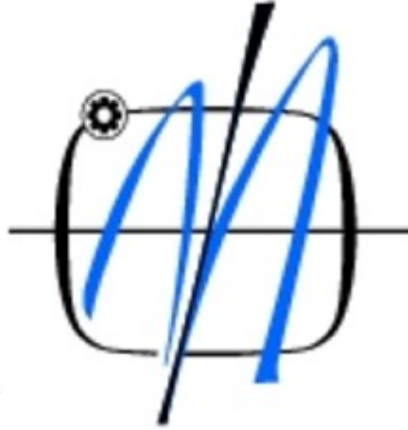


UNIVERSITY OF BELGRADE
FACULTY OF MECHANICAL ENGINEERING



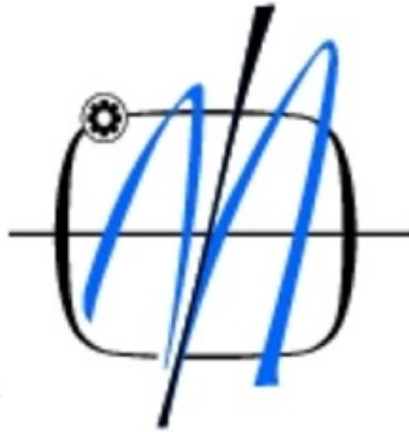
NOUREDDINE TOUMI

**NUMERICAL AND EXPERIMENTAL DIAGNOSTICS OF
BUCKLING STRUCTURAL ELEMENT BEHAVIOR**

DOCTORAL DISSERTATION

BELGARDE, 2017

УНИВЕРЗИТЕТ У БЕОГРАДУ
МАШИНСКИ ФАКУЛТЕТ



НОУРЕДДИНЕ ТОУМИ

Нумеричка-експериментална дијагностика
понашања извијања структурних елемената

Докторска дисертација

Београд, 2017

Mentor:

Prof. Dr. Taško Maneski, full professor

University of Belgrade, Faculty of Mechanical Engineering

**Members of the
Committee**

Prof. Dr. Nina Anđelić, full professor

University of Belgrade, Faculty of Mechanical Engineering.

Prof. Dr. Igor Balać, full professor

University of Belgrade, Faculty of Mechanical Engineering.

Prof. Dr. Vladimir Buljak, assistant professor

University of Belgrade, Faculty of Mechanical Engineering.

Prof. Dr. Dragan Ignjatović, full professor

University of Belgrade, Faculty of Mining and Geology.

Date of defense:

*The thesis is dedicated to all of my parents, wife, children, brothers
and sister whose love, guidance, sacrifices and encouragement is
boundless*

ACKNOWLEDGEMENTS

First of all, I am sincerely grateful to my supervisor Professor Taško Maneski, for his expertise, guidance and constructive suggestions over the last few years and the valuable assistance in many ways.

I would like to thank the Libyan Ministry of Higher Education and Scientific Research (www.highereducation.gov.ly) for providing me the financial support. Thanks also to the all members of the Faculty of Mechanical Engineering at the University of Belgrade for providing the necessary facilities and technical support.

Many thanks to the wonderful people who have supported me on this journey. Without their help, I would not be able to finish my thesis successfully.

I would like to express my deep and sincere appreciation to all of my wife, children and brothers and sister as well. They made a great part of this adventure possible and showed me with patience and optimism all the way to the end. To all of my colleagues who studied with me at the University of Belgrade for their measureless help during the journey.

Finally, a special word of appreciation to my parents and also to my friends, for their endless support, encouragement and love throughout the duration of this study.

Author

Belgrade, 2017

TABLE OF CONTENTS

ACKNOWLEDGEMENTS	i
TABLE OF CONTENTS	ii
ABSTRACT	vii
NOMENCLATURE	xii
LIST OF FIGURES	xv
LIST OF TABLES	xxii
1. INTRODUCTION	1
1.1 GENERAL INTRODUCTION.....	1
1.2 RESEARCH PURPOSE AND AIM	5
1.3 CONTENTS OF THE THESIS.....	6
2. LITERATURE REVIEW	8
2.1 THE CONCEPT OF BUCKLING	8
2.2 AN OVERVIEW OF SHELL BUCKLING.....	9
2.3 PLATE AND BEAM-COLUMN BUCKLING HISTORY	10
2.4 ELASTIC PLATE BUCKLING	10
2.4.1 BUCKLING OF SIMPLY SUPPORTED PLATES UNDER UNIFORM COMPRESSION (SSSS).....	17
2.4.2 BUCKLING OF SIMPLY SUPPORTED-FREE PLATE UNDER UNIFORM COMPRESSION (SSSF)	23
2.4.3 LINEAR BUCKLING OF STIFFENED PLATES	24
2.4.3.1 TRANSVERSE STIFFENERS	25
2.4.3.2 LONGITUDINAL STIFFENERS	26
2.5 LOCAL BUCKLING.....	27

2.6 GLOBAL BUCKLING.....	28
3. BUCKLING ANALYSES WITH FINITE ELEMENTS.....	30
3.1 INTRODUCTION	30
3.2 FINITE ELEMENT METHODS SOLUTIONS	32
3.2.1 LINEAR STATIC ANALYSIS.....	32
3.2.2 LINEAR BUCKLING ANALYSIS METHOD.....	34
3.2.3 FINITE ELEMENT DISCRETIZATION	37
3.2.4 FORMULATION AND CALCULATION OF FINITE ELEMENT MATRICES.....	39
3.2.4.1 THE STIFFNESS MATRIX OF SHELL ELEMENT	39
3.2.4.2 STIFFNESS MATRIX OF A BAR ELEMENT	40
3.2.4.3 STIFFNESS MATRIX OF A BEAM ELEMENT	42
3.2.4.4 STIFFNESS MATRIX OF SPACE FRAME STRUCTURES	44
3.3 CONCLUDING REMARKS.....	46
4. THE BUCKLING BEHAVIOUR OF A THIN PLATE	47
4.1 INTRODUCTION	47
4.2 FINITE ELEMENT MODELLING OF THIN PLATE	47
4.2.1 GEO-METRIC MODELLING AND NUMERICAL ANALYSIS	47
4.2.2 BOUNDARY CONDITIONS AND FINITE ELEMENT MESH.....	48
4.2.3 FULLY SIMPLY SUPPORETED OF THIN PLATE EDGES UNDER COM-PRESSIVE LOAD (SSSS).....	50
4.2.4 SIMPLY SUPPORETED FREE OF THE THIN PLATE UNDER EDGES COMPRESSIVE LOAD (SSSF).....	53
4.2.5 SIMPLY SUPPORETED CLAMPED FREE OF THE THIN PLATE UNDER EDGES COMPRESSIVE LOAD (SSCF).....	57

4.2.6 CLAMPED FREE OF THE THIN PLATE UNDER EDGES COMPRESSIVE LOAD (CFFF)	61
4.3 CONCLUDING REMARKS	65
5. THE BUCKLING BEHAVIOUR OF BEAM-COLUMN TRANSVERSELY AND LONGITUDINALLY STIFFENED.....	67
5.1 INTRODUCTION	67
5.2 FINITE ELEMENT MODELLING OF STIFFENED BEAM-COLUMN	68
5.2.1 GEO-METRIC MODELLING AND NUMERICAL ANALYSIS	68
5.2.2 BOUNDARY CONDITIONS AND FINITE ELEMENT MESH	70
5.3 MESH CONVERGENCY STUDY	71
5.4 BUCKLING BEHAVIOUR OF THE BEAM-COLUMN WITH STIFFENERS. 72	
5.4.1 A STIFFENED BEAM-COLUMN WITH ONLY TRANSVERSE STIFFENERS	72
5.4.2 A STIFFENED BEAM-COLUMN WITH TRANSVERSE AND LONGITU- DINAL STIFFENERS.....	77
5.4.2.1 A STIFFENED BEAM-CLOUMN WITH TRANSVERSE AND TWO LONGITUDINAL STIFFENERS.....	77
5.4.2.2 A STIFFENED BEAM-COLUMN WITH TRANSVERSE AND FOUR LONGITUDINAL STIFFENERS.....	82
5.5 EFFECT OF TRANSVERSE STIFFENER'S THICKNESS ON THE CRIT-ICAL BUCKLING LOAD.....	87
5.5.1 CRITICAL LOCAL BUCKLING RESPONSE AT DIFFERENTTS THIC- KNESSES.....	87
5.5.2 CRITICAL GLOBAL BUCKLING RESPONSE AT DIFFERENT TS THIC- KNESSES.....	92
5.6 CONCLUDING REMARKS.....	96

6. THE BUCKLING BEHAVIOUR OF FRAME STRUCTURE TRANSVERSELY AND LOGNITUDINALLY STIFFENED	98
6.1 INTRODUCTION	98
6.2 FINITE ELEMENT MODELLING OF STIFFENED FRAME STRUCTURE ...	99
6.2.1 GEO-METRIC MODELLING AND NUMERICAL ANALYSIS	99
6.2.2 FRAME MODELS DESCRIPTION	102
6.2.3 FRAME BASE BOUNDARY CONDITIONS, LOAD AND FINITE ELEMENT MESH	104
6.3 BUCKLING RESPONSE OF THE STIFFENED FRAME MODELS.....	107
6.3.1 STIFFENED FRAME MODELS BY USING TRANSVERSE STIFFENERS ONLY	107
6.3.2 STIFFENED FRAME MODELS BY USING TRANSVERSE AND LONGITUDINAL STIFFENERS	112
6.3.2.1 STIFFENED FRAME MODEL BY USING TRANSVERSE AND TWO LONGITUDINAL STIFFENERS	112
6.3.2.2 STIFFENED FRAME MODELS BY USING TRANSVERSE AND FOUR LONGITUDINAL STIFFENERS	118
6.4 EFFECT OF TRANSVERSE STIFFENERS THICKNESS ON THE CRITICAL BUCKLING LOAD.....	123
6.4.1 CRITICAL LOCAL BUCKLING RESPONSE AT DIFFERENT TS THICKNESSES	123
6.4.1.1 CRITICAL GLOBAL BUCKLING RESPONSE AT DIFFERENT TS THICKNESSES	127
6.5 CONCLUDING REMARKS.....	131
7. EXPERIMENTAL BEHAVIOR OF STEEL STRUCTURAL ELEMENTS ..	132
7.1 INTRODUCTION	132
7.2 TEST SPECIMENS	133

7.3 TEST SETUP	135
7.4 LOAD AND BOUNDARY CONDITIONS	136
7.5 TEST RESULTS.....	137
7.6 CONCLUDING REMARKS.....	152
8. CONCLUSIONS AND FUTURE WORK.....	153
8.1 SUMMARY	153
8.2 CONCLUSIONS	154
8.3 FUTURE WORK.....	156
REFERENCES	158

ABSTRACT

The linear buckling phenomenon is obviously a failure in the stability of structural systems. However, the performance and characteristic of any thin structural system are known to be significantly influenced by a range of buckling modes. For instance, local buckling, global buckling and distortional buckling. These buckling problems generally due to some different factors which affect the buckling behaviour and characteristic. Therefore the ultimate performance and capacity of the thin plate structural components, are effected by load, boundary conditions, material properties and structural geometry. Therefore, it is important to eliminate or delay these types of buckling problems in order to increase the capacity resistance of the structure. Nowadays, the understanding of the local and global buckling behaviour and its resistance capacity of any thin-walled plate structure is at a quite complicated. The determination of buckling resistance is an important characteristic of the design of steel structure.

This research contains a detailed description and contribution to the area of buckling by developing finite element modeling strategies. A solution procedure has made by using the advantages of the computational technology with commercially available FE package ABAQUS.

The work of this thesis provides an in-depth understanding of the local and global buckling failure mechanics associated with unstiffened and stiffened beam-column and frame structures with thin plates that are subjected to axial compression load. Besides, the presence of transverse and longitudinal stiffeners in structural plate elements has a vital role in order to increase critical buckling load capacity. However, these stiffeners cause redistribution in buckling behaviour in terms of local and global buckling. In this thesis the transverse and longitudinal stiffeners were employed on a real beam-column and frame structure to maximize the critical buckling loads. The objective function is to find the optimum location and geometrical characteristics of stiffeners. The effect of stiffeners on structural performance is detailed for beam-column and frame structures which called in attached stiffeners. Based on the finite element method, numerical models are made in order to observe the critical buckling capacity. Consequently, this thesis has enabled the accurate prediction of the behaviour and capacity of the compression members with beam-

column and frame structure and to be as a paved way for efficient and economical use of these members in the design. The last part of this thesis is the experimental tests which are used for validation by comparing with the theoretical or numerical solutions. Therefore, some specific standard sections have been experimentally investigated in order to follow their fail due to local or global critical buckling load before the plastic capacity is reached.

АПСТРАКТ

Феномен линеарног извијања је очигледно слабост структурних система у њиховој стабилности. Међутим, перформансе и карактеристика сваке танкозиде структуре значајно утичу на нежељену појаву локалног извијања, глобалног извијања и извијања при увијању. Ови проблеми извијања углавном потичу од различитих фактора који утичу на понашање структурних система и на перформансе и капацитет носивости танких структурних плоча. Такође, наведени проблеми зависе и од оптерећења, ослањања и својства материјала. Стога је важно да се елиминише могућност појаве наведених облика извијања у циљу повећања носивости структуре. Данас, знање и разумевање локалног и глобалног понашања извијања и њене отпорности на извијање било које танкозидне структуре је на прилично захтевном нивоу због интензивних истраживања који су постигнути у овој области студија. Отпорности на извијање је важна карактеристика дизајна челичне конструкције и њу је потребно одредити.

Ово истраживање садржи детаљан опис и допринос у области извијања. Развијен је процес моделирања и процедура решавања понашања танкозидних структура на извијање користећи комерцијални софтвер коначних елемената ABAQUS. Рад ове тезе даје дубље разумевање локалних и глобалних механизма извијања на неукрућеним и укрућеним (ојачаним) гредама и оквирним конструкцијама са танким плочама које су изложене аксијалном притисном оптерећењу. Осим тога, присуство попречних и уздужних укрућења у структурним елементима плоче имају кључну улогу у циљу повећања критичне силе извијања. Међутим, ови укрућења изазивају прераспodelу понашања на извијање у смислу локалног и глобалног извијања.

У овој тези уведена су трансверзална и уздужна ојачања на реалној како би се максимизирале критичне силе извијања. Функција циља је била да се пронађе оптимално место увођења укрућења и његове геометријске карактеристике. Ефекат укрућења на перформансе структуре урађен је детаљно за реалним структурама греда и рамова. На основу методе коначних елемената, нумерички модели су направљени и генерисани са циљем да се одреди понашање структуре на извијање. Према томе, ова

теза је омогућио прецизне процене понашања и носивости танкозидих структура на извијање.

Последњи део ове тезе су експериментални тестови који су коришћени за валидацију теоријских или нумеричких резултата. Због тога су експериментално истражене неке специфичне стандардне секције. При томе за све секције су одређена критична оптерећења која изазивају њихово локално и глобално извијање.

Key words: Local and global buckling, beam-column, frame structural, thin plate, finite element method, transverse and longitudinal stiffeners.

Scientific discipline: Mechanical Engineering

Scientific sub-discipline: Strength of materials

UDC: 624.072.2:519.6(043.3)
624.014:519.6(043.3)

NOMENCLATURE

a	Plate length
A	Element area
b	Plate width
B	Strain displacement matrix
D	flexural rigidity
$\{D\}$	System displacement
$\{D\}_{ref}$	System reference displacement
e	Element number
E	Young's modulus
$[E]$	Elastic stiffness matrix
G	Shear modulus
$[k]$	Element stiffness matrix
$[K]$	Global stiffness matrix
$[K_{\sigma}]$	Stress stiffness matrix
$[K_{\sigma}]_{ref}$	Reference stress stiffness matrix
l	Element length
m	Number of the half wave
M_{xx}, M_{yy}	Bending moments per unit length on x and y planes
M_{xy}	Twisting moment per unit length on x plane
n_x, n_y	Number of half waves of the buckling mode along x and y direction
N_{cr}	Critical load

N_x	Force per unit length in x direction
N_y	Force per unit length in x direction
N_{xy}	Shearing force per unit length
$[N]$	Shape function matrix
$\{P\}$	External load vector
q	Nodal degree of freedom in the local coordinate system
Q_x, Q_y	Shear force per unit length on x and y plane
$\{R\}$	Internal load vector
$\{R\}_{\text{ref}}$	Arbitrary reference load
t	Transverse stiffener thickness
t_p	Plate thickness
T	External work
u_x	Longitudinal displacement component along x-direction
$\{u\}$	Nodal displacement vector
U	Strain energy
v	Transverse displacement component along y direction
w	Vertical displacement component along z direction
W	Work done due to uniaxial loads
x, y, z	Longitudinal, transverse and vertical axis (direction) of the coordinate system
$\gamma_{xy}, \gamma_{yz}, \gamma_{xz}$	Shear strain in the xy, yz and xz plane
λ	Eigenvalue
λ_{cr}	Smallest eigenvalue
ε	Measured deformation

ν	Poisson's ratio
$\varepsilon_{xx}, \varepsilon_{yy}, \varepsilon_{zz}$	Normal strains in x , y and z direction
σ_{cr}	Critical stress
σ_{xx}, σ_{yy}	Normal stress on the x , y
σ_{xy}	Shear stress on the x plane and parallel to the y direction
α	Constant
Ω_0	Domain occupied by the mid-plane of the plate
Γ	Integration boundary
Π	Potential energy

LIST OF FIGURES

Figure 1.1 A transporter crane (Bajina-Bašta, Serbia)	4
Figure 1.2 A FE model of the transporter crane	4
Figure 2.1 Load-displacement curve (Chen et al., 1996)	9
Figure 2.2 Thin rectangular plate under uniaxial load.....	11
Figure 2.3 Stress resultants on a plate element.....	12
Figure 2.4 System bifurcation at point A	15
Figure 2.5 Simply supported plate under uniform compression load, a. Dubas & Gehri [38], b. FE model.....	19
Figure 2.6 The buckling load coefficient for a simply supported thin plate, Timoshenko and Gere [21].....	21
Figure 2.7 Representative buckling mode of a rectangular plate, having an aspect ratio $a/b=3$ by FE model	22
Figure 2.8 Buckled pattern of a plate free along one edge by FE model	23
Figure 2.9 Buckling coefficients of plate free along one edge	24
Figure 2.10 Beam-column with transverse & longitudinal stiffeners [64].....	27
Figure 2.11 Typical local buckling modes of: a) plate, b) beam-column, c) frame structure	28
Figure 2.12 Typical global buckling modes of: a) beam-column, b) frame structure ...	29
Figure 3.1 The sequence of steps in the solution of a technological, after Hattel in [74]	32
Figure 3.2 Linear static analysis in ABAQUS.....	34
Figure 3.3 Flowchart of a standard procedure for linear buckling analysis with multiple	36
Figure 3.4 Typical two & three dimensional elements with nodes	38
Figure 3.5 Two nodes bar element	40
Figure 3.6 Two nodes beam element.....	42
Figure 3.7 Deformation of a beam in x-y plane [84].....	43
Figure 3.8 Frame element in space with twelve DOFs.....	45

Figure 4.1 Typical geometry of a thin plate using in the study	48
Figure 4.2 Mesh generation on the model of square thin plate	49
Figure 4.3 A plate under uniform uniaxial compression load	49
Figure 4.4 Length-to-width vs. critical buckling load for SSSS with different thicknesses, $b_{\text{constant}} = 1.2\text{m}$	50
Figure 4.5 Deformation images (a) and growth of von Mises stresses (b) with different aspect ratios and thicknesses of Figure 4.4	52
Figure 4.6 Width-to-thickness vs. critical buckling load for SSSS with different length-to-width ratios, ($b_{\text{constant}} = 1.2\text{m}$)	53
Figure 4.7 Length-to-width vs. critical buckling load for SSSF with different thicknesses, ($b_{\text{constant}} = 1.2\text{m}$).....	55
Figure 4.8 Deformation images (a) and growth of von Mises stresses (b) with different aspect ratios and thicknesses of Figure 4.7	56
Figure 4.9 Width-to-thickness vs. critical buckling load for SSSF with different length-to-width ratios, ($b_{\text{constant}} = 1.2\text{m}$).....	57
Figure 4.10 Length-to-width vs. critical buckling load for SSCF with different thicknesses, ($b_{\text{constant}} = 1.2\text{m}$).....	59
Figure 4.11 Deformation images (a) and growth of von Mises stresses (b) with different aspect ratios and thicknesses of Figure 4.10	60
Figure 4.12 Width-to-thickness vs. critical buckling load for SSCF with different length-to-width ratios, ($b_{\text{constant}} = 1.2\text{m}$)	61
Figure 4.13 Length-to-width vs. critical buckling load for CFFF with different thicknesses, ($b_{\text{constant}} = 1.2\text{m}$).....	63
Figure 4.14 Deformation images (a) and growth of von Mises stresses (b) with different aspect ratios and thicknesses of Figure 4.13	64
Figure 4.15 Width-to-thickness vs. critical buckling load for CFFF with different length to-width ratios, ($b_{\text{constant}} = 1.2\text{m}$).....	65
Figure 5.1 Typical geometry of a hollow beam-column using in the study.....	69
Figure 5.2 Geometry of transverse stiffener configuration (TS).....	69
Figure 5.3 Geometry of longitudinal stiffener configuration (LS).....	69
Figure 5.4 Typical FE model of a hollow beam-column.....	71
Figure 5.5 Loading configurations of a simply supported hollow beam-column.....	71

Figure 5.6 Mesh convergence study of a compressed beam-column	72
Figure 5.7 A specimen section of the beam-column using TS only (<i>model-1_b</i>).....	73
Figure 5.8 A sample of 1 st local Eigen buckling mode of the beam-column (<i>model-1_b</i>)	73
Figure 5.9 A sample of 1 st global Eigen buckling mode of the beam-column (<i>model-1_b</i>)	73
Figure 5.10 ($P_{cr-unstiffened}$) / P_{cr} vs. distance between TS for <i>model-1_b</i> (Local).....	74
Figure 5.11 Effect of TS on the critical local buckling load of the beam-column <i>model-1_b</i>	75
Figure 5.12 ($P_{cr-unstiffened}$)/ P_{cr} vs. distance between TS for <i>model-1_b</i> (Global).....	76
Figure 5.13 Effect of TS on the critical global buckling load of the beam-column <i>model-1_b</i>	76
Figure 5.14 Geometrical section of the beam-column for <i>model-2_b</i>	77
Figure 5.15 A sample of 1 st local Eigen buckling mode of the beam-column for <i>model-2_b</i>	78
Figure 5.16 A Sample of 1 st global Eigen buckling mode of the beam-column for <i>model-2_b</i>	78
Figure 5.17 ($P_{cr-unstiffened}$) / P_{cr} vs. distance between TS for <i>model-2_b</i> (Local).....	79
Figure 5.18 Effect of TS & two LS on the critical local buckling load of the beam- column (<i>model-2_b</i>).....	80
Figure 5.19 ($P_{cr-unstiffened}$)/ P_{cr} vs. distance between TS for <i>model-2_b</i> (Global).....	81
Figure 5.20 Effect of TS and two LS on the critical global buckling load of the beam- column (<i>Model-2_b</i>).....	81
Figure 5.21 Geometrical section of the beam-column for <i>model-3_b</i>	82
Figure 5.22 A sample of 1 st local Eigen buckling mode of the beam-column <i>model-3_b</i>	83
Figure 5.23 A sample of 1 st global Eigen buckling mode of the beam-column <i>model-3_b</i>	83
Figure 5.24 ($P_{cr-unstiffened}$) / P_{cr} vs. distance between TS for <i>model-3_b</i> (Local)	84
Figure 5.25 Effect of TS and four LS on the critical local buckling load of the beam- column (<i>model-3_b</i>)	85
Figure 5.26 ($P_{cr-unstiffened}$) / P_{cr} vs. distance between for <i>model-3_b</i> (Global).....	86

Figure 5.27 Effect of TS and four LS on the critical global buckling load of the beam-column (<i>model-3_b</i>).....	86
Figure 5.28 Samples of critical local buckling modes for all models of the stiffened beam-column at different TS thicknesses.....	89
Figure 5.29 Effect of transverse stiffener thickness on the critical local buckling load for all models of the beam-column at TS thickness equals to 15mm.....	90
Figure 5.30 Effect of transverse stiffener thickness on the critical local buckling load for all models of the beam-column at TS thickness equals to 20mm.....	90
Figure 5.31 Effect of transverse stiffener thickness on the critical local buckling load for all models of the beam-column at TS thickness equals to 25mm.....	91
Figure 5.32 Effect of transverse stiffener thickness on the critical local buckling load for all models of the beam-column at TS thickness equals to 30mm.....	91
Figure 5.33 Critical global buckling modes for all models of the beam-column at different TS thicknesses.....	93
Figure 5.34 Effect of transverse stiffener thickness on the critical global buckling load for all models of the beam-column at TS thickness equals to 15mm.....	94
Figure 5.35 Effect of transverse stiffener thickness on the critical global buckling load for all models of the beam-column at TS thickness equals to 20mm.....	95
Figure 5.36 Effect of transverse stiffener thickness on the critical global buckling load for all models of the beam-column at TS thickness equals to 25mm.....	95
Figure 5.37 Effect of transverse stiffener thickness on the critical global buckling load for all models of the beam-column at TS thickness equals to 30mm.....	96
Figure 6.1 Unstiffened hollow frame structure used in the study.....	100
Figure 6.2 Geometry of transverse stiffener configuration (TS) type-1.....	100
Figure 6.3 Geometry of transverse stiffener configuration (TS) type-2.....	101
Figure 6.4 Geometry of horizontal longitudinal stiffener configuration (LS) type-1.....	101
Figure 6.5 Geometry of vertical longitudinal stiffener configuration (LS) type-2.....	101
Figure 6.6 Geometry of stiffened frame <i>Model-1_f</i>	102
Figure 6.7 Geometries of stiffened frame <i>Model-2_f</i>	103
Figure 6.8 Geometries of stiffened frame <i>Model-3_f</i>	103
Figure 6.9 Frame connections of the model (FE model).....	105
Figure 6.10 Frame connections on site.....	106

Figure 6.11 Typical FE of the frame model	106
Figure 6.12 Mesh sensitivity study on critical buckling load	107
Figure 6.13 A sample of 1 st local Eigen buckling mode of the frame for <i>Model-1_f</i>	108
Figure 6.14 A sample of 1 st global Eigen buckling mode of the frame (<i>Model-1_f</i>).....	108
Figure 6.15 ($P_{cr-unstiffened}$) / P_{cr} vs. distance between TS for <i>Model-1_f</i> (Local).....	110
Figure 6.16 Effect of TS on the critical local buckling load of the frame for <i>Model-1_f</i>	110
Figure 6.17 ($P_{cr-unstiffened}$) / P_{cr} vs. distance between TS for <i>Model-1_f</i> (Global). 111	111
Figure 6.18 Effect of TS on the critical global buckling load of the frame for <i>Model-1_f</i>	112
Figure 6.19 A sample of 1 st local Eigen buckling mode of the frame (<i>Model-2_f</i>).....	113
Figure 6.20 A sample of 1 st global Eigen buckling mode of the frame (<i>Model-2_f</i>).....	114
Figure 6.21 ($P_{cr-unstiffened}$) / P_{cr} vs. distance between TS for <i>Model-2_f</i> (Local)...	115
Figure 6.22 Effect of TS on the critical local buckling load of the frame for <i>model-2_f</i>	116
Figure 6.23 ($P_{cr-unstiffened}$) / P_{cr} vs. distance between TS for <i>Model-2_f</i> (Global). 117	117
Figure 6.24 Effect of TS on the critical global buckling load of the frame <i>Model-2_f</i> 117	117
Figure 6.25 A sample of 1 st local Eigen buckling mode of the frame <i>Model-3_f</i>	118
Figure 6.26 A sample of 1 st global Eigen buckling mode of the frame <i>Model-3_f</i>	119
Figure 6.27 ($P_{cr-unstiffened}$) / P_{cr} vs. distance between TS for <i>Model-3_f</i> (Local) ...	120
Figure 6.28 Effect of TS on the critical local buckling load of the frame for <i>Model-3_f</i>	120
Figure 6.29 ($P_{cr-unstiffened}$) / P_{cr} vs. distance between TS for <i>Model-3_f</i> (Global). 122	122
Figure 6.30 Effect of TS on the critical global buckling load of the frame for <i>Model-3_f</i>	122
Figure 6.31 Critical local buckling modes for the samples of all models at difference TS thicknesses	124
Figure 6.32 Effect of TS thickness on the critical local buckling load for all models at TS thickness =5mm	125
Figure 6.33 Effect of TS thickness on the critical local buckling load for all models at TS thickness =10mm	125

Figure 6.34 Effect of TS thickness on the critical local buckling load for all models at TS thickness =15mm	126
Figure 6.35 Critical global buckling modes for all models at difference TS thicknesses	128
Figure 6.36 Effect of TS thickness on the critical global buckling load for all models at TS thickness = 5mm	129
Figure 6.37 Effect of TS thickness on the critical global buckling load for all models at TS thickness equals 10mm	130
Figure 6.38 Effect of TS thickness on the critical global buckling load for all models at TS thickness = 15mm	130
Figure 7.1 Test setup facility	135
Figure 7.2 General view of the test stand with mounted sample and Force sensor....	136
Figure 7.3 Data acquisition set-up	136
Figure 7.4 The applied boundary conditions during testing	137
Figure 7.5 First local buckling mode for specimen C1, a. Exp, b. FE.....	138
Figure 7.6 First global buckling mode for specimen C1; a. Exp. , b. FE.	138
Figure 7.7 Critical buckling load response for specimen C1.....	139
Figure 7.8 First local buckling mode for specimen C2; a. Exp. , b. FE.	140
Figure 7.9 First global buckling mode for specimen C2; a. Exp. , b. FE.	140
Figure 7.10 Critical buckling load response for specimen C3.....	141
Figure 7.11 First Local buckling mode for specimen C3, a. Exp, b. FE.	142
Figure 7.12 Critical buckling load response for specimen C3.....	143
Figure 7.13 First local buckling mode for specimen C4 (L = 900 mm), a. Exp, b. FE	144
Figure 7.14 First global buckling mode for specimen C4 (L = 900 mm) by FE.....	144
Figure 7.15 First local buckling mode for specimen C4 (L = 510 mm) by FE	145
Figure 7.16 Critical buckling load response for specimen C4, L = 900 mm.....	146
Figure 7.17 Critical local buckling load location of Figure 7.16.....	146
Figure 7.18 Critical global buckling location of Figure 7.16	147
Figure 7.19 First global buckling mode for specimen C4, L=510mm	147
Figure 7.20 First local buckling mode for specimen C5, a. Exp, b. FE.....	148
Figure 7.21 First global buckling mode for specimen C5, a. Exp, b. FE	149

Figure 7.22	Critical local & global buckling load locations for specimen C5	149
Figure 7.23	First global buckling mode for specimen C6, a. Exp, b. FE	150
Figure 7.24	Second global buckling mode for specimen C6 by FE	151
Figure 7.25	Critical buckling load response for specimen C6.....	152

LIST OF TABLES

Table 5.1 Boundary conditions of simply supported model.....	71
Table 6.1 Boundary conditions of supported frame model.....	105
Table 7.1 Models specimens.....	133
Table 7.2 Geometrical details of test specimens.....	134

CHAPTER 1

1. INTRODUCTION

1.1 GENERAL INTRODUCTION

The applications of thin-walled structures are widely utilized and have become increasingly in various engineering technologies such as mechanical, civil, building and aerospace engineering. Stiffened plates, beam-columns and frame structures can all be categorized as thin-walled structures as long as the width-to-thickness ratios. These types of members are commonly used as structural components which are jointed together by means of welding, riveting or cold-formed. Thin-walled plates are mostly quite capable of carrying axial tensile loads while when these structural members subject to axial compression loading are at risk and failure due to the weakness of their axial-stiffness properties. Therefore, it is significant to diagnostic and to be able to accurately predict the buckling capacities of the plates, beam-columns and frame structures which have thin thicknesses in order to avoid any unexpected breakdown. Some of the early development in thin flat plates and beam-column has been made with the purpose of developing mathematical models which can work out the strength and represent the real behaviour of the members under different applied loads and boundary conditions throughout the loading process. Another type of buckling in which the edges of members unloaded and subjected to different support boundary conditions, has been examined by Rhodes & Harvey [1][2] in order to observe the behaviour of uniformly and linearly plates. It is worth pointing out that the boundary conditions and member's thickness should be taken into account in case of the analysis of buckling. From the findings, the behaviour of the plates and beam-column are completely different compared with each other. An exact solution procedure has been developed by Kang and Leiss [3] or plates with simply supported edges and linearly varying load. The obtained results showed that under these conditions, the plate behaved with more critical compared with the other types of loading profiles. The behaviour of plates subjected to transversely and longitudinally loaded have studied by Bakker et al. [4] who have developed a formula in

order to describe the plate's behaviour. Alexandrov and Eisenberger [5] have examined through the mathematical formulations, the behaviour of isotropic rectangular fully compressed plates with varying thicknesses. Many researchers have been investigated the subject of buckling during the years and a number of design specifications regarding to the buckling of thin plates structural parts have been published. Most of the studies have been performed with the aim of understanding the behaviour of thin plates and beam-column with different kind of boundary conditions, end support conditions and loadings. In 1976 at the University of Sydney, Hancock et al [6] has been described a comprehensive numerical work in predicting the buckling behaviour of thin-walled structural members due to global, local and distortional buckling. The study was to investigate the different buckling modes and the interaction between modes by using the finite strip method where the theoretical approaches have been successfully compared with the experiments tests. Since 1990 some experimental works have been carried out for beam-column structures, plates and plate structures by Hancock & Rasmussen and Rhodes [7][8][9]. The researchers presented and provided a good continuation of history through the field of buckling analysis. Some others of investigators have been expanded the research work of thin flat plates and the thin-walled plate structures. For instance, Azhari et al. [10] and Tan et al. [11] who developed mathematical equations and formulations on elastic buckling of triangular thin plates. Currently, the concept of critical buckling in thin-walled structures must be understood to any engineer and to be as the basic requirement of engineering knowledge. The buckling behaviour of thin-walled structures under compressive load is mostly dependent on multi parameters, such as the materials models, section geometries, boundary conditions and geometrical imperfections in nonlinear buckling. Notably, the slenderness ratio is the most important factor in thin-walled structures which are associated with the member width, the member thickness, the member length. The buckling behaviour has different modes; hence these modes could interfere with each other. Therefore, the coupled mode interference might be formed, for instance, local buckling with global buckling or torsional buckling with flexural buckling. This type of interference between the modes of buckling may decrease the risk of failure load of the thin-walled structures if compared to other when only one buckling mode. The first important analysis of thin-walled structure has been made in the 18th century. In order to apply a suitable solution method to analyze the linear behaviour of buckling of different structural systems depends mostly on the complexity of

the problem. It is noticed during the analysis that the failure mechanism is developed after the critical buckling load in particular when the stresses exceed the material yielding criterion. As a result, the plate or the beam-column or frame structures become unable to carry any additional load due to the development of the deformation which became a permanent in plastic form. Therefore, the post-buckling should be considered to be geometrically nonlinear problem due to the previous results that appear after the occurrence of critical buckling, but in this research only linear analysis is considered. A set of methods for buckling solution can be utilized in thin-walled compression members to find the failure mechanisms and stability behaviour. For example the finite strip method, the analytical mathematical method and finite element method are generally the numerical solution procedure able to deal with complex problems. In spite analytical mathematical methods have been evolved over the years, but these methods are still unable to solve the whole complex problems in particular with the complexity of the nonlinear problems. The complexities of the problems are associated with boundary conditions, geometry and etc. However, the finite element methods are able to deal with all of these aspects which are considered the most appropriate, powerful and flexible approach at the current time. Finite element methods are employed by selecting the suitable analysis solution procedures and finite element simulation packages are used to model the structural components. The task of this thesis is to develop appropriate finite element modelling strategies, solution procedures and to study the local buckling and global buckling modes of transversely and longitudinally stiffened plates. A real structure is considered as shown in Figure 1.1 where a transporter crane machine which used as a lifter upon the river in Bajina-Bašta, Serbia has taken as a sample of the analysis. It will illustrate in next sections various investigators have carried out a considerable amount of work over the years on the plate, the beam-column and the frame structures subjected to uniaxial compression load and thus the knowledge of the subject is considered to be at a fairly sophisticated level. The newly developed modelling strategies and finite element modelling in this thesis have enhanced the knowledge of the buckling subject by improving the understanding of the buckling failure mechanics of the thin plate, the beam-column and the frame structures. Therefore, research must be carried out to develop a finite element model for the same assembled transporter crane as shown in Figure 1.2



Figure 1.1 A transporter crane (Bajina-Bašta, Serbia)



Figure 1.2 A FE model of the transporter crane

1.2 RESEARCH PURPOSE AND AIM

The main purpose of this research was to diagnostic structural element behaviour of the plate, the beam-column and the frame structures under buckling load conditions. Furthermore, to develop adequate simplified numerical methods for the safe, economical buckling analysis and design of stiffened beam-columns, similar to those that exist in the frame steel structures.

The purpose of the work presented within this thesis regarding the local and global buckling resistance was:

- To investigate the local and global buckling behaviour of structural elements subject to axial compression load using advanced numerical methods. The three governing cases are to be considered in this research, i.e., local and global buckling of unstiffened-stiffened elements for (a) plate element, (b) beam-column using transverse and longitudinal stiffeners, (c) frame structure using also transverse and longitudinal stiffeners.
- To investigate if a buckling resistance of mentioned members will reinforce with only transverse stiffeners or with both.
- To investigate the effect and applicability of stiffeners on the buckling behaviour for unstiffened and stiffened elements for previous members.

The aim of this thesis was, regarding to both the local and global buckling resistance

- To diagnose and develop a suitable method for previous compression members which are subject to both the local and global buckling.
- To validate the finite element models of previous compression members by compression with experimental test results.
- To develop accurate finite element models which are capable of simulating the local and global buckling behaviour of steel element structures.

The work has focused upon the influence of transverse and longitudinal stiffeners on the buckling resistance of the plate, the beam-column and the frame structure. The members are subjected to uniformly distributed compressive load as mentioned earlier to improve the capacity and resistance of some specific structural elements to buckling loads with the aid of both advanced numerical analyses and experimental. In order to do so, finite element

models will be created for each case. A highly scientific based and internationally recognized software package in the field of structural analysis of engineering related applications is ABAQUS which will use in the analysis to obtain the numerical results of the elastic local and global buckling load and behaviour.

1.3 CONTENTS OF THE THESIS

Chapter one describes a brief general introduction to thin plate structures, the purpose and aim of research, and the contents of the thesis. Buckling behavior and finite element method in general are presented which identifies the need for the development of accurate linear buckling finite element modeling.

Chapter two a summary of literature review relevant to the analysis of thin-walled structures subjected to uniaxial compressive load are provided. It includes some topics which relevant to the buckling analysis as follow: an overview of shell buckling, plate and beam-column buckling history and some important titles associated with linear buckling.

Chapter three is about some of the basic concepts on which the linear finite element method. It includes the introduction of the basic sequential process in the finite element method, comprehensive introduction of the static and linear buckling analysis. The theoretical of finite element discretization, formulation of stiffness matrixes for the bar element, the beam element and the frame structures are described in this chapter.

Chapter four the buckling behavior of finite element modelling strategies and solution procedures for the analysis of thin plate structural members are developed. The effects of different lengths, thicknesses and boundary conditions on the buckling in terms of buckling modes of thin plate are examined. The obtained results are demonstrated with each other, in order to show the influence of buckling and capability of developed finite element strategies.

Chapter five finite element analyses of typical beam-column transversely and longitudinally stiffened are examined and presented to highlight the improvement in the structural performance of the beam-column due to the attachment of stiffeners. In order to examine the changes in the both the local and global buckling behavior, the influence of stiffeners parameters such as the stiffener location and thickness is varied.

Chapter six presents the application of the developed finite element simulation strategy to examine the local buckling and global buckling behavior of frame structures also transversely and longitudinally stiffened. As in chapter 5, the effects of the stiffeners on the buckling characteristics are examined, in order to develop an in-depth understanding of the load capabilities of the frame structures.

Chapter seven presents the experimental steel elements in order to compare it with the finite element simulation solutions and to be considered as validation producers.

Chapter eight presents a brief summary, general conclusion and a projection of future work that could be done in this field.

CHAPTER 2

2. LITERATURE REVIEW

In this section, a literature review of the buckling behaviour of rectangular plates, beam-column and frame structures are presented to provide the background information for the present investigation. The review focused on published research work that has been carried out by many researchers over the years in the field of buckling. Moreover, the review focuses on homogenous isotropic thin plates, beam-columns and frame structures.

2.1 THE CONCEPT OF BUCKLING

The theory of elastic is usually applied and used in the majority of building structure by simply selected allowable stress values for the used materials and by giving ratios as limits to meet serviceability requirements. Figure 2.1 shows the first and second order elastic methods which used in (i.e. different paths of buckling), to analyze the behavior of load deflection of a structure. Galambos[11] [12], Allen and Bulson [13] and Chen et al. [14] have been discussed this issue to find out more details in it. It is clear and can be understood from the figure that the critical buckling load is important and also needed for the evaluation of the effective length of members. Therefore, the critical buckling load may be determined directly by the Eigenvalue analysis, which represents the simplest way instead of first or second order elastic analysis in which the solution can be worked out in a rather simple way. The load at which buckling occurs depends on the stiffness of a component, not upon the strength of its materials. Buckling refers to the loss of stability of a component and is usually independent of material strength. This loss of stability usually occurs within the elastic range of the material. Two phenomena are governed by different differential equations. Buckling failure is primarily characterized by a loss of structural stiffness and is not modeled by the usual linear finite element analysis, but by a finite element Eigenvalue-Eigenvector.

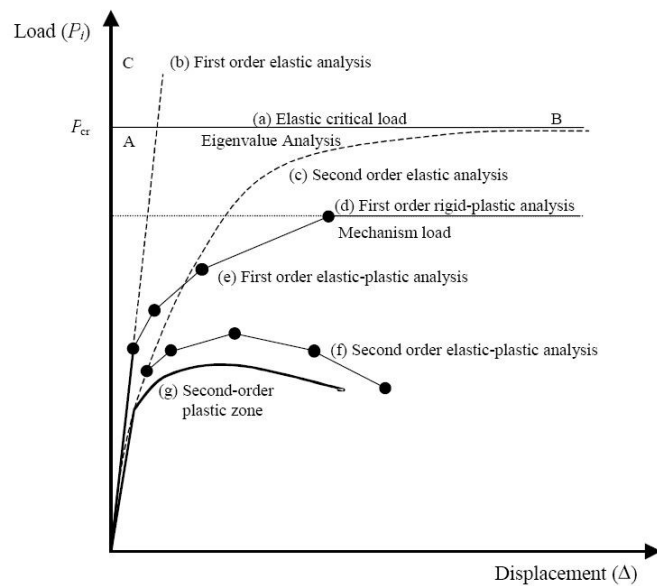


Figure 2.1 Load-displacement curve (Chen et al., 1996)

2.2 AN OVERVIEW OF SHELL BUCKLING

The buckling is a phenomenon of failure of a structure with a large deformation. A number of researchers state that the buckling phenomenon generally occurs before the large deformation which happens to the structures. Bushnell [15] states that the structure may slightly deform or to be not deformed, in spite that buckling phenomena are appearing. In mechanics and civil engineering structures, the buckling is an important phenomenon to study, because this thing frequently leads to failure of structures. Calladine [16] states that buckling occurs without any noticeable caution, especially in shell structures. The critical buckling load is an important parameter which was used as a primary design up to the end of the 1960s. The structural geometry, boundary conditions, material properties and the applied loading conditions are the factors which critical buckling load depends on it. Bryan [17] introduced the first equation in 1890, for determining the elastic buckling of flat plates under axial compression load. Shell structures are widely used in many fields. The buckling behaviour and stability analysis of shell structure are an active research area in recent years. Failure is supposed to be caused by either local buckling or global buckling of the shell. By contrast, failure controlled by loss of material strength is not very common in practical shell structures. Exploration of the buckling behaviour of plate, beam-column and frame shells involve many different aspects.

2.3 PLATE AND BEAM-COLUMN BUCKLING HISTORY

Usually beam-column is an assembly of plates. It can be considered that buckling in beam-column as plate buckling phenomenon where the specific boundary conditions caused by the restraint of stiffeners with the rest parts of the whole structure that intersect the web plate determine member strength. Plate buckling studying has a long story during the early time, in terms of critical buckling loads and stress. Bryan [17] introduced the full analysis of the critical elastic stress for a plate under uniform axial compression stress in rectangular shape with simply supported boundary conditions at whole edges. Energy method is the method which used in the solution for plate stability cases, when Timoshenko [18] used it for the plate to find the buckling stress at different conditions under compression stresses. The first study in the stability of rectangular plates in order to reinforce the plate by using the stiffeners as supports was studied theoretically by Timoshenko [18]. In addition to that, Timoshenko has examined the producers and questions of the required and optimum stiffness of the stiffeners to avoid buckling of the plate. His results showed that the stiffeners subdivided the plate into short panels in which stress is redistributing, where the increase in critical buckling load is considerably appeared.

2.4 ELASTIC PLATE BUCKLING

The theory of plates says that the behaviour of a thin plate under compressive forces can be divided into two parts; firstly the calculation of the critical load and secondly the determination of the ultimate load level. The critical load level is by definition the load or a point where the ideal structure, or members, in question loses its stability. The buckling of an elastic plate is described by the partial differential equation which derived by St. Venant [19]. The definition of the critical load of a structure is where it loses its stability that means the structure reached to a specific load to fail which called critical buckling load. In order to calculate the critical buckling load, the theory of elasticity can be done. Two analytical calculations can be used, either by of an energy method or by solving differential plate equation. Figure 2.2 represents a rectangular thin plate of length a , width b , and thickness t , subjected to uniaxial compressive load N_x . By taking the rectangular coordinates x, y and z in Cartesian system and where the uniaxial load N_x is parallel to the x axis. Kirchhoff proposed a simple theory of the plate with some unique assumptions for the solution as follows:

- a) Deflections are small compared with the plate's thickness,

- b) During bending the middle plane of the plate remains neutral.
- c) During bending the plane sections rotate to remain normal to the neutral surface, and without distortion.
- d) The dimensions are high compared with the plate's thickness.
- e) The effect of shearing forces is neglected and the bending moments are resisted by applied loads.

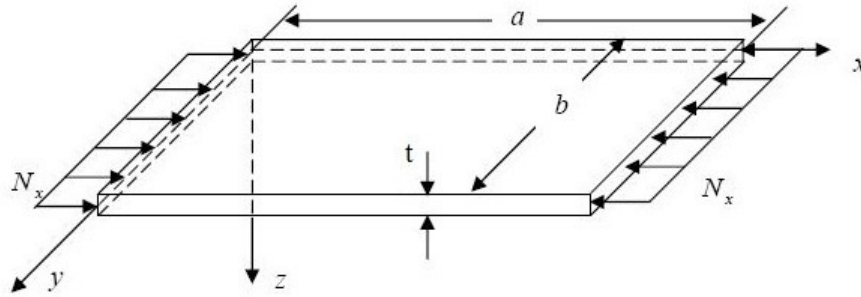


Figure 2.2 Thin rectangular plate under uniaxial load

According to the assumptions that mentioned above, the displacement functions may be expressed as the following:

$$\bar{u}(x, y, z) = -z \frac{\partial w}{\partial x}, \quad (2.1)$$

$$\bar{v}(x, y, z) = -z \frac{\partial w}{\partial y}, \quad (2.2)$$

$$\bar{w}(x, y, z) = w(x, y, z), \quad (2.3)$$

Where u , v and w are the displacement components along the x , y and z directions, where w is the transverse deflection of a point on the mid-plane (i.e., $z = 0$).

The linear strains (i.e., non-zero) related to the displacements are:

$$\varepsilon_{xx} = \frac{\partial \bar{u}}{\partial x} = -z \frac{\partial^2 w}{\partial x^2} \quad (2.4)$$

$$\varepsilon_{yy} = \frac{\partial \bar{v}}{\partial y} = -z \frac{\partial^2 w}{\partial y^2} \quad (2.5)$$

$$\gamma_{xy} = \frac{\partial \bar{u}}{\partial y} + \frac{\partial \bar{v}}{\partial x} = -2z \frac{\partial^2 w}{\partial x \partial y} \quad (2.6)$$

Where ε_{xx} and ε_{yy} are the normal strains and γ_{xy} is the shear strain.

Based on the Kirchhoff plate theory that is given by Ugural [20] for the virtual strain energy

$$\delta U = \iint_{\Omega_0} \left[\int_{-t/2}^{t/2} (\sigma_{xx} \delta \varepsilon_{xx} + \sigma_{yy} \delta \varepsilon_{yy} + \sigma_{xy} \delta \gamma_{xy}) dz \right] dx dy \quad (2.7)$$

$$\delta U = - \iint_{\Omega_0} \left(M_{xx} \frac{\partial^2 \delta w}{\partial x^2} + M_{yy} \frac{\partial^2 \delta w}{\partial y^2} + 2M_{xy} \frac{\partial^2 \delta w}{\partial x \partial y} \right) dx dy \quad (2.8)$$

Where Ω_0 denotes the domain occupied by the mid-plane of the plate, $(\sigma_{xx}, \sigma_{yy})$ the normal stresses, σ_{xy} the shear stress and (M_{xx}, M_{yy}, M_{xy}) the moments per unit length, as shown in Figure 2.3.

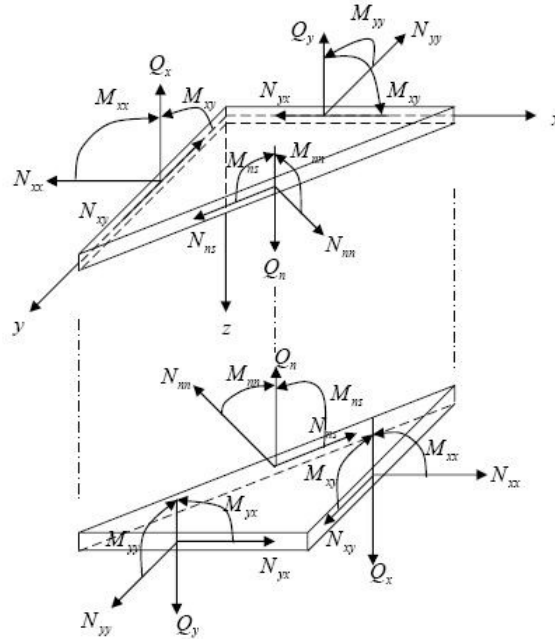


Figure 2.3 Stress resultants on a plate element

Again, based on the Kirchhoff plate theory that the virtual strain energy related to the transverse shear strain is equal to zero (i.e. $\gamma_{yz} = \gamma_{xz} = 0$).

There is a relationship between the moments and stresses where are given by:

$$M_{xx} = \int_{-t/2}^{t/2} \sigma_{xx} z dz \quad (2.9)$$

$$M_{yy} = \int_{-t/2}^{t/2} \sigma_{yy} z dz \quad (2.10)$$

$$M_{xy} = \int_{-t/2}^{t/2} \sigma_{xy} z dz \quad (2.11)$$

The uniaxial load N_x produces the work W , due to displacement w only

$$W = -\frac{1}{2} \int_{\Omega_0} N_x \left(\frac{\partial w}{\partial x} \right)^2 dx dy \quad (2.12)$$

The virtual work δW due to the uniaxial load N_x is given by:

$$\delta W = \int_{\Omega_0} N_x \frac{\partial w}{\partial x} \frac{\partial \delta w}{\partial x} dx dy \quad (2.13)$$

The principle of virtual displacements requires that $\delta \Pi = \delta U - \delta W = 0$, i.e.

$$\delta \Pi = - \int_{\Omega_0} \left(M_{xx} \frac{\partial^2 \delta w}{\partial x^2} + M_{yy} \frac{\partial^2 \delta w}{\partial y^2} + 2M_{xy} \frac{\partial^2 \delta w}{\partial x \partial y} + N_x \frac{\partial w}{\partial x} \frac{\partial \delta w}{\partial x} \right) dx dy = 0 \quad (2.14)$$

By using the divergence theorem, one obtains

$$\begin{aligned} \delta \Pi = & - \int_{\Omega_0} \left(M_{xx,xx} + 2M_{xy,xy} + M_{yy,yy} - N_x \frac{\partial^2 w}{\partial x^2} \right) \delta w dx dy \\ & - \oint_{\Gamma} \left[\left(M_{xx} n_x + M_{xy} n_y \right) \frac{\partial \delta w}{\partial x} + \left(M_{xy} n_x + M_{yy} n_y \right) \frac{\partial \delta w}{\partial y} \right] ds \\ & + \oint_{\Gamma} \left[\left(M_{xx,x} + M_{xy} - N_x \frac{\partial w}{\partial x} \right) n_x + \left(M_{yy,y} + M_{xy,x} \right) n_y \right] \delta w ds = 0 \end{aligned} \quad (2.15)$$

For clarifying, a comma followed by subscripts denotes differentiation with respect to the subscripts, i.e., $M_{xx,x} = \frac{\partial M_{xx}}{\partial x}$, and so on, (n_x, n_y) denote the direction cosines of the unit

Normal \bar{n} on the boundary Γ , and ds denotes the incremental length along the boundary.

If the unit normal vector is oriented at an angle θ from the positive x -axis, then $n_x = \cos \theta$ and $n_y = \sin \theta$. Since δw is arbitrary in Ω_o , it is independent of $\partial \delta w / \partial x$, and $\partial \delta w / \partial y$ on the boundary Γ , it follows that

$$\frac{\partial^2 M_{xx}}{\partial x^2} + 2 \frac{\partial^2 M_{xy}}{\partial x \partial y} + \frac{\partial^2 M_{yy}}{\partial y^2} - N_x \frac{\partial^2 w}{\partial x^2} = 0, \text{ in } \Omega_o \quad (2.16)$$

The above equation represents the equilibrium equation for rectangular plates under uniaxial load.

The kook's law can be applied to the isotropic material of the plate in this case, and by applying the relation between stress and strain can write as follows:

$$\sigma_{xx} = \frac{E}{1-\nu^2} (\epsilon_{xx} + \nu \epsilon_{yy}) \quad (2.17)$$

$$\sigma_{yy} = \frac{E}{1-\nu^2} (\epsilon_{yy} + \nu \epsilon_{xx}) \quad (2.18)$$

$$\sigma_{xy} = G \gamma_{xy} = \frac{E}{2(1+\nu)} \gamma_{xy} \quad (2.19)$$

Where E is the Young's modulus, G the shear modulus, and ν the Poisson's ratio. By substituting eqs. (2.17) into eqs. (2.9) and carrying out the integration over the plate thickness, one obtains

$$M_{xx} = \int_{-t/2}^{t/2} \sigma_{xx} z dz = \frac{E}{1-\nu^2} \int_{-t/2}^{t/2} (\epsilon_{xx} + \nu \epsilon_{yy}) z dz = -D \left(\frac{\partial^2 w}{\partial x^2} + \nu \frac{\partial^2 w}{\partial y^2} \right) \quad (2.20)$$

$$M_{yy} = \int_{-t/2}^{t/2} \sigma_{yy} z dz = \frac{E}{1-\nu^2} \int_{-t/2}^{t/2} (\epsilon_{yy} + \nu \epsilon_{xx}) z dz = -D \left(\frac{\partial^2 w}{\partial y^2} + \nu \frac{\partial^2 w}{\partial x^2} \right) \quad (2.21)$$

$$M_{xy} = \int_{-t/2}^{t/2} \sigma_{xy} z dz = G \int_{-t/2}^{t/2} \gamma_{xy} z dz = -(1-\nu) D \frac{\partial^2 w}{\partial x \partial y} \quad (2.22)$$

Where D is the flexural rigidity and is given by

$$D = \frac{Et^3}{12(1-\nu^2)} \quad (2.23)$$

By substituting eqs. (2.20), (2.21) and (2.22) into eq. (2.16), yields the governing equation for buckling of plate subjected to a uniaxial load:

$$D \left(\frac{\partial^4 w}{\partial x^4} + 2 \frac{\partial^4 w}{\partial x^2 \partial y^2} + \frac{\partial^4 w}{\partial y^4} \right) + N_x \frac{\partial^2 w}{\partial x^2} = 0 \quad (2.24)$$

The above equation was derived under certain assumptions where the behavior of the material deals as ideally elastic way i.e., without imperfections such as geometrical defects or residual stresses. In addition to that, the plate deformation is assumed to be small. As a result, the plate shows that there is no lateral deformation till the critical load or stress. Figure 2.4 shows that the deflection might be either negative or positive, according to the coordinate system of the plate, and there are no lateral deformations till the critical stress level.

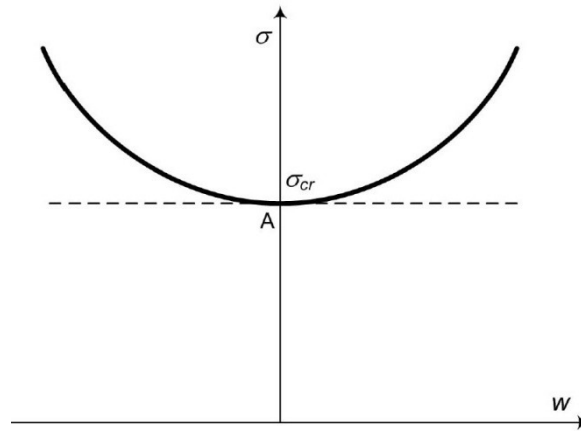


Figure 2.4 System bifurcation at point A

The investigation of stability of thin plates is normally to achieve the equilibrium of the system by using the energy method which is known as the principle of stationary value of the total potential energy of the plate. According to the correlation between the internal energy bending and the external work which done by the forces acting in the middle plane of the plate the energy solution was built on them. The bending strain energy stored in a

small element of linear elastic material due to the applied bending and twisting moments are as follows:

$$dU_b^1 = -\frac{1}{2} \left(M_x \frac{\partial^2 w}{\partial x^2} + M_y \frac{\partial^2 w}{\partial y^2} \right) dx dy \quad (2.25)$$

$$dU_b^2 = \left(M_{xy} \frac{\partial^2 w}{\partial x \partial y} \right) dx dy \quad (2.26)$$

The bending moments and twisting moment can be expressed in terms of lateral displacement and are as follows:

$$M_x = -D \left(\frac{\partial^2 w}{\partial x^2} + \nu \frac{\partial^2 w}{\partial y^2} \right) \quad (2.27)$$

$$M_y = -D \left(\frac{\partial^2 w}{\partial y^2} + \nu \frac{\partial^2 w}{\partial x^2} \right) \quad (2.28)$$

$$M_{xy} = -D(1 - \nu) \left(\frac{\partial^2 w}{\partial x \partial y} \right) \quad (2.29)$$

The substitution into eqs (2.27) by eqs (2.25) and (2.26) yields the following equations:

$$dU_b^1 = \frac{D}{2} \left[\left(\frac{\partial^2 w}{\partial x^2} \frac{\partial^2 w}{\partial y^2} \right)^2 - 2(1 - \nu) \left(\frac{\partial^2 w}{\partial x^2} \frac{\partial^2 w}{\partial y^2} \right) \right] dx dy \quad (2.30)$$

$$dU_b^2 = D(1 - \nu) \left(\frac{\partial^2 w}{\partial x \partial y} \right)^2 dx dy \quad (2.31)$$

The superposition method that can be applied here in order to obtain the resultant of the strain energy and is following

$$dU_b = dU_b^1 + dU_b^2 \quad (2.32)$$

After the integration the above equation over the plate,

$$U_b = \frac{1}{2} D \iint \left[\left(\frac{\partial^2 w}{\partial x^2} + \frac{\partial^2 w}{\partial y^2} \right) - 2 \cdot (1 - \nu) \cdot \left(\frac{\partial^2 w}{\partial x^2} \cdot \frac{\partial^2 w}{\partial y^2} - \left(\frac{\partial^2 w}{\partial x \partial y} \right)^2 \right) \right] dx dy \quad (2.33)$$

The foregoing equation (expression) represents the strain energy which stored in the deformed plate, where the work conducted by the externally applied forces can be describing by

$$T = \frac{1}{2} \iint \left[N_x \frac{\partial^2 w}{\partial x^2} + N_y \frac{\partial^2 w}{\partial y^2} + 2N_{xy} \frac{\partial^2 w}{\partial x \partial y} \right] dx dy \quad (2.34)$$

According to the previous assumptions, the two last equations are only valid for small deformations. There are two cases concerning the stability of the plate in question at the bifurcation point, according to Timoshenko and Gere [21]

- a. if $U > T$, the flat form of equilibrium of the plate is stable,
- b. if $U < T$, the plate is unstable and buckling occurs.

However, the critical load amplitude may be found by setting

$$T = U \Leftrightarrow U = T \quad (2.35)$$

The change in energy potential must have a minimum value for a stable equilibrium to be solved. This condition may be used for the differential equation derivation from of the equilibrium, equation (2.24). Another method to solve the problem is to apply an expression for the lateral deformation of the plate.

2.4.1 BUCKLING OF SIMPLY SUPPORTED PLATES UNDER UNIFORM COMPRESSION (SSSS)

For the simply supported edges plate case, the equation has solved by Bryan [1][17]. Timoshenko [18] has solved different other cases with different boundary conditions. The elastic critical load in a complex structure is one difficult part in calculation in particular with stiffeners. Lundquist and Stowell [22] extended the work of Timoshenko and Gere [21] for the elastic plate buckling, by introduced practical methods for working out the stability of assembled plates. Kollbrunner and Hermann[23] have been examined the CSSS plates. The results found that when the tension edge of the plate is clamped edge, the critical load factors do not differ greatly compared with those which have both edges simply supported. In order to solve the buckling problem of ESSS plates, the Lagrangian

multiplier is employed by Schuette and McCulloch [24]. The Galerkin's method has been used by Walker [25] to give precise values of critical load for a number of the edge conditions as noted before. Xiang et al. [26] applied the Levy's method to work out the elastic buckling of uniaxially loaded rectangular plate with an internal line hinge. The method succeeded in presenting the exact solution for several different boundary conditions, for instant CSCS, SSCS, SSSS, FSSS, and FSFS plates. The variety of boundary conditions considered include (i.e. CSCS, SSCS, SSSS, FSSS, ESSS, S- simply supported edge, F-free edge, C-clamped edge and E-elastic). In addition to the buckling analysis, some other researchers have also analyzed the vibration of plates which subjected to in-plane stress field such as Bassily and Dickinson [27], Kielb and Han [28], Kaldas and Dickinson [29], Leissa and Kang [30], Sukajit and Singhatanadgid [31]. Bifurcation buckling may be seen as a particular instance of the vibration problem; that is, determining the in-plane stresses which cause vibration frequencies to bring down to zero. The "effective width" solution was based on von Kármán et al. [32] and the experimental corrections of Winter [33]. Notably, both Chilver and Harvey [34] properly included the interaction of elements in determining the local buckling stress. As mentioned earlier, Buckling phenomena often occur without advance warning to any structure which includes different slender parts, cross sections that have to be dealt carefully to avoid unexpectedly fail. According to some researchers, one Theodor von Kármán [32] states that the local buckling is based on the effective width to length. George Winter [33] introduced a new modified issue of the effective width concept followed to the original version of Theodor von Kármán. In determining the local buckling stress, the interaction of elements is included Chilver and Harvey [34] Moreover, to increase local buckling Chilver [35] states that for lipped open channels, the reinforcing lips should be sufficiently stiff. During the years, the column research focused on the interaction between local and overall (i.e. global) buckling modes. Kalyanaraman et al. [36] investigated a work on unstiffened elements while Desmond [37] on intermediate and edge stiffeners. Figure 2.5 shows a plate subjected to uniformly compressive distributed forces in x-direction. By applying a general case with applied loads which are acting in all the in-plane direction. To determinate the critical load of the plate in the equation is simplified to only with uniaxial forces which are acting in x-direction. Since the only load applied to the plate, in the form of a uniform distributed

compressive force, acting along the edges $x = 0$ and $x = a$, the rest of the external applied loads according to eq. (2.24) equals to zero:

$$N_y = N_{xy} = 0 \quad (2.36)$$

The boundary condition which applied to constrain the plate leads to the following: along four edges $x = 0$ and $x = a$,

$$w = \frac{\partial^2 w}{\partial x^2} = 0 \quad (2.37)$$

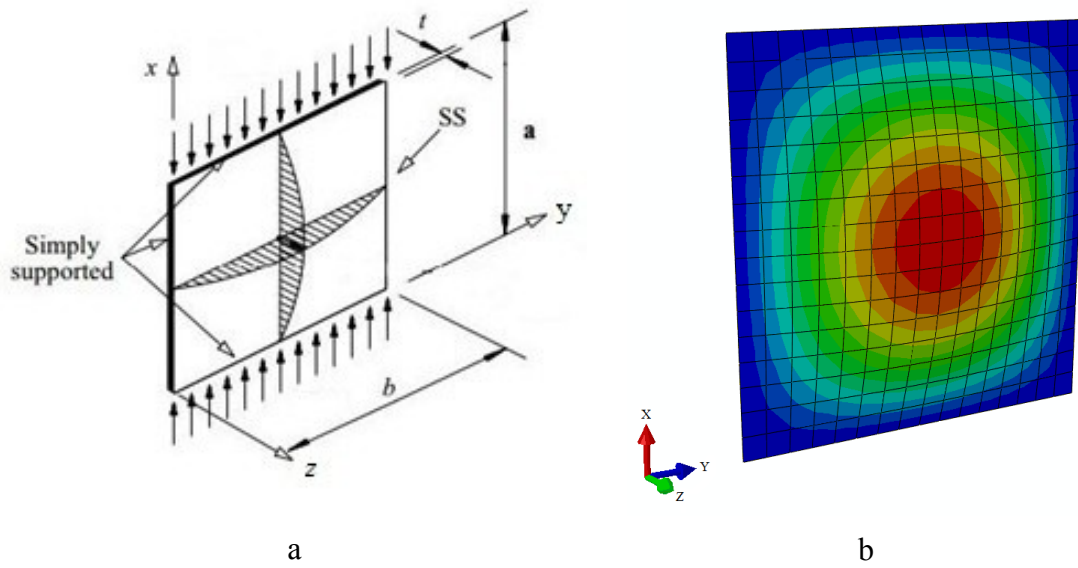


Figure 2.5 Simply supported plate under uniform compression load, a. Dubas & Gehri [38], b. FE model

Along three edges $y = 0$ and $y = b$,

$$w = \frac{\partial^2 w}{\partial y^2} = 0 \quad (2.38)$$

By applying a double trigonometric Fourier series on the deformed shape of simply supported plate and the boundary conditions may be described on the following form

$$w = \sum_{m=1}^{\infty} \sum_{n=1}^{\infty} a_{mn} \sin \frac{m\pi x}{a} \sin \frac{n\pi y}{b}, \quad m, n = 1, 2, 3, \dots \quad (2.39)$$

Eq. (2.39) represents the lateral deflection that can be substituted into eq. (2.33) and eq. (2.34) based on the conditions in eq. (2.36) and (2.37) eq. (2.38) and by using eq. (2.35), we get a new relation after some mathematical procedures,

$$\left[D \left(\left(\frac{m\pi}{a} \right)^2 + \left(\frac{n\pi}{b} \right)^2 \right)^2 + N_x \left(\frac{m\pi}{a} \right)^2 \right] a_{mn} \sin \frac{m\pi x}{a} \sin \frac{n\pi y}{b} = 0 \quad (2.40)$$

In order to apply the eq. (2.40) for all positions on the plate, the simplified equation will be as the following,

$$D \left(\left(\frac{m\pi}{a} \right)^2 + \left(\frac{n\pi}{b} \right)^2 \right)^2 + N_x \left(\frac{m\pi}{a} \right)^2 = 0 \quad (2.41)$$

Or

$$N_x = \frac{D \left(\left(\frac{m\pi}{a} \right)^2 + \left(\frac{n\pi}{b} \right)^2 \right)}{\left(\frac{m\pi}{a} \right)^2} \quad (2.42)$$

Timoshenko and Gere [21] state that the lowest value of critical load is reached when the plate buckles in a form such that one half sinus wave, hence the integral parameter $n = 1$. Then the last equation may be eliminated, such as

$$N_{cr} = \frac{a^2 \cdot \pi^2 \cdot D}{m^2} \left(\frac{m^2}{a^2} + \frac{1}{b^2} \right), \quad \text{where } m = 1, 2, 3, \dots \quad (2.43)$$

Where the parameter m describes the number of the half waves over the plate length in x -direction,

$$N_{cr} = k_{cr} \frac{\pi^2 D}{b^2} \quad (2.44)$$

The parameter k_{cr} is the buckling load coefficient with dimensionless and is given by

$$k_{cr} = \left(\frac{mb}{a} + \frac{a}{mb} \right)^2 \quad (2.45)$$

By instating eq. (2.23) for the flexural rigidity of the plate in eq. (2.44), we get the critical stress of the plate as,

$$\sigma_{cr} = k_{cr} \cdot \frac{\pi^2 \cdot E}{12 \cdot (1 - \nu^2)} \cdot \left(\frac{t}{b}\right)^2 \quad (2.46)$$

From eq. (2.45) the buckling coefficient k_{cr} is a function of the plate width b , length a and the number of sinus half waves over the length, m . Figure 2.6 shows different values of the plate width to length ratio a/b with k_{cr} .

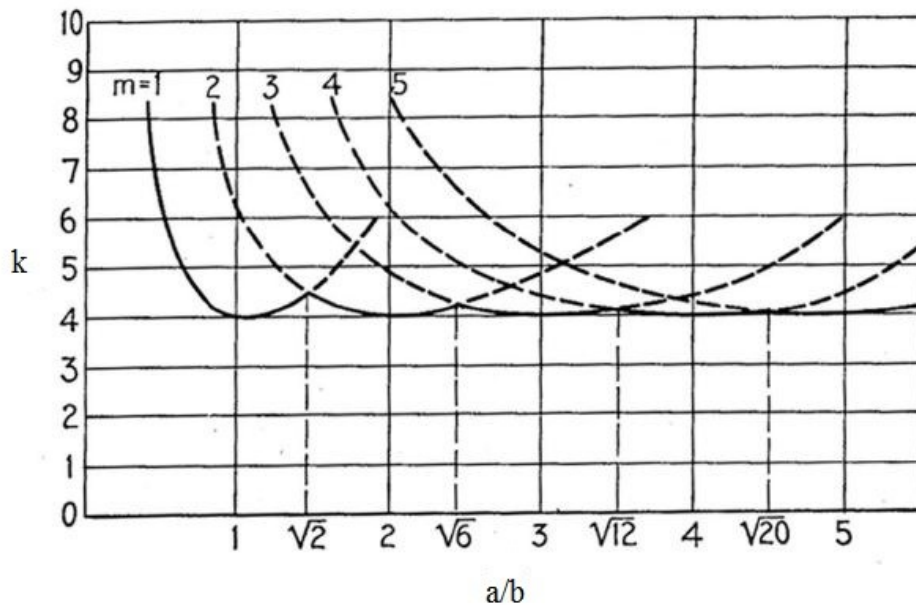


Figure 2.6 The buckling load coefficient for a simply supported thin plate, Timoshenko and Gere [21]

As for a rectangular plate, having an aspect ratio $a/b = 3$ (i.e. $a=240\text{mm}$, $b=80\text{mm}$), the buckling mode in which the lowest value of the critical buckling stress (with $k_{cr} = 4.0$) will be divided the plate into three units of squares as shown in Figure 2.7, and having an equally large buckling in each unit (i.e. $m = 3$).

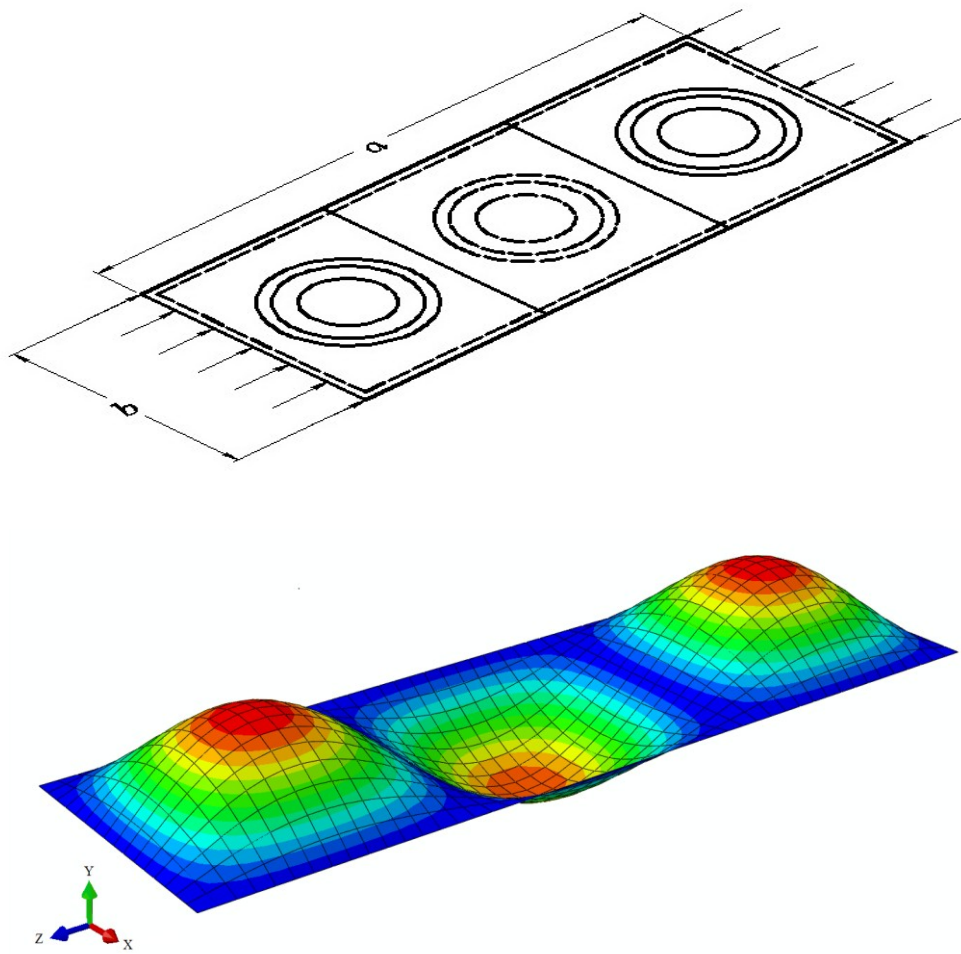


Figure 2.7 Representative buckling mode of a rectangular plate, having an aspect ratio $a/b=3$ by FE model

2.4.2 BUCKLING OF SIMPLY SUPPORTED-FREE PLATE UNDER UNIFORM COMPRESSION (SSSF)

As illustrated in Figure 2.8, a flat plate is simply supported along one longitudinal edge and two transverse edges, and is free along the fourth edge. The buckling differential equation of equilibrium of the plate is still the same as in eq. (2.45).

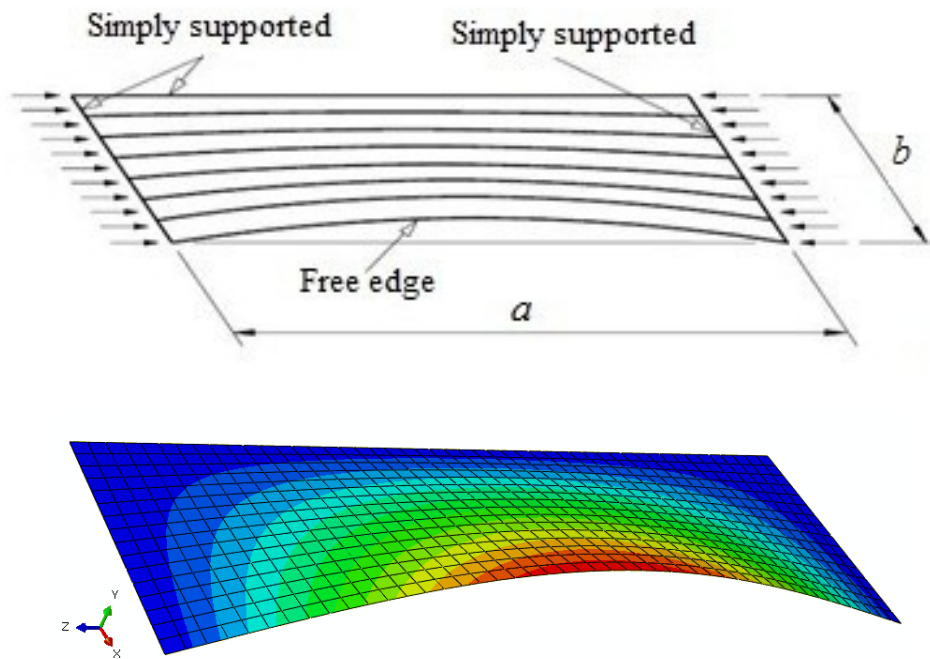


Figure 2.8 Buckled pattern of a plate free along one edge by FE model

The shape of the buckling which satisfies this difference, however, based on the approximately square buckles of the simply supported plate as shown in Figure 2.7. The dissimilar boundary conditions along the free edge reason, the plate buckles with a one half wave along its length as shown in Figure 2.8. Although, the elastic buckling stress solution may still be expressed in the form of eq. (2.24), in which the buckling coefficient k_{cr} is estimated by eq. (2.47) and as shown in Figure 2.9.

$$k_{cr} = 0.425 + \left(\frac{b}{a}\right)^2 \quad (2.47)$$

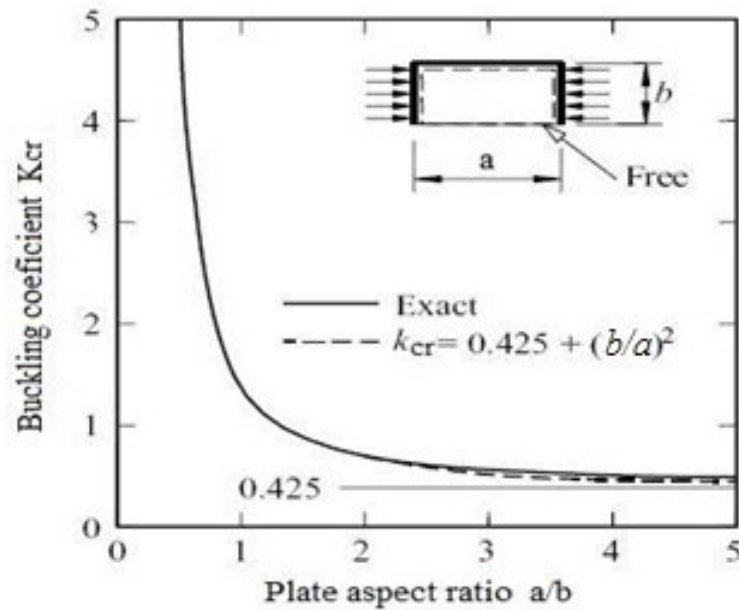


Figure 2.9 Buckling coefficients of plate free along one edge

2.4.3 LINEAR BUCKLING OF STIFFENED PLATES

The main feature of buckling is that the load at which it occurs depends basically on some parameters such as (elastic modulus E , the cross-section shape and properties), and it is virtually independent of the material strength. Stiffened plates have been widely utilized as essential auxiliary components for many basic frameworks subjected to compressive loads, and are may be exposed against various types of buckling phenomena. Based on and according to the investigative analysis of stiffened plates and structures, two essential sorts of buckling modes may be considered. The global buckling mode is one possible mode, which usually occurs for the entire stiffened plate, which the second one is called local buckling mode which occurs for the stiffener or the main plate. Murray [39] and Bonello et al. [40] have been discovered four largely familiar forms of structural failure in stiffened plates: (i) major plate originated global buckling; (ii) stiffener originated global buckling; (iii) local buckling of the stiffener or the major plate and (iv) stiffener tripping, which is connected with the plastic collapse of the stiffeners in a localized mechanism. Global buckling is described by instantaneous buckling of the stiffener and the major plate performing as one single curvature and usually referred to as Euler buckling.

The shear buckling of infinitely long plates has studied by Cook and Rokey [41] with clamped and simply supported boundary conditions. Their tests conducted on a closed section of transverse stiffeners. The obtained results showed that the buckling resistance of the web plates was significantly improved and the researchers proposed to use such as stiffeners. With regard to the shear buckling of girders and in use of transverse stiffeners, a sequence of tests conducted by Nishino and Okumura [44] in order to work out the safety coefficients where the stiffeners placed at girders' boundaries. The depth-to-thickness was one of their changing parameters and noticed that after the web buckling load all test girders have significant excessive carrying capability. The collapse behaviour of the plate girders with transversely and longitudinally attached stiffeners. The fail behaviour of plate girders has discussed by Komatus [43] with use transverse and longitudinal stiffeners where for four types of modes have provided in order to determinate the ultimate strength of plates. The influence of flange stiffness on the buckling patterns demonstrated by Skaloud [44] for the early work of Rokey and Skaloud [48] and also on the failure mechanism of steel web at high with-to-thickness ratio. Another factor which has a crucial effect on the buckling behaviour is the variation of stiffeners geometry. Plank and Williams [46] have studied the behaviour of the stiffened panels with different stiffener geometries subjected to combined shear and compressive loads. Consequently, the influence of the different stiffener geometries on the panels was obvious through the interaction curves. Consequently, in general, the purpose of both transverse and longitudinal stiffener is to enhance the critical buckling load, stress and it has to be stiff enough to be able to remain straight structure members.

2.4.3.1 TRANSVERSE STIFFENERS

Transverse stiffeners are often used to reinforce and support the plates or columns at their webs to increase buckling capacity and to avoid rapid fails. The diagonal tension field theory for stiffened webs has been developed by Wagner [44]. In order to use the transverse stiffeners in the best manner in terms of increase the resistance of the structure to buckling, there are some conditions should take into account: First, the moment of inertia of the stiffeners must be minimized as possible to maintain the almost zero deflection of the line when buckling is appeared. Secondly, the required stiffeners' area is minimized to give sufficient strength. The influence of transverse stiffeners on the axial force due to tension or compression field has been demonstrated by a number of studies which made by Lee et

al. [48][49], Horne and Grayson [50], Stanway et al. [51], Rahal and Harding [52][53]. The largest demand on transverse stiffeners according to Kim, Jung and White [54] in straight curved plates were when the web panel has a square shape. Figure 2.10 shows the beam-column with transverse stiffeners which used in this study.

2.4.3.2 LONGITUDINAL STIFFENERS

Longitudinal stiffeners are fundamental structural components in plates, beam-columns and frames. The primary purpose of longitudinal stiffeners between two adjacent transverse girders is to produce compressive longitudinal stresses by hull girder bending moment. The location, dimensions of longitudinal stiffener and attached plates have an effect on the buckling modes from local or global buckling of the panel could be occurring. Several researchers were devoted to the buckling study of stiffened plates, beam-columns. A research has made by Fujikubo and Yao [55] to study the restraining effect of the longitudinal stiffeners on the edges of the plate between stiffeners. A series of Elasto-plastic large deflection analyses has developed by Yao et al. [56] for stiffened panels with flat stiffeners. Dubas [57] established that the optimum position of the longitudinal stiffener on a plate subjected to uniform bending. The requirements of minimum stiffener were defined by Chwalla and Kromm [58][59] where both of them considered longitudinally stiffened plates under uniform bending. A series of charts have been provided by Kloppel and Scheer [60], which include various stiffener positions and loading conditions for simply supported longitudinally stiffened rectangular plates. Massonet [61] concluded that an increase of 25% in the safety factor can be obtained in the resistance of the girders using longitudinal stiffeners. The interactions of the web, plate, flexural and torsional buckling of Z-stiffeners have studied by Van der Neut [62] where the strip theory is used. In addition to Van Der Neut, Hughes and Ma [63] have also studied the interaction of plate, web, beam-column type flexural buckling, and torsional buckling of stiffeners by the same method. Figure 2.10 shows the beam-column with longitudinal stiffeners which used in this study.

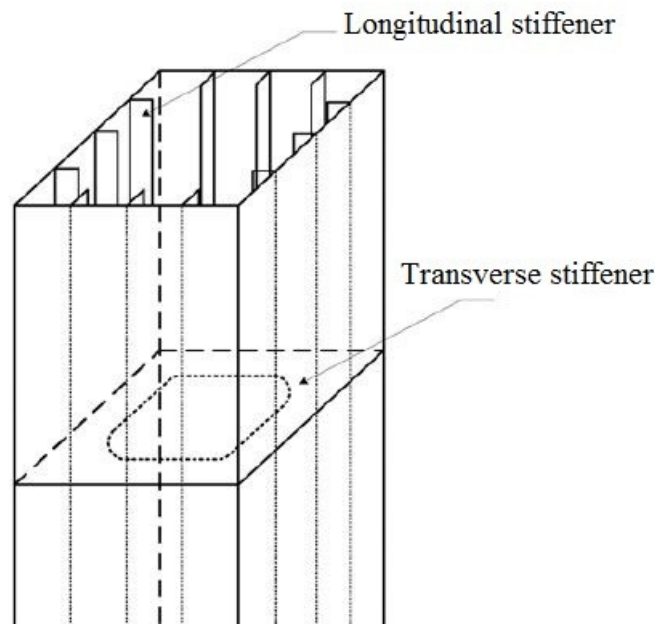


Figure 2.10 Beam-column with transverse & longitudinal stiffeners [64]

2.5 LOCAL BUCKLING

As previously described the plate, beam-column or any assembled structure sections are commonly have a thin thickness compared with their width or length and based on that the local buckling may occur before section yielding. The fundamental phenomenon of local buckling is shown in Figure 2.11 which shows the real local buckling behavior in an unstiffened plate, beam-column and frame structure where refer to flexural displacement of the plate elements. It is clear from the figure that the line junction between elements of the plate remains still straight. Consequently, the local buckling may occur in compression, shear or bending. As mentioned earlier, buckling phenomena often occur without advance warning to any structure which includes different slender parts, cross sections that have to be dealt carefully to avoid unexpectedly fail. In general, the local buckling is particularly common and also is characterized by wavelength which relatively short and frequent of thin-walled elements. An investigation has made by Nishino et al. [65] on the fabricated square plates welded together. Research work was to clarify the effect of residual stresses influence against local buckling. Dwight et al presented tests on the local buckling for rectangular square boxes. The tests were in previously tested and reported by Dwight and Moxham [66] with the aim of filling gaps.

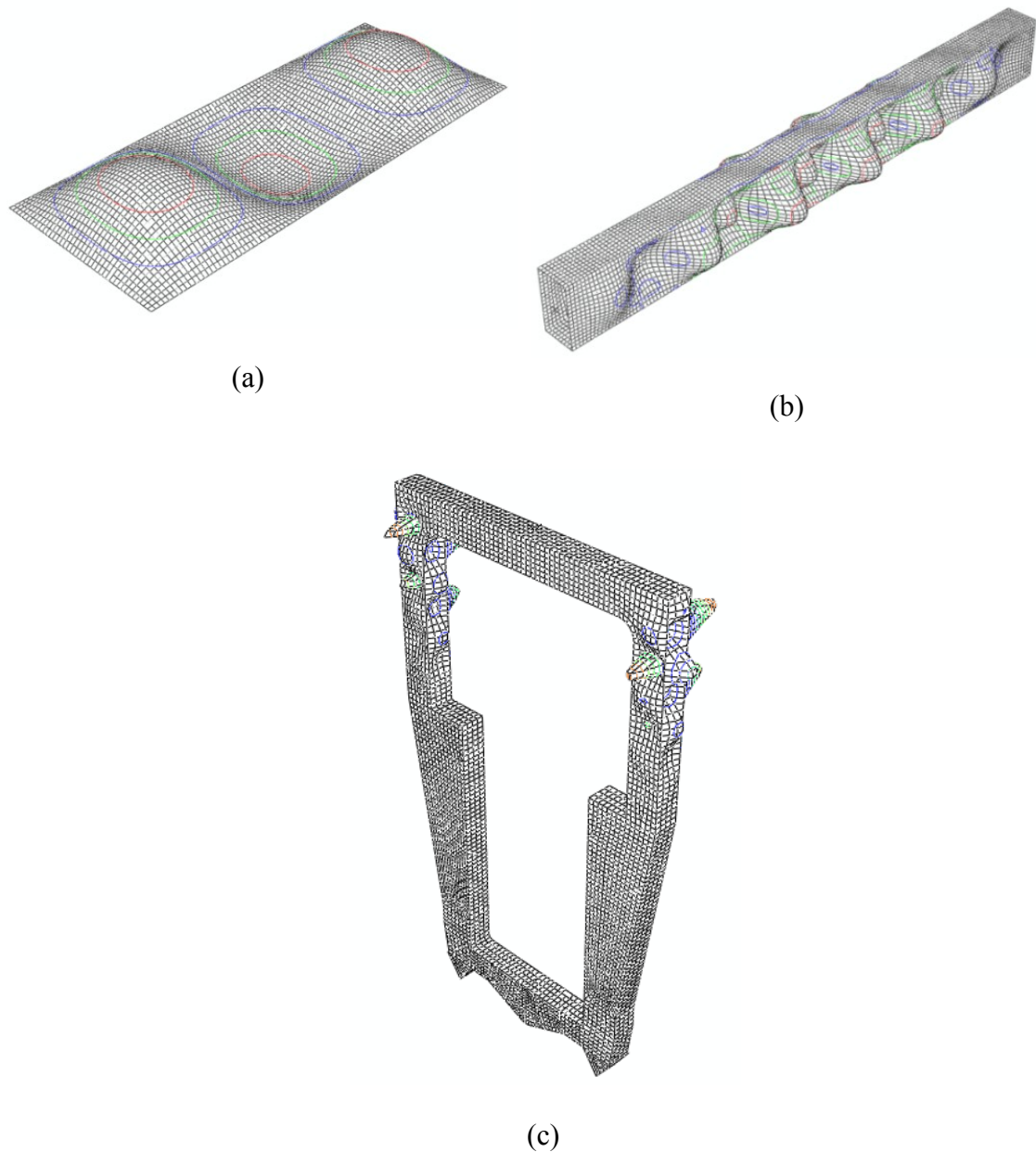
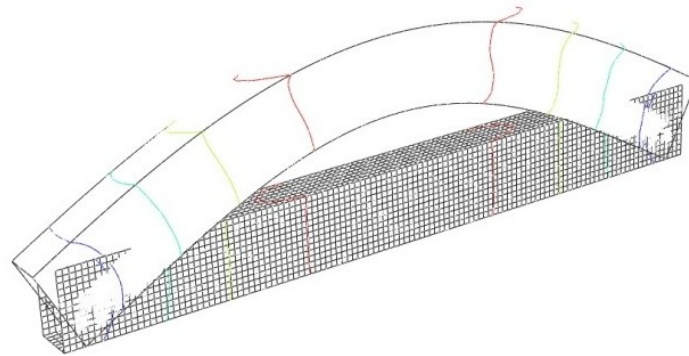


Figure 2.11 Typical local buckling modes of: a) plate, b) beam-column, c) frame structure

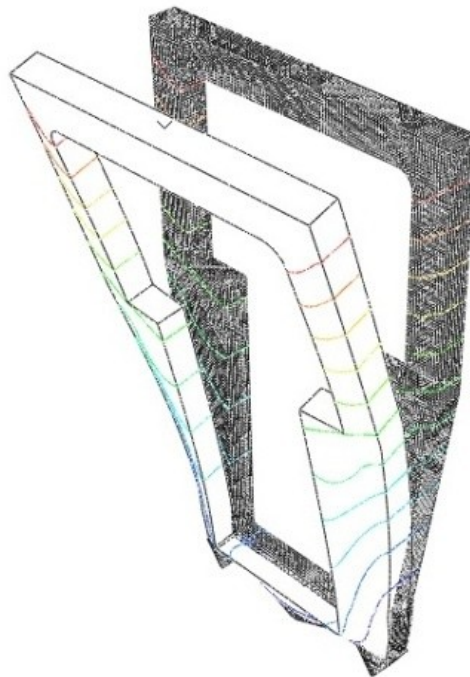
2.6 GLOBAL BUCKLING

Global buckling or overall buckling is another mode of buckling in which compression members bend curvedly about its symmetric point. This type of buckling can be flexural, torsional, or flexural-torsional. The member deflects laterally until the plate or column becomes unstable as it approaches the critical buckling load. Some examples of global buckling modes of the beam-column and the frame structure without stiffeners in pure

compression predicted by finite element modelling are shown in Figure 2.11. In addition to that, global buckling mostly occurs in long columns.



(a)



(b)

Figure 2.12 Typical global buckling modes of: a) beam-column, b) frame structure

CHAPTER 3

3. BUCKLING ANALYSES WITH FINITE ELEMENTS

3.1 INTRODUCTION

The finite element method is one of powerful numerical methods and the most broadly used for solving a lot of problems in different engineering fields. One of the basic purposes of the finite element is to predict the behavior of the structure under consideration, to estimate, understanding the strength of the structure and its failure mechanisms. In general, the finite element with recent complications in engineering for solving problems such as geometries, material behavior, loadings and constraints, has significantly improved. The computational tools that perform specific tasks by using the finite element have widely developed with very superb versatility. Finite element method is a numerical method that requires the solution of various simultaneous algebraic equations in order to solve many different complex engineering problems. During the years, the finite element method became more common and it represented many different and significant developments in the history of computational methods. The theoretical mechanics and science have changed into the practical by applying the finite element method which became the essential tools for a huge number of technological developments. At the beginning of the 1940s was born a theory called FEM theory, where the first formula which was developed as matrix method for structural analysis. The first assembly of triangular elements and the minimum of potential energy to torsion problems was introduced by Courant [67]. Furthermore, the Finite Element expression was introduced by Clough [68] in his paper which was cooperated with Turner, Martin and Topp . Their study focused on the assembled complex structures in terms of their stiffness and deflection. Twenty years thereafter, the finite element method started again in enhancing by some researchers and scientists as Zienkiewicz [69][70], Hinton and Owen [71] to more general for many different engineering problems. Laplace and Poisson's equations which used to solve problems have been applied by Zienkiewicz and Cheung [72] in order to solve by finite element method. Crisfield [73] carried out the

modeling and solution of nonlinear problems. In the finite element process, the first thing is to simplify the actual structure. In order to do this, the structure is discretised or meshing into a set of finite elements. The connecting points where finite elements may be connected together are called nodes (nodal points). Afterwards, the mathematical model is made for analysis. In the finite element model, the material properties, loads and constraints represent the full and real structure. Usually the finite element methods are used to validate or find a solution for the analytical methods or in case of complex problems for any type of structures. Although, the basic assumptions for both analytical and numerical methods are identical but the way of the solution is different. The basic step in the finite element analysis of any structural problem is the formulation of the equations of problem which called a shape function. In the finite element method, the shape function means the deflection function which is usually assumed for each element as the first or second order polynomial. The whole structure is the effect of displacement of each element of the final deflection. In order to apply a program based on the finite element method as a numerical solution or validate the theoretical analysis, it is essential to generate an appropriate model. The last step is in this technique, the real structure is transformed into a finite element model by employing pre-processor programs (e.g. ABAQUS, ANSYS etc.) to provide an input file to a FEM solver program in order to perform the desired analysis. In this chapter some basic knowledge of the finite element methods is described. The main aim of using the advanced finite element solution procedures described in the next sections is to show and develop the reliable and recent finite element simulation strategies. The novel approaches are used in the subsequent chapters to generate various models for the thin plate, the beam-column and frame elements structural in order to precisely predict their buckling behavior with an in-depth understanding. Figure 3.1 illustrates the task's sequence steps in finite element method, from the realization of a technological problem to technological problems. As known, the numerical solution usually is an approximation especially for a complex model, whereas for a simple problem, the analytical solution is an exact. Therefore, in both cases the solution has to be understood or interpreted for the original physical problem. The main part in finite element is the mathematical model task, because the risk of the wrong model leading to incorrect results.

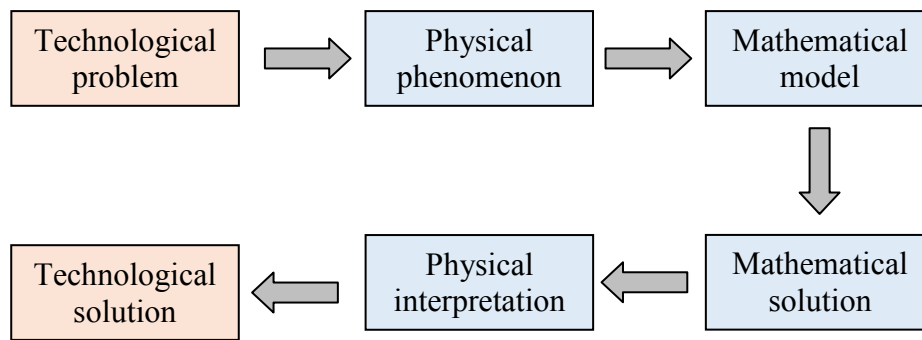


Figure 3.1 The sequence of steps in the solution of a technological, after Hattel in [74]

3.2 FINITE ELEMENT METHODS SOLUTIONS

3.2.1 LINEAR STATIC ANALYSIS

In order to analyze statically thin-walled structures, finite shell elements seem to be the appropriate choice due to the flexibility in the degree of freedom in the shell element, so as to map smoothly deformations. The connection between all elements to each other is at grid points with six degrees of freedom in terms of rotations and translations. Finite element method depends on chosen of element type, an efficient mesh density and appropriate boundary conditions, all of these factors play a significant role in terms of obtaining the most accurate results close to the reality. The linear FE method is most commonly applied technological aid for buckling and stress analysis in the first step design stages of complex structures. In the mechanic and also in all engineering fields the linear finite element method considers the basic expressions and equations and has become an essential part in the analysis. There are some advantages of linear analysis of the finite element method which are usually fairly obvious. Without the need for complicated numerical iterative schemes and increments, the simple direct solution may be obtained. Moreover, Hilton [74] has made a study for superimposed various load cases, boundary conditions and the set of constant material in order to illustrate and able to form the behaviour are kept at minimum. Wullschleger [75] states that " The mostly applied FE method for structural stability investigations consist of a linear static stress analysis with subsequent linear eigenvalue extraction, although the scheme of this linear analysis method may be traced back to a nonlinear FE formulation". In order to apply the static analysis on the structure some assumptions are made in terms of motions under certain types of loadings and boundary

conditions. The basic objective of static analysis is the equilibrium system or structure between the applied and internal loads which should be equal to the each other and expressed as;

$$\{P\} = \{R\} \rightarrow \{P\} - \{R\} = 0 \quad (3.1)$$

Where $\{P\}$ and $\{R\}$ are the external and internal load vectors respectively. As mentioned before, the factors which effect on the structure to resist the applied loads depend on the structure' material and its geometry. For static analysis, and regarding to the finite element, the internal loads can be expressed:

$$\{R\} = [k]\{u\} \rightarrow \{P\} = [k]\{u\} \quad (3.2)$$

Where $\{u\}$ is the displacement vector and $[k]$ is the stiffness of the material. With the equilibrium of structure and when the stiffness property is known, the displacement of the structure can be worked out as follows:

$$\{u\} = [k]^{-1} \{P\} \quad (3.3)$$

In order to find a solution for the unknown parameters in the above equation, the finite element program task is: to find the element stiffness matrices $[k]$ by using the given data for the geometry, material properties and element properties; to gather the entire stiffness matrices $[k]$ into a total stiffness matrix $[K]$ of the structure and then to determine the displacement $\{u\}$ in equation (3.3). One thing is advantage in the linear static analysis, the total stiffness of the structure does not change and also the stiffness matrix is done once. By applying the loads and boundary conditions to constrain the mathematical model which is generated the matrix equation can be solved. Once obtained the displacements, the rest of the other unknowns can be calculated such as the reaction forces stresses and strains. The post-processing program ABAQUS software is used to represent the obtained results to create it easily visualized. This step is very important since the output data (i.e. results) can be immense. Figure 3.2 shows the entire process of carrying out linear static analysis in ABAQUS program.

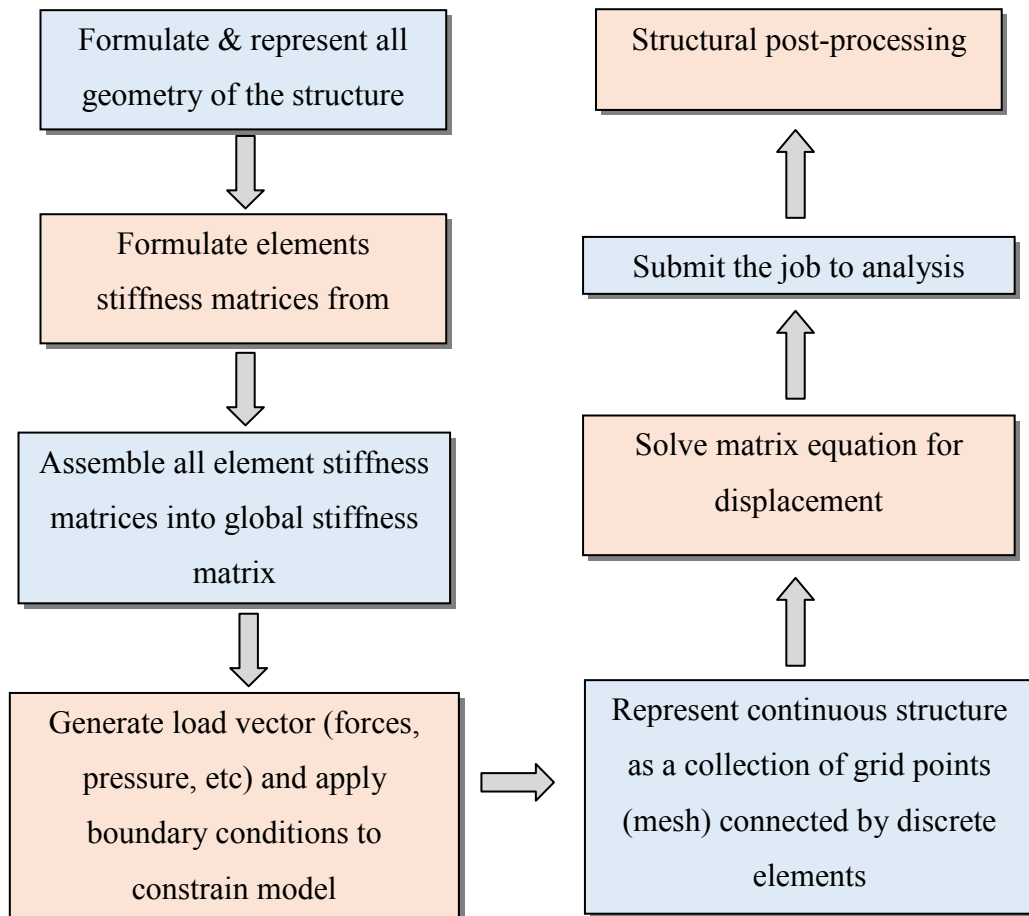


Figure 3.2 Linear static analysis in ABAQUS

3.2.2 LINEAR BUCKLING ANALYSIS METHOD

This section explains the types of finite element solution sequences of ABAQUS for linear buckling, which are employed to analyze the thin plate structures and discusses in brief the formulation of linear buckling analysis. Linear buckling is the most common analysis of the structural problems, and known as eigenvalue-based buckling analysis. The buckling mode frequently presents the shape of the structure which used to evaluate the elastic stability associated with the structural systems. Structural equilibrium is a main point in the engineering design, and the load type which is applied in such way in terms of static or a combination that produces the deflections in the structure leads to instability. From finite element point of view Campbell et al. and Lee [76][77] state that the procedure when performing a buckling analysis of a structure consists of three steps. First, a linear buckling analysis is carried out and it describes by Cook et al. [78] as an eigenvalue problem which involves the solution of a homogenous algebraic equation system whose smallest root

eigenvalue corresponds to critical buckling load and the associated eigenvector represents the first buckling mode. Using the standard finite element approach, the governing equation for buckling, then takes the form of the standard eigenvalue problem:

$$[K]\{D\} = \{R\}_{ref} \quad (3.4)$$

Where $[K]$ is the stiffness matrix, $\{D\}$ is the displacement and $\{R\}_{ref}$ is an arbitrary load on the structure. When the displacements are known, the stresses can be calculated for the used forces, $\{R\}_{ref}$ which can be used to form the stress stiffness matrix $[K_{\sigma}]_{ref}$. Since the stress stiffness matrix $[K_{\sigma}]_{ref}$ is proportional to the load vector $\{R\}_{ref}$, an arbitrary stress stiffness matrix and an arbitrary load vector $\{R\}$ may be defined by a constant λ as:

$$[K_{\sigma}] = \lambda[K_{\sigma}]_{ref} \text{ when } \{R\} = \lambda\{R\}_{ref} \quad (3.5)$$

The conventional stiffness matrix $[K]$ is unchanged by the applied load, because the problem is presumed linear. When the buckling displacement increment $\{\delta D\}$ takes place relative to displacements $\{D\}_{ref}$ of the reference configuration. Because, external loads do not change at a bifurcation point,

$$([K] + \lambda_{cr}[K_{\sigma}]_{ref})\{D\}_{ref} = \lambda_{cr}\{R\}_{ref} \quad (3.6)$$

$$([K] + \lambda_{cr}[K_{\sigma}]_{ref})(\{D\}_{ref} + \{\delta D\}) = \lambda_{cr}\{R\}_{ref} \quad (3.7)$$

By subtraction of eq. (3.6) from eq. (3.7), gives an eigenvalue problem of eq. (3.8) where the smallest root λ_{cr} defines the smallest load and there is a bifurcation, eq. (3.9)

$$([K] + \lambda_{cr}[K_{\sigma}]_{ref})\{\delta D\} = \{0\} \quad (3.8)$$

$$\{R\}_{cr} = \lambda_{cr}\{R\}_{ref} \quad (3.9)$$

Figure 3.3 shows the procedure steps of the buckling analysis which made by Felippa [80] using finite element methods. The first input data to start the analysis is the number of load combinations n that picked based on the given problem (i.e. compression forces, moments or shear), subsequently the combination of load which indicates by i is applied to the structure on specific positions. When the first phase is completed the second phase will start for the static analysis. As previously mentioned that the solution loop will start to solve the static analysis step in order to work out the unknown parameter in eq. (3.4).

The majority of commercial finite element programs are used two methods to work out the integration element stiffness matrix which is usually performed numerically. These

methods are Gauss integration or Simpson integrations, which have a good accuracy and computational time. Once the static analysis is completed and to complete the solution loop is to calculate the stress stiffness matrix $[K_\sigma]$ which is given by

$$[K_\sigma^e] = \int_{V_e} [G]^T [S][G] dV^2 \quad (3.10)$$

Where the $[G]$ is obtained from shape functions by appropriate differentiation, and $[S]$ contains the initial stresses which are obtained from the static analysis. Finally, the global stress stiffness matrix is assembled as the global stiffness matrix. Therefore, two unknown required parameter are now computed, the linear buckling problem is ready to determine which is indicated by eq. (3.8).

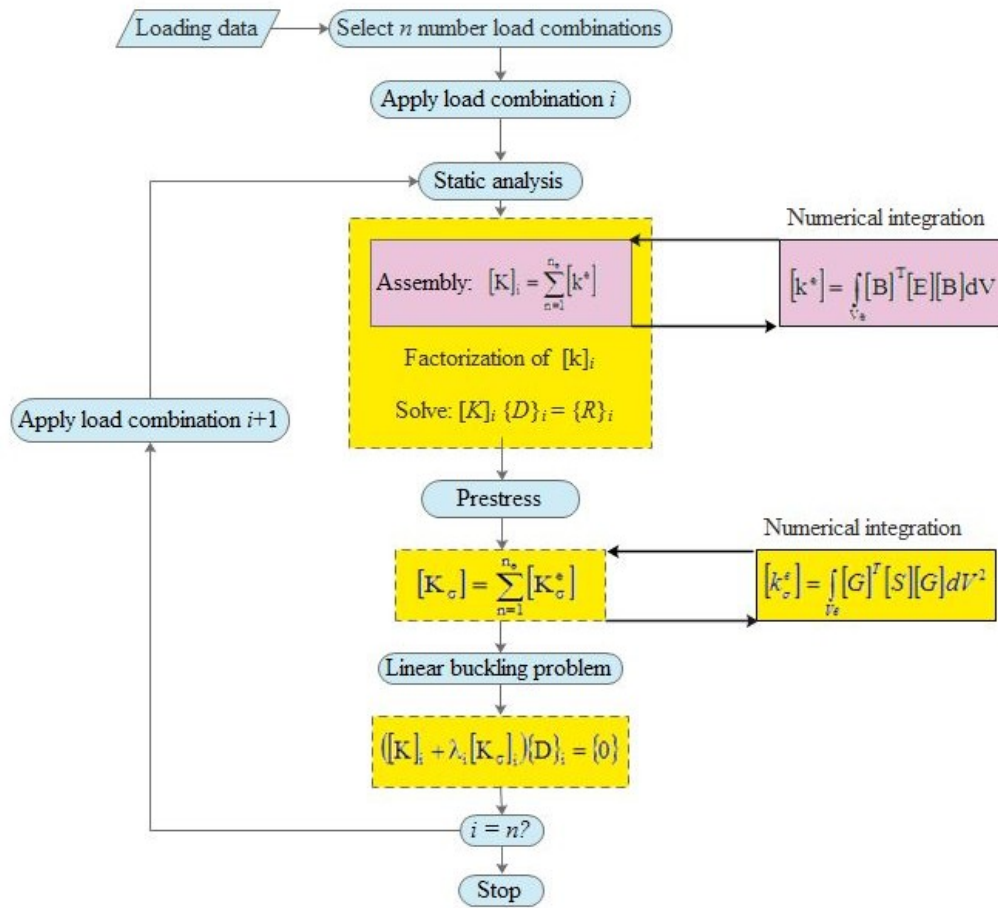


Figure 3.3 Flowchart of a standard procedure for linear buckling analysis with multiple load combinations n , when using the finite element method.

In order to solve eigenvalue problem, the built-in ABAQUS is used, which is quite quick and reliable. However, it is always possible and sometimes desirable to create a faster eigenvalue solver that is designed for the specific case to be solved. Two Eigen solvers are available in ABAQUS to extract the eigenvalue, namely the Lanczos iteration and the Subspace method. Lanczos and Subspace iteration methods are applied in ABAQUS to solve Eigen value problem and also widely used in FE programs. The Lanczos method [80], is generally faster when a large number of Eigen modes is required for a system with many degrees of freedom while the Subspace method [81], be faster when only a few (less than 20) Eigen modes are needed. The second step of the analysis is nonlinear buckling analysis in which large deformations and geometrical and/or material non-linearities are included. This type of analysis may include some imperfections after a linear buckling analysis. Post buckling analysis is the third step that may be carried out for investigating if the structure continues to carry the load after it has reached its critical limit or if it loses all its stiffness and collapses. In a general eigenvalue buckling problem is looking for the loads that lead to the model stiffness matrix to be singular and has nontrivial solutions. In this study only a linear buckling analysis is considered, because the analysis is done for “stiff” structures, so it is not necessary to include the effect of geometry change in establishing equilibrium for the base state. As a result, the important point in this numerical solution of a linear buckling analysis is the assumptions that assumed where a perfect geometry is used and therefore the obtained critical buckling. The main thing that should be pointed out is to understand that this numerical solution of a linear buckling analysis was assumed that the geometry is perfect without any imperfections. Therefore, the obtained critical load will be higher than the real critical load with geometry imperfection.

3.2.3 FINITE ELEMENT DISCRETIZATION

As is very common, the number and type of distribution of elements in FE method have a significant influence on the obtained results of calculations. The model discretized with a few or not sufficient number of elements is stiffer than the original structure, and this leads to unreal or wrong results. On the other hand, a huge number of elements used for discretization, needs to a high computer speed and leads to time-consuming calculations. Another factor should be taken into account, is the convergence analysis, the number of element density is chosen on the basis of the solution. As a result, an increase in the number

of elements increases the number of nodes and degrees of freedom for the model, which allows for mapping the highest buckling mode. Full three-dimensional FE model along with finite element statistics for the flat plate developed in ABAQUS is shown in Figure 4.2. The element type in buckling analysis that used is S4R (linear reduced integration 4-node doubly curved element). Figure 3.4 shows two and three dimensional shell elements which mean that it could be used. A two dimensional element is used when forces or moments are applied in one plane, while a three dimensional elements which can be used when forces or moments are in three perpendicular directions. Further details about the selected elements may be found in ABAQUS manual [82].

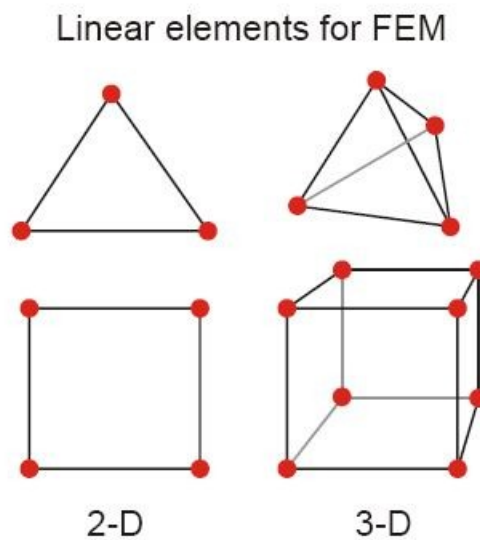


Figure 3.4 Typical two & three dimensional elements with nodes

3.2.4 FORMULATION AND CALCULATION OF FINITE ELEMENT MATRICES

The calculation of the finite element matrices is a very important phase in the finite element solution. The main idea of this section is to achieve the relationship between the element displacements at any point and the element nodal point displacements directly by using the interpolation functions.

3.2.4.1 THE STIFFNESS MATRIX OF SHELL ELEMENT

The relation between displacements and applied loads is given by the global stiffness matrix $[K]$. As eq. (3.11) shows that stiffness matrix is defined with an integration of the strain displacement matrix $[B]$ and the matrix of elastic stiffness $[E]$.

$$[k^e] = \int [B^T][E][B]dV \quad (3.11)$$

Where $[k^e]$ is the element stiffness matrix for one element only and $[B]$ is a matrix that defines the relation between the strain $\{\varepsilon\}$, and the displacement $\{u\}$, for an element as shown in eq. (3.12).

$$\{\varepsilon\} = [B]\{u\} \quad (3.12)$$

The global stiffness matrix $[K]$ is represented for entire assembled elements. By a coordinate transformation $[E] = [T^T][E'][T]$, it can possible to obtain the matrix $[E]$ from $[E']$, $[T]$ where is the transformation matrix. There is a case that leads to equality between $[E] = [E']$, this condition is when all elements are planar and defined in the same plane.

The eq. (3.13) represents the $[E']$ for an isotropic element,

$$[E'] = \begin{bmatrix} E' & \nu E' & 0 & 0 & 0 & 0 \\ \nu E' & E' & 0 & 0 & 0 & 0 \\ 0 & 0 & 0 & 0 & 0 & 0 \\ 0 & 0 & 0 & G' & 0 & 0 \\ 0 & 0 & 0 & 0 & G' & 0 \\ 0 & 0 & 0 & 0 & 0 & G' \end{bmatrix} \quad (3.13)$$

Where $E' = E/(1-\nu^2)$, $G = E/2(1+\nu)$, $G' = 5G/6$ and E is the Young's modulus while ν is the Poisson's ratio. Based on the finite element, the variation of transverse shear strain through the thickness direction is represented by a factor equal to 5/6 as shown in [83]. With the existence of the plane stress assumption of the shell element, this led to zero values in the third column of the eq. (3.13).

3.2.4.2 STIFFNESS MATRIX OF A BAR ELEMENT

For a two node bar element as shown in Figure 3.5, the only possible variation of the displacement $u(x)$ is linear, and expressed by the interpolation formula:

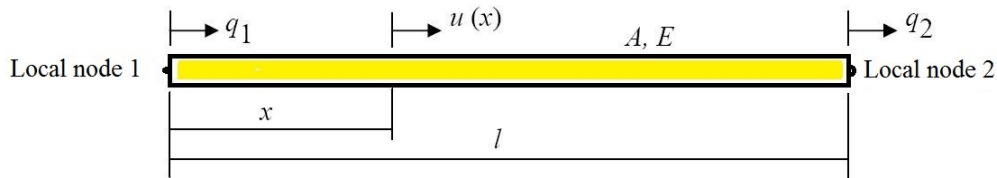


Figure 3.5 Two nodes bar element

Deflection (displacement) is approximated by

$$u(x) = [N] \overset{\rightarrow(e)}{q} \tag{3.14}$$

Where $[N]$ the shape function is

$$[N] = \left(\frac{x}{l} - \frac{x^2}{l^2} \right) \tag{3.15}$$

This can be written as a scalar product

$$\overset{\rightarrow(e)}{q} = \left\{ \begin{matrix} q_1 \\ q_2 \end{matrix} \right\}^{(e)} \tag{3.16}$$

Where q_1 and q_2 represent the nodal degree of freedom in the local coordinate system, and the superscript e denotes the element number.

For the calculation of element stiffness matrix, it needs to find the element strains

$$\varepsilon_{xx} = \frac{\partial u_x}{\partial x} \quad (3.17)$$

Where

$$\varepsilon_{xx} = \frac{q_2 - q_1}{l} \quad (3.18)$$

Or

$$\varepsilon_{xx} = [B]q^{(e)} \quad (3.19)$$

Where

$$[B] = \begin{bmatrix} -\frac{1}{l} & \frac{1}{l} \end{bmatrix} \quad (3.20)$$

In general, the strain-displacement transformation matrix is a function of the natural coordinates, and it therefore evaluates the stiffness matrix volume integral by integrating over the natural coordinates.

$$[k^{(e)}] = \iiint_{V^e} [B]^T [D] [B] dV \quad (3.21)$$

Then, evaluating eq. (3.21), it obtain the well-known matrix as in eq. (3.22)

$$[k^{(e)}] = A \int_{x=0}^l \begin{Bmatrix} -\frac{1}{l} \\ \frac{1}{l} \end{Bmatrix} E \begin{Bmatrix} -\frac{1}{l} & \frac{1}{l} \end{Bmatrix} dx \quad (3.22)$$

$$[k^{(e)}] = \frac{AE}{l} \begin{bmatrix} 1 & -1 \\ -1 & 1 \end{bmatrix} \quad (3.23)$$

3.2.4.3 STIFFNESS MATRIX OF A BEAM ELEMENT

Consider a two-dimensional beam element with 2-nodes depicted in Figure 3.6. The element has two nodes; each node has four degrees of freedom which are indicated by q_1 , q_2 , q_3 and q_4 . Due to the existence of four nodal displacements, the cubic displacement is assumed for $v(x)$ as illustrated in Figure 3.6 and expressed as following,

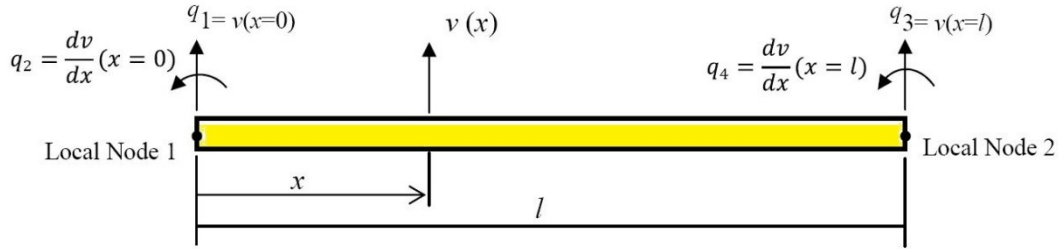


Figure 3.6 Two nodes beam element

$$v(x) = \alpha_1 + \alpha_2 x + \alpha_3 x^2 + \alpha_4 x^3 \quad (3.24)$$

Where $\alpha_1, \alpha_2, \alpha_3$ and α_4 are constants and can be worked out by applying some boundary conditions:

$$\text{At } x = 0 \Rightarrow v(x) = q_1 \text{ and } \frac{dv}{dx} = q_2$$

$$\text{And at } x = l \Rightarrow v(x) = q_3 \text{ and } \frac{dv}{dx} = q_4$$

By rewrite and substitution into eq. (3.24) by new symbols, it can be as following:

$$v(x) = [N] \overset{\rightarrow(e)}{q} \quad (3.25)$$

Where $[N]$ is given by

$$[N] = [N_1 \quad N_2 \quad N_3 \quad N_4]$$

Where

$$\begin{aligned}
 N_1(x) &= \frac{2x^3 - 3lx^2 + l^3}{l^3} \\
 N_2(x) &= \frac{x^3 - 2lx^2 + l^2x}{l^2} \\
 N_3(x) &= \frac{x^3 - lx^2}{l^2}
 \end{aligned} \tag{3.26}$$

And also

$$\vec{q} = \begin{Bmatrix} q_1 \\ q_2 \\ q_3 \\ q_4 \end{Bmatrix} \tag{3.27}$$

Figure 3.7 of Figure 3.6 which shows the section plane of beam under deformation, where the plane sections remained in the same plane after deformation based on the beam theorem. Therefore, due to the transverse displacement v , it can be expressed on axial displacement u as following:

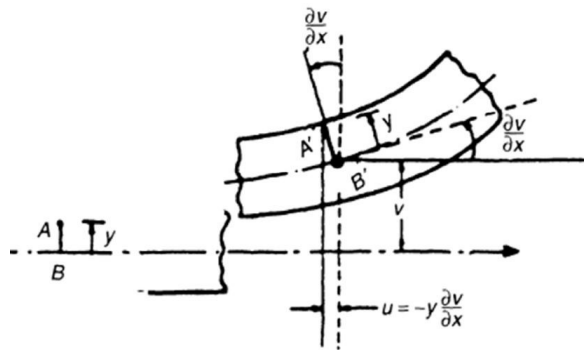


Figure 3.7 Deformation of a beam in x-y plane [84]

$$u = -y \frac{\partial v}{\partial x} \tag{3.28}$$

Where y is the distance from reference axis (i.e. neutral axis) for single element, then the axial strain is:

$$\varepsilon_{xx} = \frac{\partial u}{\partial x} = -y \frac{\partial^2 v}{\partial x^2} = [B] \vec{q} \tag{3.29}$$

Where the matrix [B] is defined as

$$[B] = -\frac{y}{l^3} \{(12x - 6l) \quad l(6x - 4l) \quad - (12x - 6l) \quad l(6x - 2l)\} \quad (3.30)$$

When $[D] = [E]$, the stiffness matrix of beam element can be written as following:

$$[k^{(e)}] = \iiint_{V^e} [B]^T [D] [B] dV = E \int_{x=0}^l dx \iint_A [B]^T [B] dA \quad (3.31)$$

The final approximate solution becomes

$$[k^{(e)}] = \frac{EI_z}{l^3} \begin{bmatrix} 12 & 6l & -12 & 6l \\ 6l & 4l^2 & -6l & 2l^2 \\ -12 & -6l & 12 & -6l \\ 6l & 2l^2 & -6l & 4l^2 \end{bmatrix} \quad (3.32)$$

Where $I_z = \iint_A y^2 dA$ is the moment of inertia about z-axis.

3.2.4.4 STIFFNESS MATRIX OF SPACE FRAME STRUCTURES

A straight bar of an uniform cross section is formulated to model a frame element, which has capability to resist not only the axial forces but also the bending moments in the directions perpendicular to the axis of the bar. Therefore, a frame element is seen to have the properties of both beam and truss elements. Figure 3.8 shows the frame element with nodes labeled 1 and 2 at each end of the element. As mentioned above, a frame element contains both the properties of the truss element and the beam element. To construct the stiffness matrix for the frame element, it can be simply formulated by combining element matrices for beam and truss elements, without going through the detailed process of formulating shape functions and using the constitutive equations for a frame. In order to obtain the stiffness matrix of the frame element, the superposition is applied. The same steps which applied in previous cases for bar element will be done for space element.

$$[k^{(e)}] = \iiint_{V^e} [B]^T [D] [B] dV \quad (3.33)$$

3.3 CONCLUDING REMARKS

This chapter has described an overview about the theoretical background of the finite element method and plate theory with particular focused on the linear buckling analysis to analyse the response of the buckling structural system. The main emphasis has been upon a basic of finite element process by highlighting its various characteristics associated to buckling analysis.

Linear static analysis and linear buckling analysis with finite element methods have been briefly presented. In order to obtain the equilibrium between applied forces on the nodal and internal generalized nodal forces, the linear static analysis has been applied. The linear behaviour structure is able to hold any amount of loading before reaching to the critical buckling point. Furthermore, before critical point any deformation in the structure disappears and system returns to its original shape without generating any imperfections or residual stresses. The linear static analysis has made upon some basic assumptions. The relationship between the applied load and resulting deflections assumed to be linear. The development of deflections is based on the theory of small displacement. Throughout the static analysis, the behaviour of the material is supposed to remain elastic. In order to determine the elastic stability of the element structures, the linear buckling analysis is applied or used. The ability of ABAQUS program is applied to perform linear buckling analysis.

CHAPTER 4

4. THE BUCKLING BEHAVIOUR OF A THIN PLATE

4.1 INTRODUCTION

In this chapter, the finite element techniques and solution strategies, which are appropriate for the linear buckling analysis of thin-walled plates, have been developed. The buckling and ultimate strength of plates subjected to pure axial compression force is governed, to a largely extent, by different aspect ratio and boundary conditions. Therefore, the right choice of boundary conditions plays an important role in the analysis in order to get precise results. Suitable constraints for each case of analysis will discuss in detail. Moreover, the solution strategies involving the selection of suitable solution parameters such as the element selection, load case and element discretization, etc. are comprehensively defined. The findings for each thin-walled section are discussed at length. In order to develop a detailed understanding of the critical buckling load of thin plates, the influence of different support boundaries on the critical buckling loads of the thin plates is thoroughly examined. In addition, the details of other important parameters involved in the simulation procedures that could potentially affect the critical buckling analysis are also explained, for instance aspect ratio of the plates and their thicknesses.

4.2 FINITE ELEMENT MODELLING OF THIN PLATE

4.2.1 GEO-METRIC MODELLING AND NUMERICAL ANALYSIS

In this section the procedures and strategies of the finite element simulation are described which used to analyze the thin plate subjected to pure axial compression buckling load. In order to develop a finite element solution of a thin plate structure subjected to axial compressive load, three-dimensional finite elements should used because the model would capture the real structural behaviour including not only global effects of the member but also various local effects. Figure 4.1 shows fully geometry of the hollow beam-column, which fully used in the analysis later and a chosen plate specimen. in order to analyse the plate specimen, some parameters are varied. The length-to-width ratio (a/b) of the thin plate

is changed from 0.5 to 2.5 where b is 1.2m (constant) and while the plate thickness is changing from 15mm to 30mm to study their influence on the critical buckling load characteristics. The plate thicknesses chosen were such as to illustrate local buckling and global buckling behaviour of the thin plate under compression load.

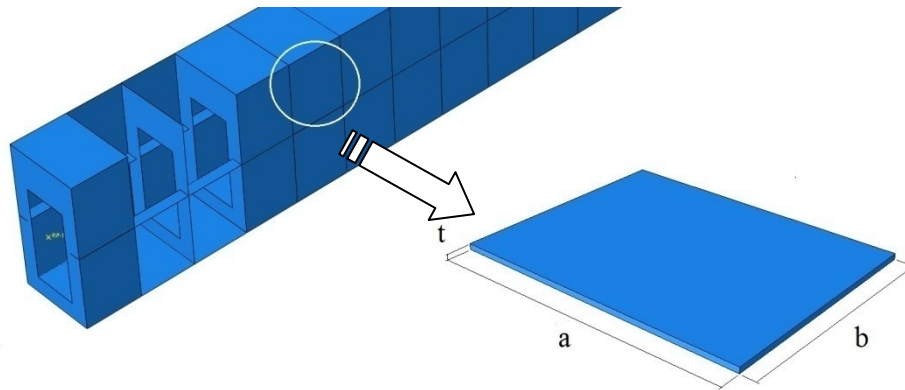


Figure 4.1 Typical geometry of a thin plate using in the study

4.2.2 BOUNDARY CONDITIONS AND FINITE ELEMENT MESH

The boundary conditions play an important role in the finite element modeling of any type of structures. However, both boundary conditions and load have very significant effects on the critical buckling mode. The main purpose of applying appropriate boundary conditions on the thin plates in both linear and nonlinear static analysis is to obtain the non-singular global stiffness matrix. To achieve the no singularity of the global stiffness matrix is only if the overall structure is motionless. Therefore, under applied load the movement of rigid body of the structure is prevented in all directions by applying appropriate displacement constraints at node (i.e. nodal displacement). However, when the boundary conditions allow to the structural elements to move which means that the structure can be deformed internally. However, when the boundary conditions allow to the structural elements to move which means that the structure can be deformed internally. The different results of the structural problems at different boundary conditions based on the change in support conditions are presented. The general-purpose elastic shell element is used in numerical simulations to discretise the model in order to build the finite element models for the Eigen value. Four noded doubly curved shell element with reduced integration S4R [81] and six degrees of freedom per node were used. In order to obtain the most optimized, accurate

solutions, the fine mesh has been chosen where the element size used for thicker plate is chosen and kept to be 0.025m. This element size chose through the appropriate convergence studies to ensure the accuracy of the solution. Figure 4.2 demonstrates the discretised configuration of the thin plate with mesh size equal to 0.025m. This type of element shows the accurate solution and satisfactory performance in verification work previously described for both thin and thick shell elements [85][86]. The thin plate structure is applied statically by a distributed compressive buckling load of 1(N/m) at plate ends as shown in Figure 4.3, where the load has a load factor with a default value of 1.0 and the entire load case can be multiplied with any numerical or alternatively loads if required. The simplified von-Mises elastic-perfectly material model is used for the isotropic steel with an elastic modulus of 210 N/mm², Poisson ratio of 0.3 and yield stress value of 350 N/mm².

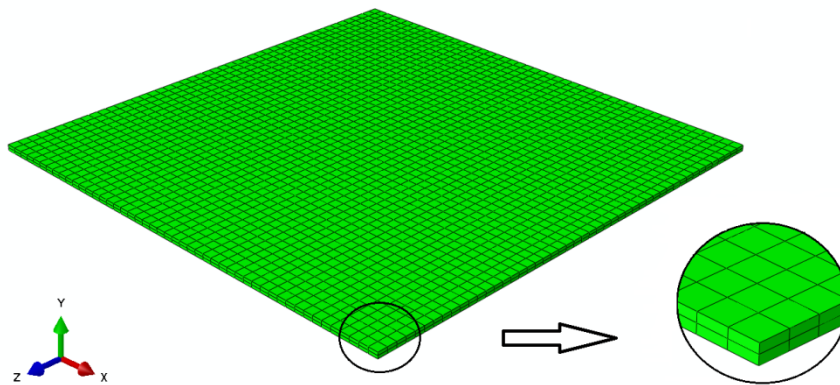


Figure 4.2 Mesh generation on the model of square thin plate

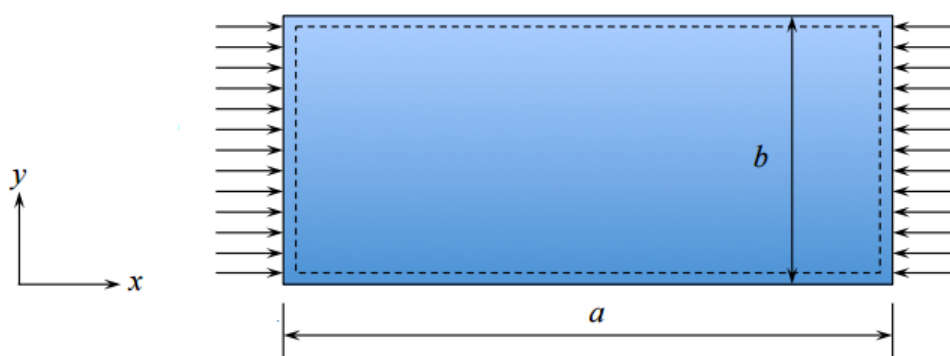


Figure 4.3 A plate under uniform uniaxial compression load

4.2.3 FULLY SIMPLY SUPPORTED OF THIN PLATE EDGES UNDER COMPRESSIVE LOAD (SSSS).

Thin plate subjected to a compressive loading is examined for the buckling analysis. The length-to-width aspect ratio (a/b) and thickness (t_p) of the plate are considered in the analysis. The study was carried out to examine the effects of plate aspect ratio and its thickness on the critical buckling load. Figure 4.4 shows the critical buckling load against aspect ratio (a/b) for different thicknesses and it can clearly observe that a considerable amount of the critical buckling is present for the case of the plate corresponding to the width-to-thickness ratio (b/t_p) in Figure 4.6. From the results that the critical buckling load of the plate is seen to increase significantly with increase in the plate thickness. On the other hand, the critical buckling load of the plate is also noted to increase substantially at $a/b = 1.5$, but it is of some significance to mention that the critical buckling load of the plate reduces with decrease in the plate thickness, due to essentially, to the higher critical buckling stress. The results obtained from finite element simulations have been thoroughly examined in order to develop a complete and in-depth understanding of the buckling behaviour of the thin plate.

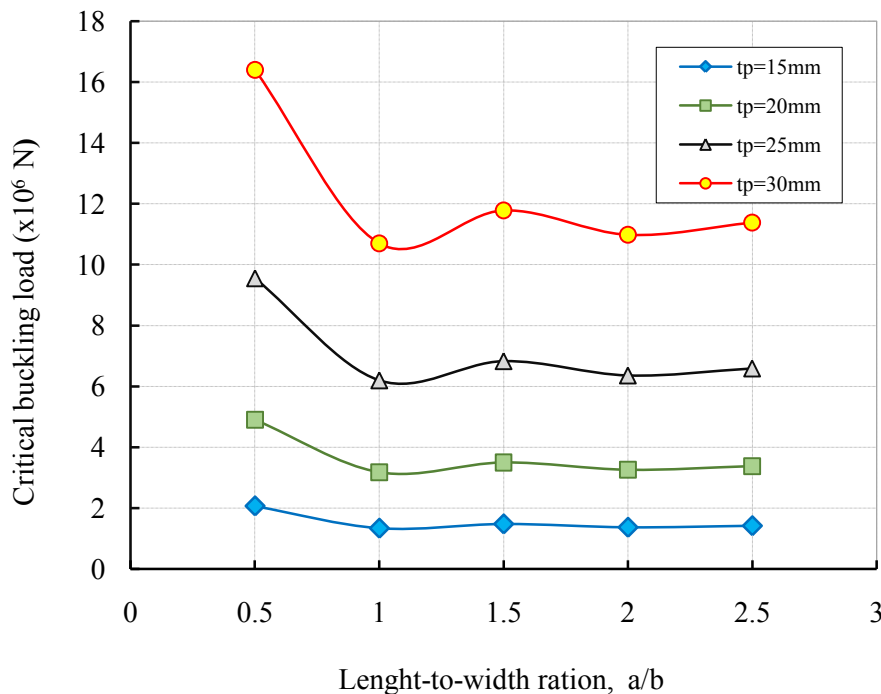
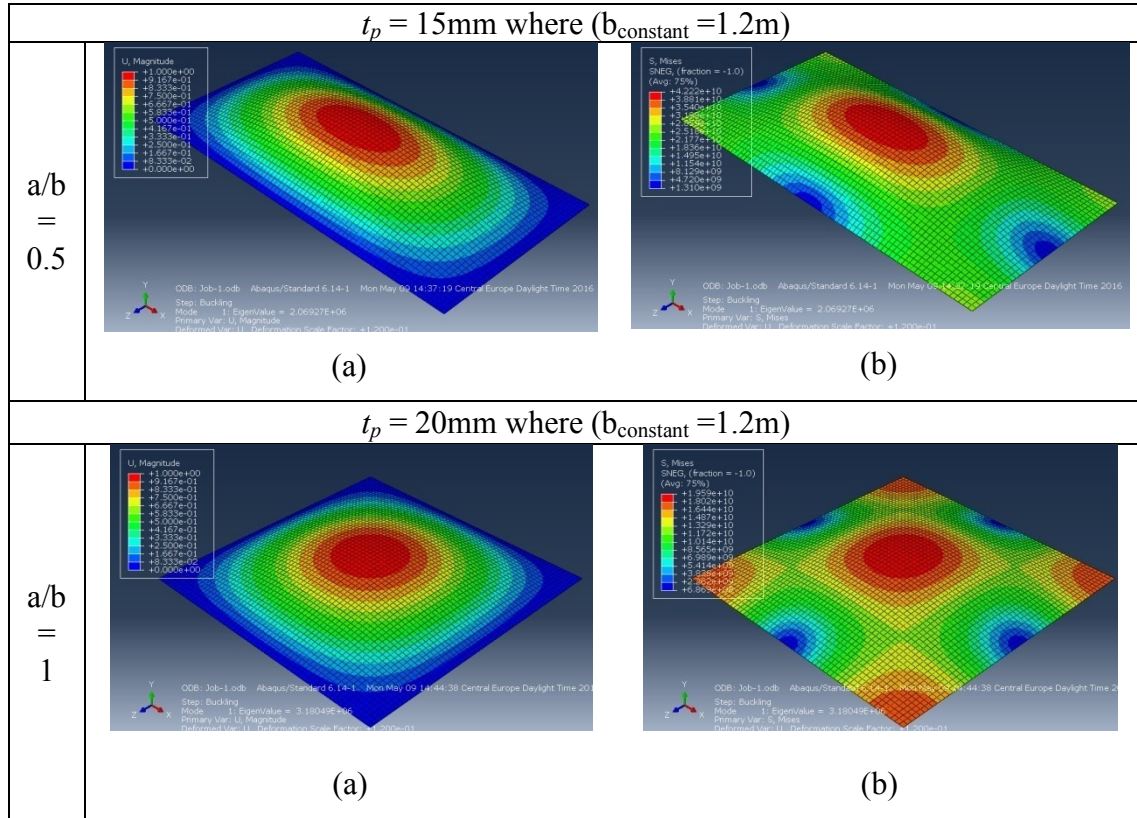


Figure 4.4 Length-to-width vs. critical buckling load for SSSS with different thicknesses,

$b_{\text{constant}} = 1.2\text{m}$

Figure 4.5 shows the deformation shapes and development of von Mises stresses during the loading in order to visualize the spread of elastic yielding with load and to determine the possible mechanism of critical buckling load. The blue and red colours on the deformation and stress spectrum represent the minimum and maximum respectively as shown in Figure 4.5. Firstly, deformation is seen to appear at the plate centres corresponding to loading for all cases. However, the stresses are at the middle-centre surface for aspect ratio equal to 0.5. The Von-Mises stresses corresponding to the aspect ratios (a/b) from 1 to 2.5 are seen to be at centres and edges corners of the plate on all surfaces. It is to be observed that the stress distribution does not remain constant on middle and corners surfaces. It is clear that the plate is not able to withstand any additional aspect ratio after 2.5 and with the increase in its thickness. Furthermore, it is noticed that from the deformation images of aspect ratios 1.5 and 2 respectively, the number of buckling waves jumped from 1 to 2 as illustrated in Figure 4.5. It is clear from this that aspect ratio also taken place through plate thickness as well. From the observations made with respect to length-to-width aspect ratio (a/b) with load, it is perhaps most relevant to point out that critical buckling behaviour is closely associated with complete width-to-thickness.



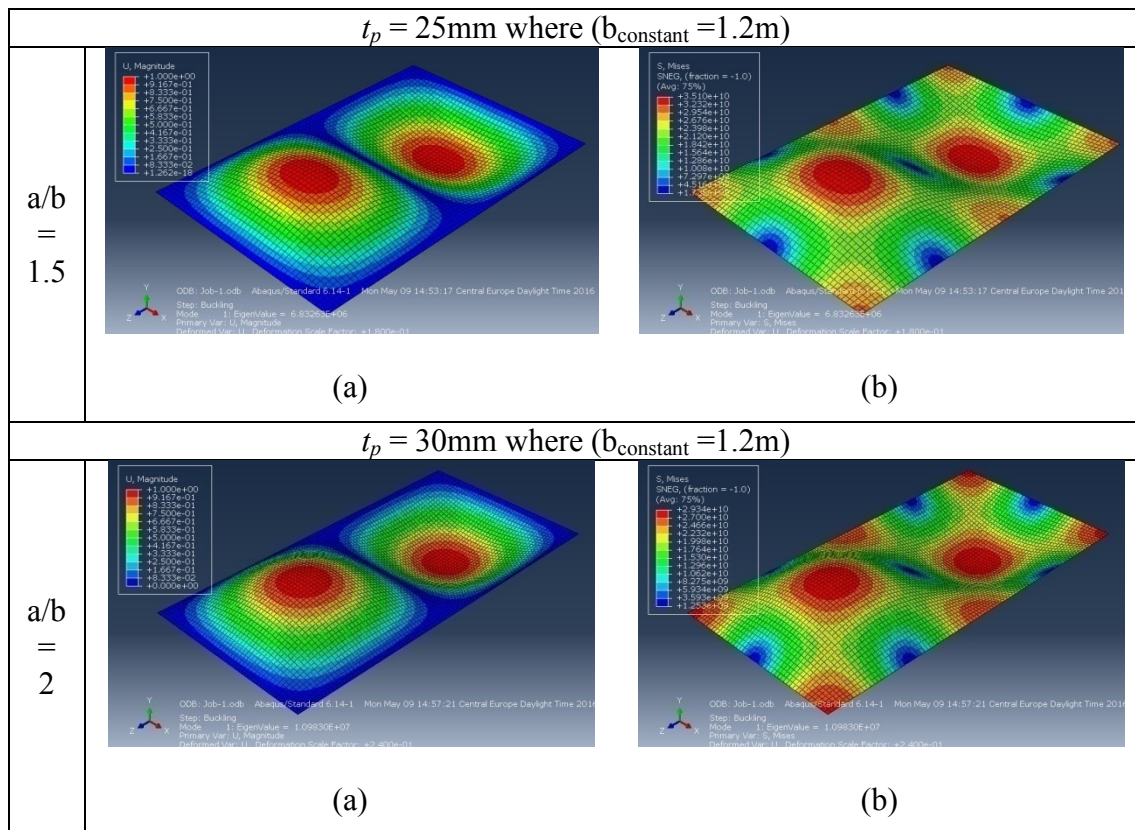


Figure 4.5 Deformation images (a) and growth of von Mises stresses (b) with different aspect ratios and thicknesses of Figure 4.4

The influence of change in the plate width-to-thickness ratio, (b/t_p), on critical buckling load is highlighted in detail in Figure 4.6. The critical buckling load is plotted against the non-dimensional width-to-thickness, (t_p/b), of the plate. Notable increase in the critical buckling load (maximum value) occurred at $a/b=0.5$ for all different of (b/t_p) conditions is, of course, due to the short length of the plate. However, it can be noticed for the other cases with (b/t_p) greater than 1 to 2.5 that the finite element value of critical buckling load is found lower and close to each other. The decline of critical buckling load of the plate is seen to be quite slow with further increase in the plate length-to-width ratio, (a/b), and it is noted that the value of the critical buckling load drops instantaneously to just over 87% of its maximum buckling value at $a/b=0.5$. Consequently, thin plate with high width-to-thickness ratio demonstrates buckling failure at very low levels of applied load. This is due to the fact that the buckling failure for high plate width-to-thickness ratio is considered a sudden geometrical phenomenon. Whereas on the other hand for low plate width-to-

thickness ratio, the plate is not very flexible to permit the load easily unlike the slender plate due to the high value of plate thickness.

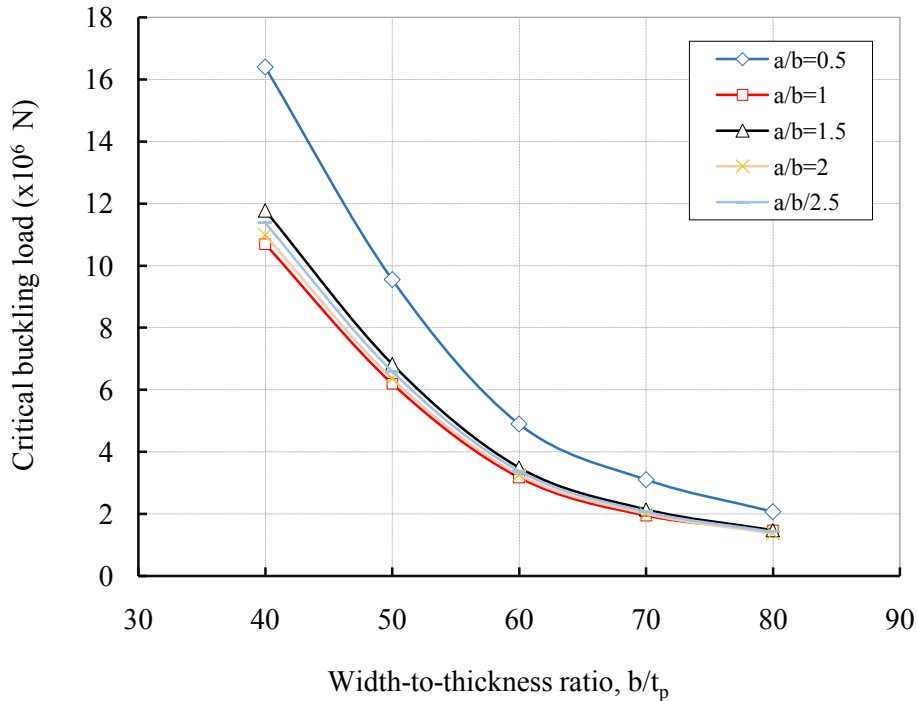


Figure 4.6 Width-to-thickness vs. critical buckling load for SSSS with different length-to-width ratios, ($b_{\text{constant}}=1.2\text{m}$)

4.2.4 SIMPLY SUPPORTED FREE OF THE THIN PLATE UNDER EDGES COMPRESSIVE LOAD (SSSF)

In this section the critical buckling load characteristics of three simply supported edges with one free edge with different length-to-width (a/b) and width-to-thickness (b/t_p) aspect ratios are examined. Figure 4.7 shows the non-dimensional length-to-width vs. critical buckling load for (SSSF) with different plate thicknesses. It is evident from the presented curves in Figure 4.7 that the behavior of critical buckling of the plate with simply supported and free edges boundaries is slightly different to that of fully simply supported boundary conditions. It is of note that the critical buckling load of the plate is noticed to be almost at same trend and level. However the critical buckling load of the plate is seen to be decreased enormously for all considered (t_p) values compared to that with SSSS edges load boundary conditions. Contrary to the case of SSSS with normal edges load boundary conditions, the critical buckling load of the plate does not seem to increase significantly with increase in

the plate thickness. For aspect ratio $a/b = 1.5$ and more, the critical buckling load seems to be in steady condition without any notable increase or decrease due to the long length of the plate. For instance the difference in critical buckling load between $a/b = 0.5$ to 2.5 and at $t_p = 15\text{mm}$ is $1.29 \times 10^6 \text{ N}$ with drop down to 83% of its pre-value at $a/b = 0.5$. As a result, critical buckling load begins to decrease with further increase in the length-to-width (a/b) ratio and it is to be observed that the loss of critical buckling load, is noticed to remain at steady trend at later stages of (a/b) ratio. The results obtained from finite element simulations have been thoroughly examined in order to develop a complete and in-depth understanding of the buckling behaviour of the thin plate. Figure 4.8 shows the deformation shapes and development of von Mises stresses during the loading in order to visualize the spread of elastic yielding with load and to determine the possible mechanism of critical buckling load. The blue and red colours on the deformation and stress spectrum represent the minimum and maximum values respectively. Firstly, deformation is seen to appear at the front plate centres corresponding to loading for all cases. However the stresses concentrated on the front-middle surface but almost it cover the majority of the surface at all aspect ratios. The Von-Mises stresses corresponding to the aspect ratios (a/b) from 0.5 to 2 are seen to be at centres and edge corners of the plate on all surfaces. It is to be observed that the stress distribution does not remain constant on the middle surfaces. An interesting point was mentioned in the Figure 4.8 that the stress distribution for $a/b=2$ and greater than were on the free and load edges corners, of course, due to the long length of plate. It is clear that the plate is not able to withstand any additional aspect ratio after $a/b=2.5$ and with the increase in its thickness. It is noticed that from the deformation images of aspect ratios 0.5 to 2.5 respectively, the number of buckling waves remained only one wave as illustrated in the figure. It is clear from this that aspect ratio also taken place through plate thickness as well. From the observations made with respect to length-to-width aspect ratio (a/b) with the load it is perhaps most relevant to point out that critical buckling behaviour is closely associated with complete width-to-thickness.

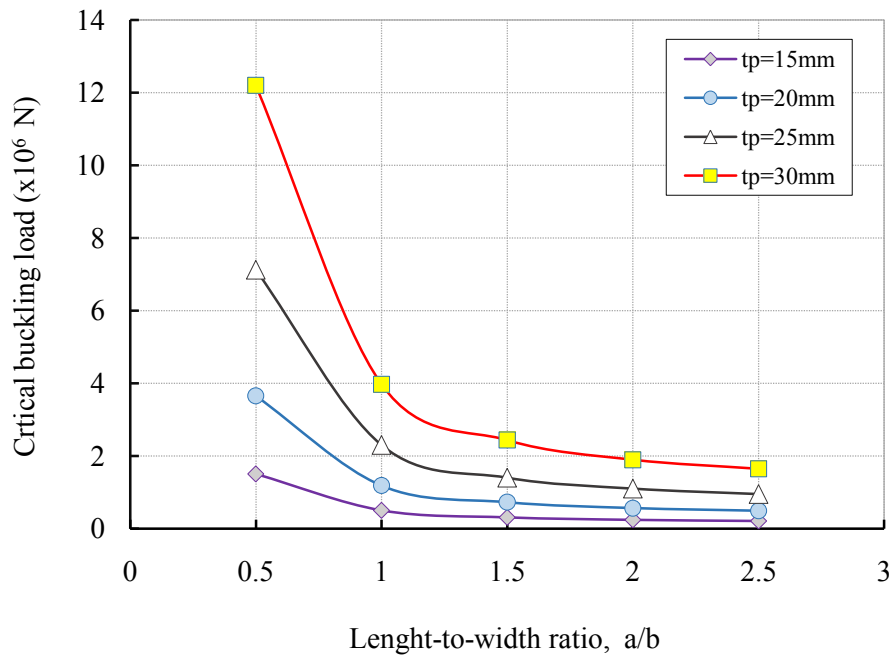
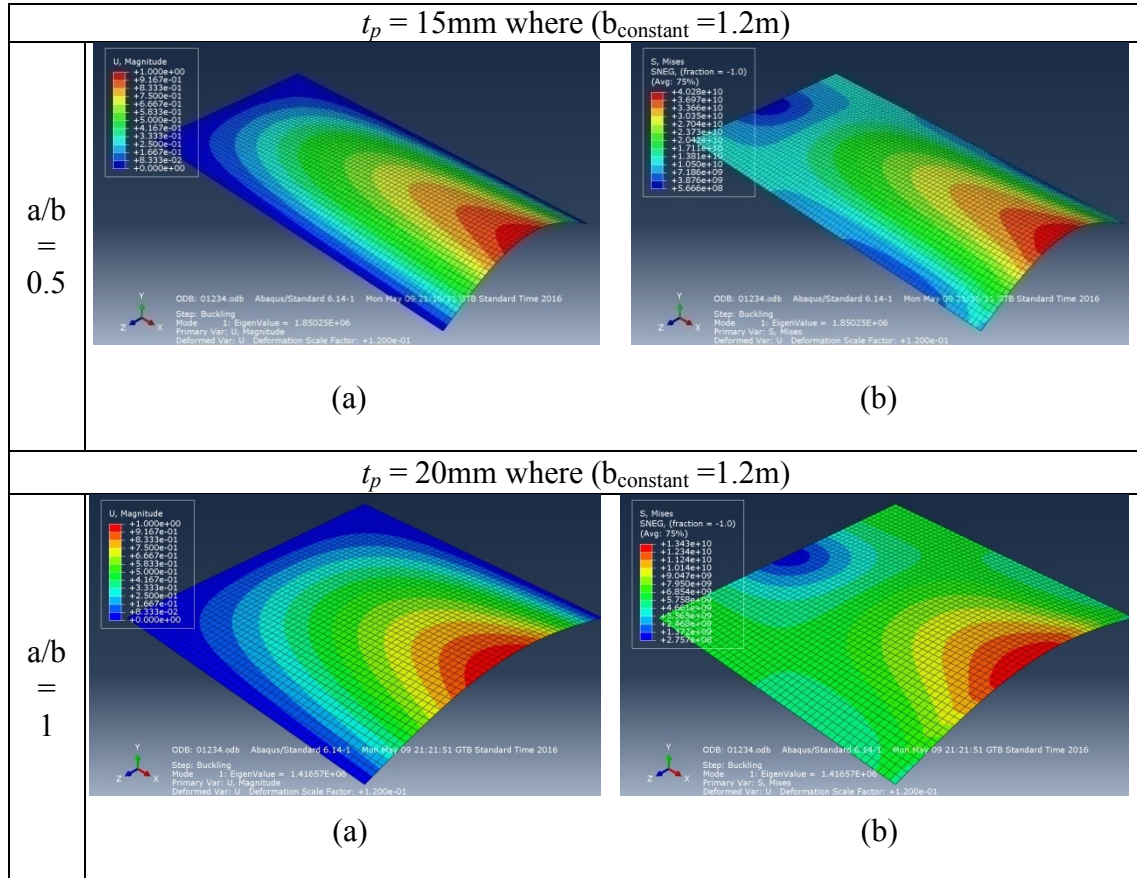


Figure 4.7 Length-to-width vs. critical buckling load for SSSF with different thicknesses, ($b_{\text{constant}} = 1.2\text{m}$)



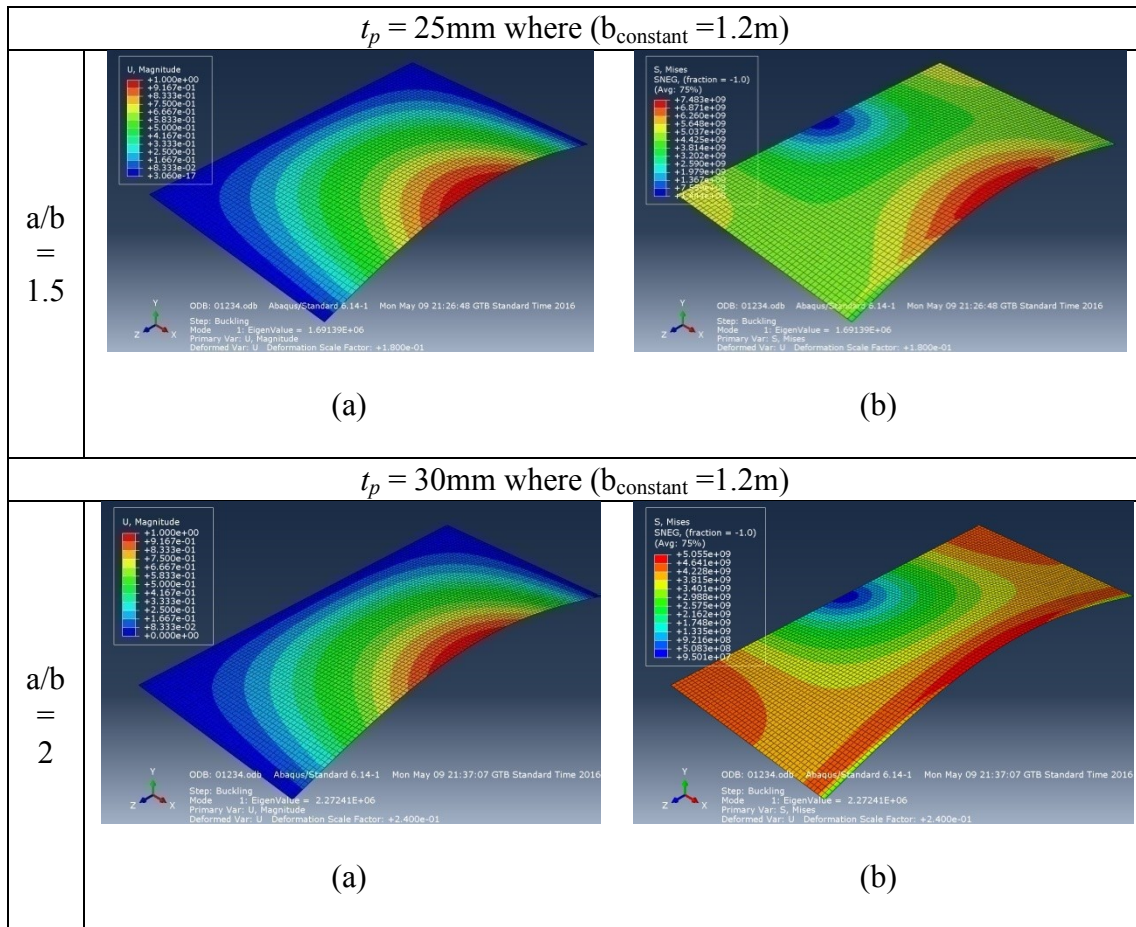


Figure 4.8 Deformation images (a) and growth of von Mises stresses (b) with different aspect ratios and thicknesses of Figure 4.7

The influence of change in the plate width-to-thickness ratio (t_p/b) on critical buckling load is highlighted in detail in Figure 4.9. The critical buckling load is plotted against the non-dimensional width-to-thickness, (t_p/b), of the plate. Notable increases in the critical buckling load (maximum value) occurred at $a/b=0.5$ for all different of (b/t_p) conditions is, of course, due to the short length of the plate. However, it can notice for the other cases with (b/t_p) greater than 1 to 2.5 that the finite element value of critical buckling load has found lower and close to each other. The decline of critical buckling load of the plate is seen to be quite slow with further increase in the plate width-to-thickness ratio, (b/t_p), and it is noted that the value of the critical buckling load drops instantaneously to just over 83% of its maximum buckling value when $a/b = 0.5$ and at all b/t_p values. Consequently, thin plates with high plate width-to-thickness ratios demonstrate buckling failure at very low levels of applied load. This is due to the fact that the buckling failure for high plate width-

to-thickness ratio is considered a sudden geometrical phenomenon. Whereas on the other hand for small plate width-to-thickness ratios the plate is not very flexible to permit the load easily, unlike the slender plate due to the high value of the plate thickness.

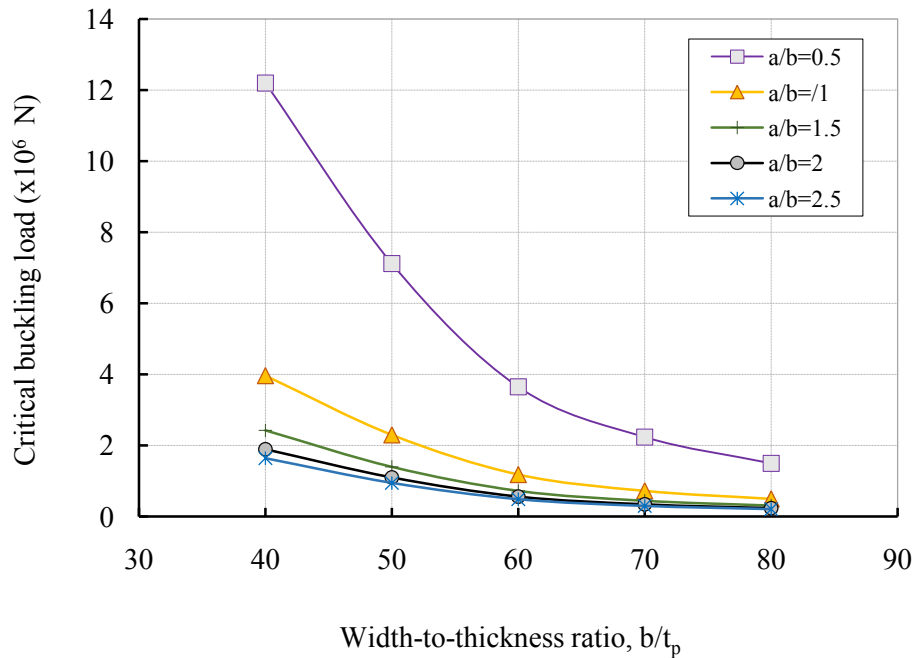


Figure 4.9 Width-to-thickness vs. critical buckling load for SSSF with different length-to-width ratios, ($b_{\text{constant}}=1.2\text{m}$)

4.2.5 SIMPLY SUPPORTED CLAMPED FREE OF THE THIN PLATE UNDER EDGES COMPRESSIVE LOAD (SSCF)

In this section the critical buckling load characteristics of two simply supported edges and one free- clamped edges with different length-to-width (a/b) and width-to-thickness (b/t_p) aspect ratios are examined. Figure 4.10 shows the length-to-width vs. critical buckling load for (SSCF) with different plate thicknesses. It is evident from the presented curves in Figure 4.10 that the behavior of critical buckling of the plate simply supported and free-clamped edges boundaries is slightly different to that of fully simply supported boundary conditions. It is of note that the critical buckling load of the plate is noticed to be almost at same trend and level. However the critical buckling load of the plate is seen to be decreased enormously for all considered (t_p) values compared to that with SSSF and edges load boundary conditions. Contrary to the case of SSSF with normal edges load boundary conditions, the critical buckling load of the plate does not seem to increase significantly

with increase in the plate thickness. For $a/b=1.5$ and greater than, the critical buckling load seems to be in steady condition without any notable decrease due to the long length of the plate. As a result, the critical buckling load for SSCF has almost similar behavior with the case of SSSS, of course with some differences in its values in terms of maximum and minimum. The results obtained from finite element simulations have been thoroughly examined in order to develop a complete and in-depth understanding of the buckling behaviour of the thin plate. Figure 4.11 shows the deformation shapes and development of von Mises stresses during the loading in order to visualize the spread of elastic yielding with load and to determine the possible mechanism of critical buckling load. The blue and red colours on the deformation and stress spectrum represent the minimum and maximum values respectively. Firstly, deformation is seen to appear at the front plate centres corresponding to loading for all cases. However, the stresses concentrated on the front-middle surface and on the back middle of the surface almost for all aspect ratios. It is to be observed that the stress distribution does not remain constant on the middle surfaces. An interesting point was mentioned in the Figure 4.11 that the stress distribution for $a/b=2$ and greater than was maximum at back edges of the plate, of course, due to the long length of plate. It is clear that the plate is not able to withstand any additional aspect ratio after $a/b=2.5$ and with the increase in its thickness. It is noticed that from the deformation images of aspect ratios 0.5 to 2.5 respectively, the number of buckling waves remained only one wave as in the previous case and as illustrated in the figure. It is clear from this that aspect ratio also has taken place through plate thickness as well. From the observations made with respect to length-to-width aspect ratio (a/b) with the load it is perhaps most relevant to point out that critical buckling behaviour is closely associated with complete width-to-thickness.

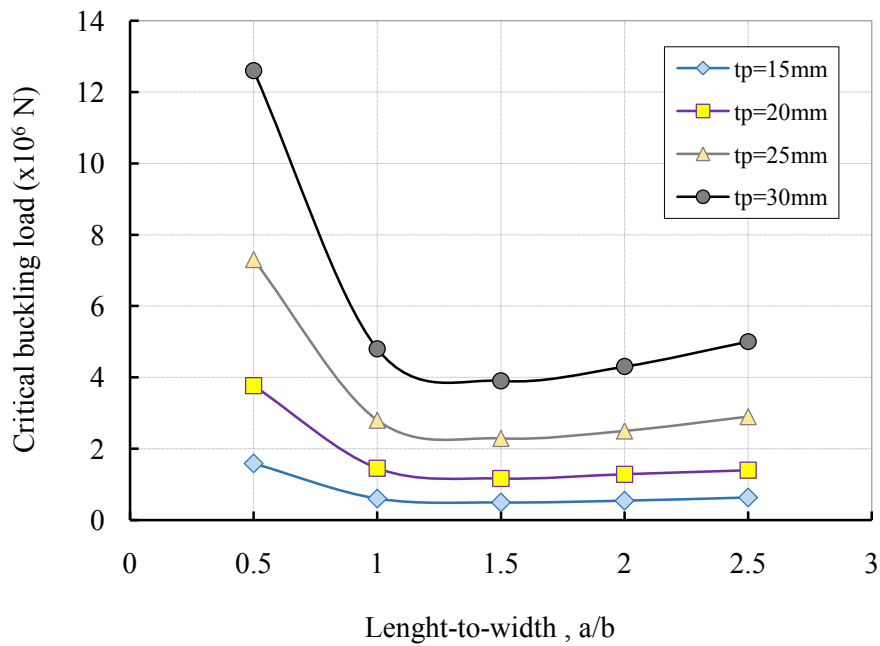
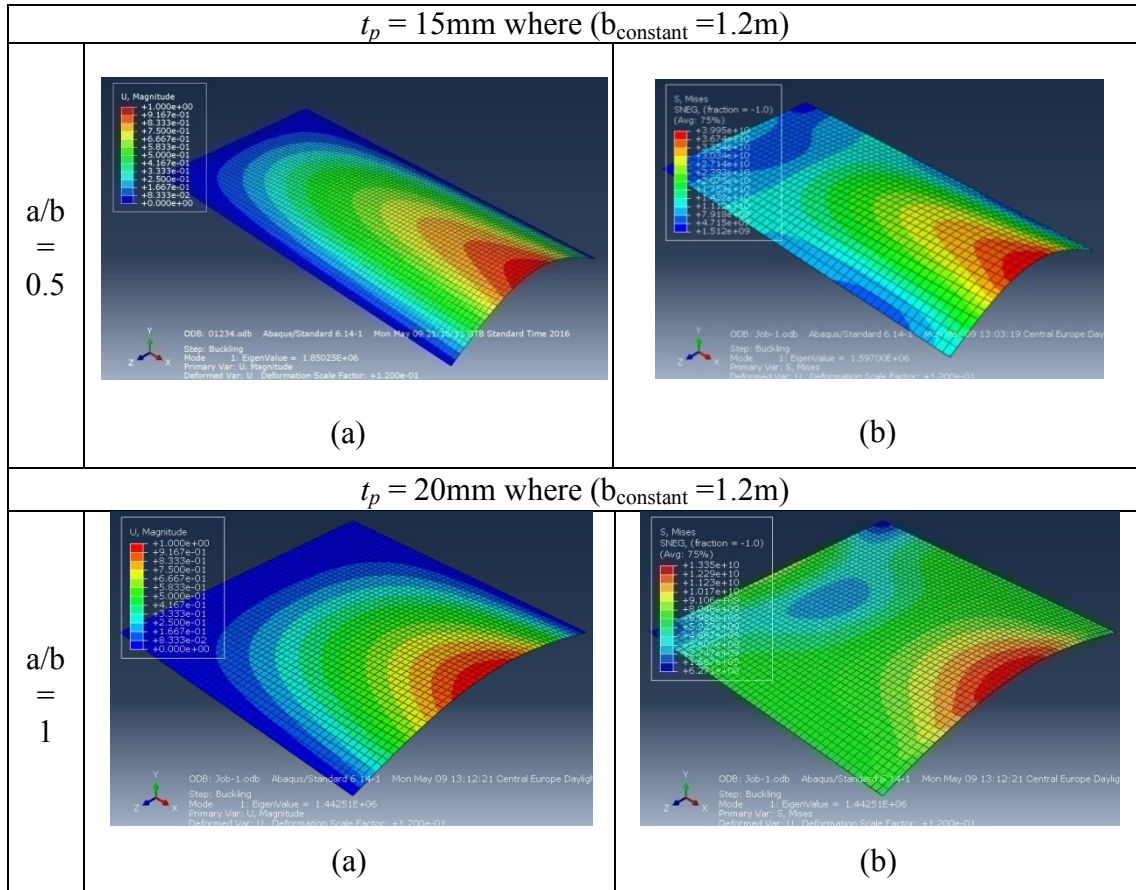


Figure 4.10 Length-to-width vs. critical buckling load for SSCF with different thicknesses, ($b_{\text{constant}} = 1.2\text{m}$)



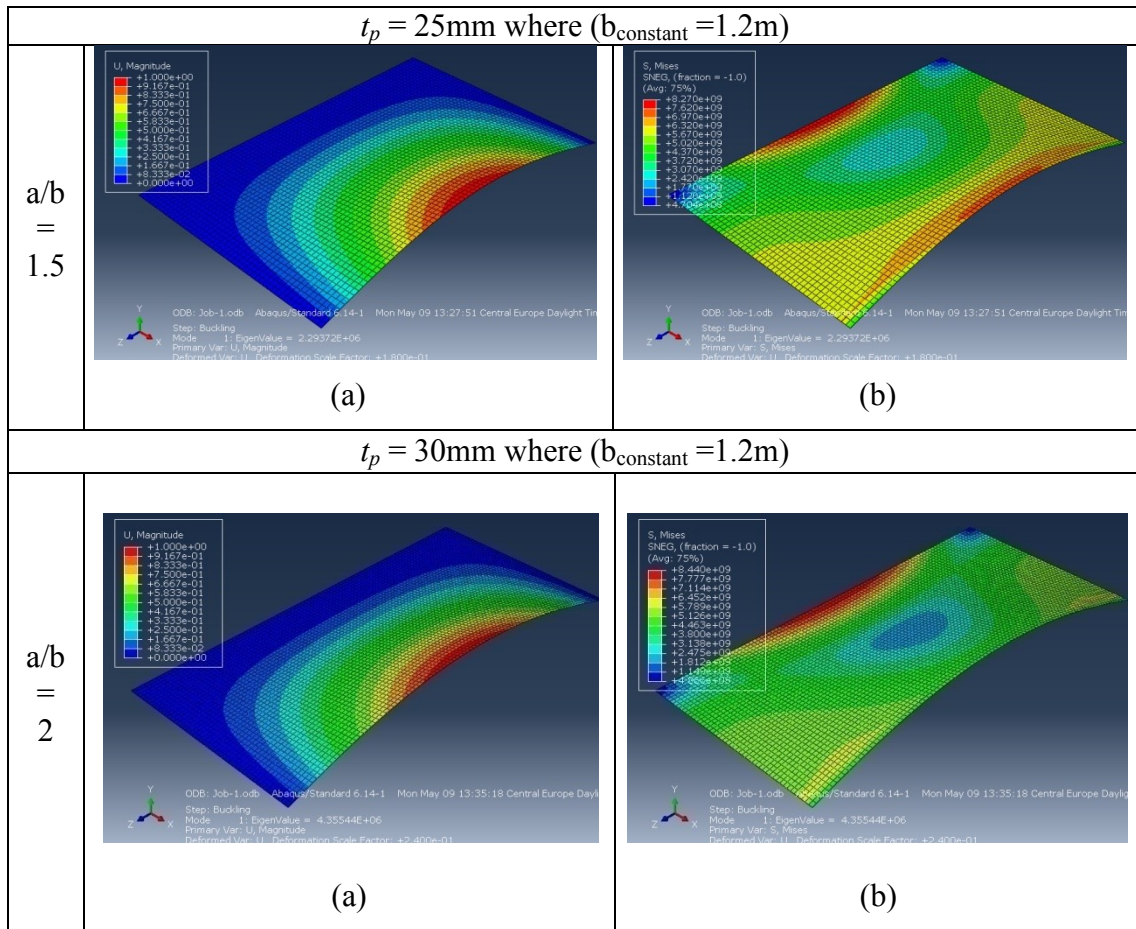


Figure 4.11 Deformation images (a) and growth of von Mises stresses (b) with different aspect ratios and thicknesses of Figure 4.10

The influence of change in the plate width-to-thickness ratio, (b/t_p), on critical buckling load is highlighted in detail in Figure 4.12. The critical buckling load is plotted against the non-dimensional width-to-thickness, (t_p/b), of the plate. Figure 4.12 shows the obtained results with different length-to-width aspect ratio, (a/b). Notable increase in the critical buckling load (maximum value) occurred at $a/b = 0.5$ for all different of (b/t_p) conditions is, of course, due to the short length of the plate. However, it can be noticed for the other cases with (b/t_p) greater than 1 to 2.5 that the finite element value of critical buckling load is found lower and close to each other. The decline of critical buckling load of the plate is seen to be quite slow with further increase in the plate length-to-width ratio, (a/b), and it is noted that the value of the critical buckling load drops instantaneously to just over 87% of its maximum buckling value at all (b/t_p) values. Consequently, thin plate with high width-to-thickness ratio demonstrates buckling failure at very low levels of applied load. This is

due to the fact that the buckling failure for high plate width-to-thickness ratio is considered a sudden geometrical phenomenon. Whereas on the other hand for small plate width-to-thickness ratio, the plate is not very flexible to permit the load easily unlike the slender plate due to the high value of plate thickness.

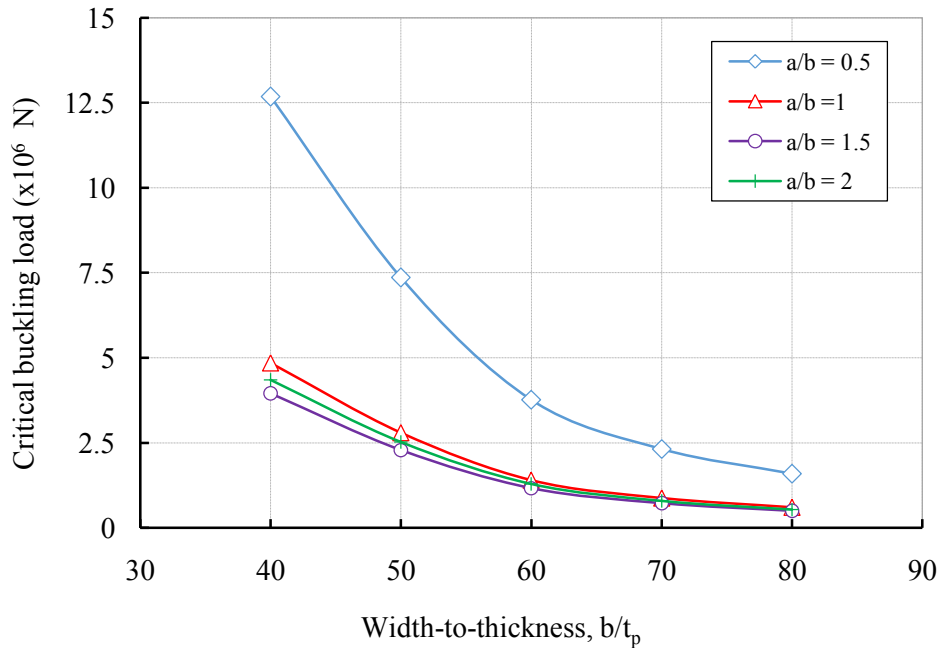


Figure 4.12 Width-to-thickness vs. critical buckling load for SSCF with different length-to-width ratios, ($b_{\text{constant}} = 1.2\text{m}$)

4.2.6 CLAMPED FREE OF THE THIN PLATE UNDER EDGES COMPRESSIVE LOAD (CFFF)

So far the buckling behaviour results associated with fully simply supported, simply supported free boundary conditions are discussed in detail however the critical buckling of the plate with regard to the simply supported clamped boundary conditions is also described for various web length-to-width and width-to-thickness ratios. In this section the critical buckling characteristics of one clamped edge of thin plate with different length-to-width a/b ratio at different thicknesses is examined. The length-to-width a/b is plotted versus the critical buckling load as shown in Figure 4.13 for clamped free thin plate boundary conditions. The results presented are for different plate length-to-width (a/b) ratios and at different plate thicknesses. It is evident from the curves presented in Figure 4.13 that the critical buckling response of the plate with clamped free edges boundaries is

entirely different to that of fully simply supported, simply supported-free and clamped boundary conditions. It is of note that the critical buckling load of the plate with clamped free boundary conditions is noticed to be almost at same level. However, the critical buckling load is seen to be enhanced enormously for all considered plate thicknesses values compared to that for previous cases of boundary conditions. An interesting point was mentioned in the Figure 4.14 that as a/b progresses more than 2, the critical buckling load would remain unchanged (i.e. constant). The results obtained from finite element simulations have been thoroughly examined in order to develop a complete and in-depth understanding of the buckling behaviour of the thin plate. Figure 4.14 shows the deformation shapes and development of von Mises stresses during the loading in order to visualize the spread of elastic yielding with load and to determine the possible mechanism of critical buckling load. The blue and red colours on the deformation and stress spectrum represent the minimum and maximum values respectively. Firstly, deformation is seen to appear at the front plate corners corresponding to loading for a/b until 1.5. While at $a/b=2$ and more the deformation is seen to appear at both the front edges and centre of the plate. Secondly, the images of the stress in Figure 4.15 are showing its growth and distribution on the plate surface with different plate thicknesses. At each thickness which corresponds to a/b , the von Mises stresses on surfaces can be visualized, where the location of the maximum stress concentrated was at the back-corners of the plate (i.e. at clamped edge) for all aspect ratios (a/b).

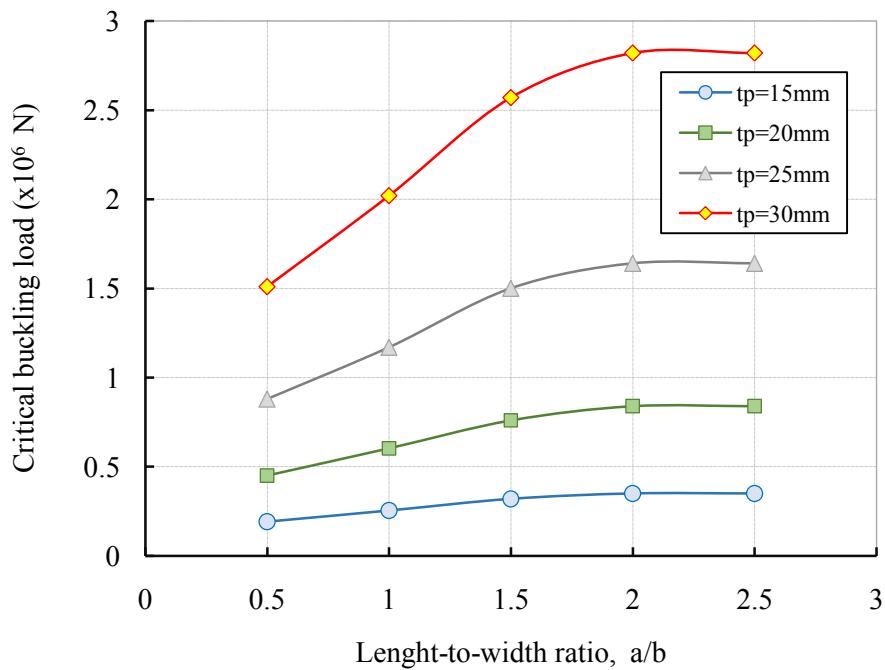
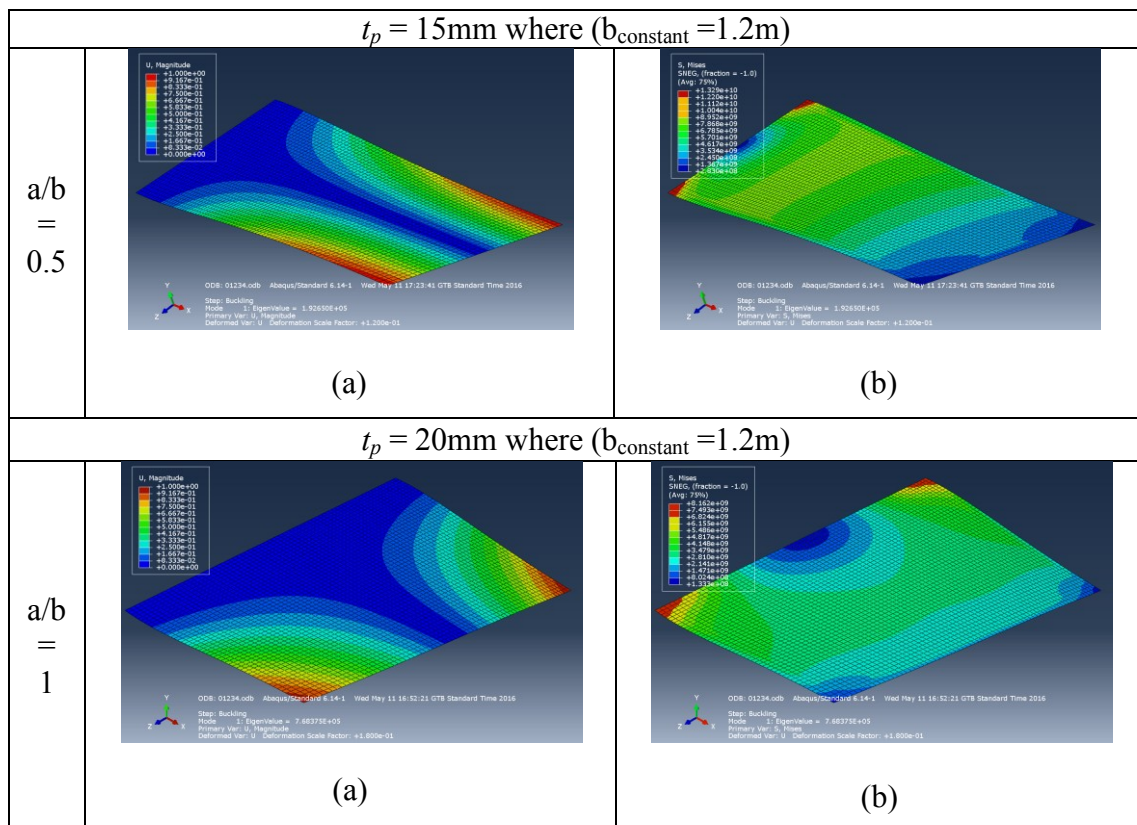


Figure 4.13 Length-to-width vs. critical buckling load for CFFF with different thicknesses, ($b_{\text{constant}}=1.2\text{m}$)



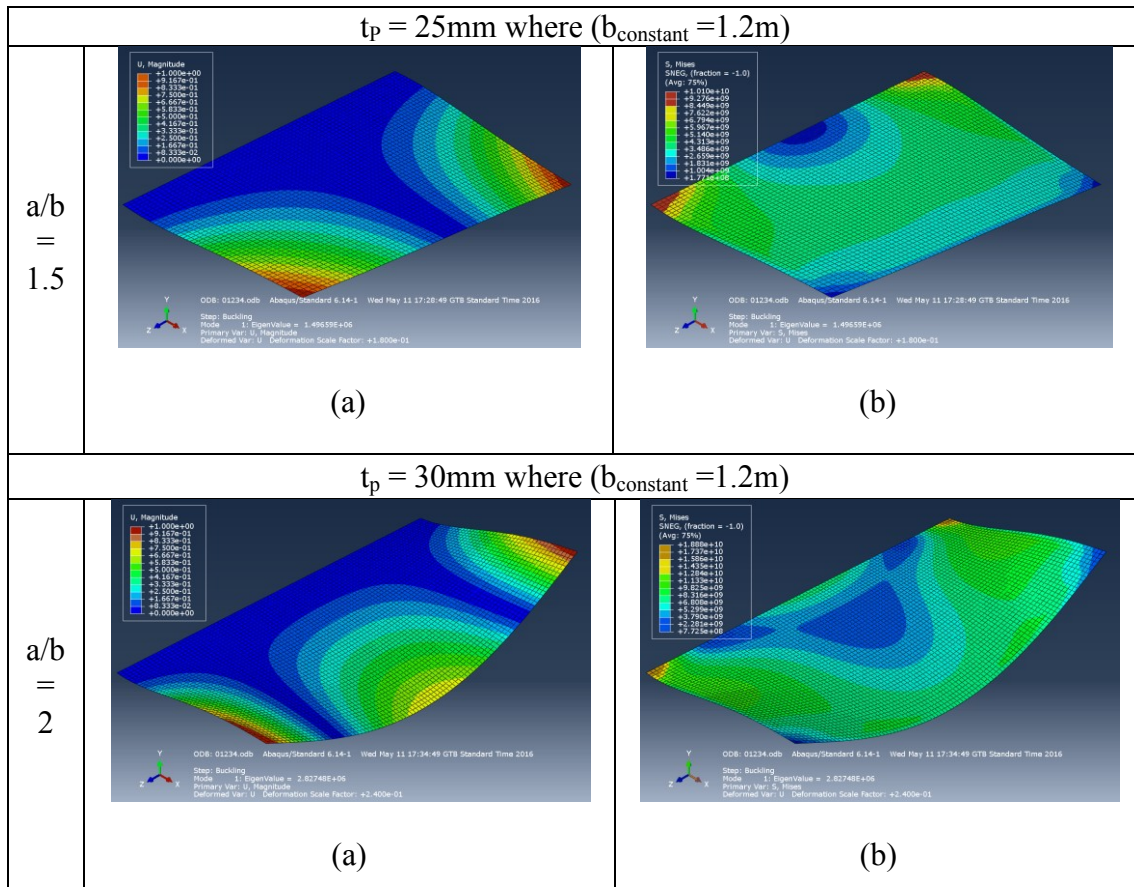


Figure 4.14 Deformation images (a) and growth of von Mises stresses (b) with different aspect ratios and thicknesses of Figure 4.13

The influence of change in the plate width-to-thickness ratio, (b/t_p), on critical buckling load is highlighted in detail in Figure 4.15. The critical buckling load is plotted against the non-dimensional width-to-thickness, (t_p/b), of the plate. Figure 4.15 shows the obtained results with different length-to-width aspect ratio, (a/b). Notable increase in the critical buckling load (maximum value) occurred at $a/b=0.5$ for all different of (b/t_p) conditions is, of course, due to the short length of the plate. However, it can be noticed for the other cases as (b/t_p) progresses more than 1 that the change in critical buckling load is found lower and close to each other. The decline of critical buckling load of the plate is seen to be quite high with further decrease in the plate length-to-width ratio, (a/b), specially for $b/t_p = 40$, and it is noted that the value of the critical buckling load increase instantaneously to just over 46% of its minimum buckling value. Consequently, thin plate with low width-to-thickness ratio demonstrates buckling failure at very high levels of applied load. This is due

to the fact that the buckling failure for low plate width-to-thickness ratio is considered a sudden geometrical phenomenon. Whereas on the other hand for high plate width-to-thickness ratio, the plate is not very flexible to permit the load easily unlike the slender plate due to the high value of plate thickness.

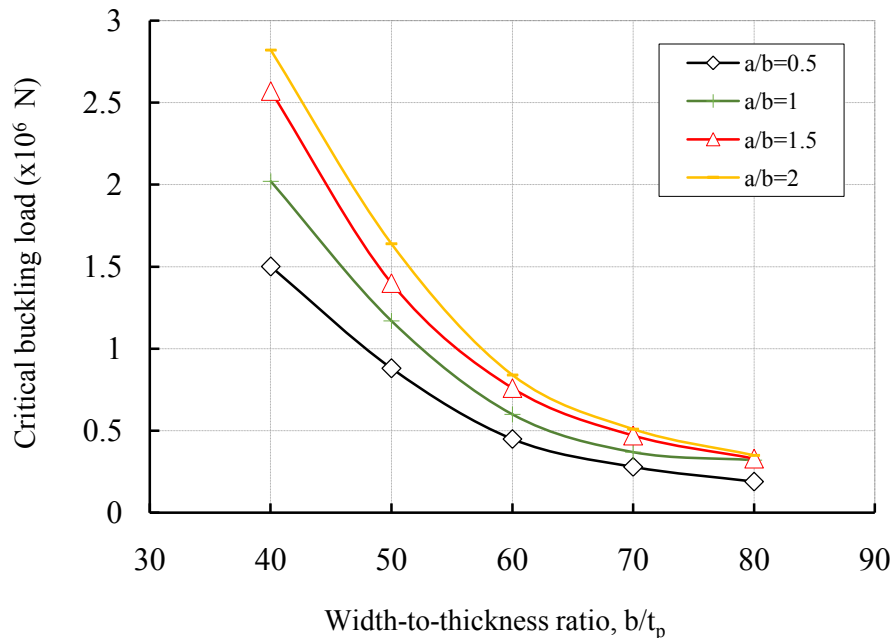


Figure 4.15 Width-to-thickness vs. critical buckling load for CFFF with different length-to-width ratios, ($b_{\text{constant}}=1.2\text{m}$)

4.3 CONCLUDING REMARKS

This chapter presents the suitable finite element simulation strategies to investigate the elastic buckling behaviour of thin plates subjected to the axial compression load. Moreover, this chapter has examined the effect of different thickness and length on the critical buckling loads and deformation behaviour of the square thin plate with different boundary conditions subjected to axial compression loading. The critical buckling behaviour of different thin plates is investigated to obtain an in-depth understanding with regard to the critical buckling failure. Also, it has been in this chapter that the critical buckling load at different boundary conditions is considerably decreased with change in the length to width ratio as well as the width to thickness ratio. The visualization of deformation growth and distribution of stress at the critical buckling load can be readily monitored and the geometric influence. It is worth pointing out that the importance of this chapter is the fact

that the critical buckling load of the thin plate has been shown to be closely associated with complete thin column-beam as well as the thin frame structure.

CHAPTER 5

5. THE BUCKLING BEHAVIOUR OF BEAM-COLUMN TRANSVERSELY AND LONGITUDINALLY STIFFENED

5.1 INTRODUCTION

This chapter examines the local and global buckling response of stiffened beam-column plates with plain flat outstands when subjected to pure axial compression load. The buckling capacity and capabilities of beam-columns subjected to axial pure compressive load can, of course, be improved through the introduction of stiffening elements such as Transverse and Longitudinal stiffeners (TS< respectively). Their flexural and torsional rigidities can contribute to significantly increase towards a critical buckling load of structural system. In order to see the effect of both stiffeners on the local and global buckling of a beam-column, finite element modelling strategies and solution procedures are developed, which enable the accurate determination of critical buckling loads and to visualize the response of the stiffened beam-column. Transverse stiffeners in the form of plain flat outstands are attached and distributed asymmetrically through the length of the beam-column with a variation of the distance between each one in order to highlight the significant influence of the stiffeners. The analysis is considered based on the equally spaced between the stiffeners. The thickness of the stiffener is varied in order to investigate the corresponding effect on the structural behaviour and performance. The modelling procedures are able to describe the complete local and global buckling behaviour of the stiffened beam-column structure. The critical buckling of stiffened beam-column was investigated by employing a unit load to start the solution sequence of buckling while giving due consideration to geometric and elastic material. Numerical simulations of the stiffened beam-columns are able to provide an in-depth understanding of the buckling analysis for such structural element. The results presented are for the case of beam-columns

with transverse stiffeners only and longitudinal stiffeners which are located at half and one third of the column's height. Furthermore, the results of critical buckling loads are presented with respect to the thickness of transverse stiffeners and their distances. In the buckling modes the stiffeners are heavily involved in both local and global types of buckling along with the length of the beam-column. The obtained results are also presented for the case of a beam-column with transverse stiffeners and longitudinal stiffeners which are located at the top part of the column height. According to the buckling behaviour, there is, of course, a transition region from local buckling to global buckling as the rigidity and thickness of the stiffeners approaches the critical level. The results illustrated in this chapter give an overview of a comprehensive detailed account of the complete critical buckling loads of the stiffened beam-columns.

5.2 FINITE ELEMENT MODELLING OF STIFFENED BEAM-COLUMN

5.2.1 GEO-METRIC MODELLING AND NUMERICAL ANALYSIS

The critical buckling capacities of beam-columns are quite complex, especially when approaching their ultimate failure. In this section the procedures and strategies of the finite element simulation are described that are used to analyze the stiffened beam-column subjected to pure axial compression load. In order to develop a finite element solution of beam-column structure subjected to axial compressive load, three dimensional finite elements must be used because the model would capture the real structural behaviour including not only global effects of the member but also various local effects. Figure 5.1 shows fully dimensions of the used hollow beam-column, which is taken and reassembled from the full frame as shown previously in Figure 1.2 for the analysis. The geometries of the transverse and longitudinal stiffeners are illustrated in Figure 5.2 and Figure 5.3 respectively. The thickness of the transverse stiffeners is changed from 15mm to 30mm to study the influence of the stiffener thickness on the critical buckling load characteristics, while the longitudinal stiffeners thickness is fixed at 15mm. The transverse stiffener thicknesses chosen were such as to illustrate local buckling and global buckling behaviour of the stiffened under compression load.

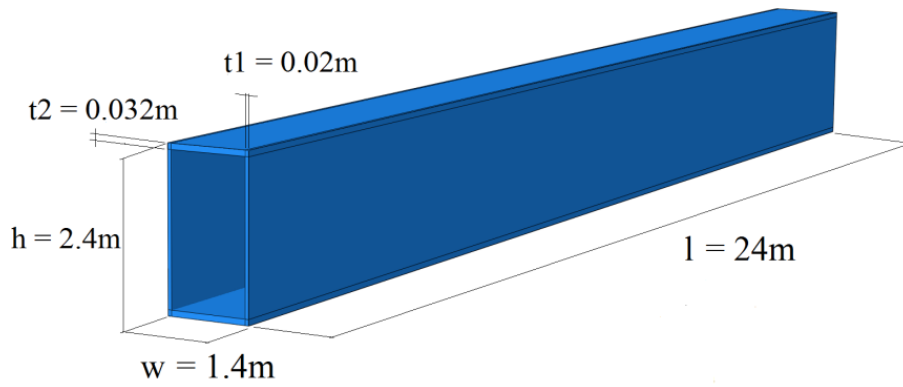


Figure 5.1 Typical geometry of a hollow beam-column using in the study

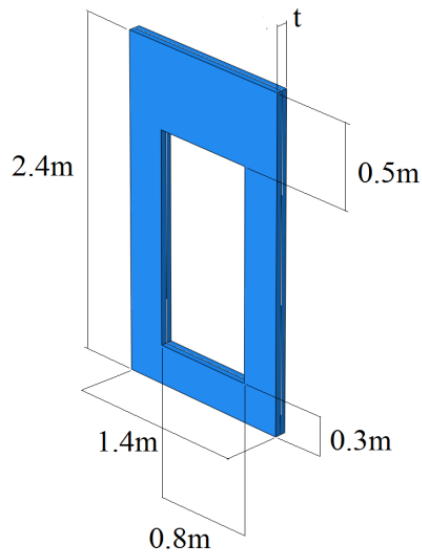


Figure 5.2 Geometry of transverse stiffener configuration (TS)

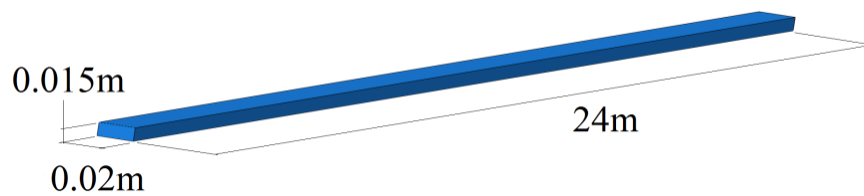


Figure 5.3 Geometry of longitudinal stiffener configuration (LS)

5.2.2 BOUNDARY CONDITIONS AND FINITE ELEMENT MESH

One of the important steps in the finite element modeling of structure is the boundary conditions. The main point of the boundary conditions when applying them is to obtain the non-singular global stiffness in linear or nonlinear static analysis. However, both boundary conditions and load have very significant effects on the critical buckling mode. In order to achieve the non-singularity of the global stiffness matrix is when the entire structure is motionless. Therefore, under applied load the movement of rigid body of the structure is prevented in all directions by applying appropriate displacement constraints at node (i.e. nodal displacement). However, when the boundary conditions allow to the structural elements to move which means that the structure can be deformed internally. The different results of the structural problems at different boundary conditions based on the change in support conditions are presented. As a result, the global stiffness matrix is either decreased or increased for a given loading condition. A beam-column with simply supported at its ends is considered in the analysis while the rest of the structure is left free to remain either normal or straight. A rigid body constraint has been used to tie the beam-column ends via node-to-node tie constraint relationship to reference points RP1 and RP2 which available in ABAQUS [82]. The reference points used to accomplish the boundary conditions to be tied to the end beam- column surfaces. The used boundary conditions are given in table 1 and the beam-column is applied statically by a central buckling load of 1N at RP1 (Figure 5.4 and Figure 5.5). The simplified Von-Mises elastic-perfectly material model is used for the isotropic steel with an elastic modulus of 210 N/mm^2 , Poisson ratio of 0.3 and yield stress values of 350 N/mm^2 . The general purpose elastic shell element is used in numerical simulations to discretise the model in order to build the finite element models for the Eigenvalue. Four noded doubly curved shell element with reduced integration S4R [81] and with six degrees of freedom per node were used. In order to obtain the most optimised accurate solutions, the fine mesh has been chosen where the element size used for the beam-column and as well as for the stiffeners is chosen and kept to be 0.1 meters. This element size is chosen through the appropriate convergence studies to ensure the accuracy of the solution as shown in Figure 5.6. Figure 5.4 demonstrates the discretised configuration of the beam -column without stiffeners. This type of element shows the accurate solution and satisfactory performance in verification work previously described for both thin and thick shell elements [85][86].

Table 5.1 Boundary conditions of simply supported model.

	Boundary conditions (Free: ○ , Constrained: ●)					
	u	v	w	θ_x	θ_y	θ_z
RP1	●	●	○	○	●	●
RP2	●	●	●	○	●	●

u, v, w are translations in x, y, z axes and $\theta_x, \theta_y, \theta_z$ are rotations about x, y, z axes.

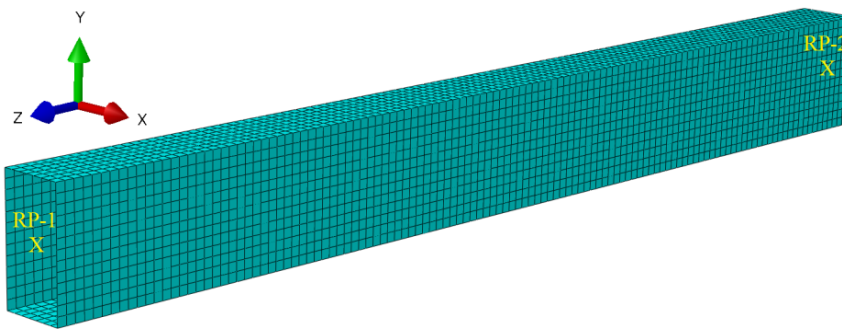


Figure 5.4 Typical FE model of a hollow beam-column



Figure 5.5 Loading configurations of a simply supported hollow beam-column

5.3 MESH CONVERGENCY STUDY

In order to choose the suitable size and to get the mesh independent results of finite element across the beam-column that gives a solution with a reasonable accuracy, a convergence study has been made. By applying the load and boundary conditions with suitably refined finite element models were developed for simulation. Many different sizes and numbers of elements have been considered, where the Figure 5.6 shows the obtained results. The figure depicts the response of the column-beam covering the onset of critical buckling load

through linear phase. Consequently, the chosen mesh is based on the mesh sensitivity analysis performed for successive mesh refinements. The minimum critical buckling load attained during the analysis is considered as the basis for mesh refinement. As shown in Figure 5.6, it is clear that no further increase in minimum critical buckling load is achieved if the number of elements is increased beyond 20×10^3 .

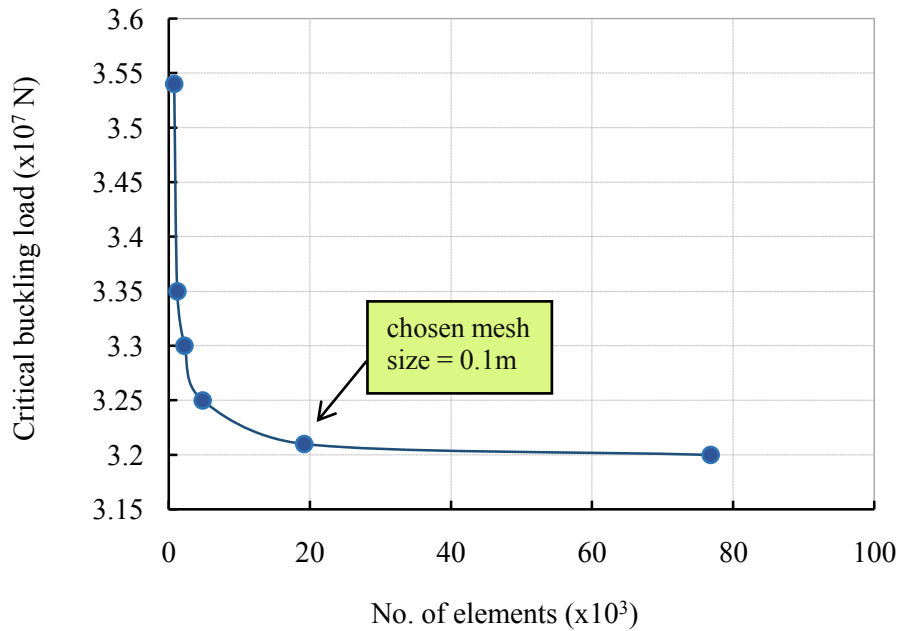


Figure 5.6 Mesh convergence study of a compressed beam-column

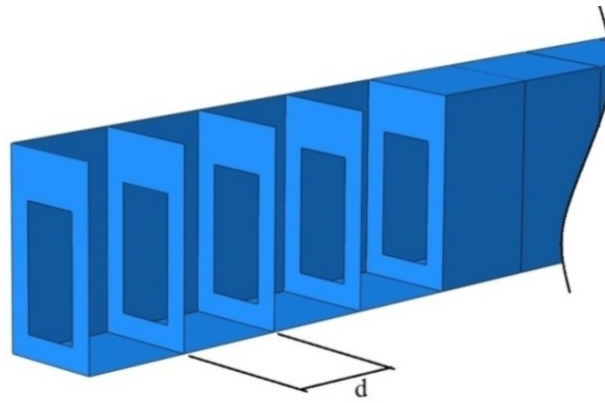
5.4 BUCKLING BEHAVIOUR OF THE BEAM-COLUMN WITH STIFFENERS

In this section the local and global buckling behaviour of the stiffened beam column is investigated in detail. A beam-column is considered with different cases for analysis, which are involved both transverse and longitudinal stiffeners. The effect of a change in stiffener locations and thicknesses on the buckling characteristics as well as the structural performance of the stiffened beam-column is highlighted.

5.4.1 A STIFFENED BEAM-COLUMN WITH ONLY TRANSVERSE STIFFENERS

The analysis in this section is done in the case of *model-1_b* which is placed only transverse stiffeners through the beam-column length at different distances between each one of the transverse stiffeners as shown in Figure 5.7. The dimensions of the transverse stiffener have been previously illustrated in section 5.2.1. The distance (d) is changing from 0.5 to 3

meters with 0.5 increments. The first Eigen buckling modes on deformed shapes at critical local & global buckling loads for one sample is shown in Figure 5.8 and Figure 5.9 respectively. Obviously, the onset of buckling modes can be seen along with distribution of magnitude deformation over the surfaces.



TS distance variation (d) = 0.5, 1, 1.5, 2, 2.5 and 3m.

Figure 5.7 A specimen section of the beam-column using TS only (*model-1_b*)

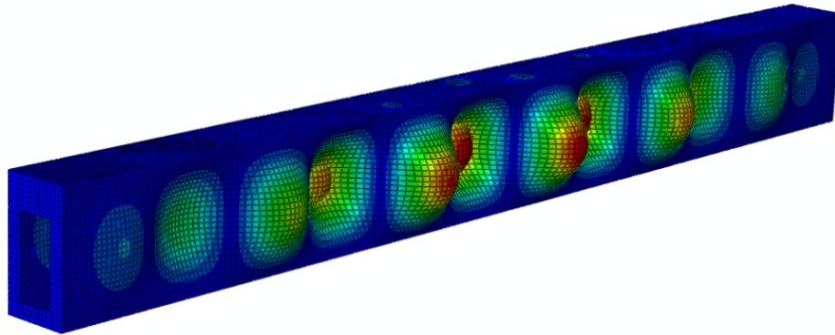


Figure 5.8 A sample of 1st local Eigen buckling mode of the beam-column (*model-1_b*)

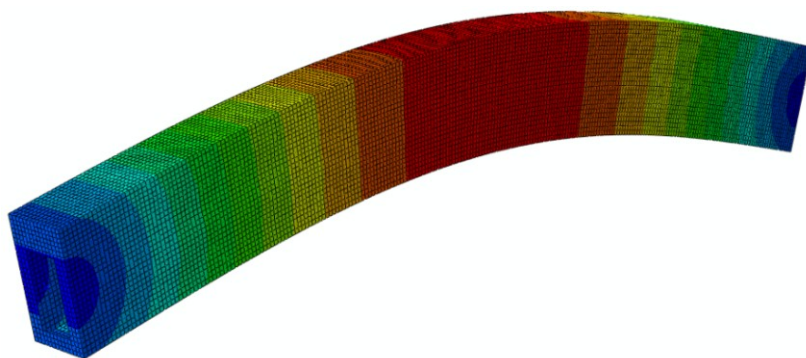


Figure 5.9 A sample of 1st global Eigen buckling mode of the beam-column (*model-1_b*)

The stiffener's thickness t and its location are changed in order to investigate its influence on the critical buckling load for local and global and structural response. The stiffened beam-column is subjected to pure axial compressive load at its ends, which are simply supported boundary conditions. The effect of a change in stiffener thickness and its locations on the critical buckling load is illustrated in Figure 5.10, where the ratio of critical local buckling load of stiffened to an unstiffened beam-column, $(P_{cr} - unstiffened) / P_{cr}$, is seen to be plotted against the distance d between transverse stiffeners.

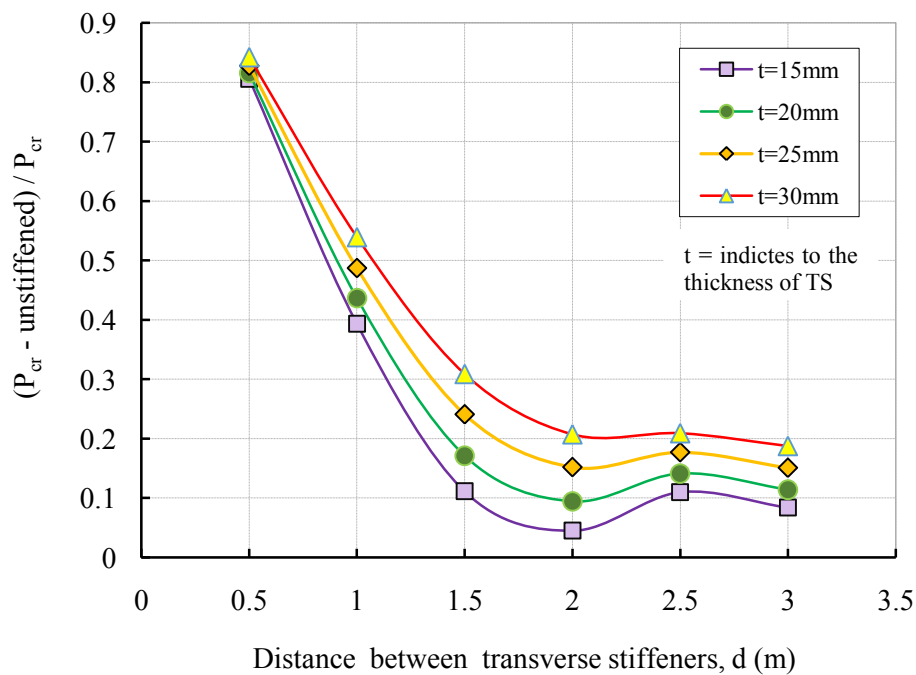


Figure 5.10 $(P_{cr} - unstiffened) / P_{cr}$ vs. distance between TS for *model-1_b* (Local)

Figure 5.10 clearly manifests that the introduction of a stiffener considerably improves the critical local buckling load performance of a beam -column. Initially, the rate of increase in the critical buckling resistance of the stiffened beam-column is seen to be maximum between 0.8 to 0.9 and with increase in the distance d between transverse stiffeners, it became significant at 2 meters before beginning of the reduction phase. As a consequence, the curves tend to the minimum value at 2 meters for all TS thicknesses and eventually decrease in the critical buckling performance becomes almost without effect. Figure 5.11 shows the influence of an increase in the transverse stiffener distance with changing of its thickness on the maximum and minimum critical local buckling load, where the effect of

stiffeners becomes lower after 2 meters which represents the optimum location. In the critical global buckling, termed as overall sometimes, the corresponding critical global buckling mode as shown previously in Figure 5.9, is clear that the beam-column buckles globally. In the global buckling mode, significant bending of the beam-column with stiffeners which are involved considering the fact that the stiffeners are not effective enough to increase the critical global buckling.

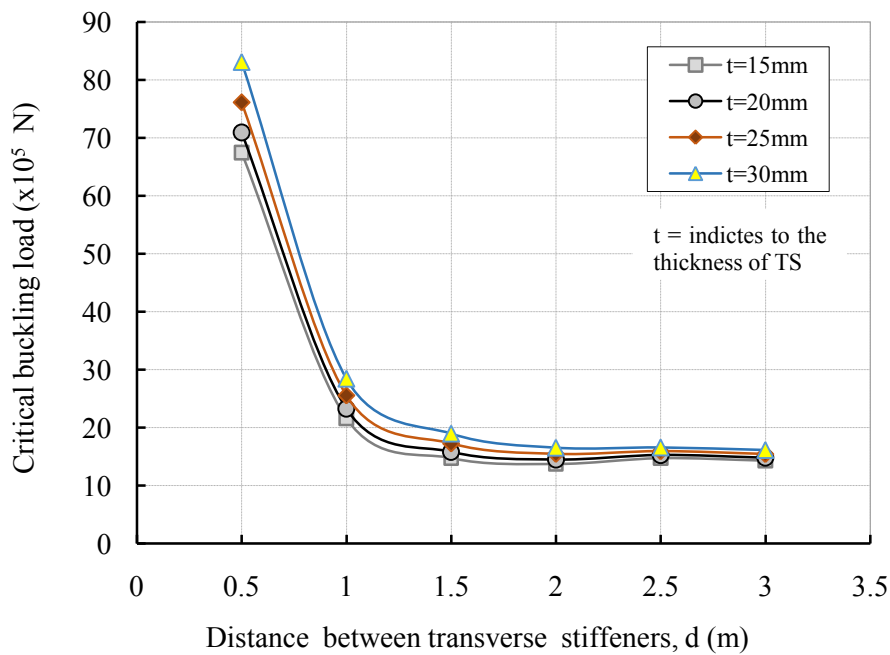


Figure 5.11 Effect of TS on the critical local buckling load of the beam-column *model-1_b*

The effect of a change in stiffener thickness and its locations on the critical global buckling load is illustrated in Figure 5.12 where the ratio of critical global buckling load of stiffened to unstiffened beam-column, $(P_{cr} - unstiffened) / P_{cr}$ is seen to be plotted against the distance between stiffener. It is of note that the increase of critical global buckling load is found to be a small order of unstiffened beam-column. As a result, it is seen that the effect of transverse stiffeners on the critical global buckling are not clear and the variation of P_{cr} ratio almost negligible at all distances and through all thicknesses according to the curves values. Figure 5.13 shows the effect change of critical global buckling where gradually begins to reduce before reaching to almost 2 meters of stiffener's distance. The stiffener distance in $d=2$ meters is found to be capable of holding the critical global buckling at optimum value based on critical local buckling and it seems useless to further increase the

distance between stiffeners since it decrease the structural weight without any notable improvement in the critical buckling.

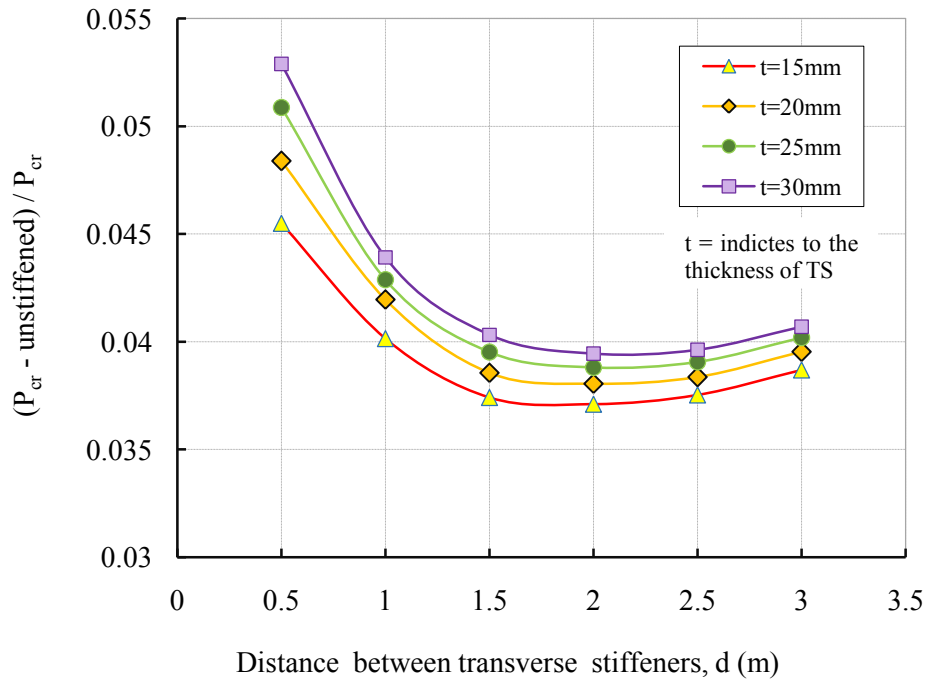


Figure 5.12 $(P_{cr} - \text{unstiffened}) / P_{cr}$ vs. distance between TS for *model-1_b* (Global)

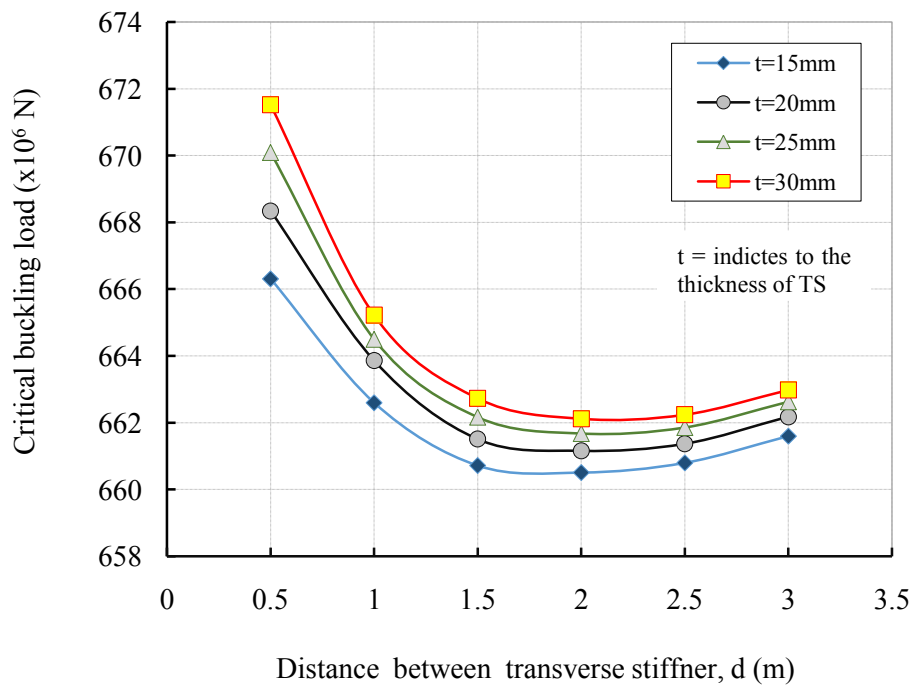
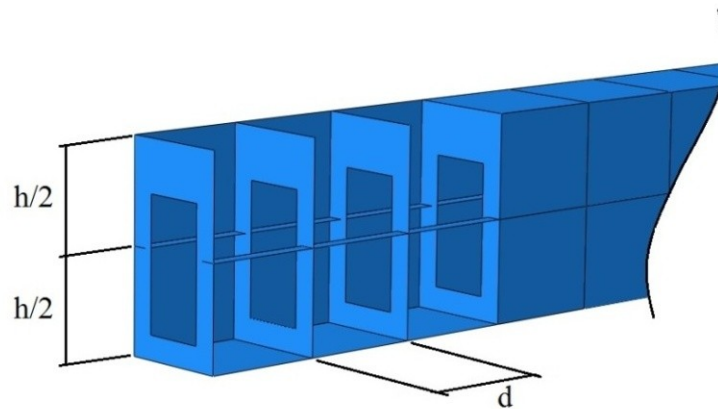


Figure 5.13 Effect of TS on the critical global buckling load of the beam-column *model-1_b*

5.4.2 A STIFFENED BEAM-COLUMN WITH TRANSVERSE AND LONGITUDINAL STIFFENERS

5.4.2.1 A STIFFENED BEAM-COLUMN WITH TRANSVERSE AND TWO LONGITUDINAL STIFFENERS

In this case the effect of change in both transverse and longitudinal stiffeners for model-2a, on the critical buckling load and buckling modes of the stiffened beam-column with two longitudinal stiffeners is investigated. Figure 5.14 illustrates a detailed geometrical assembly of a beam-column with both stiffeners where the longitudinal stiffeners are mounted at $h/2$ of beam-column height. The dimensions of both the transverse and longitudinal stiffeners have been previously illustrated in section 5.2.1. The first Eigen buckling modes on deformed shapes at critical local and global buckling loads for one sample are shown in Figure 5.15 and Figure 5.16 respectively. Obviously, the onset of buckling modes can be seen along with distribution of magnitude deformation over the surfaces. It is clearly manifest from Figure 5.15 that the effect of longitudinal stiffeners has a pivotal role in terms of redistribution of the buckling mode in particular for the local buckling. However, the behaviour of global buckling mode is in the same fashion to the previous case in section 5.4.1 with a difference, of course, in the values.



TS distance variation (d) = 0.5, 1, 1.5, 2, 2.5 and 3m, LS distance variation ($h/2$)=1.2m.

Figure 5.14 Geometrical section of the beam-column for *model-2_b*

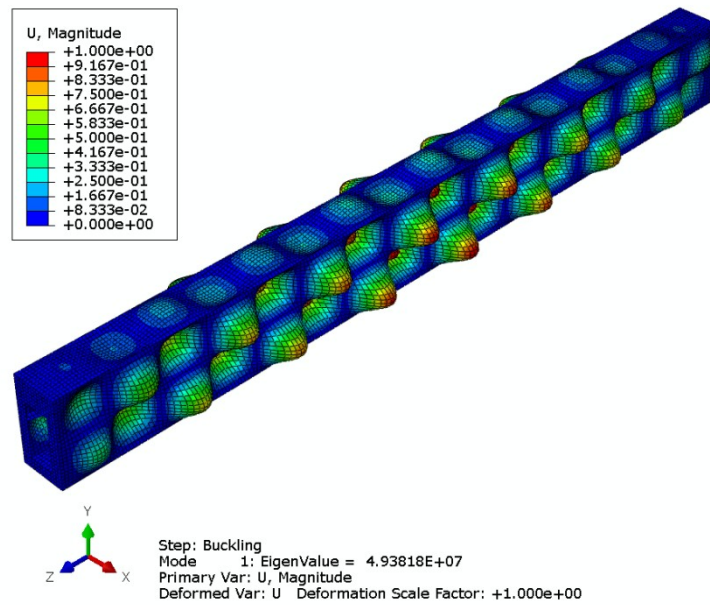


Figure 5.15 A sample of 1st local Eigen buckling mode of the beam-column for *model-2_b*

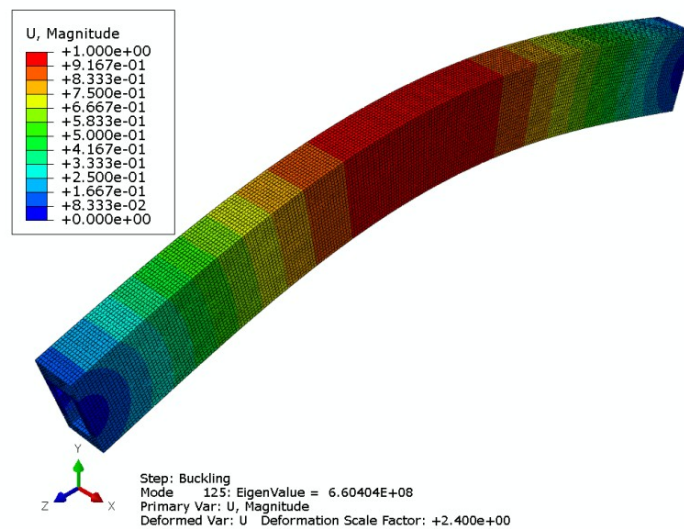


Figure 5.16 A Sample of 1st global Eigen buckling mode of the beam-column for *model-2_b*

Figure 5.17 shows a series of curves exhibiting the influence of change in the transverse stiffener distance on the ratio of critical local buckling load of stiffened to unstiffened beam-column,, is seen to be plotted against the transverse stiffener distance (d). The thickness of the transverse stiffener is varied to examine its influence on the critical buckling load of the beam-column. In Figure 5.17 the equilibrium curves are plotted for different TS thicknesses and it can be observed that a considerably amount of the critical

buckling load reserve is present for the cases of the more short distances between TS. The ratio of the beam-column is seen to increase significantly with an increase in the TS thicknesses. With an increase in the distance between TS, the ratio $(P_{cr} - unstiffened) / P_{cr}$ is also noted to decrease substantially especially after 2 meters. This is due, essentially, to the proving influence of transverse stiffeners on the critical buckling load. As a result, this improvement gives the beam-columns high buckling resistance and capacity compared to unstiffened beam-column.

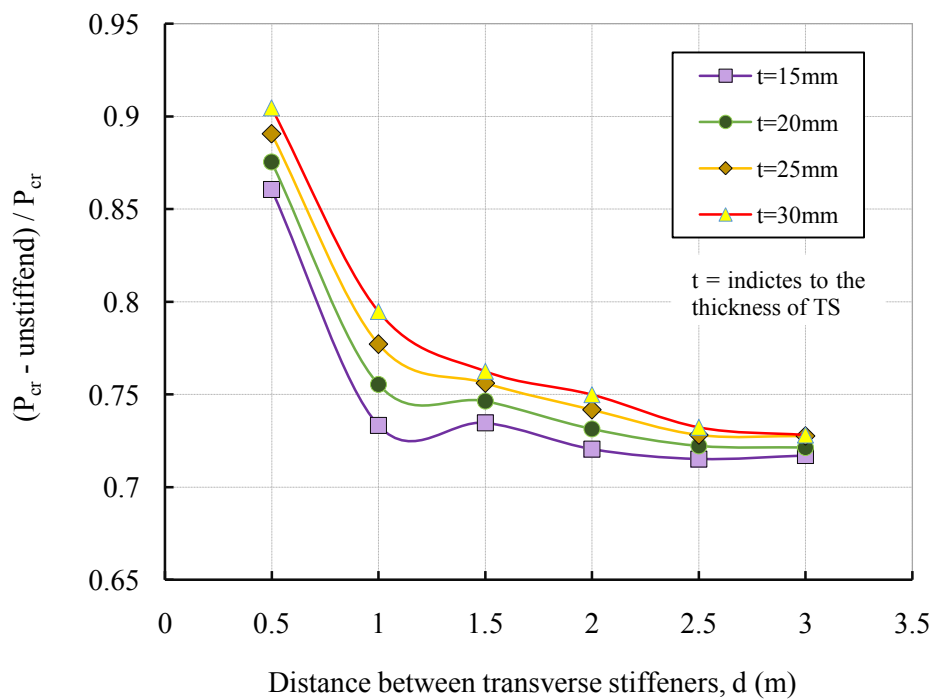


Figure 5.17 $(P_{cr} - unstiffened) / P_{cr}$ vs. distance between TS for *model-2_b* (Local)

Figure 5.18 refers to the critical buckling loads versus the distance between transverse stiffeners with the changing of its thickness on the maximum and minimum critical buckling load. It is seen from the Figure 5.18 that the effect of stiffeners becomes lower after 2 meters which represents the optimum location. By comparing the obtained results with the previous case in section 5.4.1, it is seen that there is a clear difference between the two cases. For instance, the maximum value for critical buckling was 139×10^6 N at $d = 0.5$ and $t = 30$ mm to the same condition in section 5.4.1 was 82×10^6 N. Therefore, the gain of critical local buckling is observed to be 41%. As a result, in this case which using longitudinal stiffeners with transverse stiffeners design consideration; it is suggested to increase the critical local buckling loads till a specific distance between stiffeners.

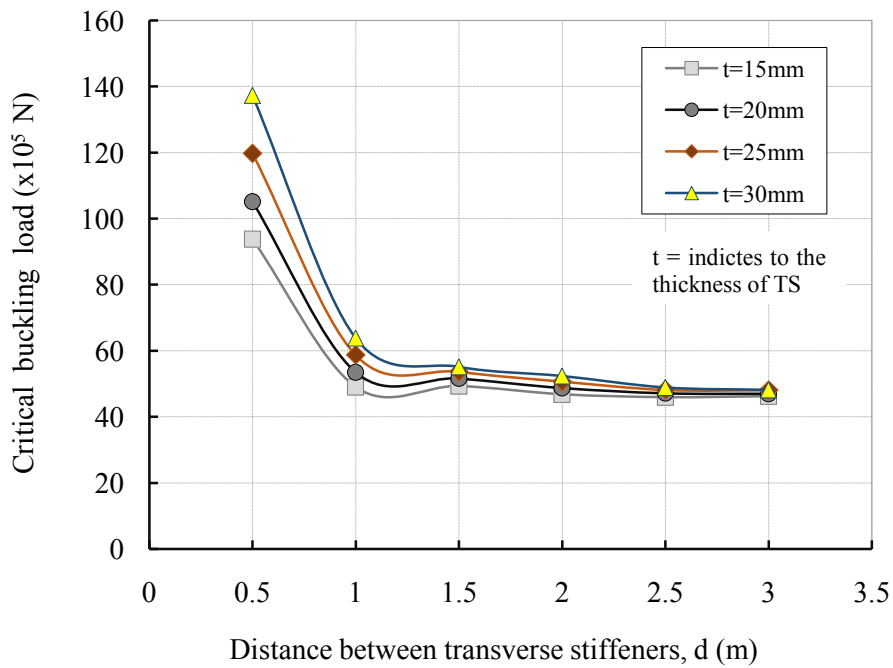


Figure 5.18 Effect of TS & two LS on the critical local buckling load of the beam-column (*model-2_b*)

Figure 5.19 shows a series of curves exhibiting the influence of change in the transverse stiffener distance on the ratio of critical global buckling load of stiffened to unstiffened beam-column, is seen to be plotted against the transverse stiffener distance (d). With the increase in the transverse stiffener distance, the ratio $(P_{cr} - unstiffened) / P_{cr}$ is decreased as well till reaching the maximum value at 2 meters where were about 20% to lowest value. This improvement gives the beam-columns high buckling resistance and capacity compared to unstiffened beam-column. It is clear from Figure 5.20 that an increase in the distance between stiffeners does not significantly improve the critical global buckling of the beam-column to unstiffened beam column. The improvement in the critical global buckling capacity of the stiffened beam-column as shown in Figure 5.19 was 28% between 0.5 meters to 2 meters of stiffeners distance and at t=30mm. The rate of change in the critical global buckling load has decreased for short stiffeners distance and then gradually increases with the increase in the stiffener distance and eventually approaches to steady state for long stiffener distance. As a result, the curve tends to level out at an optimum stiffener distance and a little increase in the critical buckling capacity of the stiffened beam-column becomes almost useless zero with further increase in the stiffener distance.

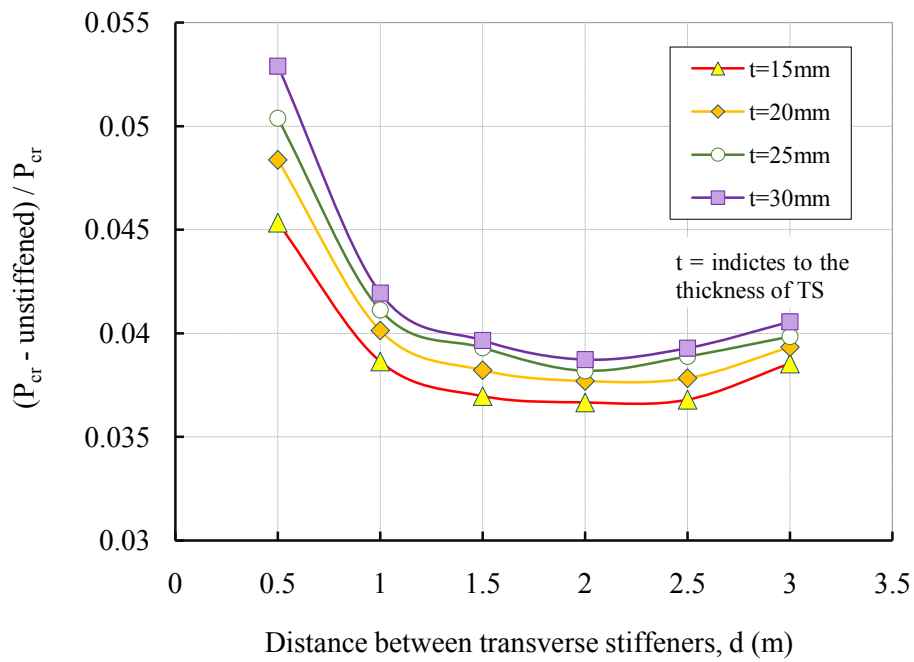


Figure 5.19 $(P_{cr} - \text{unstiffened})/P_{cr}$ vs. distance between TS for *model-2_b* (Global)

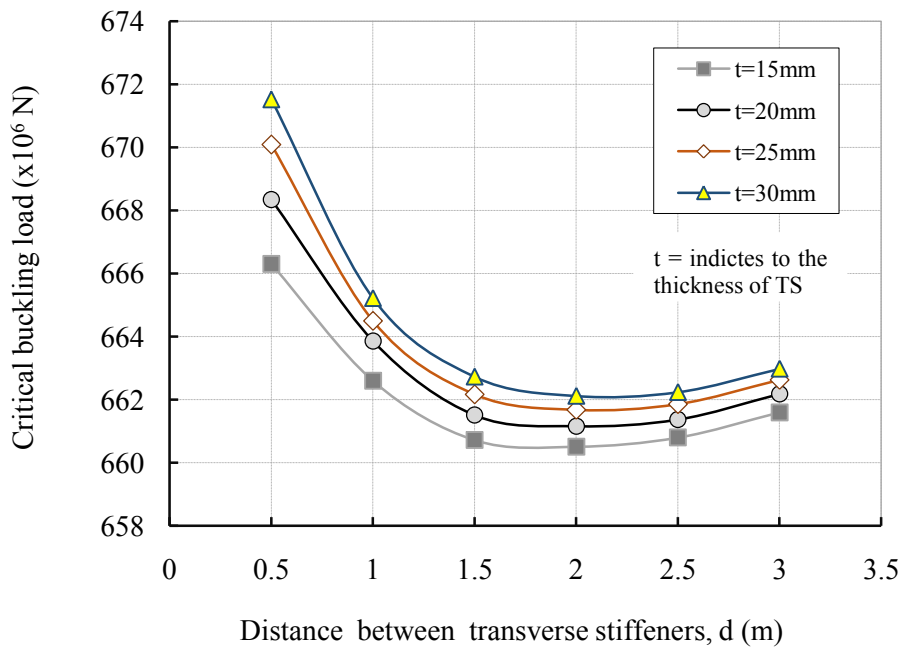
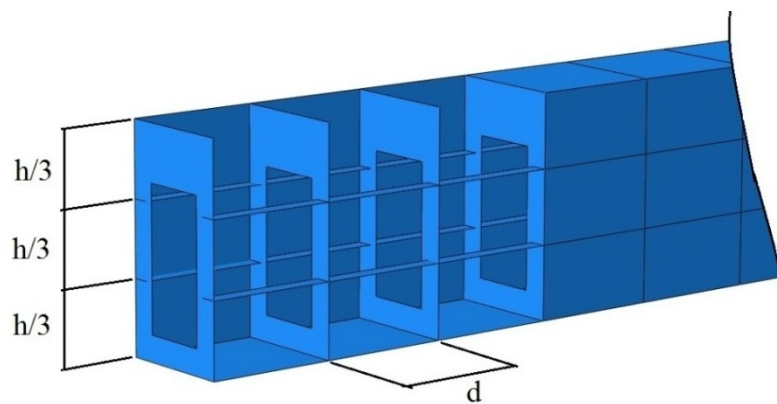


Figure 5.20 Effect of TS and two LS on the critical global buckling load of the beam-column (*Model-2_b*)

5.4.2.2 A STIFFENED BEAM-COLUMN WITH TRANSVERSE AND FOUR LONGITUDINAL STIFFENERS

In this section the effect of change in both transverse and longitudinal stiffeners for *model-3_b*, on the critical buckling load and buckling modes of the stiffened beam-column with four longitudinal stiffeners is investigated. Figure 5.21 illustrates a detailed geometrical assembly of a beam-column with both stiffeners where the longitudinal stiffeners are mounted at $h/3$ of beam's height. The dimensions of both the transverse and the longitudinal stiffeners have been illustrated in section 5.2.



TS distance variation (d) = 0.5, 1, 1.5, 2, 2.5 and 3m, LS distance variation ($h/3$)=0.8m.

Figure 5.21 Geometrical section of the beam-column for *model-3_b*

The first Eigen buckling modes on deformed shapes at critical local & global buckling loads for one sample are shown in Figure 5.22 and Figure 5.23 respectively. Obviously, the onset of buckling modes can be seen along with distribution of magnitude deformation over the surfaces. It is clearly manifested from Figure 5.22 that the effect of longitudinal stiffeners has a pivotal role in terms of redistribution the buckling mode in particular for the local buckling. However, the behaviour of global buckling mode is as the same fashion to the previous case in section 5.4.2.1 with a difference, of course, in the values.

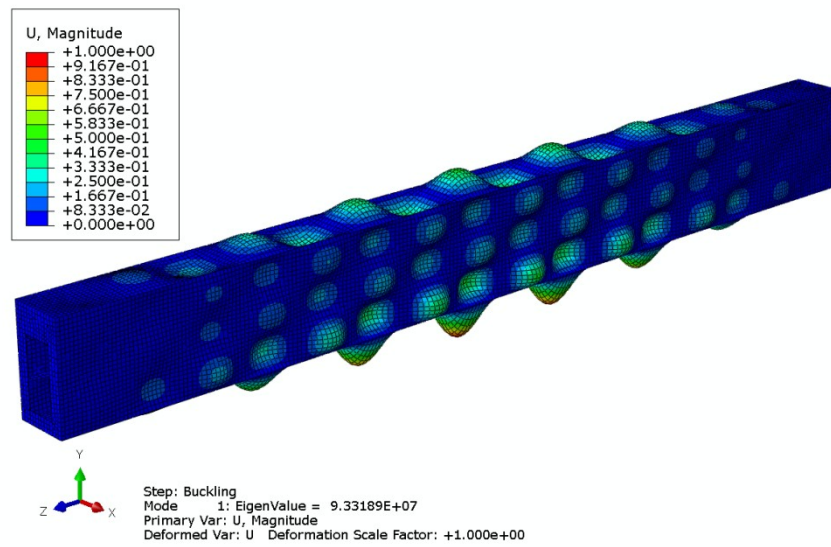


Figure 5.22 A sample of 1st local Eigen buckling mode of the beam-column *model-3_b*

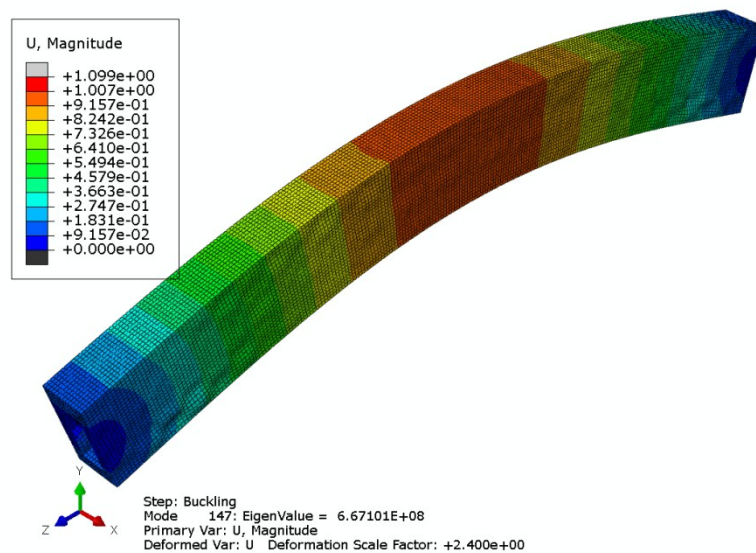


Figure 5.23 A sample of 1st global Eigen buckling mode of the beam-column *model-3_b*

The influence of the critical buckling load and the distance between the transverse stiffeners of the beam-column with different thicknesses is highlighted in detail in Figure 5.24 and Figure 5.25. The critical local buckling of stiffened to unstiffened beam-column, $(P_{cr} - unstiffened) / P_{cr}$, is seen to be plotted against the distance between transverse stiffeners (d). With further increase in the transverse stiffener distance, the ratio $(P_{cr} - unstiffened) / P_{cr}$, is decreased as well till reaching the value in which critical

buckling load sharply dropped to undesired values. The point at 2 meters distance between transverse stiffeners is a transition point that afterward the effect of transverse stiffeners is very low. As a result, the improvement in critical local buckling resistance and its capacity for this case is only in a range between 0.5 meters and 2 meters. In Figure 5.25, the curves are plotted for different transverse stiffener distances and it can be observed that a considerable changing in amount of critical local buckling loads. The critical local buckling load of the beam-column is seen to increase significantly with the increase of transverse thickness and decrease in its distance between each one. The critical local buckling loads of the beam-column is also noted to decrease substantially after 2 meters distance between transverse stiffeners This is due, essentially, to the higher distance between transverse stiffeners and to the destabilizing influence of critical local buckling load to be lower as in unstiffened beam-column. The difference between ultimate and minimum critical local buckling load for one case as an example, at thickness 30mm is found to be 60%.

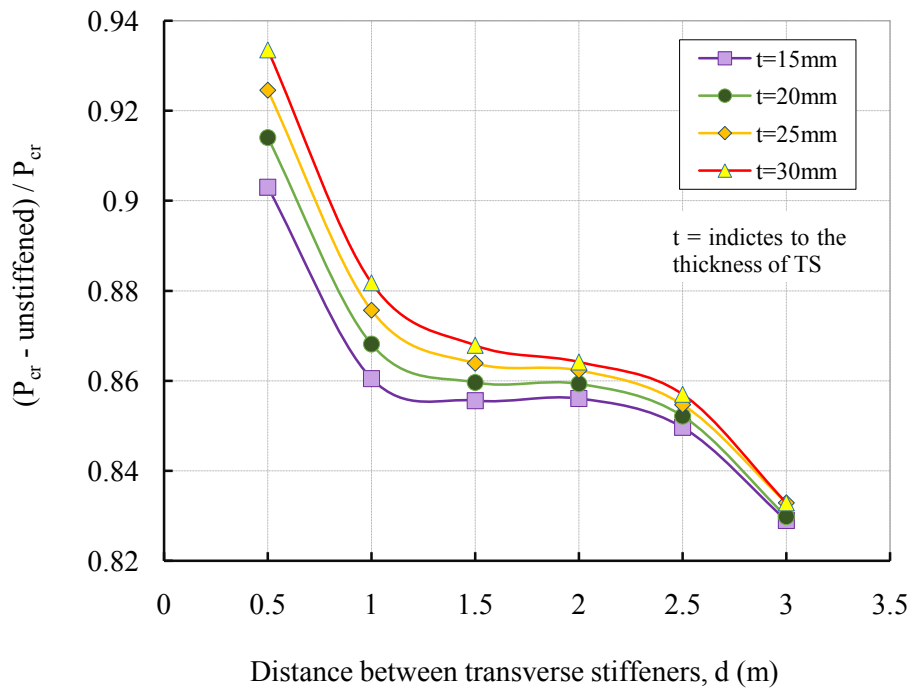


Figure 5.24 $(P_{cr} - unstiffened) / P_{cr}$ vs. distance between TS for *model-3_b* (Local)

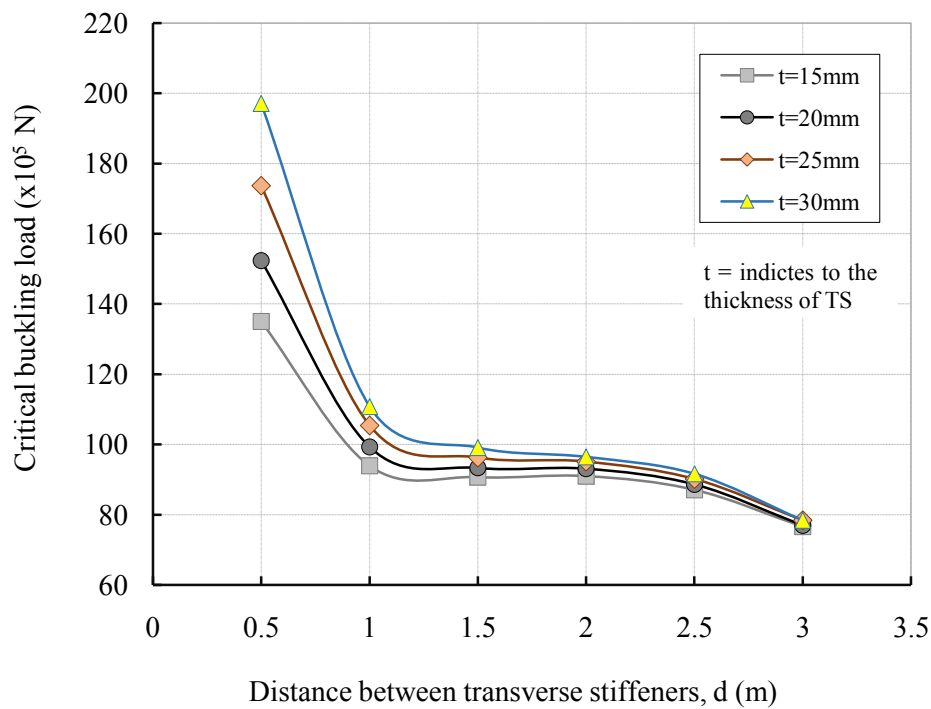


Figure 5.25 Effect of TS and four LS on the critical local buckling load of the beam-column (*model-3_b*)

Regarding the critical global buckling loads and effect of four longitudinal stiffeners which are added to the beam-column with the transverse stiffeners on it are presented in the next figures. The results obtained from the simulation for the influence of transverse stiffener thickness on the critical global buckling is detailed in Figure 5.26 and Figure 5.27. The critical buckling load ratio of the stiffened to unstiffened beam-column, $(P_{cr} - unstiffened)/P_{cr}$ is shown to be plotted against the distance between transverse stiffeners. It is clear from Figure 5.26 that the addition of transverse stiffeners after 2 meters distance did not give obvious improvement in the ratio of critical buckling loads to the stiffened beam-column where the lowest critical buckling load is at the maximum distance between transverse stiffeners. Furthermore, it can be observed from Figure 5.27 that increase in the transverse stiffeners distance does not seem to add the substantial amount of critical global buckling load to the stiffened beam-column.

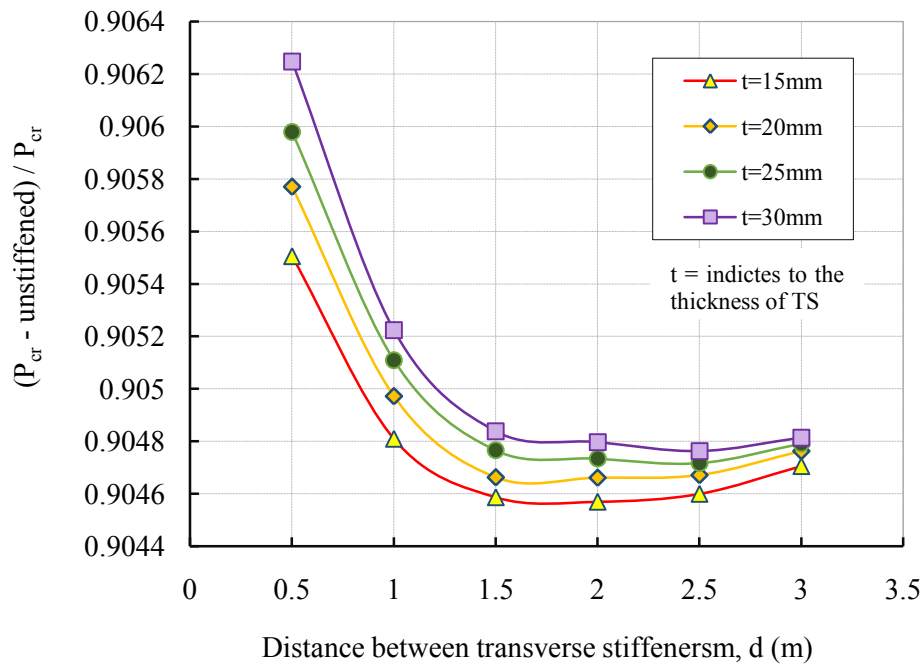


Figure 5.26 $(P_{cr} - \text{unstiffened}) / P_{cr}$ vs. distance between for *model-3_b* (Global)

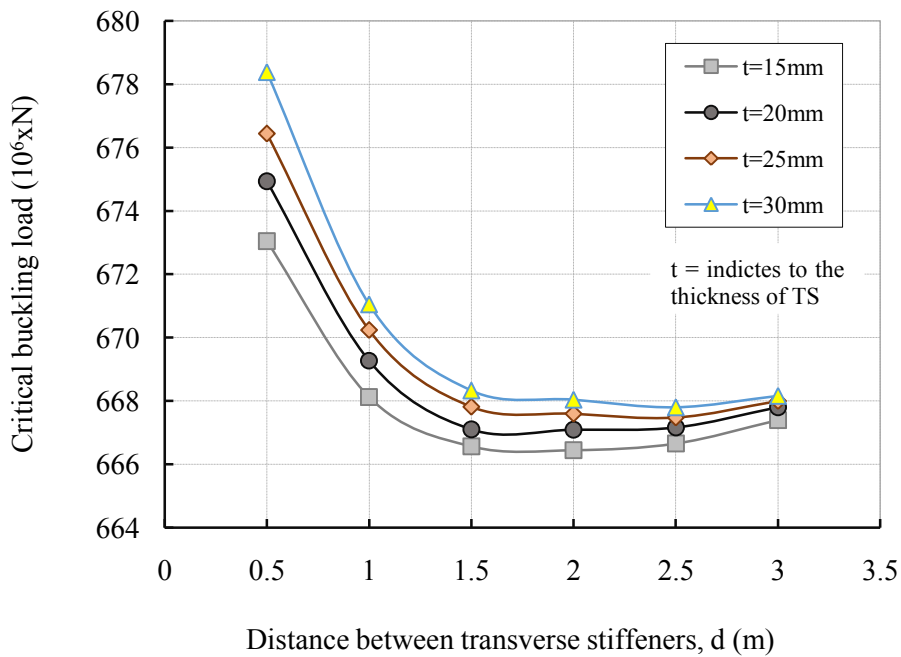


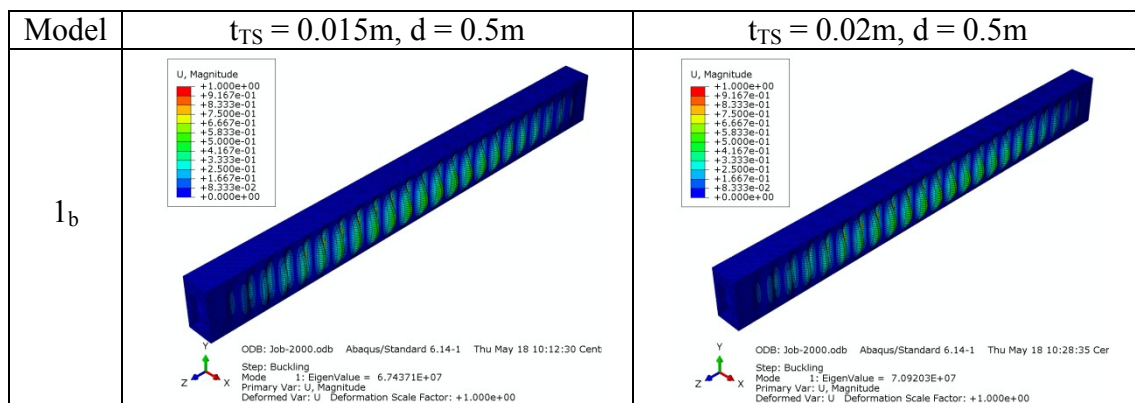
Figure 5.27 Effect of TS and four LS on the critical global buckling load of the beam-column (*model-3_b*)

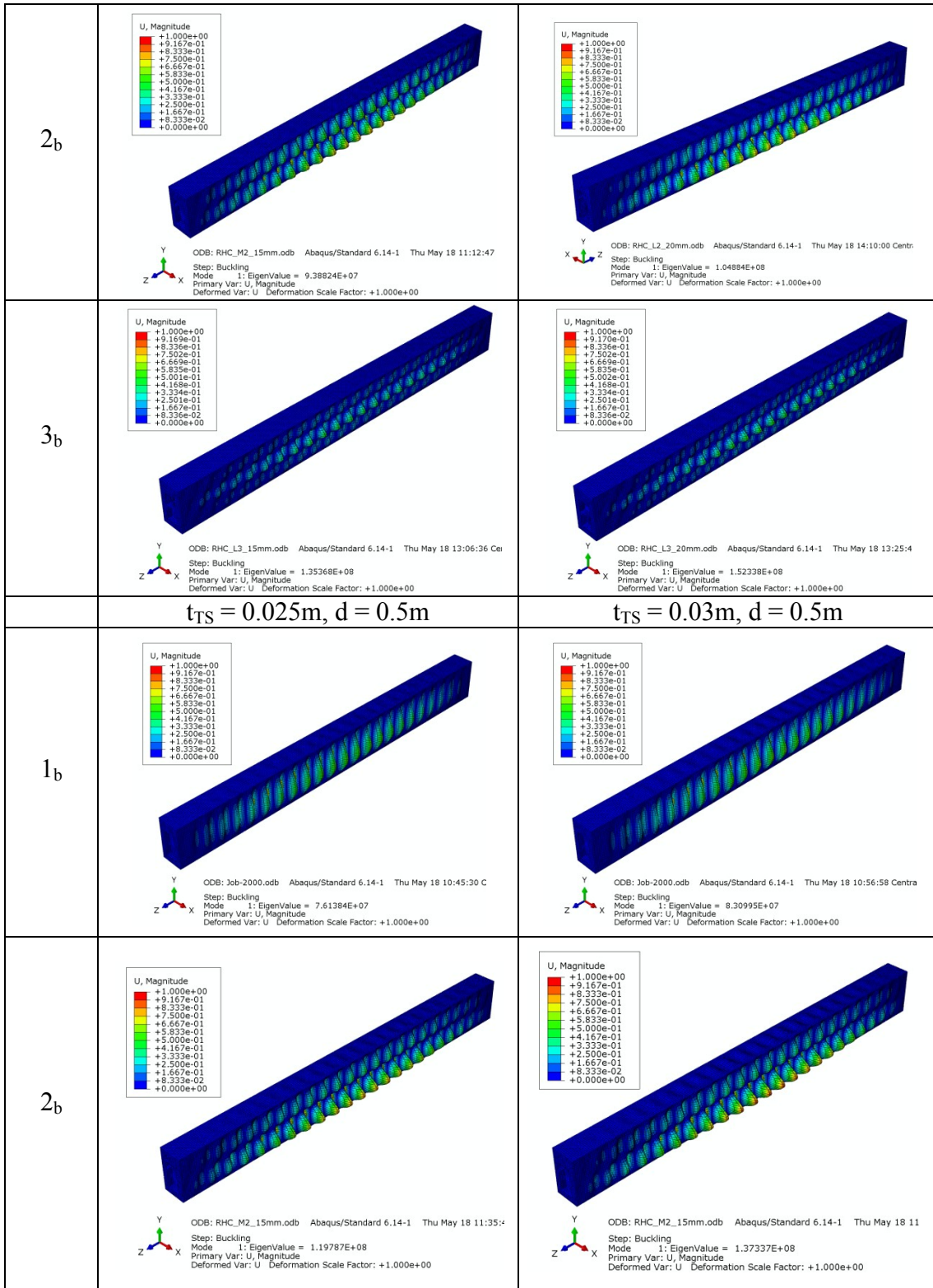
5.5 EFFECT OF TRANSVERSE STIFFENER'S THICKNESS ON THE CRITICAL BUCKLING LOAD

Another criterion which should be taken into account and has an influence along the general critical buckling load is the rigidity of the stiffener. Usually the rigidity of a stiffener depends solely on its dimensions and the critical rigidity of a stiffener corresponds to the optimum stiffeners thickness. In this section, the effect of change in transverse stiffener thickness on the critical buckling load of the stiffened beam-column with three models is investigated.

5.5.1 CRITICAL LOCAL BUCKLING RESPONSE AT DIFFERENT THICKNESSES

Figure 5.28 shows the first critical local buckling modes for three models with different TS thicknesses. Regarding *model-1_b*, the shape and location of critical local buckling loads are seen similar with each other. At $t_{TS} = 15\text{mm}$, the location of the buckling load is taking place in the middle between stiffeners. At $t_{TS} = 20\text{mm}$, the location and shape of the buckling are as the previous case, but with a difference in its value to be greater than. At $t_{TS} = 25\text{mm}$ and $t_{TS} = 25\text{mm}$, the location and shape of the buckling are noted to be also with the same behaviour and trend. *Model-2_b* shows different shapes and locations due to the adding of the longitudinal stiffeners. At all thicknesses of transverse stiffeners, the behaviour of the critical buckling shapes almost are the same with a difference of their values. By examining the buckling on *model-3_b*, with the same procedures, it is worth mentioning that the locations and shapes of the buckling are completely different compared with the other models at different TS thicknesses. Consequently, it is of note that the development in buckling has similar attitudes to changing of TS thicknesses.





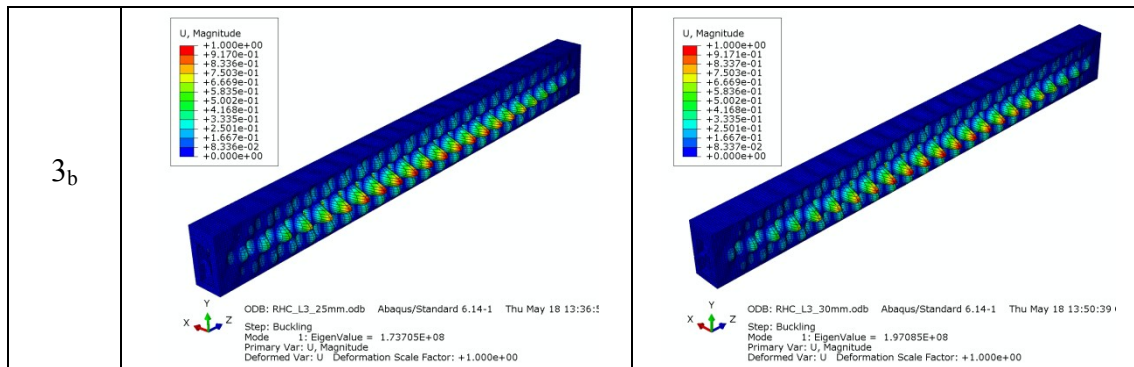


Figure 5.28 Samples of critical local buckling modes for all models of the stiffened beam-column at different TS thicknesses

The influence of transverse stiffener thickness on the critical local buckling loads of the design space associated with different distances between the transverse stiffeners is shown in Figure 5.29, Figure 5.30, Figure 5.31 and Figure 5.32. It can be observed from Figure 5.29 that the thickness of transverse stiffener has a significant effect on the critical local buckling load for stiffened models. When the distance between transverse stiffeners is between 0.5m to 1m, the results showed that the improvement in the critical local buckling load can be seen clearly in figure for all models. For *model-1_b*, *model-2_b* and *model-3_b*, which have a 15mm of TS thickness, the critical local buckling load is increased to 72%, 81% and 87% respectively. It can see also from the Figure 5.30, Figure 5.31 and that *model-1_b* and *model-2_b* and *model-3_b* are improved in terms of the values of critical buckling loads. An interesting point was mentioned in the Figure 5.32 that the value of critical buckling load for *model-3_b* is higher compared with *model-1_b* and *model-2_b*. As a result, the change of transverse stiffeners has vital effects on the critical buckling loads.

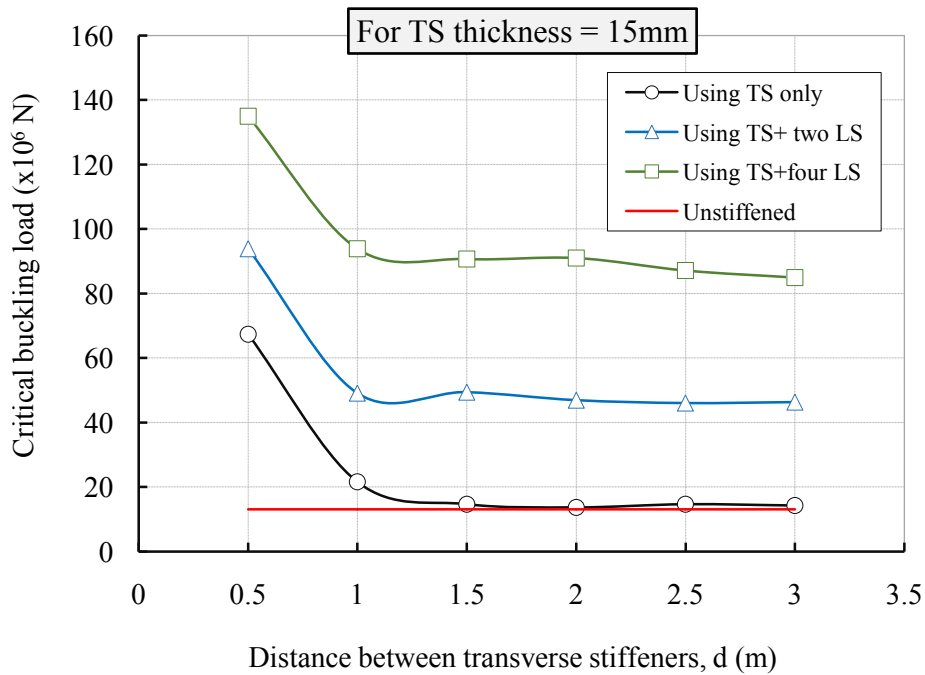


Figure 5.29 Effect of transverse stiffener thickness on the critical local buckling load for all models of the beam-column at TS thickness equals to 15mm

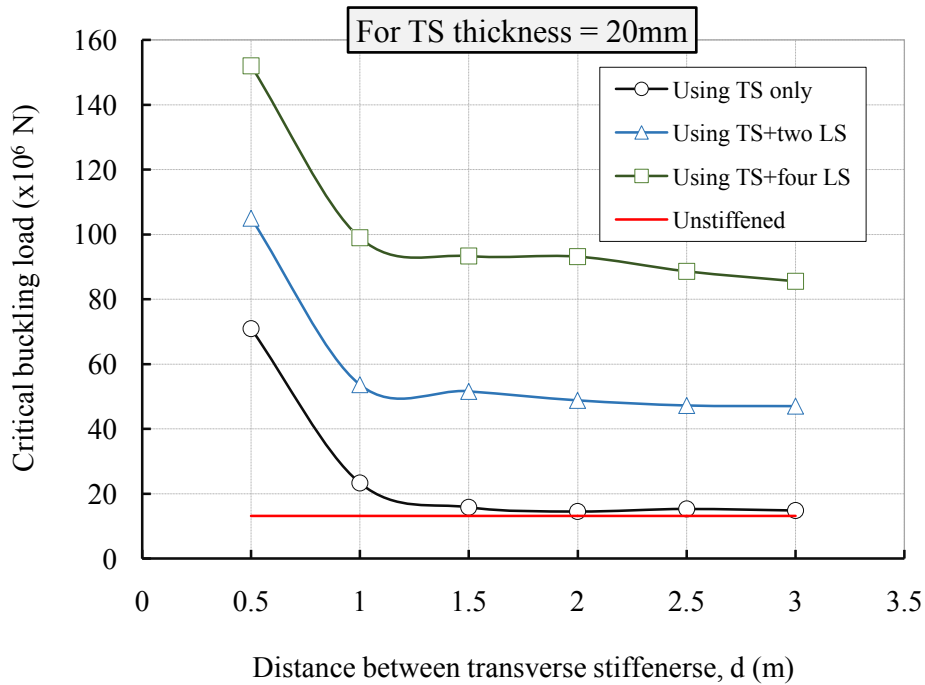


Figure 5.30 Effect of transverse stiffener thickness on the critical local buckling load for all models of the beam-column at TS thickness equals to 20mm

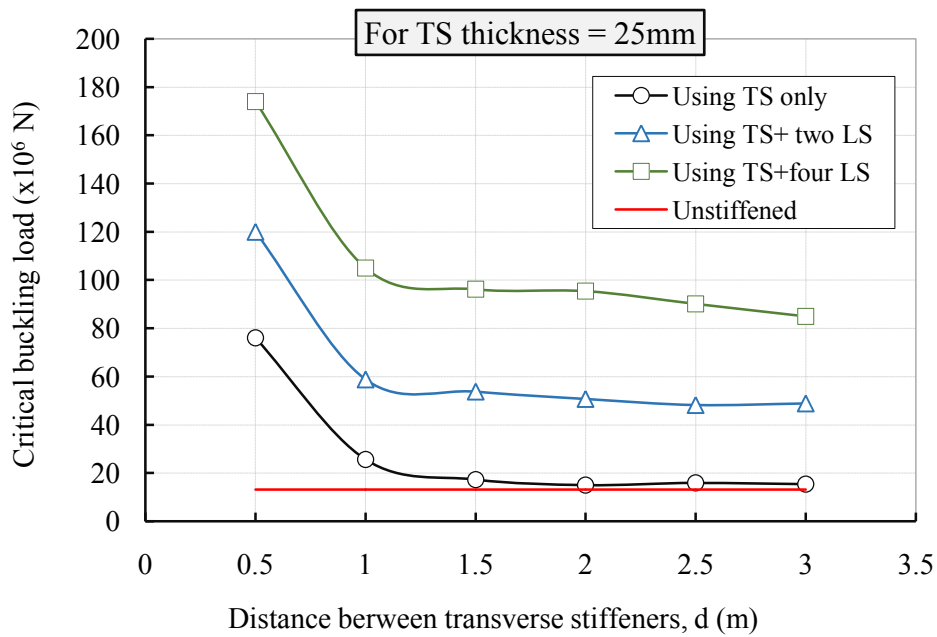


Figure 5.31 Effect of transverse stiffener thickness on the critical local buckling load for all models of the beam-column at TS thickness equals to 25mm

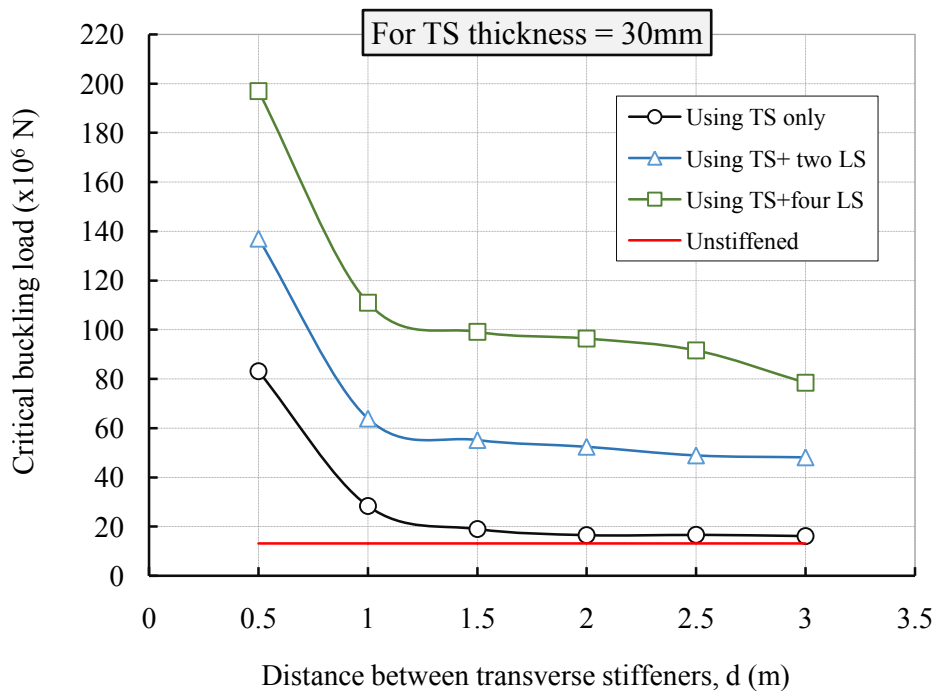
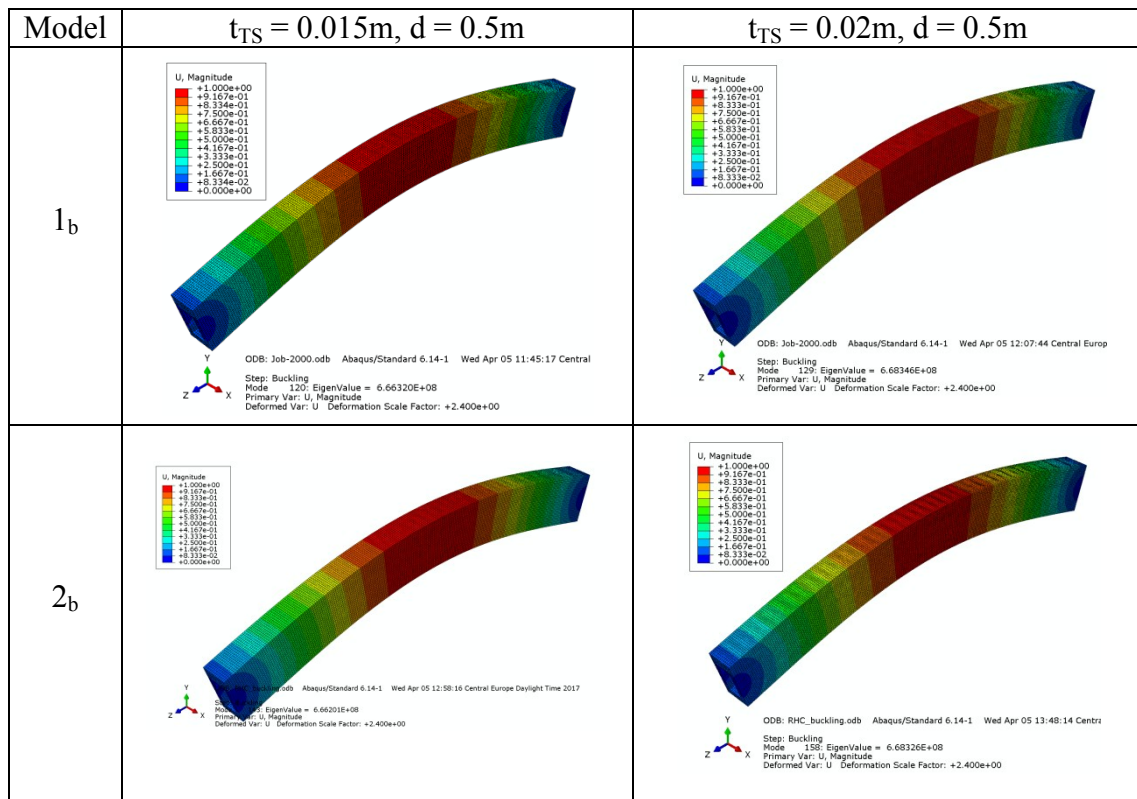


Figure 5.32 Effect of transverse stiffener thickness on the critical local buckling load for all models of the beam-column at TS thickness equals to 30mm

5.5.2 CRITICAL GLOBAL BUCKLING RESPONSE AT DIFFERENT TS THICKNESSES

Figure 5.28 shows the first critical global buckling modes for three models with different TS thicknesses. The behaviour of the curves in all cases has behaved in the same trends and to be quite identical. However, it gradually decreases in all cases with increasing in distance between stiffeners and lead eventually to almost steady state after 2 meters. A further increase in the stiffener distance does not affect the critical local buckling loads. The improvement in critical global buckling loads for the case in which TS is used by very close distance between stiffeners is found to be of the order of 4.5% corresponding to unstiffened beam-column. Whereas in the case of intermediately distance stiffener (i.e. 2 meters), the critical global buckling load of the beam-column is seen to be enhanced by 3.9% to unstiffened beam-column. Consequently, for critical global buckling capacity designs it is seen from results that global buckling is not sensitive to both stiffeners in terms of increasing in its values. Furthermore, it can say that for simply supported condition does not affect by the stiffeners on global buckling.



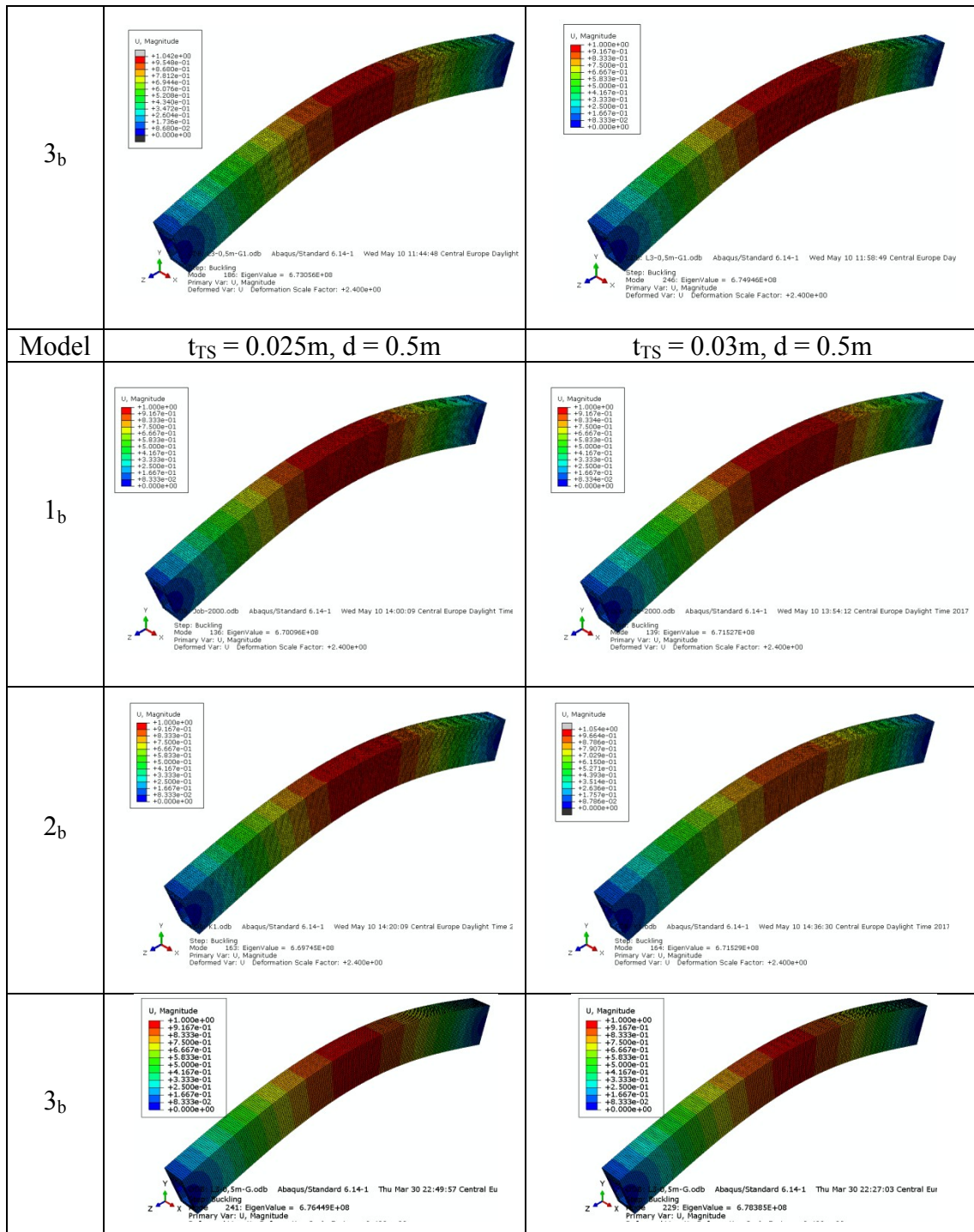


Figure 5.33 Critical global buckling modes for all models of the beam-column at different TS thicknesses

The influence of transverse stiffener thickness on the critical global buckling loads of the design space associated with different distances between the transverse stiffeners is shown in Figure 5.34, Figure 5.35, Figure 5.36 and Figure 5.37. It can be observed from all figures that the thickness of transverse stiffener has not a significant effect on the critical global buckling load for stiffened models. When the distance between transverse stiffeners is 0.5m, the results showed that the improvement in the critical global buckling load can be seen clearly in figures for all models. For *Model-1_b*, *Model-2_b* and *Model-3_b*, which have a 15mm of TS thickness, the critical global buckling load is increased to 0.5%, 0.47% and 0.45% respectively. It can see from the Figure 5.34, Figure 5.35 and Figure 5.36 that *Model-1_b* and *Model-2_b* and *Model-3_b* are improved in terms of the values of critical global buckling loads. An interesting point was mentioned in all figures that the value of critical global buckling load for all models is almost close to each other. As a result, the change of transverse stiffeners has in general a vital effect on the critical buckling loads.

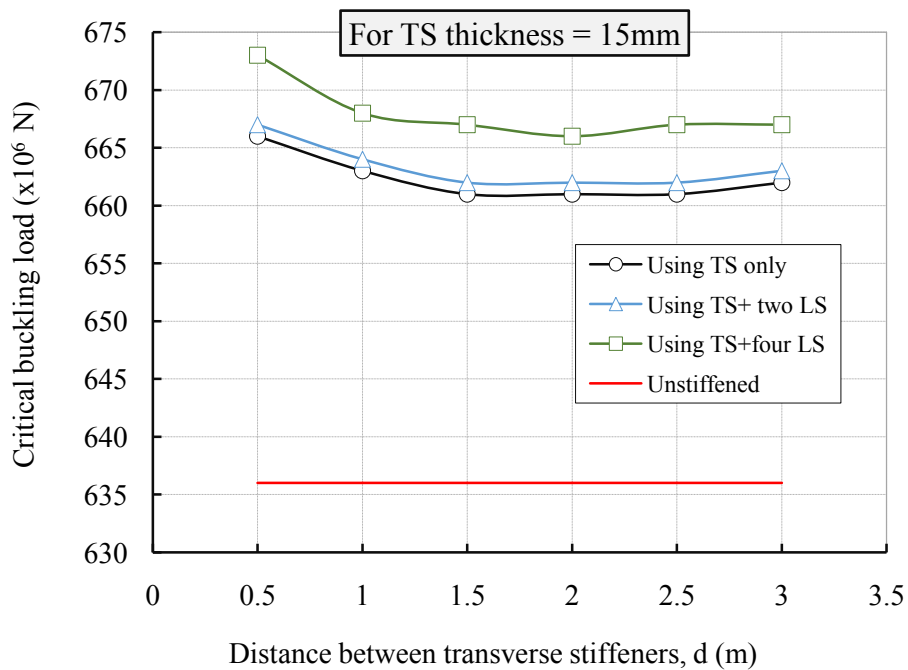


Figure 5.34 Effect of transverse stiffener thickness on the critical global buckling load for all models of the beam-column at TS thickness equals to 15mm

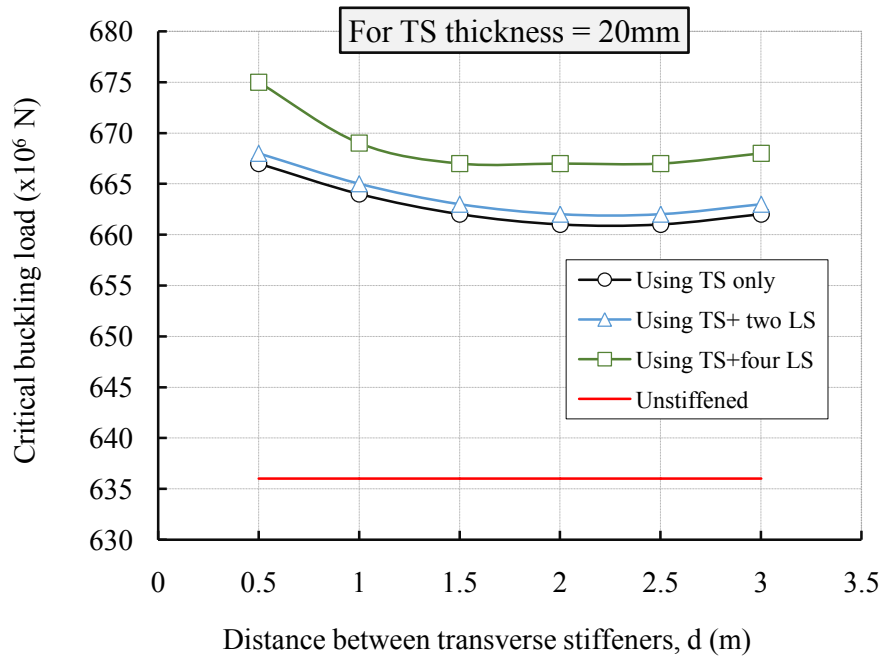


Figure 5.35 Effect of transverse stiffener thickness on the critical global buckling load for all models of the beam-column at TS thickness equals to 20mm

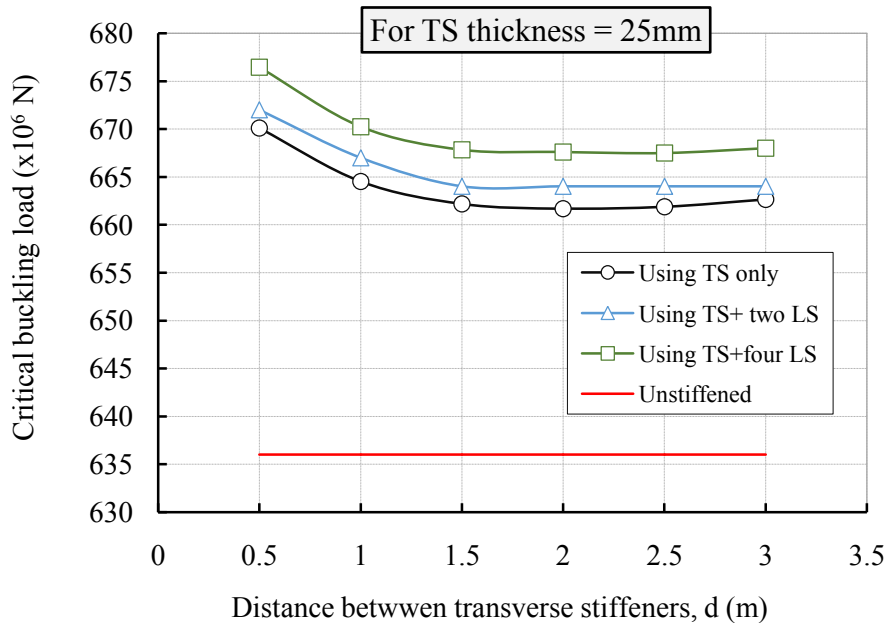


Figure 5.36 Effect of transverse stiffener thickness on the critical global buckling load for all models of the beam-column at TS thickness equals to 25mm

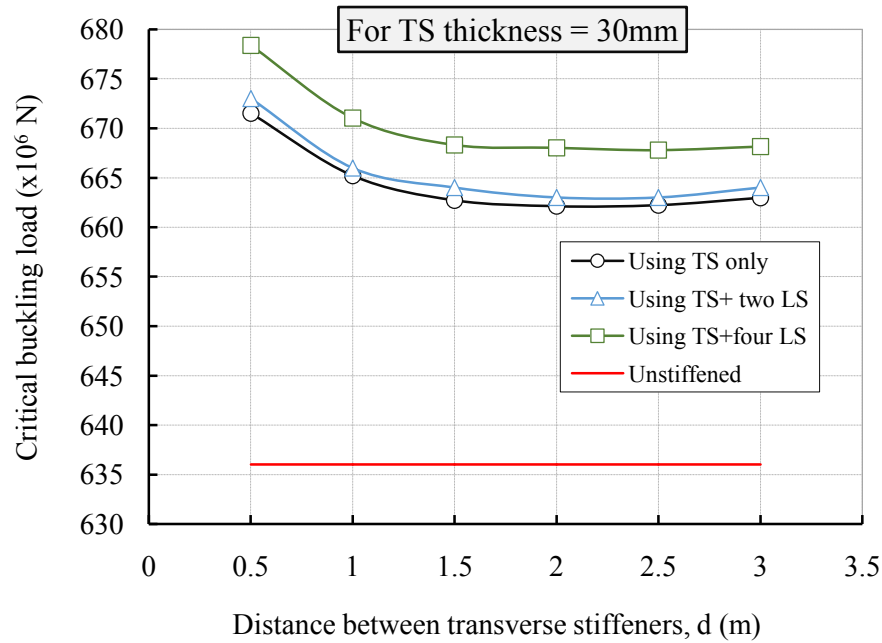


Figure 5.37 Effect of transverse stiffener thickness on the critical global buckling load for all models of the beam-column at TS thickness equals to 30mm

5.6 CONCLUDING REMARKS

In this chapter the finite element analyses of simply supported beam-column with different cases, unstiffened beam and stiffened beam by only transverse stiffeners and both transverse and longitudinal stiffeners have been presented. Simulation strategies have been applied to be able to investigate the behaviour of critical buckling load of the beam-column subjected to axial compression load. The effects of the transverse and longitudinal stiffeners on the local and global critical buckling have examined in depth on the critical buckling loads with different distances between each stiffener and its thickness in order to find the maximum and minimum distance. Three cases of stiffened beam-column applied to a simply supported case were modeled under uniaxial compression load. Linear buckling analyses of these element models predicted the critical buckling capacities and also to provide the full picture of the buckling behaviour. The percentage of critical buckling load versus the distance between stiffeners plots shows that the critical buckling load has reached maximum at short distances between stiffeners. Once the distances goes after 1.5 meter, the critical buckling load clearly is decreased. The obtained results demonstrated

that ultimate carrying capability of the beam-column has been shown to be significantly raised by adding the transverse and longitudinal stiffeners.

CHAPTER 6

6. THE BUCKLING BEHAVIOUR OF FRAME STRUCTURE TRANSVERSELY AND LOGNITUDINALLY STIFFENED

6.1 INTRODUCTION

In this chapter, the local and global buckling for a thin walled frame structure has been analysed by using the finite element techniques and solution strategies which are appropriate for such structures. The presence of local and global buckling for higher length thin-walled compression frame structures along the frame length can be accompanied by the overall instability. Longer frame columns will decrease in their global elastic Euler buckling loads as a termination of the weakening effects of local buckling and the influence of geometrical shapes, and that of unused stiffeners will, of course, further reduce the ultimate carrying capability of the frame columns members. Generally, there are some methods to determine the critical capacity of members in steel frame structures subject to such loads (buckling), numerical, experimental and analytical investigations. One of the analytical methods has been made by Ritter, who conducted the first work on the inelastic buckling theory for compression members in frames. A graphical method of constructing load-deflection curves of the column corresponding to the numerical procedures developed by Ritter to be used in computer programs. Although, Thurlimann [88] has been made another attempt to derive the connected columns load-deflection curves with double integration of the curvature, but no adequate analytical solution has been developed after Ritter's attempt. The local and global buckling behaviour of the frame structure as shown in Figure 6.13 and Figure 6.14 have been determined using the linear static solution sequence involving geometric changing by adding transverse and longitudinal stiffeners as supporters at different locations. Each particular type of case has its own mesh distribution

at the same boundary conditions. Moreover, the strategies of solution involving the selection of right solution parameters such as the element type, solution sequences, iterative procedures, load position, element discretization, etc. The results for each case will discuss at length in the next sections. In order to find an accurate and reliable solution for frame structures, a good understanding of the true structural behaviour of the frame structure should be considered. For steel frame structures, many different solutions have been provided to follow the buckling behaviour of the frames [1][89][90][91][92]. The objective of the buckling analysis of steel frame structures introduced in this chapter was to develop a numerical solution for steel frame subjected to the buckling load with transverse and longitudinal stiffeners supports which can be used in analysis, frame designs and to compare it to unstiffened frame structure. The same analysis procedures that have been made in the beam-column analysis in the previous chapter will be repeated in this chapter with a different in stiffeners distributions and locations.

6.2 FINITE ELEMENT MODELLING OF STIFFENED FRAME STRUCTURE

6.2.1 GEO-METRIC MODELLING AND NUMERICAL ANALYSIS

In this section the procedures and strategies of the finite element simulation are described which used to analyse the stiffened frame structure subjected to pure axial compression buckling load. Figure 6.1 shows fully dimensions of the unstiffened hollow frame structure which is used in the analysis. The geometries of the transverse and longitudinal stiffeners are illustrated in Figure 6.2, Figure 6.3, Figure 6.4 and Figure 6.5 respectively. The thickness of the transverse stiffeners is changed from 5mm to 15mm to study the influence of the stiffeners thickness on the critical buckling load characteristics, while the longitudinal stiffeners thickness are fixed at 10mm. The transverse stiffener thicknesses have chosen to illustrate the local buckling and global buckling behaviour of the stiffened under compression buckling load.

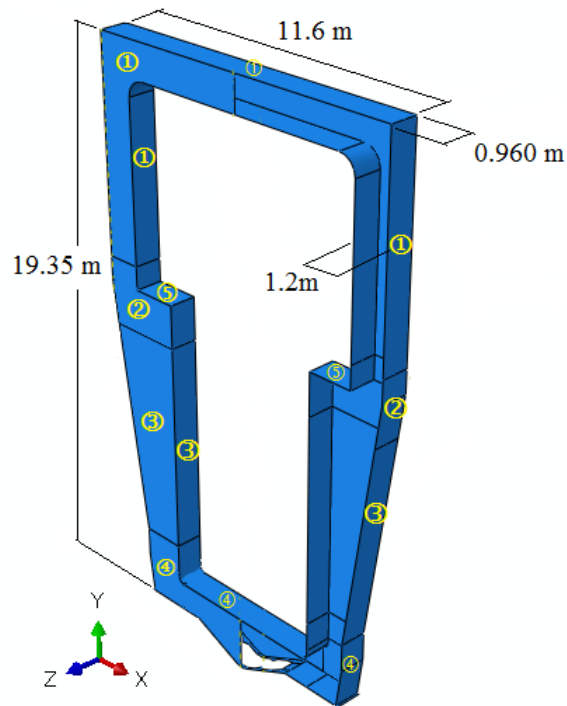


Figure 6.1 Unstiffened hollow frame structure used in the study

The frame dimensions and thicknesses chosen were such as to illustrate the local buckling and the global buckling behaviour of the stiffened frame webs. The thicknesses of the frame skins are divided into different numbered as shown in Figure 6.1 to demonstrate the real values as in the real frame. The four thicknesses of the frame skins are:

- | | | |
|----------|----------|----------|
| 1) 10 mm | 2) 20 mm | 3) 12 mm |
| 4) 15 mm | 5) 30 mm | |

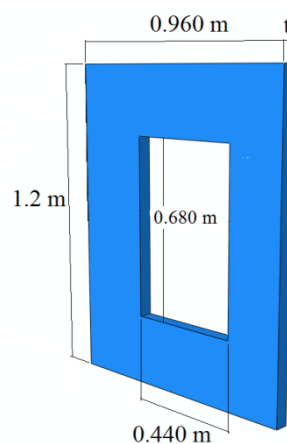


Figure 6.2 Geometry of transverse stiffener configuration (TS) type-1

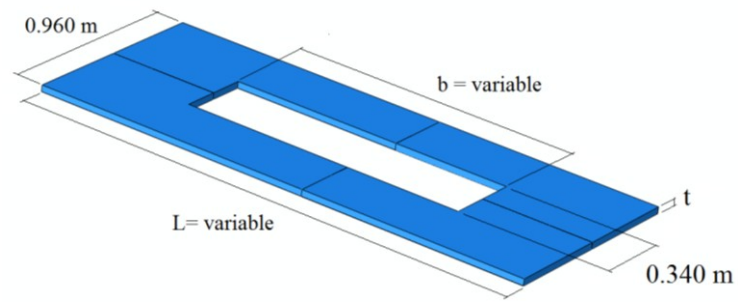


Figure 6.3 Geometry of transverse stiffener configuration (TS) type-2

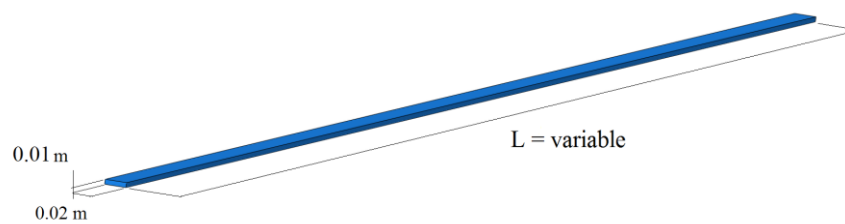


Figure 6.4 Geometry of horizontal longitudinal stiffener configuration (LS) type-1

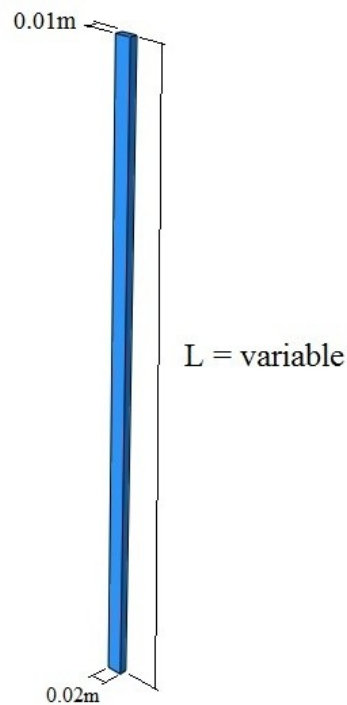


Figure 6.5 Geometry of vertical longitudinal stiffener configuration (LS) type-2

6.2.2 FRAME MODELS DESCRIPTION

The frames, which are used in this study can be categorised into three different models: 1) by adding only transverse stiffeners to unstiffened frame, 2) by adding transverse stiffeners with two longitudinal stiffeners to unstiffened frame, 3) by adding transverse stiffeners with four longitudinal stiffeners to unstiffened frame. The chosen frames in this study include all these categories and are shown in Figure 6.6 and Figure 6.7. The distance between transverse stiffeners (d) chosen for this study is varying from 0.5m to 3m as shown in Figure 6.6, while the distance between longitudinal stiffeners ($w/2$) is at the middle of the frame-beams as shown in Figure 6.7. The thickness of the transverse stiffeners is changed from 5mm to 15mm to study its influence on the critical buckling load characteristics, while the longitudinal stiffeners thickness is fixed at 10mm. In addition to that and as shown in Figure 6.4 and Figure 6.5, the length (L) depends on the frame-beams altitude. The transverse stiffener thicknesses chosen were such as to illustrate local buckling and global buckling behaviour of the stiffened under compression load.

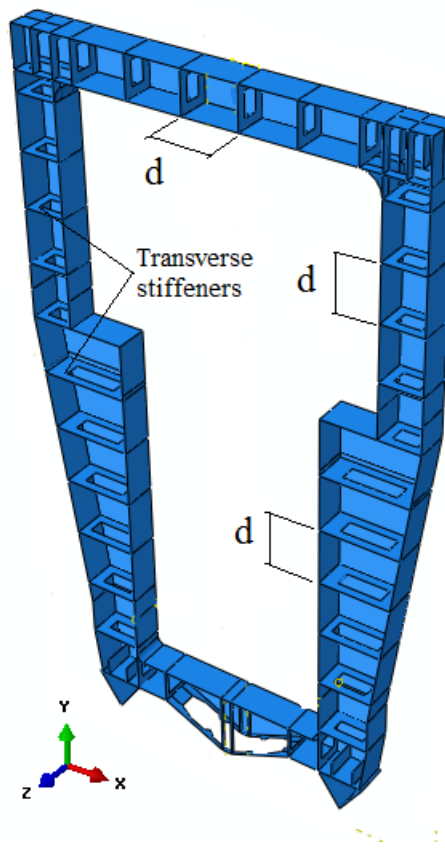


Figure 6.6 Geometry of stiffened frame *Model-1_f*

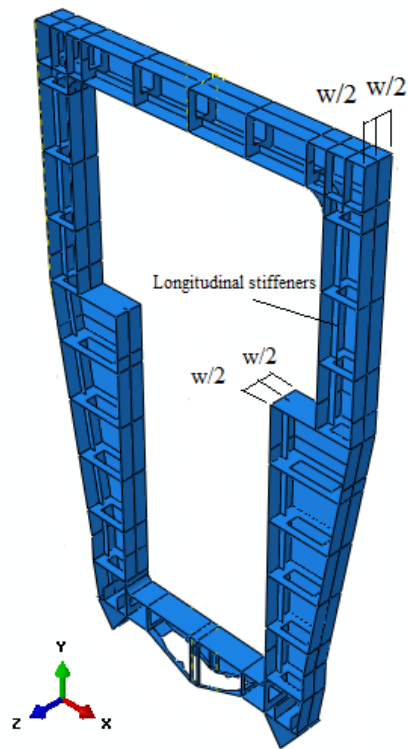


Figure 6.7 Geometries of stiffened frame *Model-2_f*

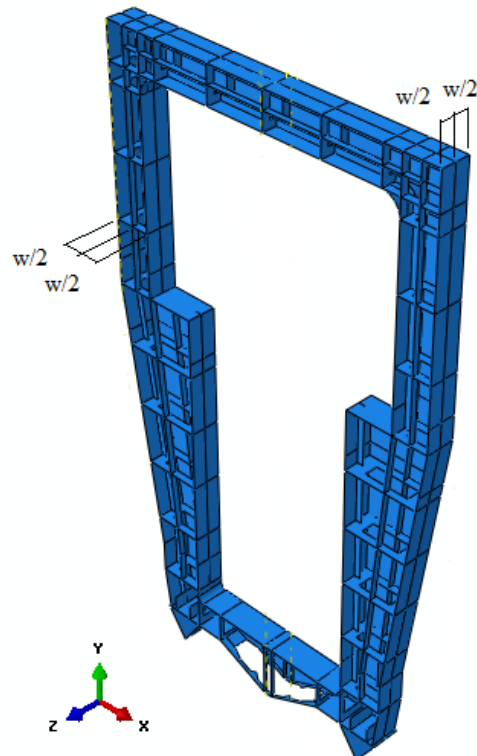


Figure 6.8 Geometries of stiffened frame *Model-3_f*

6.2.3 FRAME BASE BOUNDARY CONDITIONS, LOAD AND FINITE ELEMENT MESH

As mentioned before in pervious chapter, the boundary conditions have significant effects on the analysis results when frame structure is isolated from its real condition. In order to apply and replicate the boundary conditions on the models in this study with axial compression force assumed in the analyses were used to simply support. The boundary conditions in these models are suitable for the development such frame structures and for the study of critical buckling capacity. The boundary conditions were simulated by simply supported conditions which were assumed at the bottom of the frame structure as shown in Figure 6.9. This was achieved by using single point constraints A and B which were applied at the ends of the frame supporters to be more realistic with the original case as shown in Figure 6.10. It was assumed to have some free, fixed translations and rotations that are illustrated in Table 6.1.

Figure 6.11 shows the boundary conditions points where the frame model is fixed and considered in the analysis while the rest of the structure left free to remain either normal or straight. As shown in Figure 6.11 a rigid body constraint has been used to tie the top surface of the frame via node-to-node tie constraint relationships to reference point RP1 which is available in ABAQUS [82]. The reference point RP1 used to accomplish the axial load to be applied on the entire top surface of the frame. The frame structure is applied statically by a central buckling load of 1 at RP1 (Figure 6.11) where the load has a load factor with a default value of 1.0 and the entire load case can be multiplied with any numerical or alternatively loads if required. The simplified von-Mises elastic-perfectly material model is used for the isotropic steel with an elastic modulus of 210 N/mm^2 , Poisson ratio of 0.3 and yield stress values of 350 N/mm^2 . After defining the structural geometry, the next step is to discretise the structure with suitable elements. As it is known to all that the selection of appropriate finite elements is an essential feature in finite element modelling, considering the fact that these elements represent the true physical structure. With regard to Figure 6.11, it can be seen that the shell elements are used because they provide sufficient degrees of freedom to the buckling model analysis for such frame structure. Due to the large models, the element density of the frame models was increased compared with the simply supported column-beam models. Four noded doubly curved shell element with reduced integration S4R [81] and six degrees of freedom per node were

used in this type of geometry. S4R elements are doubly curved general-purpose, membrane strain shell elements and R stand for reduced integration with hourglass control. For shell structures which have thicknesses larger than 1/15 of the element length, the S4R is often used. The mesh density choice is usually a function of the geometrical characteristic of structures. Therefore, in order to obtain the most optimised accurate solutions, the fine mesh has been chosen where the element size used for the frame structure and as well as for the stiffeners is chosen and kept to be of 0.1m. This element size is chosen through the appropriate convergence studies to ensure the accuracy of the solution as shown in Figure 6.12. Therefore, the shell elements have widely used in structural engineering and where Avery and Kim [91][93] have used it to develop benchmark solutions for frame structures. Many different benchmark solutions have been made by different researchers for steel frame structures [94]

Table 6.1 Boundary conditions of supported frame model

Boundary conditions (Free: ○ , Constrained: ●)						
	u	v	w	θ_x	θ_y	θ_z
A	●	●	●	○	●	○
B	●	●	●	○	●	○

u, v, w are translations in x, y, z axes and $\theta_x, \theta_y, \theta_z$ are rotations about x, y, z axes

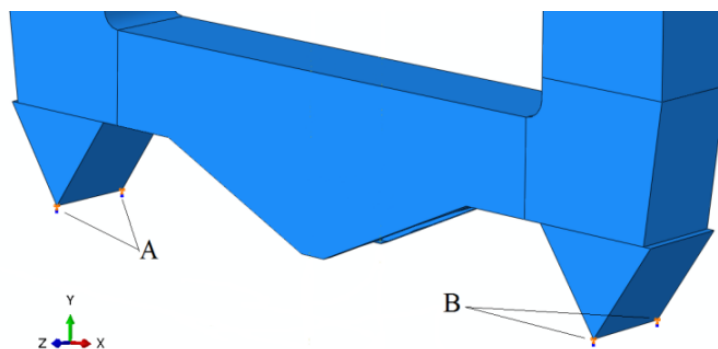


Figure 6.9 Frame connections of the model (FE model)



Figure 6.10 Frame connections on site

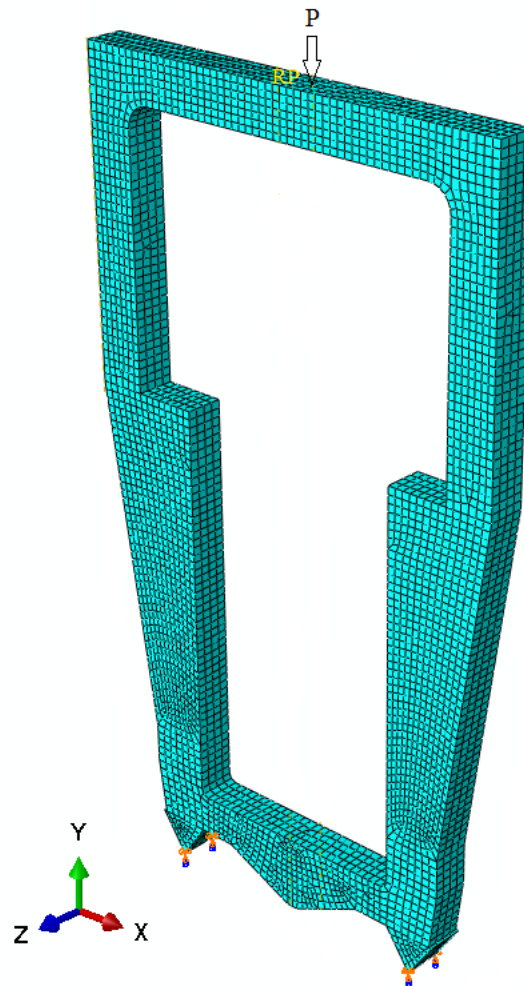


Figure 6.11 Typical FE of the frame model

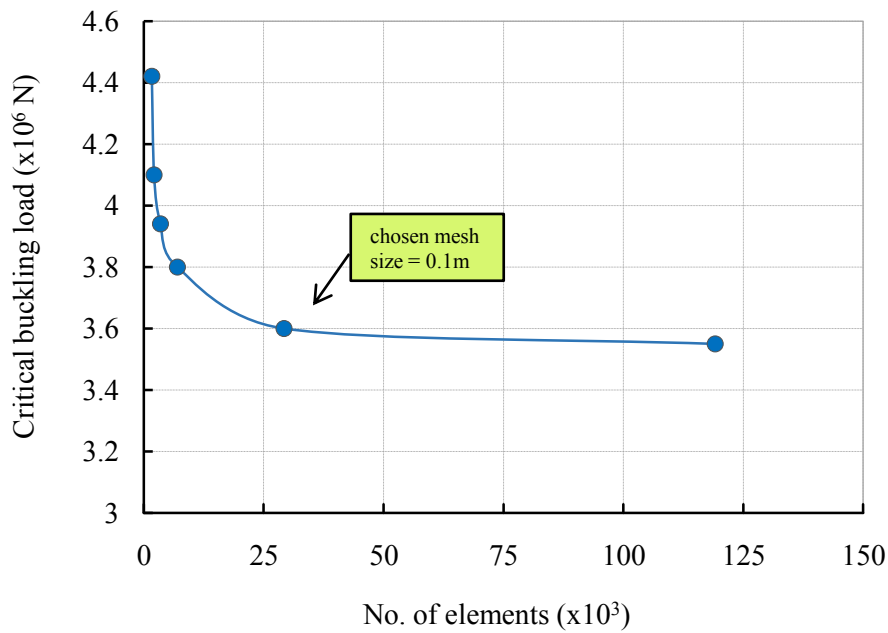


Figure 6.12 Mesh sensitivity study on critical buckling load

6.3 BUCKLING RESPONSE OF THE STIFFENED FRAME MODELS

In this section, the local and global buckling behaviour of stiffened frame models is investigated in detail. A frame model is considered in different cases for analysis, which is, involved both transverse and longitudinal stiffeners. The effect of a change in stiffener positions and its thicknesses on the critical buckling characteristics as well as the structural performance of the stiffened frame model is highlighted.

6.3.1 STIFFENED FRAME MODELS BY USING TRANSVERSE STIFFENERS ONLY

The results presented in this section are for the frame *Model-1_f* that is stiffened by only transverse stiffeners. The variation of distances between transverse stiffeners d , is varied from 0.5m to 3m and the stiffeners configurations are shown as in Figure 6.6 and Figure 6.7 respectively. The stiffened frame *Model-1_f* considered in this analysis is subjected to pure axial compression load with transverse stiffeners thicknesses from 5mm to 15mm in order to investigate its influence on the frame structural response. The first Eigen buckling modes on deformed shapes at critical local & global buckling loads for one sample are shown in Figure 6.13 and Figure 6.14 respectively. Obviously, the onset of buckling modes can be seen along with distribution of magnitude deformation over the surfaces.

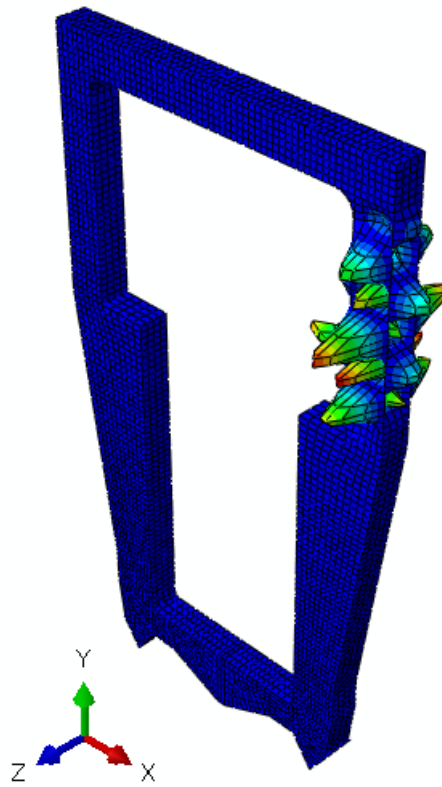


Figure 6.13 A sample of 1st local Eigen buckling mode of the frame for *Model-1_f*

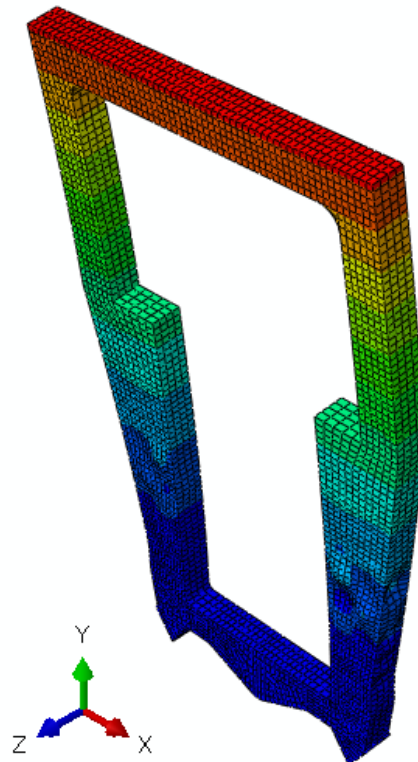


Figure 6.14 A sample of 1st global Eigen buckling mode of the frame (*Model-1*)

The obtained results of the influence of the stiffened frame models on both local and global buckling capacity are illustrated in Figure 6.15 and Figure 6.17 respectively, where the ratio of critical buckling load of the stiffened to unstiffened frame model, $(P_{cr} - \text{unstiffened})/P_{cr}$, are shown to be plotted against the distance between transverse stiffeners TS. Furthermore, the critical buckling loads corresponding to the various stiffener thicknesses are shown in Figure 6.16. Figure 6.15 clearly appears that the addition of transverse stiffeners considerably improves the local buckling performance of a frame model. Initially the percentage of increase in the local buckling resistance of the stiffened frame model is seen to be significant at 0.5m and with an increase in the distance between transverse stiffeners; it becomes gradual reduced for the period up to 1.5m before beginning of the reduction in steady state. As a result, it is clear that the addition of stiffeners has given a clear improvement in the critical buckling resistance to the unstiffened frame model and the curves trend to level down and eventually decrease in the local buckling capacity as shown in Figure 6.16. For an instant, the case of a small stiffener thickness 5mm at a distance between TS is 0.5m, an increase in the critical local buckling load is found to be of the order 58% of unstiffened frame model as shown in Figure 6.15. On the other side, for the case of a high stiffener thickness 15mm at the same case increase in the critical buckling load is found to be of the order 71% of unstiffened frame model. Consequently, with an increase in the distance between stiffeners, it is of note that the transverse stiffeners effect on the critical local buckling became effect less after 1.5m of distance between TS.

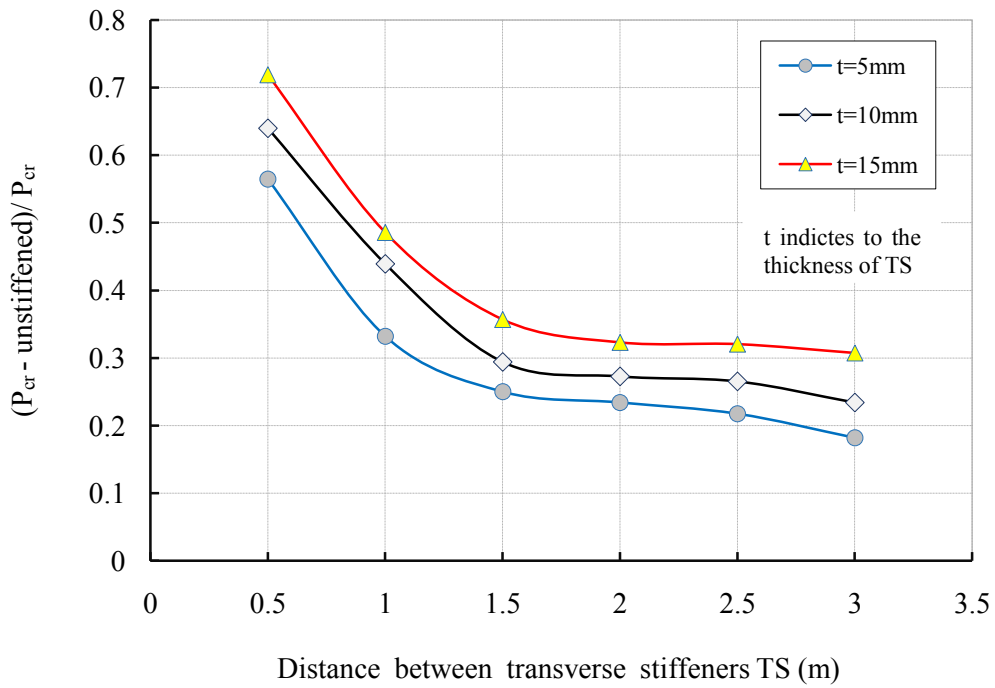


Figure 6.15 $(P_{cr} - \text{unstiffened}) / P_{cr}$ vs. distance between TS for *Model-1_f* (Local)

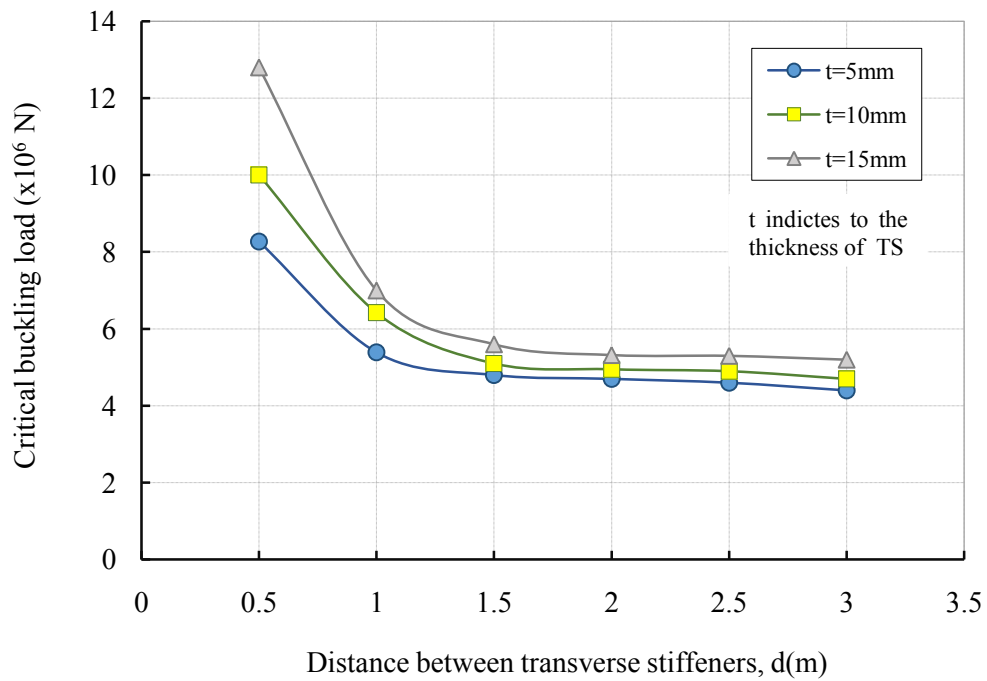


Figure 6.16 Effect of TS on the critical local buckling load of the frame for *Model-1_f*

The local buckling mode changes from local buckling to global buckling with increase in applied load. Figure 6.17 highlights the structural response of the frame *Model-1_f* that corresponding to the critical global buckling capacity, throughout the loading. The ratio of the critical global buckling capacity of stiffened to unstiffened frame model, $(P_{cr} - unstiffened) / P_{cr}$, is shown to be plotted against the distance between transverse stiffeners. It can be noticed from the Figure 6.17 that the curves for different distance between transverse stiffeners to critical global buckling tend to show similar behaviour with an increase in the stiffeners distance. It is evident that initially the notable improvement in the critical global buckling is seen at 0.5m is found to be 14.5%, 14.7% and 15.5% at different TS thicknesses of unstiffened frame respectively. Afterwards, with an increase in the distance between transverse stiffeners, the rate of change of critical global buckling load eventually approached for a small period almost zero after 1.5m of distance between transverse stiffeners as shown in Figure 6.18 and it seems useless to further increase the stiffener distance since it increased the frame model (structural) weight without any notable improvement. As a result, the global buckling performance of the stiffened frame model is noted to be enhanced substantially for close distances between transverse stiffeners, while it can be observed that does not seem to add a substantial amount of the global buckling performance for short distances between transverse stiffeners.

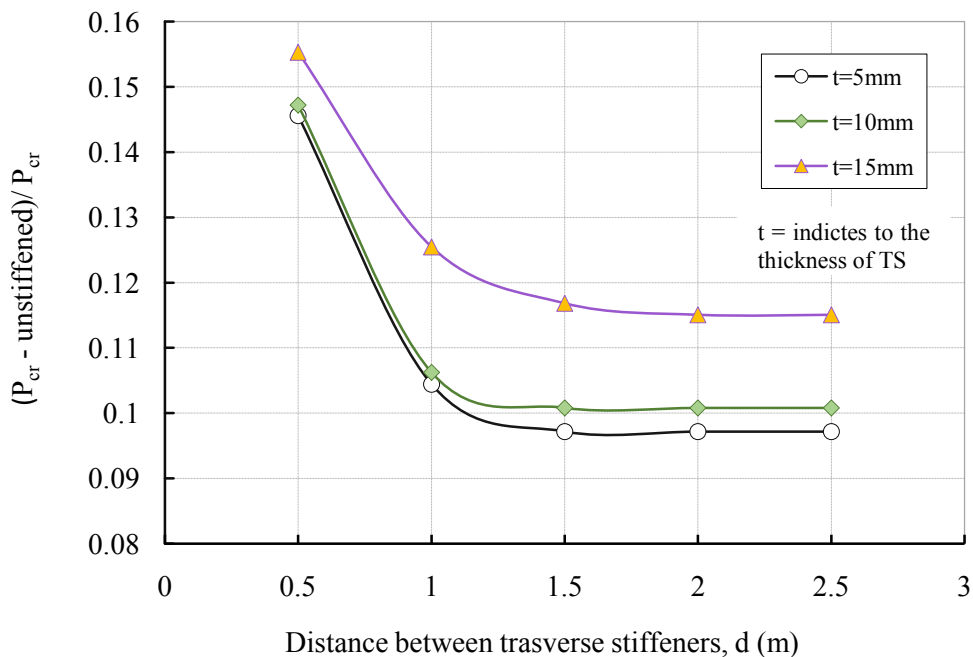


Figure 6.17 $(P_{cr} - unstiffened) / P_{cr}$ vs. distance between TS for *Model-1_f* (Global)

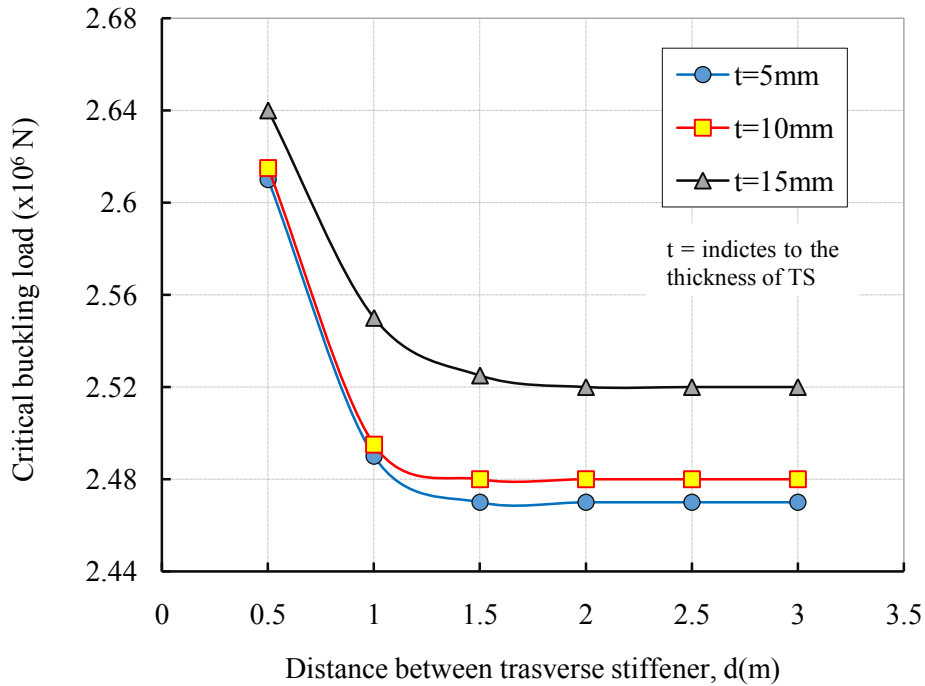


Figure 6.18 Effect of TS on the critical global buckling load of the frame for *Model-1_f*

6.3.2 STIFFENED FRAME MODELS BY USING TRANSVERSE AND LONGITUDINAL STIFFENERS

In this section, the critical local and global buckling behaviour of the frame models with transverse stiffeners and longitudinal stiffeners are investigated in detail. The influence of change in distance between transverse stiffeners and its thicknesses on the buckling capacity characteristics as well as structural performance of the stiffened frame models is illustrated. Frame models by adding longitudinal stiffeners are considered in the analysis for instance an one centrally located i.e. $w/2$ longitudinal stiffeners and of course with transverse stiffeners.

6.3.2.1 STIFFENED FRAME MODEL BY USING TRANSVERSE AND TWO LONGITUDINAL STIFFENERS

In this case, the effect of change in both transverse and two longitudinal stiffeners on the critical buckling load and buckling mode of the stiffened frame model is investigated. Figure 6.7 illustrates a detailed geometrical assembly of the frame *Model-2_f* with both stiffeners where the longitudinal stiffeners are fixed at $w/2$ of the frame-beams heights. The dimensions of the longitudinal stiffeners have been previously illustrated in section 6.2.1.

The results presented in this section are for the frame *Model-2_f* which stiffened by both types of stiffeners. The variation of distances between transverse stiffeners d , is varied from 0.5m to 3m and the stiffener configuration is that in Figure 6.2 and Figure 6.3 respectively. The stiffened frame *Model-2_f* considered in this analysis is subjected to pure axial compression load with transverse stiffeners thicknesses from 5mm to 15mm and 10mm for longitudinal stiffener's thicknesses in order to investigate their influence on the structural response. The first Eigen buckling modes on deformed shapes at critical local and global buckling loads for one sample are shown in

Figure 6.19 and Figure 6.20 respectively. Obviously, the onset of buckling modes can be seen along with distribution of magnitude deformation over the surfaces. It is clearly manifest from

Figure 6.19 that the effect of longitudinal stiffeners has a vital role in terms of redistribution the buckling mode in particular for the local buckling. However, the behaviour of global buckling mode as illustrated in Figure 6.20, is almost as the same fashion to the previous case in section 6.3.1 with a difference, of course, in its values.

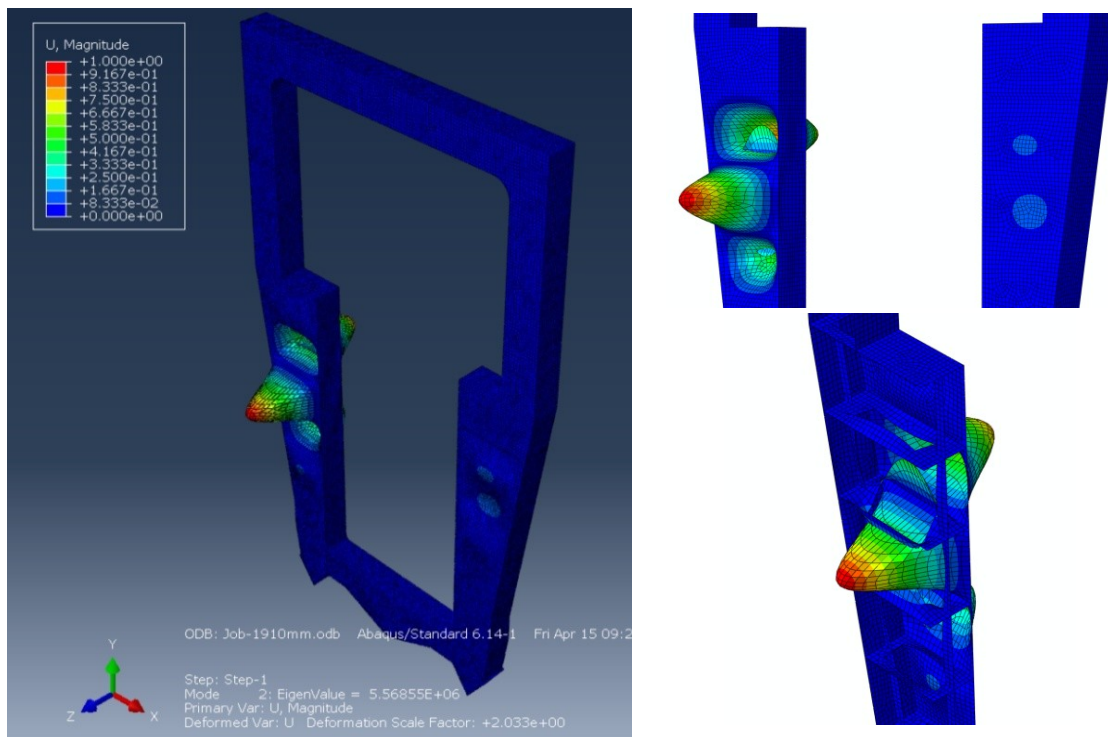


Figure 6.19 A sample of 1st local Eigen buckling mode of the frame (*Model-2_f*)

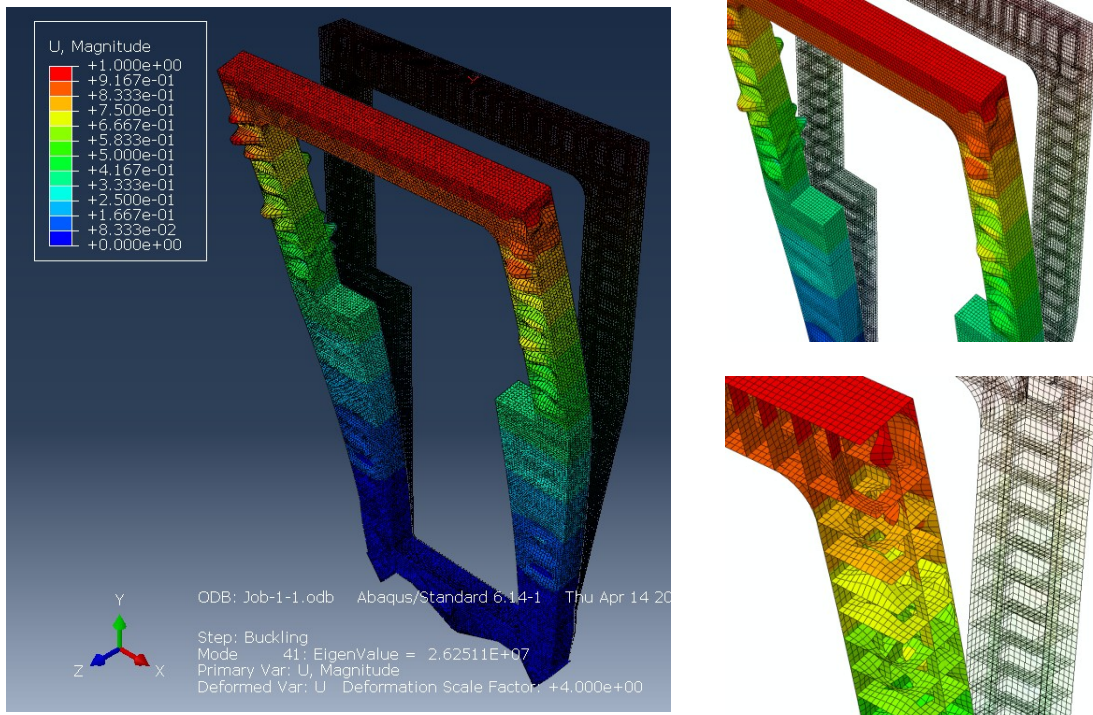


Figure 6.20 A sample of 1st global Eigen buckling mode of the frame (*Model-2*)

The obtained results of the influence of the stiffened frame models on both local and global buckling capacity are illustrated in Figure 6.21 and Figure 6.23 respectively, where the ratio of critical buckling load of the stiffened to unstiffened frame model, $(P_{cr} - unstiffened) / P_{cr}$, are shown to be plotted against the distance between transverse stiffeners TS. Furthermore, the critical buckling loads corresponding to the various stiffener thicknesses are shown in Figure 6.22. Figure 5.18 clearly appears that the addition of longitudinal stiffeners to transverse stiffeners considerably improves the local buckling performance of a frame model. Initially the percentage of increase in the local buckling capacity of the stiffened frame model is seen to be significant at 0.5m and with an increase in the distance between transverse stiffeners; it becomes gradual reduced for the period up to 1.5m before beginning of the reduction in steady state as shown in Figure 6.21. As a result, it is clear that the addition of longitudinal stiffeners has given a clear improvement in the critical local buckling capacity to unstiffened frame model and the curves trend to level down and eventually decrease in the local buckling capacity. For an instant, at a small TS thickness = 5mm and at a distance between TS = 0.5m, increase in the critical local buckling load is found to be of the order 65% of the unstiffened frame model.

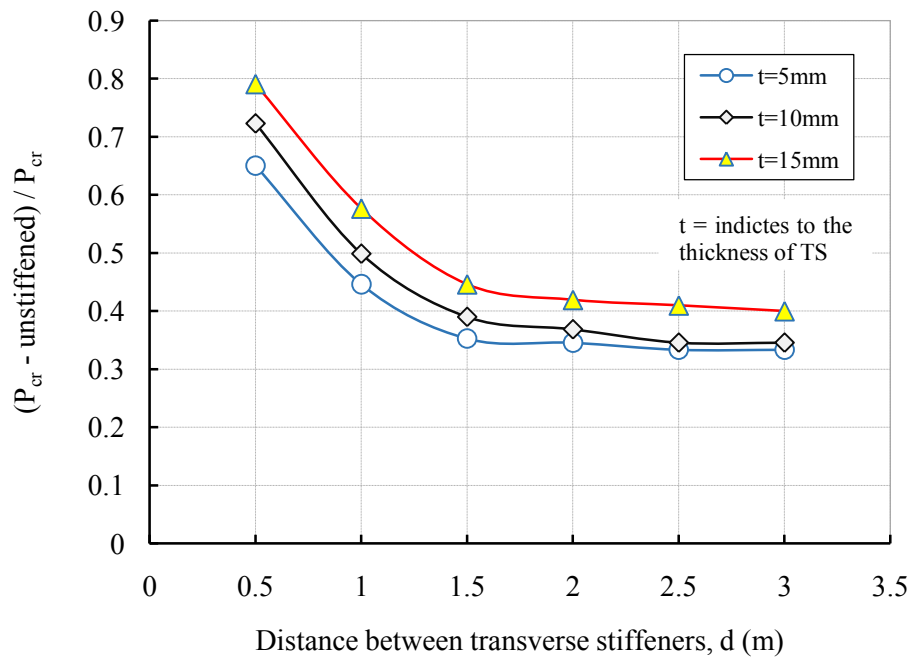


Figure 6.21 $(P_{cr} - \text{unstiffened}) / P_{cr}$ vs. distance between TS for *Model-2_f* (Local)

In comparison with the *Model-2_f* for the same condition, the percentage increased to 10% for both. Consequently, as the distance between stiffeners increase, it is of note from Figure 6.22 that the transverse stiffeners effect on the critical local buckling load became effect less after 1.5m of distance between TS . Although, similarly for distance between TS = 3m with regard to TS thicknesses = 5mm and 15mm, the critical local buckling loads are noted to be improved by 31% and 40% respectively compared with *Model-1_f*. Therefore, it can be observed that further increase in the distance between TS does not greatly improve the critical buckling loads and is not recommended for designs.

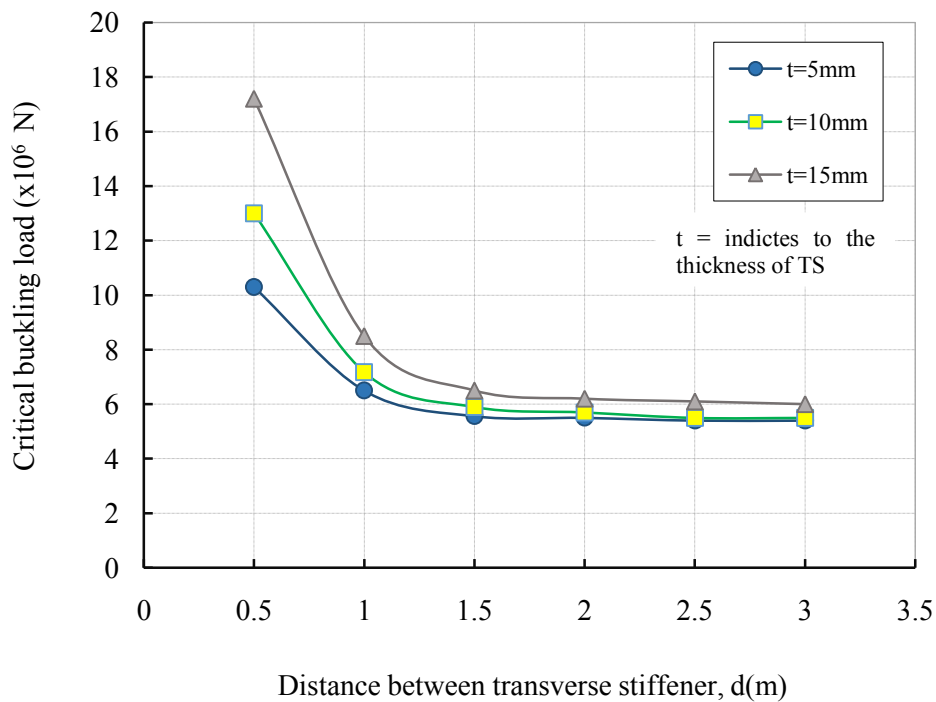


Figure 6.22 Effect of TS on the critical local buckling load of the frame for *model-2_f*

Figure 6.23 and Figure 6.24 highlights the structural response of the frame *Model-2_f* that corresponding to the critical global buckling capacity, throughout the loading. The ratio of the critical global buckling capacity of stiffened to unstiffened frame model, $(P_{cr} - \text{unstiffened}) / P_{cr}$, is shown to be plotted against the distance between transverse stiffeners. It can be noticed from the Figure 6.23 that the curves for different distance between transverse stiffeners to critical global buckling tend to show similar behaviour with an increase in the distance between TS. It is evident that initially the notable improvement in the critical global buckling is seen for 0.5m is found to be 14.5%, 14.7% and 15.5% at different TS thicknesses of unstiffened frame *Model-2_f* respectively. Afterward, as the distance between TS increase, the rate of change in critical global buckling loads eventually approached for a small period (i.e. almost zero) after 2m of distance between transverse stiffeners as shown in Figure 6.24. It seems useless to further increase the stiffener distance since it increases the frame model (structural) weight without any notable improvement. As a consequence, it can be observed that in comparison with the results of *Model-1_f* the critical global buckling remained unchanged for all cases.

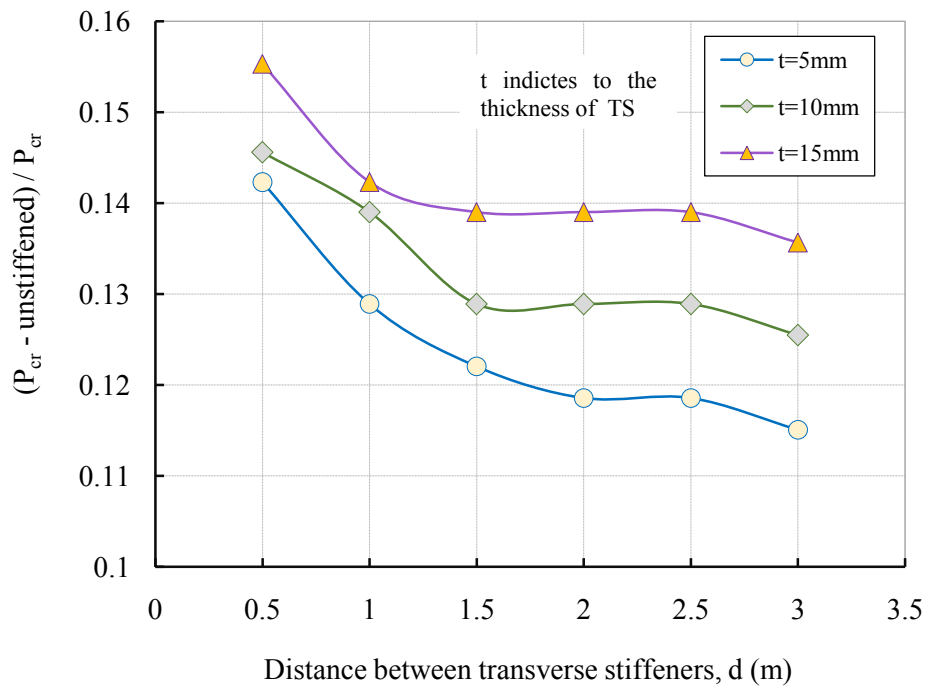


Figure 6.23 $(P_{cr} - \text{unstiffened}) / P_{cr}$ vs. distance between TS for *Model-2_f* (Global)

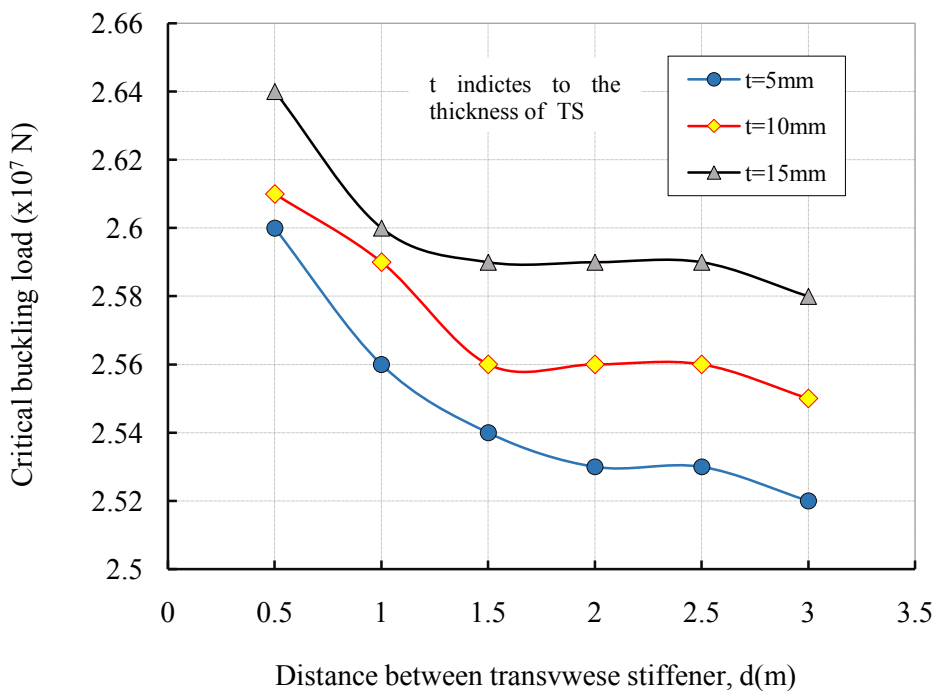


Figure 6.24 Effect of TS on the critical global buckling load of the frame *Model-2_f*

6.3.2.2 STIFFENED FRAME MODELS BY USING TRANSVERSE AND FOUR LONGITUDINAL STIFFENERS

In this case, the effect of change in both transverse, four longitudinal stiffeners on the critical buckling load and buckling mode of the stiffened frame *Model-3_f* is investigated. Figure 6.8 illustrates a detailed geometrical assembly of a frame model with both stiffeners where the longitudinal stiffeners are fixed at $w/2$ of frame-beams height. The dimensions of the longitudinal stiffeners have been previously illustrated in section 6.2.1. The results presented in this section are for the frame *Model-3_f* that is stiffened by both stiffeners. The variation of distances between transverse stiffeners denoted by d , is varied from 0.5m to 3m and the stiffener configuration is shown as in Figure 6.2 and Figure 6.3 respectively. The stiffened frame model considered in this analysis is subjected to pure axial compression load with variety of transverse stiffeners thicknesses from 5mm to 15mm and only 10mm for longitudinal stiffener's thicknesses in order to investigate their influence on the structural response. The first Eigen buckling modes on deformed shapes at critical local and global buckling loads for one sample are shown in and respectively. Obviously, the onset of buckling modes can be seen along with distribution of magnitude deformation over the surfaces. It is clearly manifest from that the effect of longitudinal stiffeners has a vital role in terms of increase the buckling mode in particular for local buckling. However, the behaviour of global buckling mode is a little bit as the same fashion to the previous case in 6.3.2.1 with a difference, of course, in the its values.

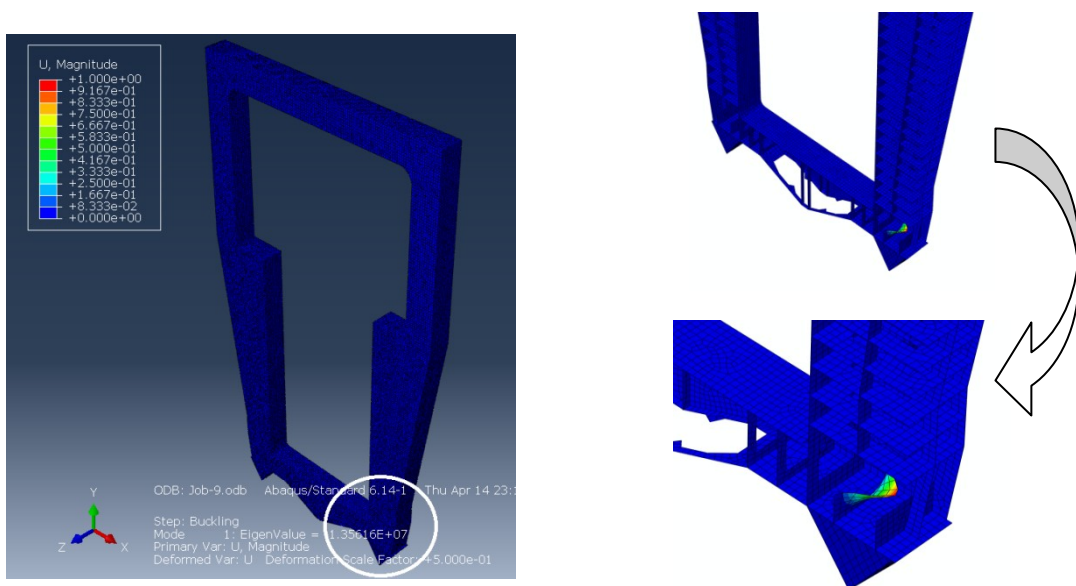


Figure 6.25 A sample of 1st local Eigen buckling mode of the frame *Model-3_f*

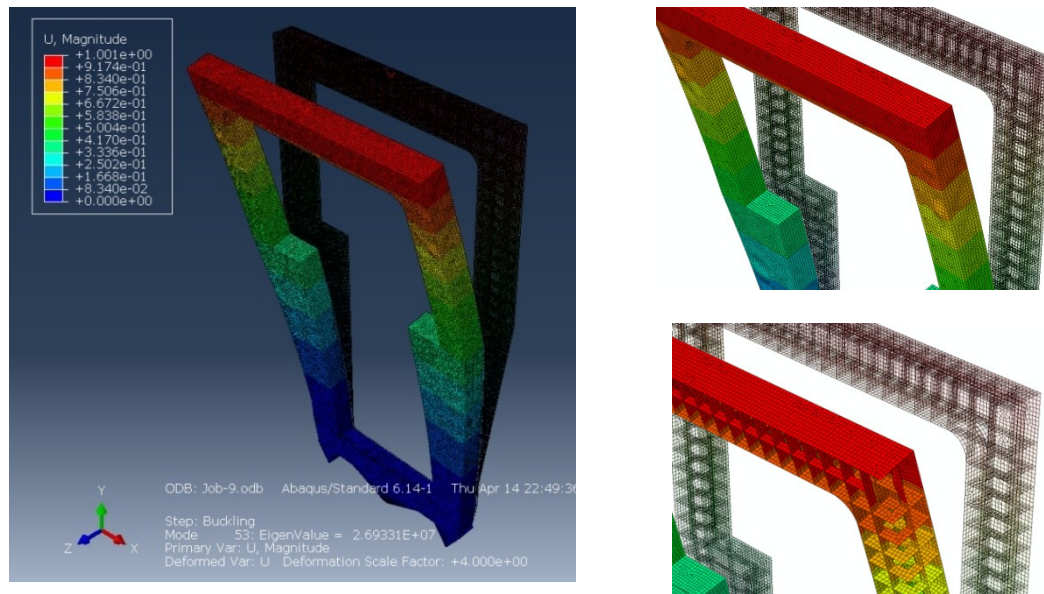


Figure 6.26 A sample of 1st global Eigen buckling mode of the frame *Model-3_f*

The obtained results of the influence of the stiffened frame models on both local and global buckling capacity are illustrated in Figure 6.25 and Figure 6.26 respectively, where the ratio of critical buckling load of the stiffened to unstiffened frame model, $(P_{cr} - \text{unstiffened})/P_{cr}$, are shown to be plotted against the distance between transverse stiffeners TS. Furthermore, the critical buckling loads corresponding to the various stiffener thicknesses are shown in Figure 6.28 and Figure 6.30, and clearly appears that the addition of longitudinal stiffeners to transverse stiffeners considerably improves the local buckling performance of the frame *Model-3_f*. It is note worthy to point out that the percentage of increase in the local buckling capacity of the stiffened frame model is seen to be significant at all thicknesses of TS. While an increase in the distance between transverse stiffeners it becomes gradual reduced for the period up to 1.5m, after this point the curves started dramatically decreasing. As a result, it is clear that the model using four longitudinal stiffeners has given a superb improvement and results in the critical buckling capacity to unstiffened frame model. For an instant, at lower distances between TS, the critical local buckling loads are found to be of order between 81% to 84.4% of the unstiffened frame model.

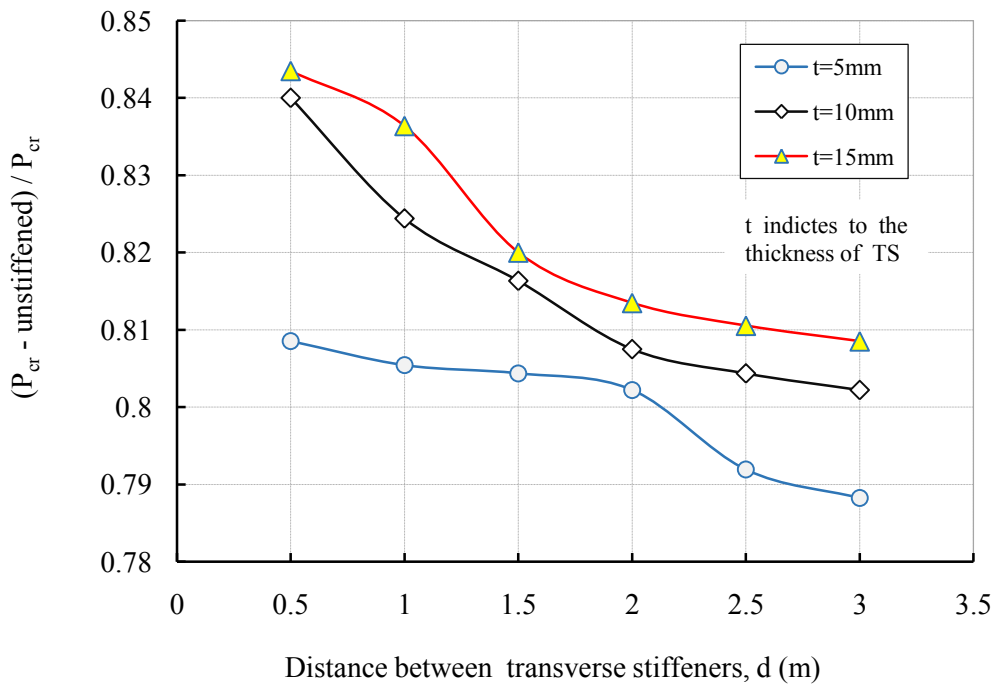


Figure 6.27 $(P_{cr} - \text{unstiffened}) / P_{cr}$ vs. distance between TS for Model-3_f (Local)

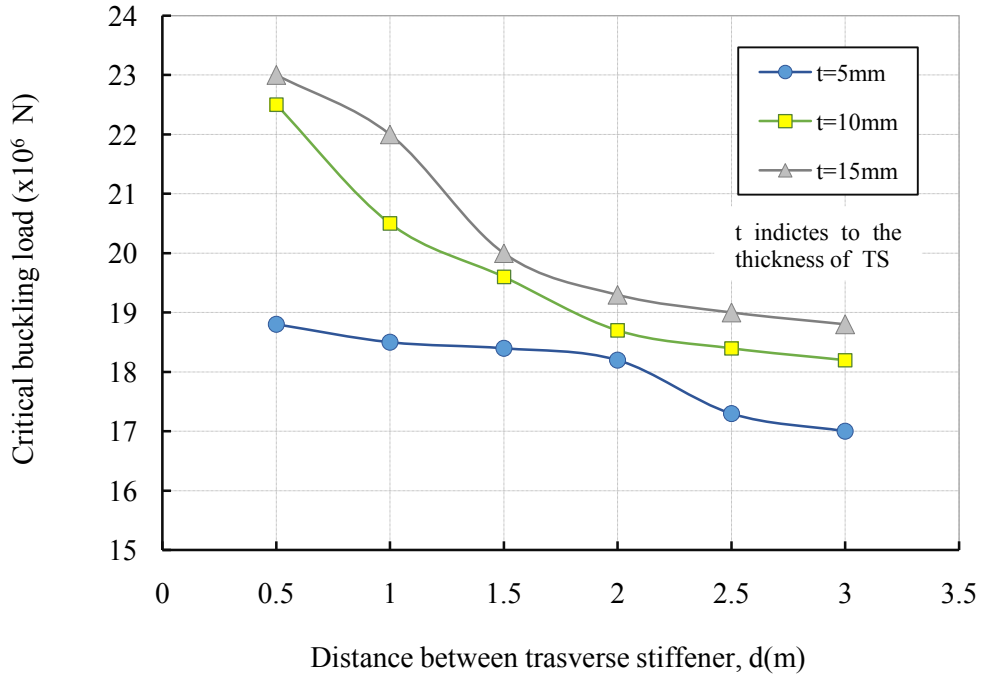


Figure 6.28 Effect of TS on the critical local buckling load of the frame for Model-3_f

In comparison with the *Model-2_f* for the same condition, the percentage increased 16% and 4% respectively. Consequently, as the distance between stiffeners increase, it is of note that the transverse stiffeners effect on the critical local buckling load became effect less. Although, similarly for distance between TS is 3m with regard to TS thicknesses 5mm and 15mm, the critical local buckling loads are improved 78.8% and 80.9% respectively. Therefore, it can be observed that further increase in the distance between TS does not greatly improve the critical buckling loads and is not recommended for designs. Again, the buckling mode changes from local buckling to global buckling with increase in applied load. Figure 6.29 highlights the structural response of the frame *Model-2_b* that corresponding to the critical global buckling capacity, throughout the loading. The ratio of the critical global buckling capacity of stiffened to unstiffened frame model, $(P_{cr} - \text{unstiffened}) / P_{cr}$, is shown to be plotted against the distance between transverse stiffeners. It can be noticed from the curves for different distance between transverse stiffeners to critical global buckling tend to show similar behaviour almost linearly with an increase in the distance between TS. It is evident that initially the notable improvement in the critical global buckling is seen for 0.5m is found to be 16.9%, 18% and 18.6% at different TS thicknesses of unstiffened frame *Model-3_f* respectively. Afterwards, as the distance between TS increase, the rate of change in critical global buckling loads eventually approached for a small period, i.e. almost similar to the maximum values of *model-2_f*. It seems useless to further increase the stiffener distance since it increases the frame model (structural) weight without any notable improvement. Consequently, it can be observed that in comparison with the results of *Model-1_f* and *Model-2_f* the critical global buckling slightly increased.

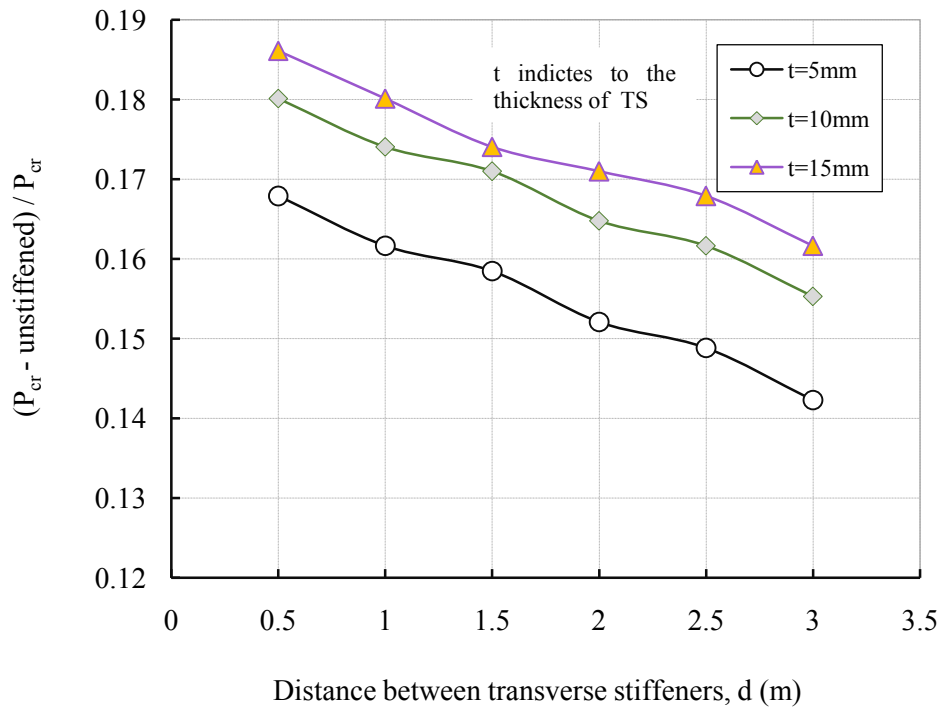


Figure 6.29 $(P_{cr} - \text{unstiffened}) / P_{cr}$ vs. distance between TS for *Model-3_f* (Global)

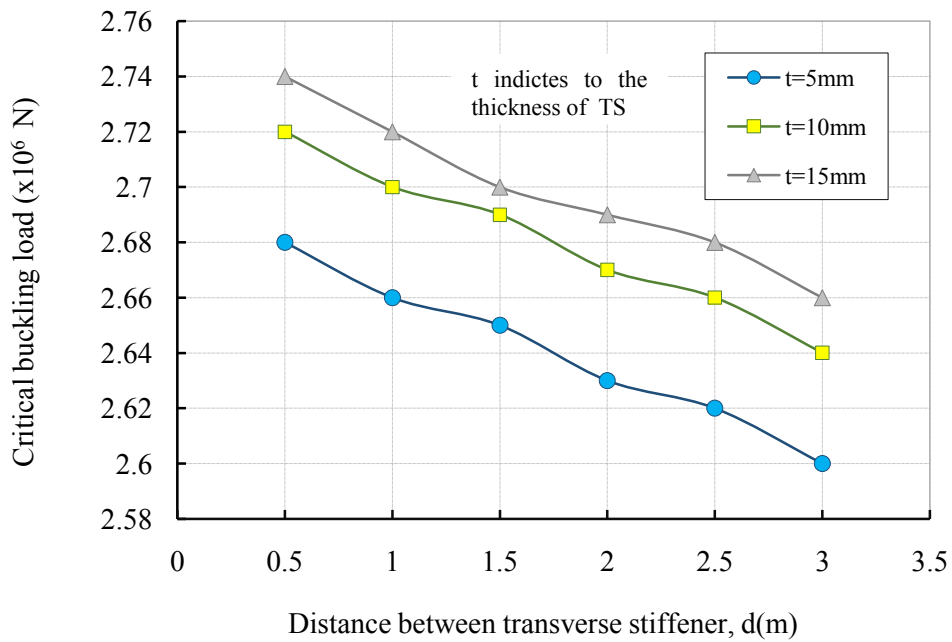


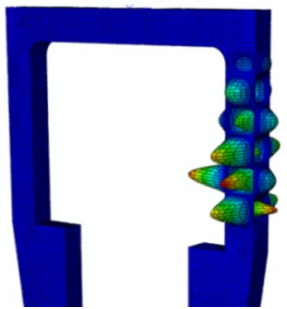
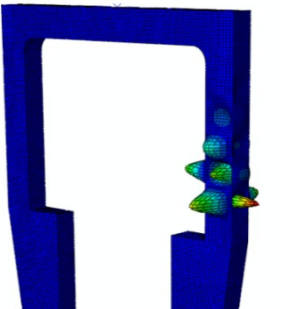
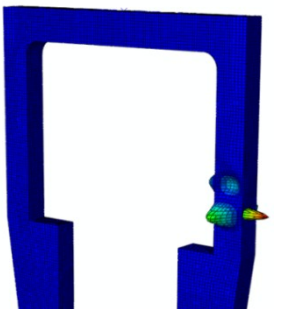
Figure 6.30 Effect of TS on the critical global buckling load of the frame for *Model-3_f*

6.4 EFFECT OF TRANSVERSE STIFFENERS THICKNESS ON THE CRITICAL BUCKLING LOAD

Another element, which takes in an outcome and influence along the general critical buckling capacity, is the rigidity of the stiffener. Usually the rigidity of a stiffener depends solely on its dimensions and the critical rigidity of a stiffener corresponds to an optimum stiffeners thickness. In this section, the effect of change in transverse stiffener thickness on the critical buckling load of the stiffened frames with three models is investigated.

6.4.1 CRITICAL LOCAL BUCKLING RESPONSE AT DIFFERENT TS THICKNESSES

Figure 6.31 shows the first critical buckling modes for three models with different TS thicknesses. Regarding *Model-1_f*, the shape and location of critical buckling loads are seen differently with each other. At $t_{TS} = 5\text{mm}$, the location of the buckling load is taking place in the right top of the section frame on the outer surface. At $t_{TS} = 10\text{mm}$, the location and shape of the buckling are changed to be less than the previous condition, but at $t_{TS} = 15\text{mm}$, the location and shape of the buckling are noted to be at the bottom and in the vicinity of the section junction. For the TS considered with $t_{TS} = 5\text{mm}$ and $t_{TS} = 10\text{mm}$, the location and shape of the buckling are almost in the same trend on the left top section of the frame as indicated in the figure. It is clear that with $t_{TS} = 15\text{mm}$ for the same model, the propagation of the buckling has not gone through the wall thickness on the right top of the frame section. By examining the buckling on *Model-3_f* with the same procedures, it is worth mentioning that the locations and shapes of the buckling are closely of each other at different TS thicknesses. Consequently, it is of note that the development in buckling has different attitudes to changing of TS thicknesses. This change depends on the location and thickness of transverse stiffener.

Model	$t_{TS} = 5\text{mm}$	$t_{TS} = 10\text{mm}$	$t_{TS} = 15\text{mm}$
1_f			

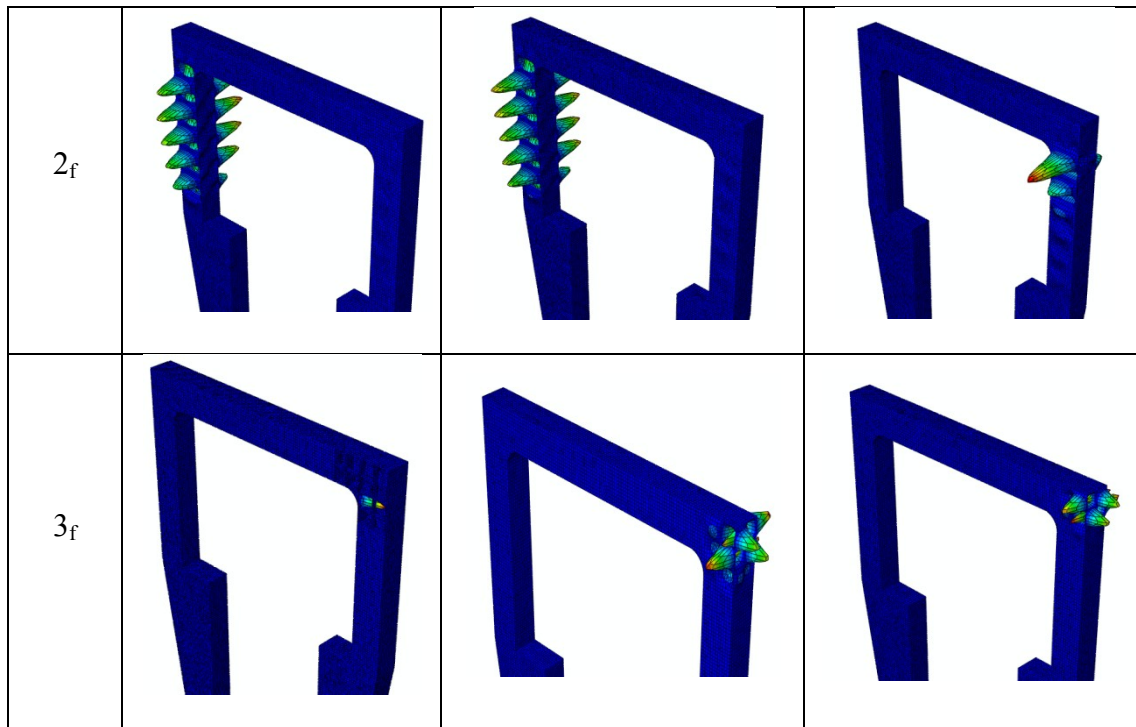


Figure 6.31 Critical local buckling modes for the samples of all models at difference TS thicknesses

The influence of transverse stiffener thickness on the critical local buckling loads of the design space associated with different distance between the transverse stiffeners is shown in Figure 6.32, Figure 5.33 Figure 6.34 respectively. It can be observed from all figures that the thickness of transverse stiffener has a significant effect on the critical local buckling load for stiffened models. When the distance between transverse stiffeners is between 0.5m to 1.5m, the results showed that the improvement in the critical local buckling load can be seen clearly in Figure 6.32 for all models. For *Model-1_f*, *Model-2_f* and *Model-3_f*, which have a 5mm of TS thickness, the critical local buckling load is increased to 55%, 64% and 80% respectively. It can see from Figure 6.32, Figure 6.33 and Figure 6.34 that *Model-1_f* and *Model-2_f* is very close to each other in terms of the values of critical buckling loads. An interesting point was mentioned in Figure 6.28 that the value of critical buckling load for *Model -3_f* is higher compared with *Model-1_f* and *Model-2_f*.

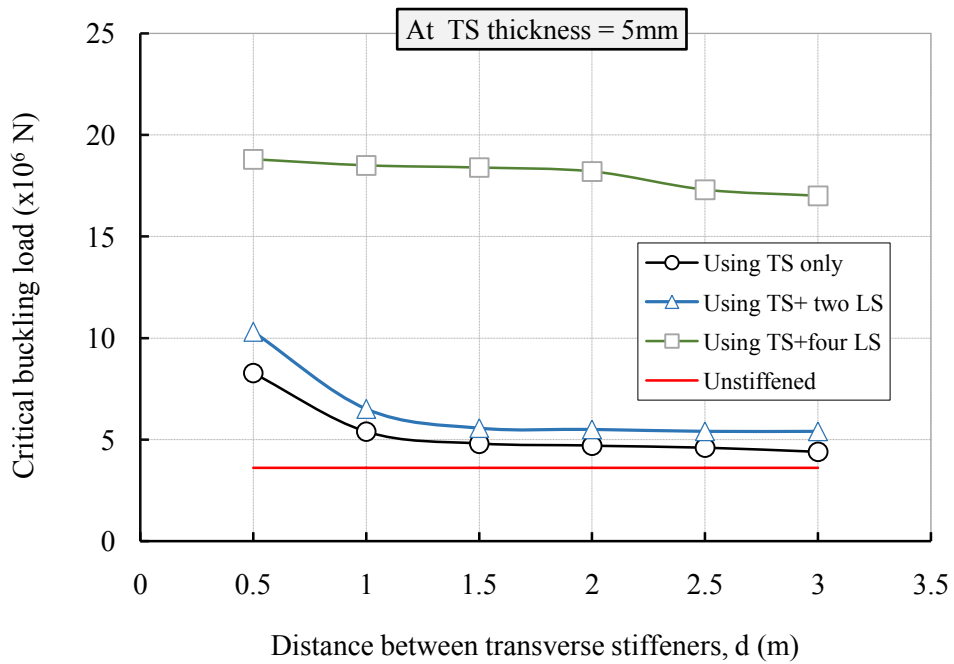


Figure 6.32 Effect of TS thickness on the critical local buckling load for all models at TS thickness =5mm

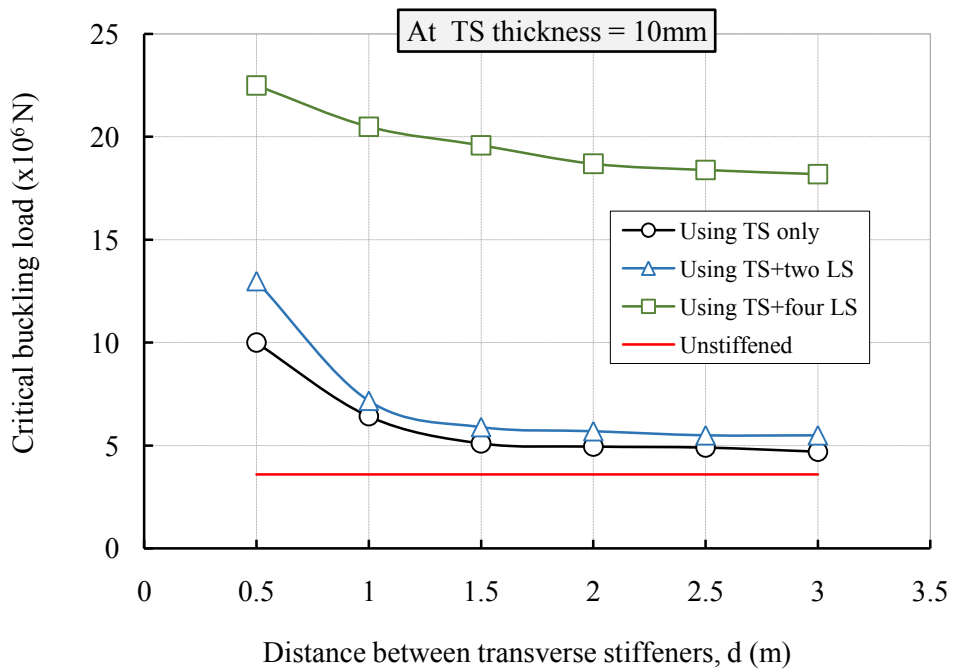


Figure 6.33 Effect of TS thickness on the critical local buckling load for all models at TS thickness =10mm

With the increase in TS thickness to 10mm by the same procedures, it can see from Figure 6.33 that did not significantly increase in the critical local buckling load with *Model-1_f* and *Model-2_f*. The values of these critical buckling loads compared to the values which found earlier at TS=5mm and d=0.5m are improved as following 64% and 72% respectively. Again, considering *Model-3_f*, the critical buckling load was increased to 84% where could be the best increase. By looking at Figure 6.34 all models after 1.5m of distance between transverse stiffeners d, and with the increase in TS thickness to 15mm, the critical buckling loads are slightly changed. It can also see that the values of critical buckling loads are almost similar to the previous cases when TS=5mm and 10mm. However, the critical buckling load increases noticeably between 0.5m and 1.5m of distance between transverse stiffeners due to the increase presence of transverse stiffener thickness. The curves with high thickness of transverse stiffeners seem to approach the higher bound estimate of the critical buckling load at small distances between transverse stiffeners.

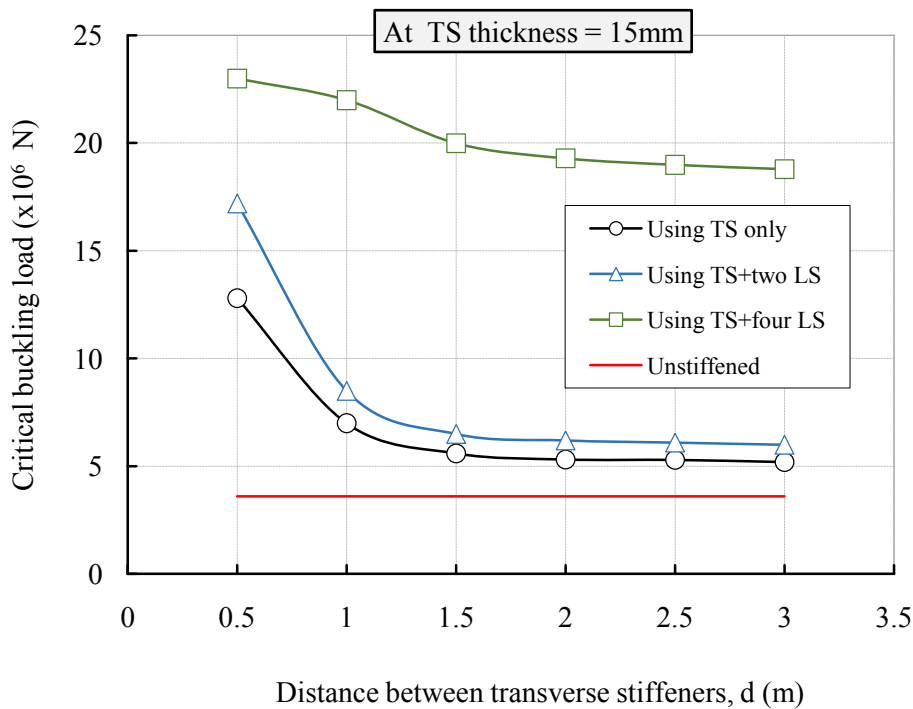
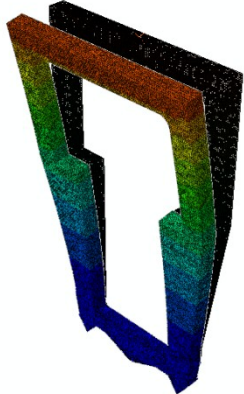
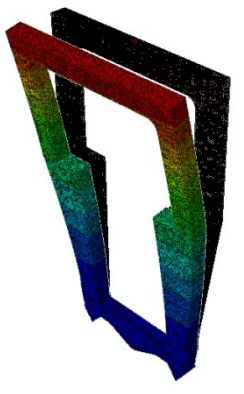
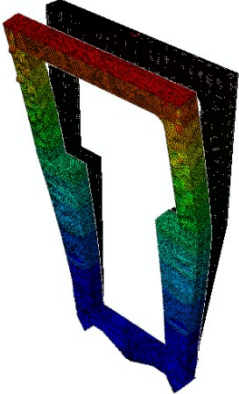


Figure 6.34 Effect of TS thickness on the critical local buckling load for all models at TS thickness =15mm

6.4.1.1 CRITICAL GLOBAL BUCKLING RESPONSE AT DIFFERENT TS THICKNESSES

The influence of transverse stiffener thickness on the critical global buckling load for three models with different TS thicknesses is depicted in Figure 6.35. For *Model-1_f*, the behaviour of critical buckling loads are seen similar with each other. At $t_{TS}=5\text{mm}$, the location of the maximum buckling load is taking place in the top of the frame. At $t_{TS} = 10\text{mm}$, also the behaviour and the shape of the buckling are changed to be more than the previous condition, but at $t_{TS}=15\text{mm}$, the location and shape of the buckling are noted increased a little bit down. For the other models, the behaviour of the global buckling is almost in the same trend with different values as indicated in the image (i.e. inside the figure). Consequently, it is of note that the development in buckling has different attitudes to changing of TS thicknesses. This change depends on location and thickness of the transverse stiffener.

Model	$t_{TS} = 5\text{mm}$	$t_{TS} = 10\text{mm}$	$t_{TS} = 15\text{mm}$
1 _f	 $P_{cr} = 2.59 \times 10^7 \text{ N}$	 $P_{cr} = 2.61 \times 10^7 \text{ N}$	 $P_{cr} = 2.64 \times 10^7 \text{ N}$
2 _f	 $P_{cr} = 2.62 \times 10^7 \text{ N}$	 $P_{cr} = 2.63 \times 10^7 \text{ N}$	 $P_{cr} = 2.64 \times 10^7 \text{ N}$

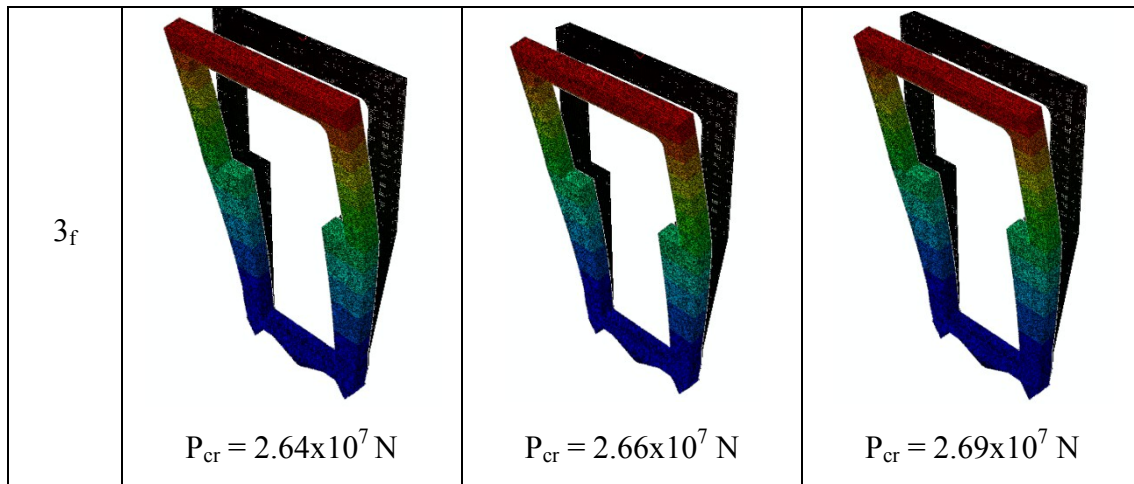


Figure 6.35 Critical global buckling modes for all models at difference TS thicknesses

The influence of transverse stiffener thickness on the critical global buckling loads of the design space associated with different distance between the transverse stiffeners is shown in Figure 6.36, Figure 6.37 and Figure 6.38 respectively. It can be observed from all figures that the thickness of transverse stiffener has an effect on the critical global buckling load for stiffened models. When the distance between transverse stiffeners is between 0.5m to 1.5m, the results showed that the improvement in the critical global buckling load can be seen clearly in Figure 6.36 for all models is limited. For *Model-1_f*, *Model-2_f* and *Model-3_f*, which have a 5mm of TS thickness, the critical local buckling load is increased to 12% , 14% and 20% respectively.

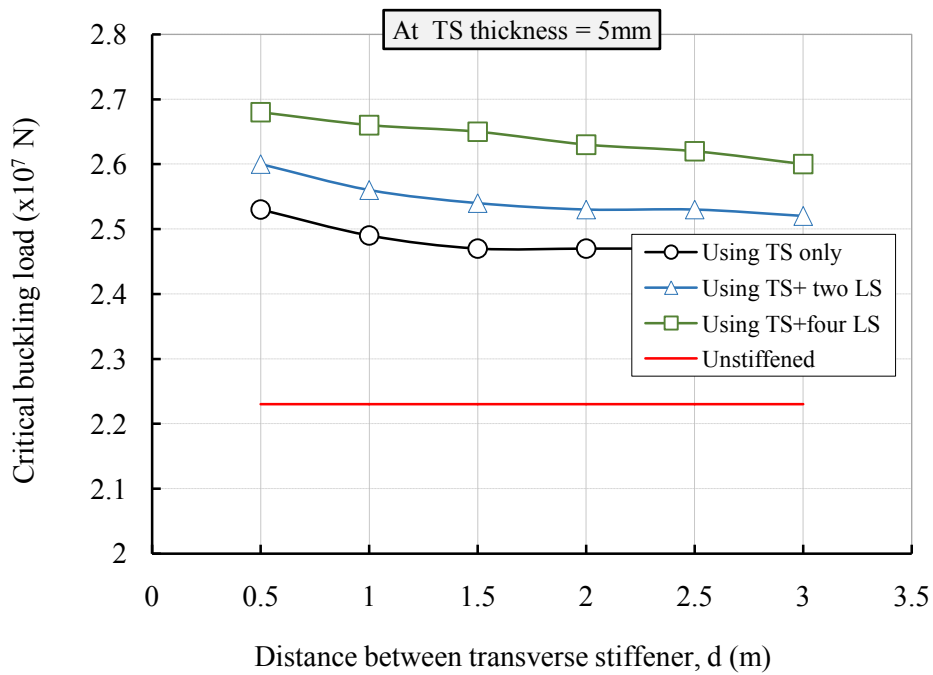


Figure 6.36 Effect of TS thickness on the critical global buckling load for all models at TS thickness = 5mm

As the increase in TS thickness to 10mm by the same procedures, it can see from Figure 6.37 that there is no significantly increase in the critical global buckling load with all models. The values of these critical buckling loads compared to the values which found earlier at TS=5mm and d=0.5m were improved as following 17%, 30% and 73% respectively.

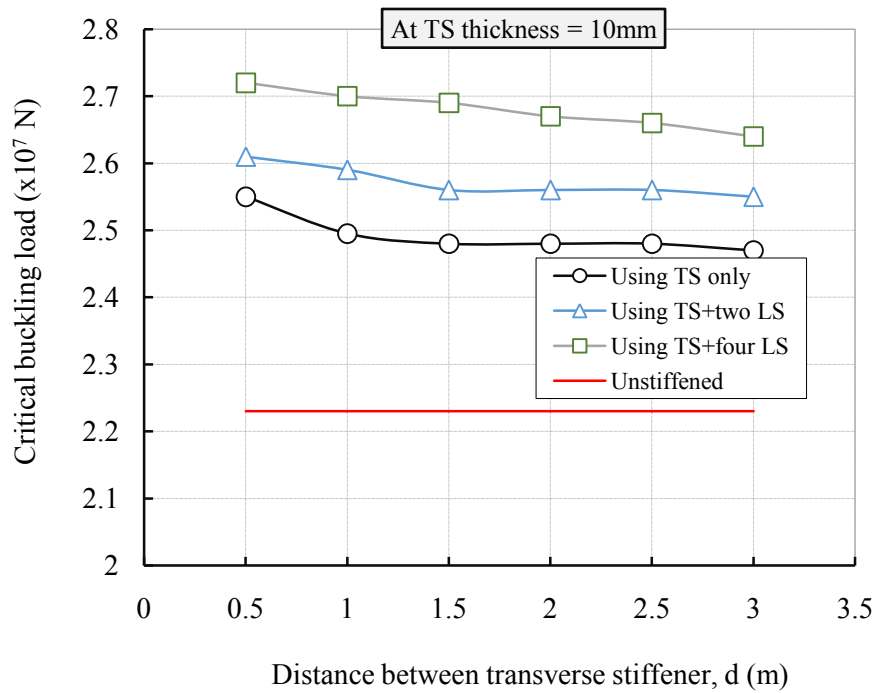


Figure 6.37 Effect of TS thickness on the critical global buckling load for all models at TS thickness equals 10mm

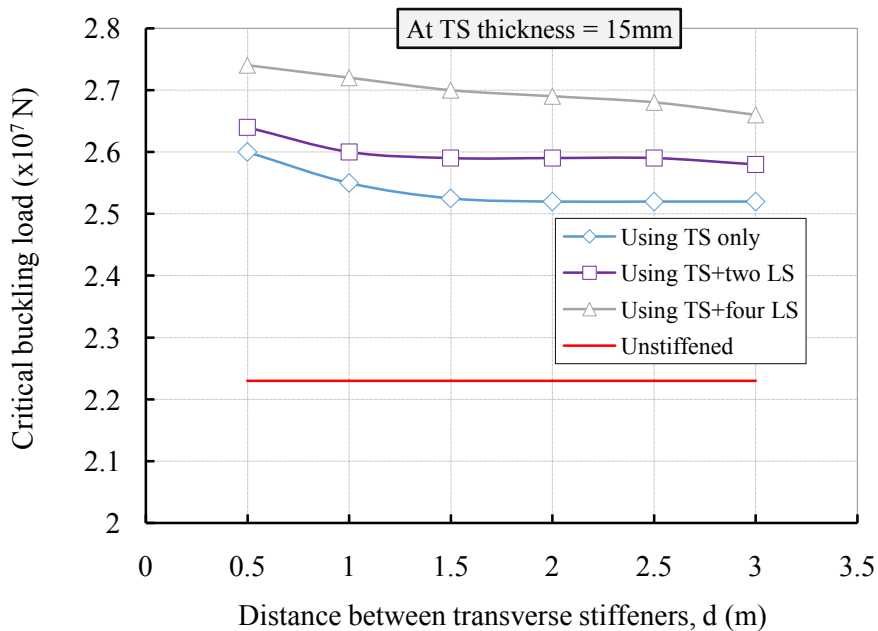


Figure 6.38 Effect of TS thickness on the critical global buckling load for all models at TS thickness = 15mm

By looking at Figure 6.38 for all models after 1.5m of distance between transverse stiffeners (d), with an increase of TS thickness to 15mm, the critical global buckling loads are slightly changed. It can also see that the values of critical buckling loads are almost similar to the previous cases when TS=5mm and 10mm. However, the critical buckling load increases noticeably between 0.5m and 1.5m of distance between transverse stiffeners due to the increase presence of transverse stiffener thickness. The curves with high thickness of transverse stiffeners seem to approach the higher bound estimate of the critical buckling load at small distances between transverse stiffeners.

6.5 CONCLUDING REMARKS

The objective of this chapter was to examine and develop finite element solutions for steel structure subjected to a compressive load. The finite element simulation strategies as described in chapter 5 were used to follow the behaviour of the frame structure in terms of local and global buckling loads under simply supported boundary conditions.

Also with the use of transverse and longitudinal stiffeners as supports to enhance the capacity of such frame structures models, these shell element models were effectively captured the buckling behaviour modes. As is described in Figure 6.1, the frame structure consists of more than one member and connections with different thicknesses. In this study, the effects of transverse and longitudinal stiffeners on the frame structures were investigated in detail. Although, it is noted that the role of both stiffeners on critical buckling is significantly affected by the different configuration of geometrical shape, but this analysis has made only on their locations. However, the charts showed that the critical buckling loads of the frame structure degraded considerably with increase in the distance between transverse stiffeners, while a lighter effect was noticed by using the longitudinal stiffeners on the global buckling behaviour.

CHAPTER 7

7. EXPERIMENTAL BEHAVIOR OF STEEL STRUCTURAL ELEMENTS

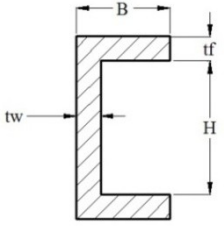
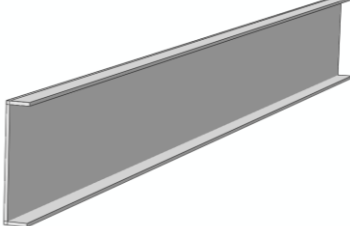
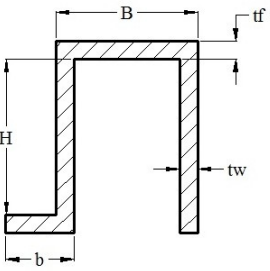
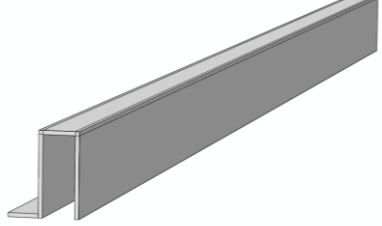
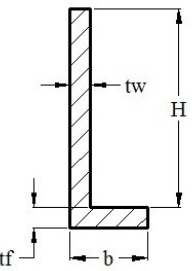
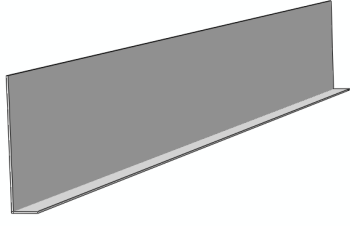
7.1 INTRODUCTION

The experimental tests are usually the base and an important for any scientific research even though are very costly and need to very long time. The numerical simulations are normally to expect the capacities of perfect members or full structures where a set of assumptions have been assumed. Therefore, the experimental tests are used for validation and comparing with the theoretical or numerical solutions and sometimes to develop further required formulas for the design. The purpose of this section is to study some specific sections that fail due to local or global buckling before the plastic capacity is reached. In the previous chapters, the basic and background of theoretical and finite element modeling aspects of the buckling behavior during thin-walled plates were discussed in details. In order to test the behaviour behind the buckling and validate the FE models, the compression test experiments are carried out. The suitable technique to guarantee the reliability of numerical simulations and to extend the utilization of the research work is by conducting the full-scale experiments with proper instrumentation for data measurement. Based on the experiments, corresponding finite element simulations have been undertaken using the ABAQUS software without any geometric imperfection in the shell. The columns were meshed using S4R, a 4-node reduced integration shell element. The compressive buckling behaviour of steel columns with has been experimentally and numerically investigated in this study. A total of 6 column tests were carried out to acquire the compressive buckling strengths with different cross sections as shown in Table 7.1.

7.2 TEST SPECIMENS

In order to investigate the buckling behavior of steel members with different types of test sections were prepared under axial compression load; it is significant that some parameters are chosen in terms of design. These parameters include the length, geometry of the cross section and thickness. A number of specimens was chosen and tested at the Faculty of Mechanical Engineering Laboratory in order to investigate the effect of these parameters. As it is known that geometrical imperfections influence the ultimate resistance buckling, but in these tests the effect of imperfection has not taken in the account. Table 7.1 and Table 7.2 respectively show the typical cross-sections geometrical details for the entire specimens which are used in the experimental tests. Generally, the lengths of specimens are different in order to observe the local and global buckling phenomena. The material considered is steel with actual stress-strain data and thus Young's modulus $E = 200\text{GPa}$, yield stress $\sigma_Y = 218\text{MPa}$ and Poisson's ratio $\nu = 0.3$.

Table 7.1 Models specimens

Specimen	Cross-section	Isometric projection
C1		
C2		
C3		

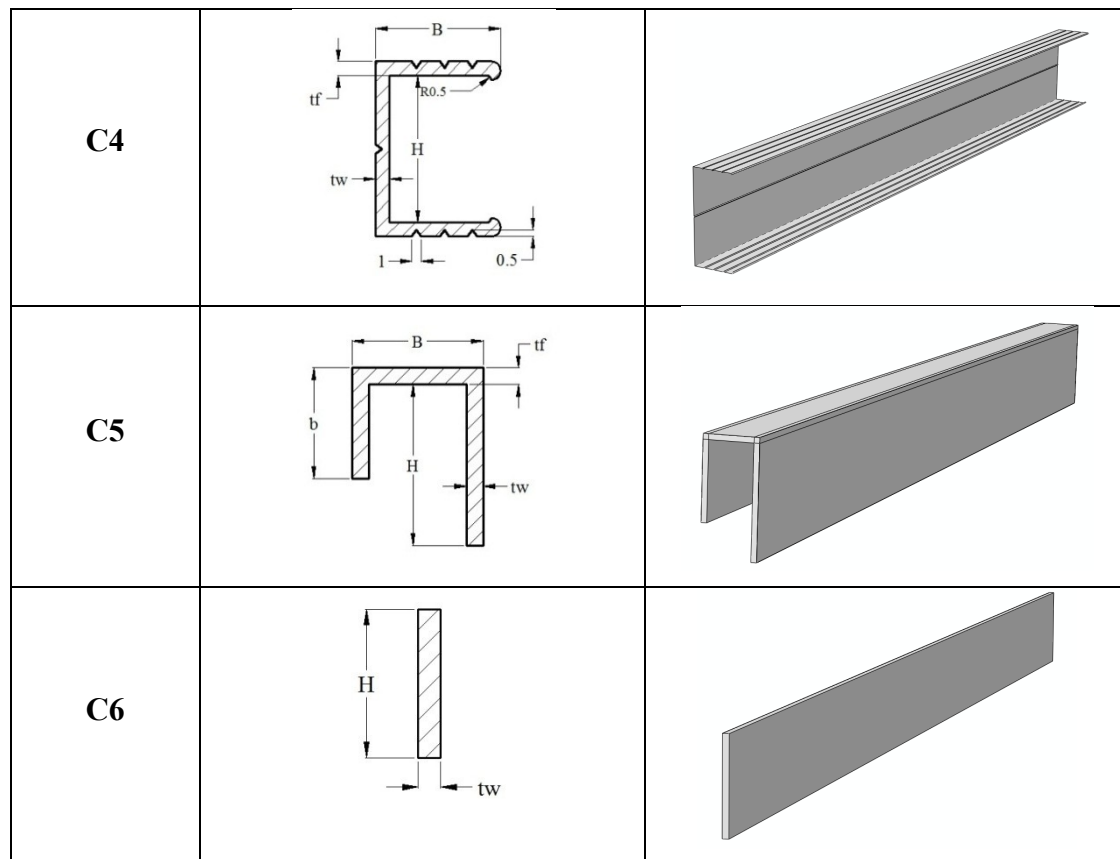


Table 7.2 Geometrical details of test specimens

Specimen	Main value					
	Section length L (mm)	Web depth H (mm)	Flange Width (mm)		Web thickness t_w (mm)	Flange thickness t_f (mm)
			B	b		
C1	1000	99	21	-	0.5	0.5
C2	960	40	20	-	1	1
C3	1000	19.5	-	20	0.5	0.5
C4	510, 900	26	27	-	0.5	0.5
C5	530	14.5	-	17	2.2	2.2
C6	540	30	-	-	-	5.5

7.3 TEST SETUP

The test was performed at the Structural Engineering Laboratory at the faculty using the compression testing frame for carrying out the tests as illustrated in Figure 3.4. The test frame was restrained by four supporting bolts on the floor which prevented any movements. The load is transmitted by an axle through a single-ended of 20 Tons hydraulic jack connected at the top of the test frame where is free in vertical direction and restrained in horizontal direction. The axial compression load which is applied on the specimen is measured by Force Sensor. The position of the force sensor is mounted at the top connection between the specimen and jack as shown in Figure 7.2. In order to measure value of the critical buckling load, the Force Sensor is connected with the computerized controller as shown in Figure 7.3 to convert the signal into force and displacement.



Figure 7.1 Test setup facility

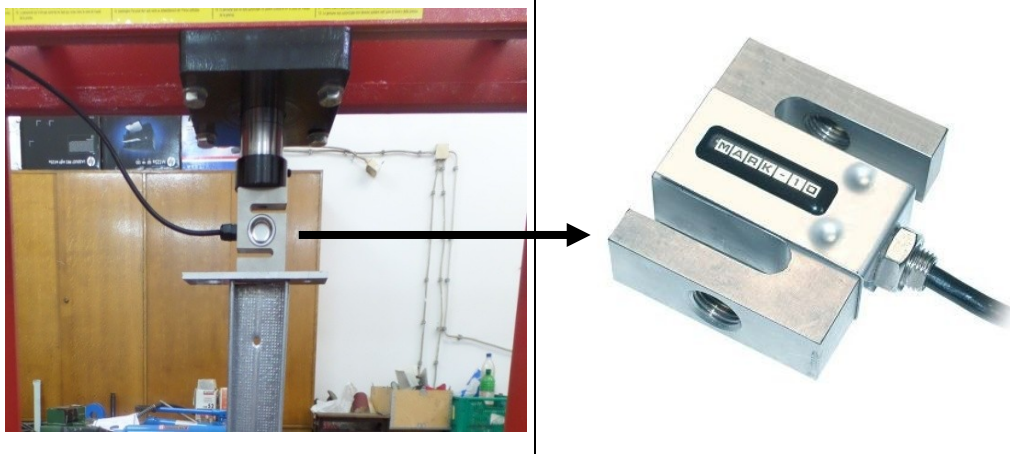


Figure 7.2 General view of the test stand with mounted sample and Force sensor

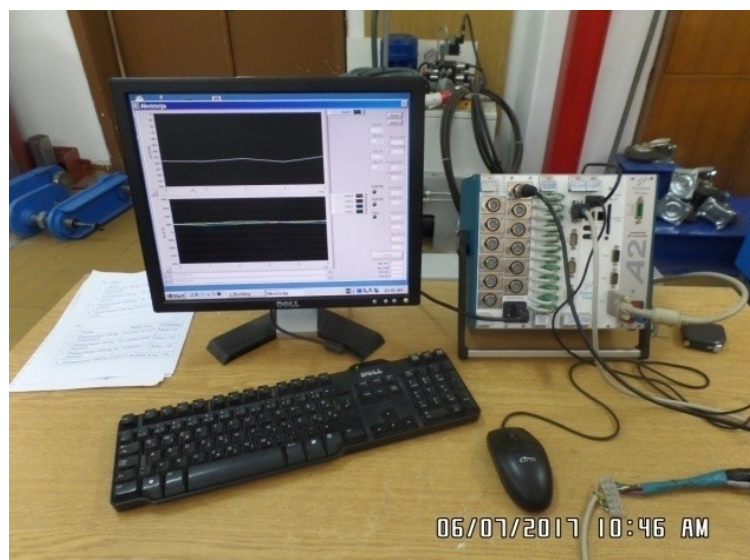


Figure 7.3 Data acquisition set-up

7.4 LOAD AND BOUNDARY CONDITIONS

The load was applied on the specimen by hydraulic jack piston which is controlled by a hydraulic pump. The load is being introduced through two steel plates by simply contact between the supports and load edge that means there is no structural connection between each other. Figure 7.4 shows the boundary conditions which are applied for all specimens in the experimental test and also during the FE simulation. The top plate is resting between the Force Sensor and specimen to distribute the load, while the bottom plate is totally fixed at the end of specimen and the base is movable to allow the specimens with various lengths to be tested as shown in the Figures. The obtained data during the test sends to the

computer as shown in Figure 7.3 where it could be read on the screen during the test and after that the data converts to readable text file then to processing.

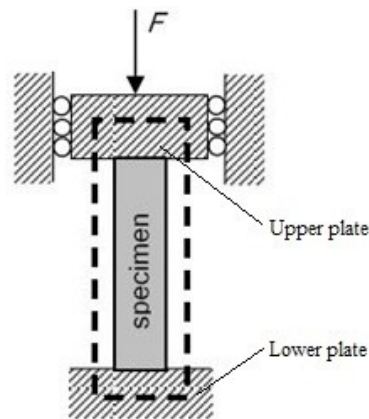


Figure 7.4 The applied boundary conditions during testing

7.5 TEST RESULTS

The buckling experiments were conducted for all specimens on the prepared test frame for validation comparison with the FE simulations results. Each specimen was positioned in the set-up alone due to that the expected mode of buckling was in a horizontal plane. In order to firm and hold the specimen in place a small load was applied to start the test. The load was then increased slowly intervals as the force approached critical load, the local and global buckling load were noted. The results of the experiments tests are briefly described as follows:

Specimen C1

Figure 7.5 shows the comparison of the local buckling behaviour for specimen C1 between the experimental and numerical models under axial compression load, where the experimental major deformation characteristic appeared similar to the FEM simulation. It can be seen from the figure that the maximum local buckling occurred in the web members than the flange members for local and global buckling. Figure 7.6 showed the global buckling mode that has the same behavior in terms of comparison with FE simulation. As a result, well agreement between the experimental and finite element models results for both local and global buckling behaviour under axial compression load.

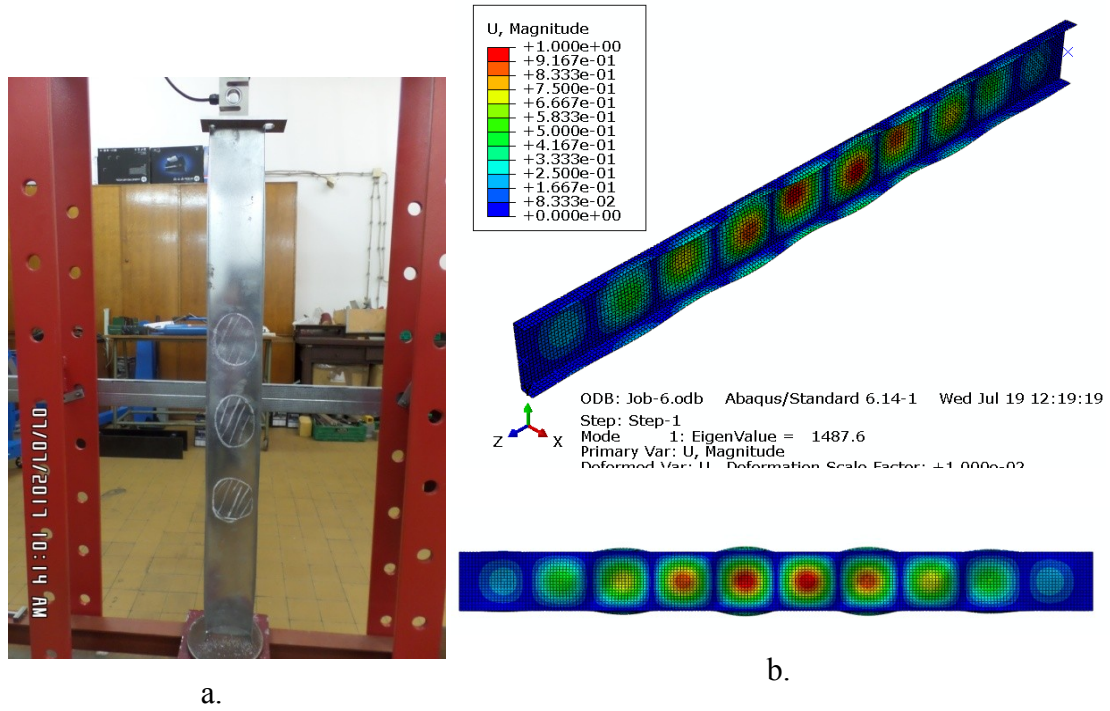


Figure 7.5 First local buckling mode for specimen C1, a. Exp, b. FE.

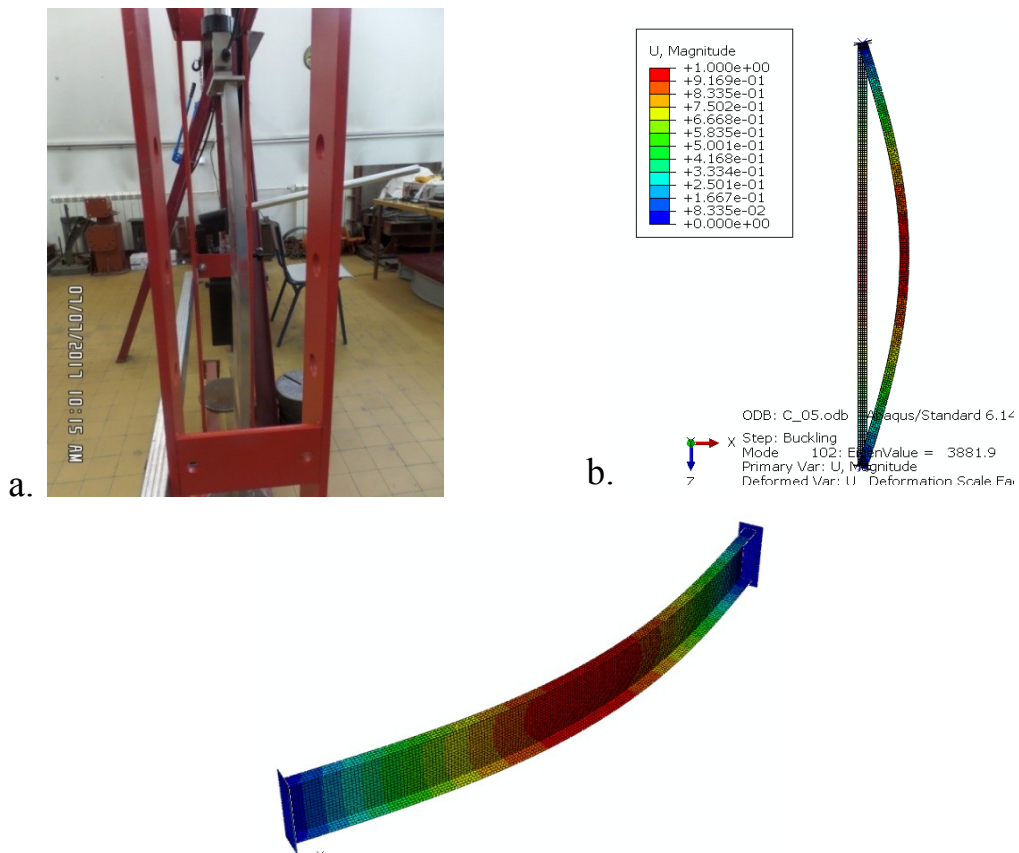


Figure 7.6 First global buckling mode for specimen C1; a. Exp. , b. FE.

The obtained load-time curve of the specimen C1 from test is shown in Figure 7.7. It is noted from the figure that before the occurrence of the local buckling, the compression load increased almost linearly till the first mode of local buckling which is occurred at 2012N. In the other hand of the solution which is made by FEM simulation and as shown in Figure 7.5, it can be seen that the first local buckling mode was at 1487.6 N. When the local buckling occurred, the axial compression load is almost at the same level for a while. The axial compression load increased further with increase of time of course until the maximum value in which the global buckling occurred that was 3125N while by FEM simulation was 3882N as shown in Figure 7.6. Consequently, the comparisons of the critical buckling modes for specimen C1 were agreed almost well with a little bit difference especially in the local buckling modes where the error was 30%.

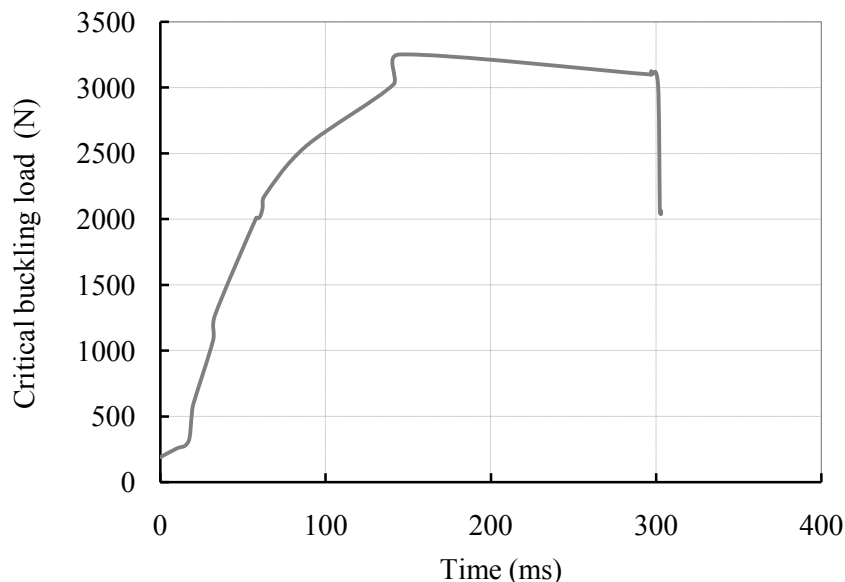


Figure 7.7 Critical buckling load response for specimen C1

Specimen C2

The description of the model and geometrical details for the specimen C2 section has been described in Table 7.1 and Table 7.2 respectively. In this specimen, another part has been added with length b as shown in Table 7.1 Models specimens. Therefore, the function of this part is to be as a longitudinal stiffer in an attempt to investigate its effect on the critical buckling in terms of value and behaviour. In order to visualize the effect of the longitudinal additional part to load and to determine the critical buckling load, there is a need to investigate the deformation shape. Figure 7.8 and Figure 7.9 show the obtained deformation

shapes and both local and global critical buckling for specimen C2. It can be seen from the Figure 7.8 and Figure 7.9 respectively that the deformation which also represents the location of the critical buckling load has occurred through and along the specimen for local buckling and at the middle of specimen for the global buckling as shown for both experimental and FE simulation.

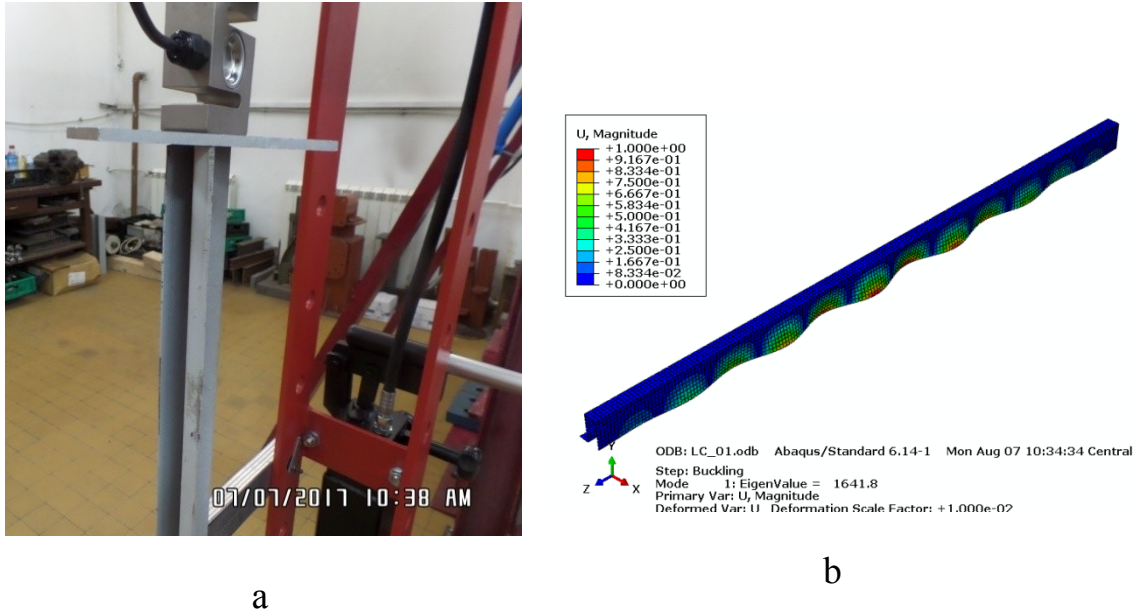


Figure 7.8 First local buckling mode for specimen C2; a. Exp. , b. FE.

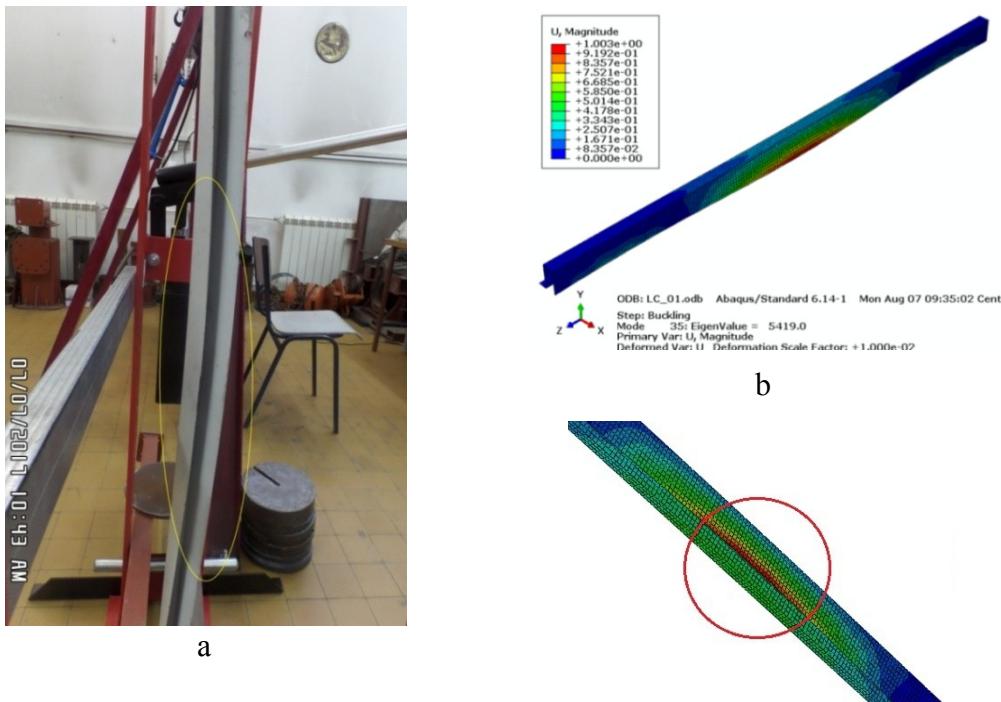


Figure 7.9 First global buckling mode for specimen C2; a. Exp. , b. FE.

The load compression response of the specimen C2 is plotted against the time of the test and is shown in Figure 7.10. The findings from the experimental test are indicated in the figure by dotted circles and more viewing for both local and global buckling. Both sets of values (i.e. Exp. & FE) demonstrate almost similar local buckling trends where are 1800N and 1641.2N respectively. The finite element simulation produced a more accurate prediction in terms of load compressive response to global buckling load where was 5420N while by experimental test was 6000N.

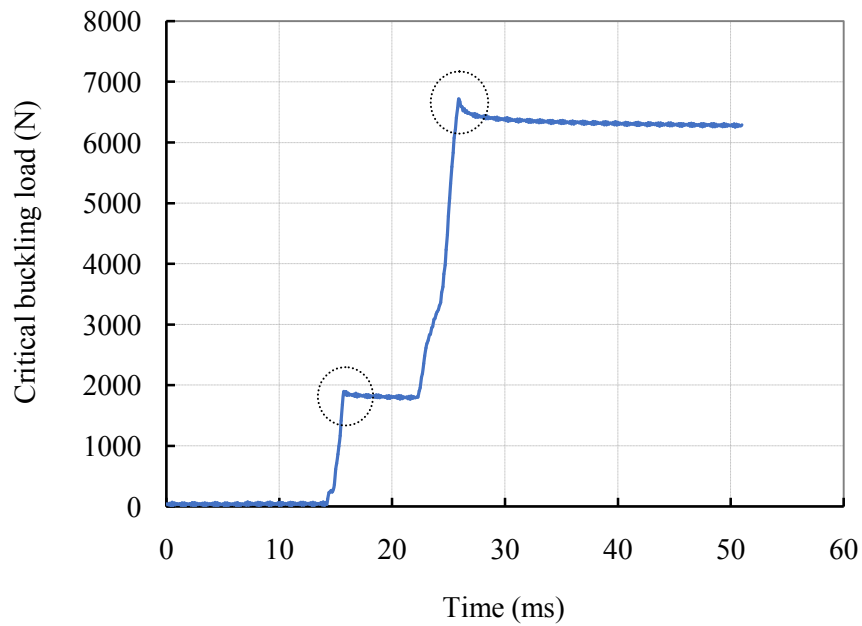


Figure 7.10 Critical buckling load response for specimen C3

Specimen C3

Figure 7.11 shows the local buckling behaviour between the experimental and numerical models for specimen C3 also under axial compression load. It can be seen from Figure 7.11 that the experimental response of specimen C3 with load whose bottom edge is buckled, is in close agreement with that of the numerical simulation solution.

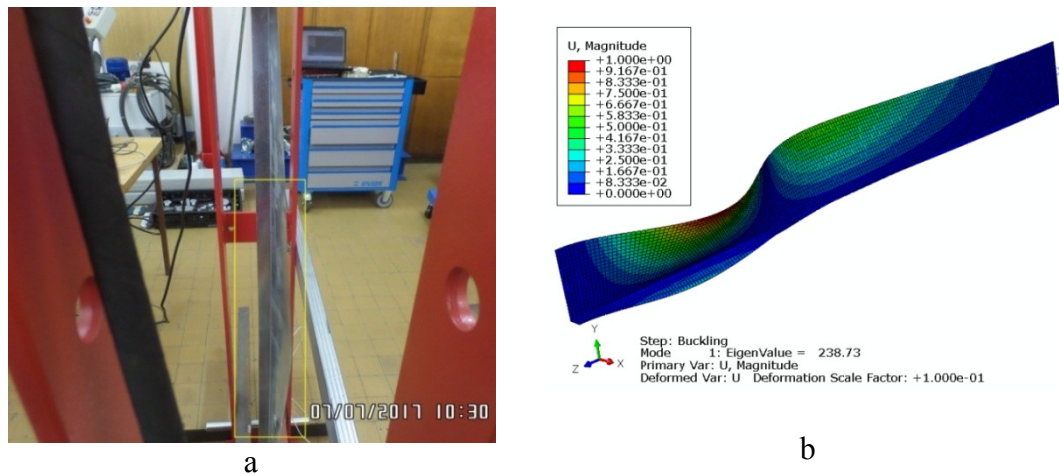


Figure 7.11 First Local buckling mode for specimen C3, a. Exp, b. FE.

Based on the experimental results which are obtained for specimen C3, the critical local buckling value is 250N. It has been noted during the test that there was not any global buckling for specimen C3 it might due to the shape of the specimen. The obtained load-time curve of the specimen C3 from test is shown in Figure 7.12. It is noted from the figure that before the occurrence of the local buckling, the compression load increased linearly till the first mode of local buckling which is occurred at 250N. On the other hand of the solution which is made by FE simulation and as shown in Figure 7.11, it can be seen that the first local buckling mode was occurred at 238.5 N. When the local buckling occurred and with increasing in the axial compression load, the critical local buckling load was almost at the same value with a little difference in its value. Consequently, the comparisons of the critical buckling modes for specimen C3 were agreed almost well with a little bit difference especially in the local buckling modes where the error was 4.6% and this value is very acceptable in design.

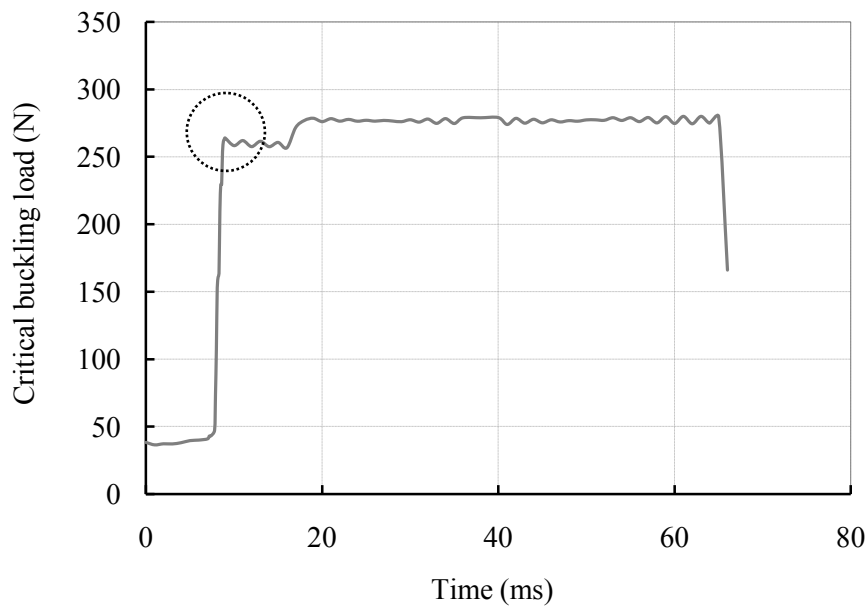


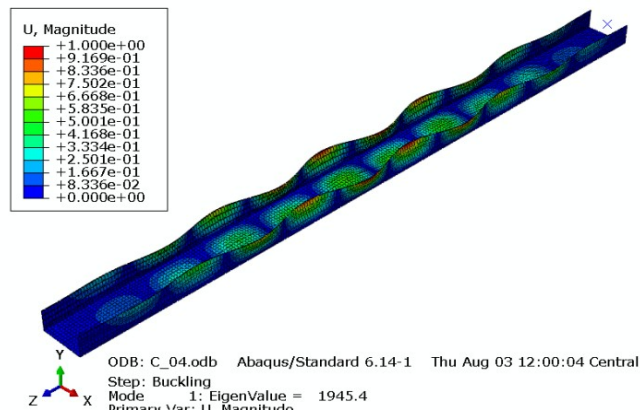
Figure 7.12 Critical buckling load response for specimen C3

Specimen C4

The specimen C4 of lengths of 900 mm and 510 mm respectively have been chosen to represent long and short columns. Other different modifications have been made on the specimen C4 as shown in Table 7.1 as zags which represent as supports in order to see its role on the buckling behaviour. Specimen C4 has two different lengths (i.e. $L = 900$ mm and $L = 510$ mm) with the same other dimensions. Figure 7.13 and Figure 7.15 also show the comparison results of the local buckling behaviour for specimen C4 at two lengths between the experimental and numerical models under axial compression load. The obtained results showed that the experimental major deformation characteristic appeared similar to the FEM simulation for two different lengths of specimen C4 as shown in the figures. It can be seen that the maximum local buckling occurred in the web member than the flange members in both cases. Figure 7.14 also shows the finite element test of the global buckling behaviour for specimen C4 at $L = 900$ mm which was very small through the experimental test and due to this reason does not show in experimental figure. It is noted from the experimental and finite element simulation that there is no global buckling for specimen C4 at length $L = 510$ mm, because of the short length. Again and as a result, well agreement between the experimental and finite element models results for both local and global buckling behaviour under axial compression load for two cases.



a



b

Figure 7.13 First local buckling mode for specimen C4 ($L = 900$ mm), a. Exp, b. FE

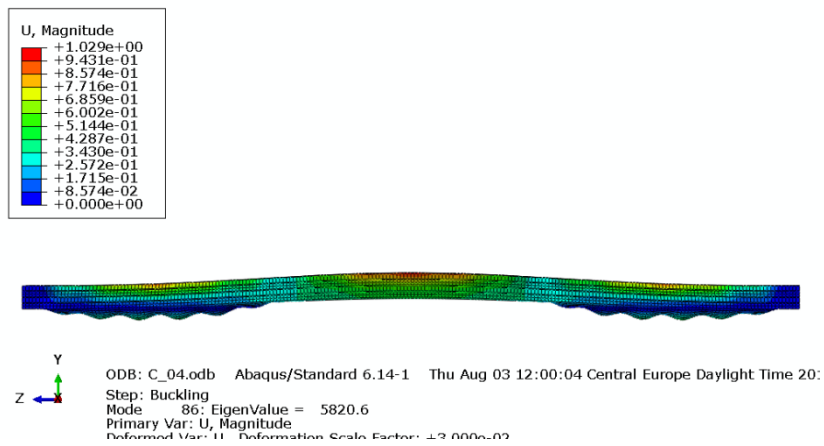


Figure 7.14 First global buckling mode for specimen C4 ($L = 900$ mm) by FE

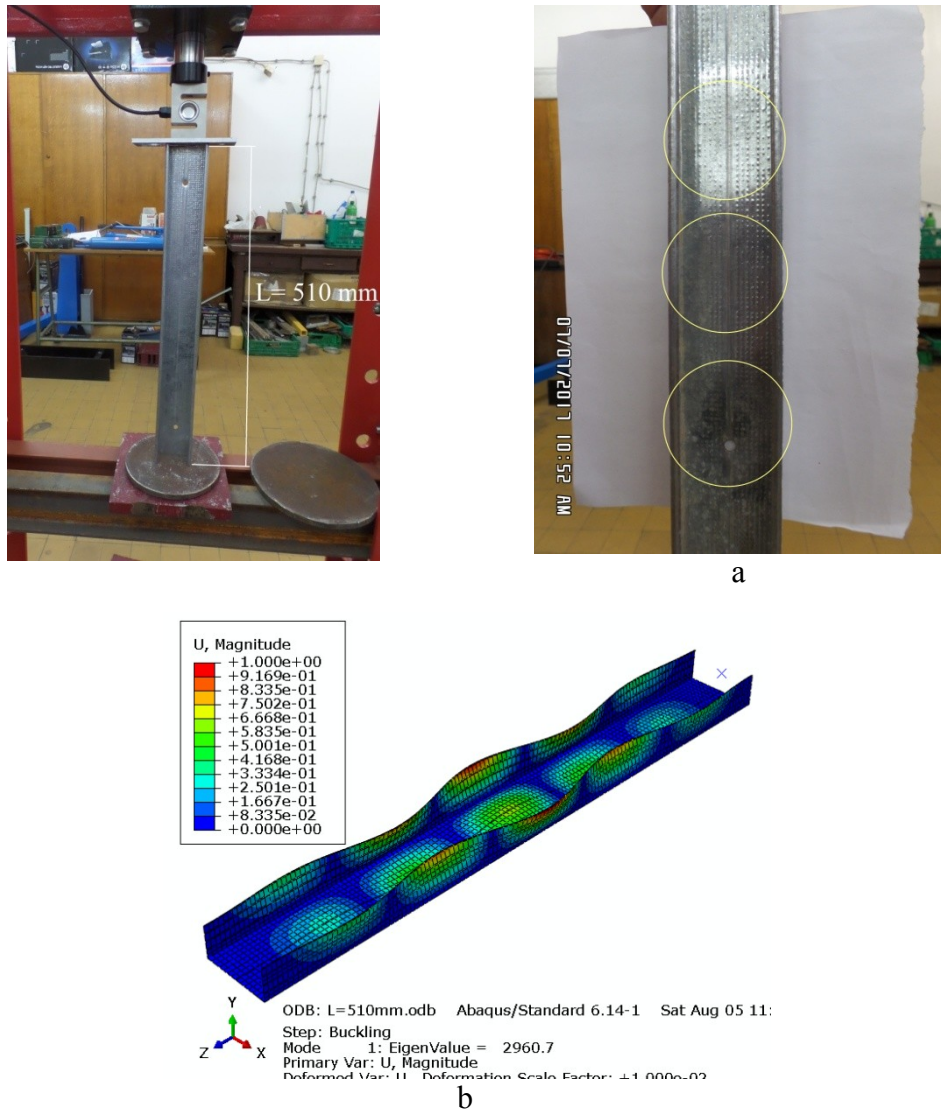


Figure 7.15 First local buckling mode for specimen C4 ($L = 510 \text{ mm}$) by FE

The load compression response of the specimen C4 when $L = 900 \text{ mm}$ and $L = 510 \text{ mm}$ is plotted against the time of the test and are shown in Figure 7.16 and Figure 7.19 respectively. The results from the experimental test are represented by more viewing at length $L = 900 \text{ mm}$ and for both local and global buckling in Figure 7.17 and Figure 7.18 respectively. Both sets of values (i.e. Exp. & FE) demonstrate almost similar local buckling trends where 1500 N and 2800 N for two lengths respectively were. However, the finite element simulations produce more accurate predictions in terms of load compressive response where were 1945 N and 2960 N as shown in Figure 7.13 and Figure 7.15 respectively.

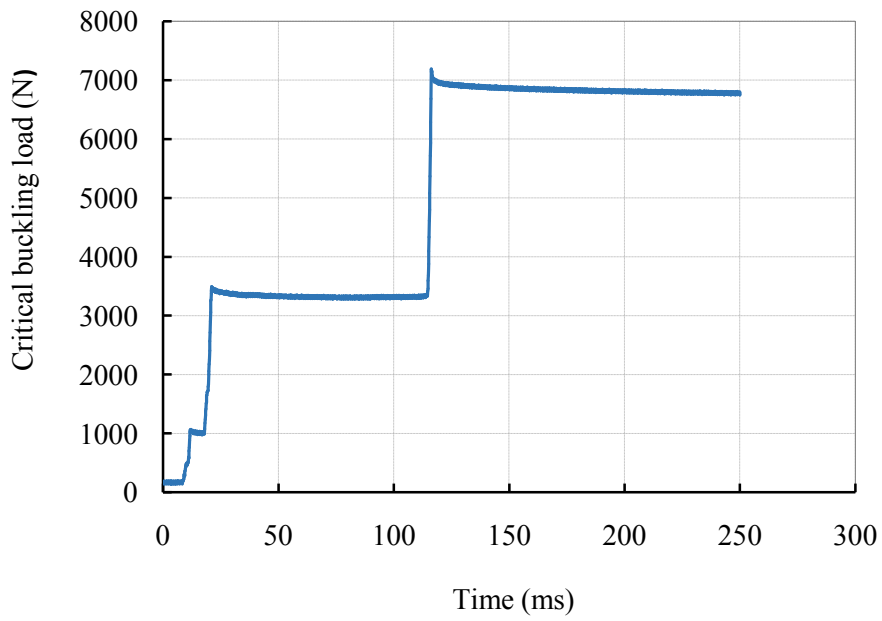


Figure 7.16 Critical buckling load response for specimen C4, L = 900 mm

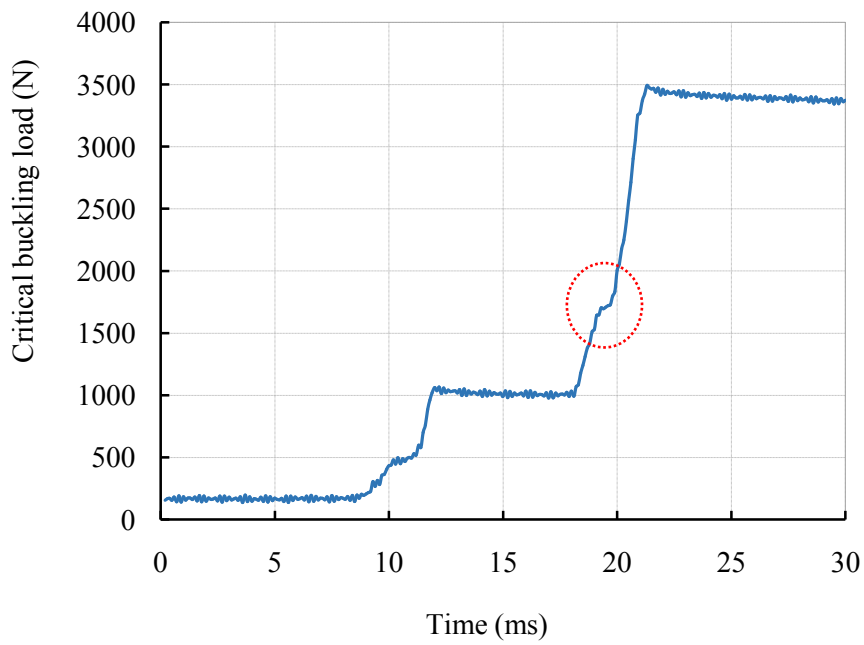


Figure 7.17 Critical local buckling load location of Figure 7.16

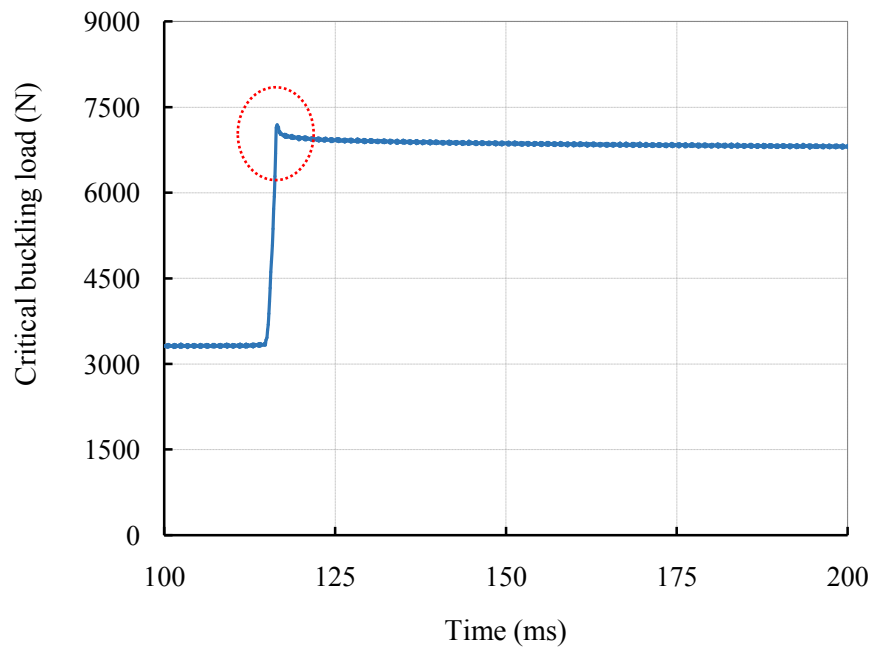


Figure 7.18 Critical global buckling location of Figure 7.16

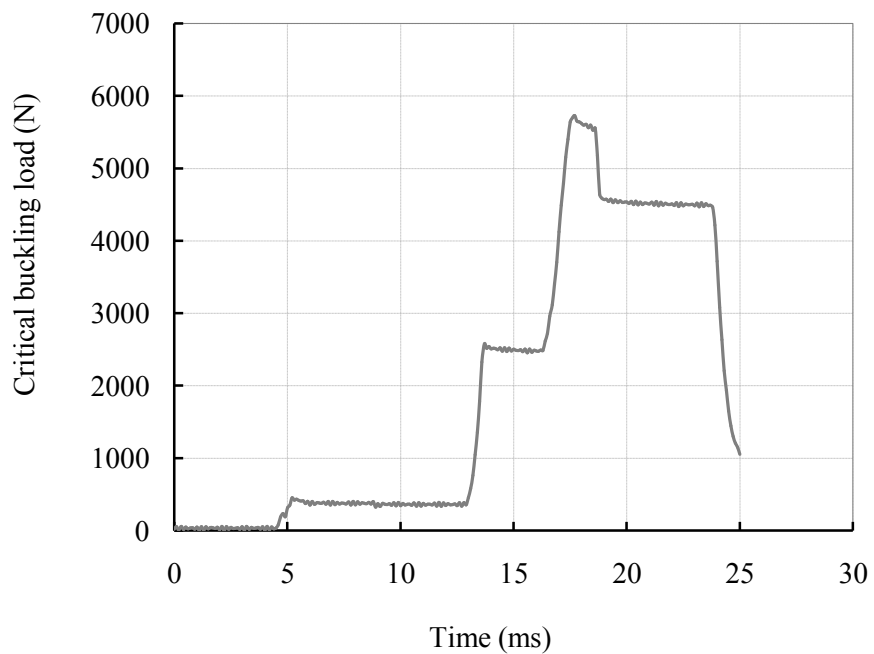


Figure 7.19 First global buckling mode for specimen C4, L=510mm

Specimen 5

Figure 7.20 shows the local buckling response from the experimental and finite element simulation for specimen C5 and the major deformation characteristic is as indicated in the figure. For specimen C5, the first local mode by FE simulation and the major deformation characteristic have been appeared similar as the experimental form and the maximum critical local buckling load for each mode are 3985N and 3500N with a difference is in the order of 12% as shown in Figure 7.20 and Figure 7.22. Figure 7.21 shows the full scale of global buckling mode that has been obviously appeared identical in two cases (i.e. Exp. and FE). The critical buckling load for specimen C5 from finite element simulation is found to be 5082N and this compares well with the test value of 5000N as indicated in Figure 7.21 and Figure 7.22.

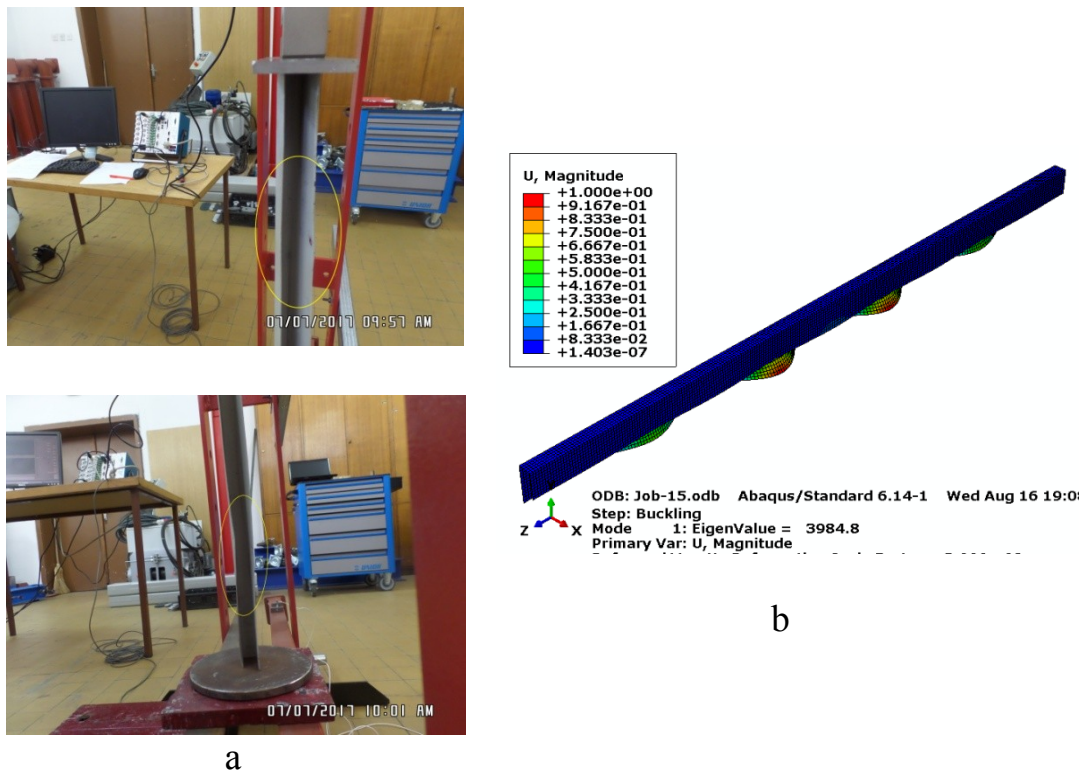


Figure 7.20 First local buckling mode for specimen C5, a. Exp, b. FE

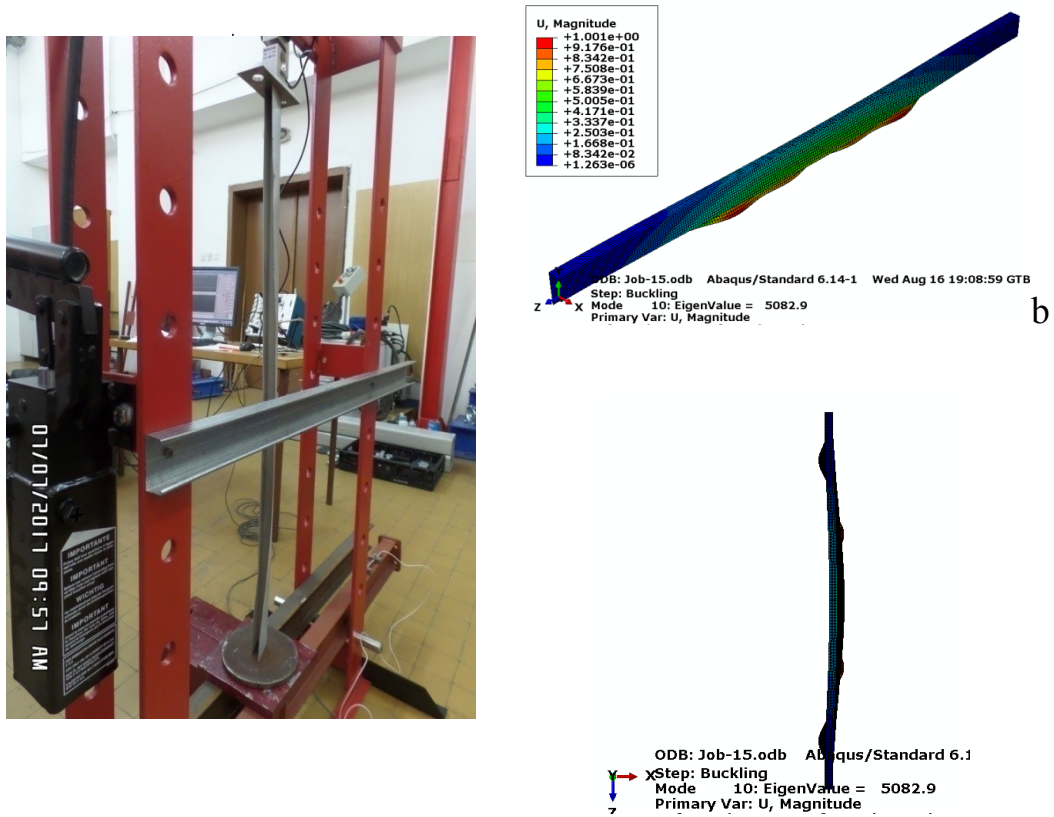


Figure 7.21 First global buckling mode for specimen C5, a. Exp, b. FE

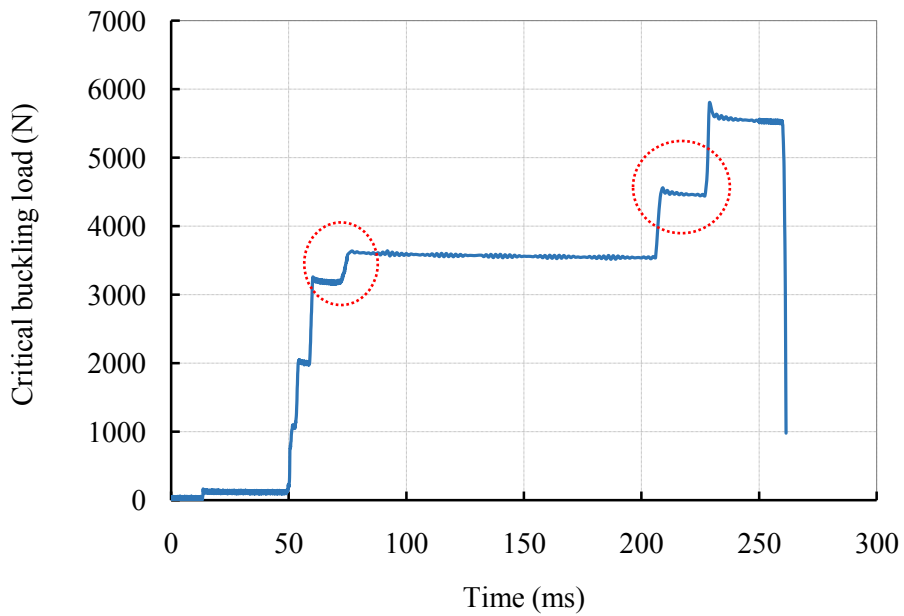


Figure 7.22 Critical local & global buckling load locations for specimen C5

Specimen 6

The specimen C6 has been chosen to represent a thick plate with $t=5.5$ mm in order to examine its influence on the critical buckling behaviour. The simply supported boundary conditions are used as previous cases with axial compression load. Figure 7.23 shows the comparison results of the global buckling behaviour for specimen C6 between the experimental and numerical models under axial compression load. The results obtained from the experimental and FE simulation showed that the major deformation characteristic appeared similar in both cases. It is noted from the experimental and finite element simulation that there is no local buckling for specimen C6. Therefore, further increase in the applied loading results a second global buckling mode as shown in Figure 7.24 which is examined by FE simulation.

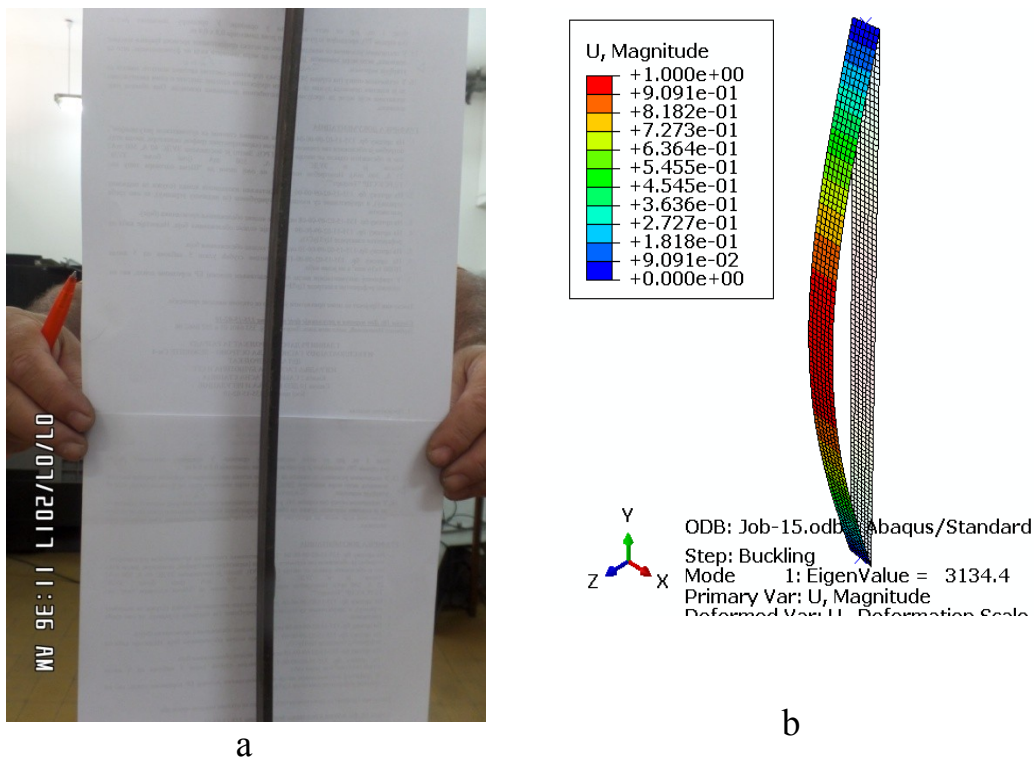


Figure 7.23 First global buckling mode for specimen C6, a. Exp, b. FE

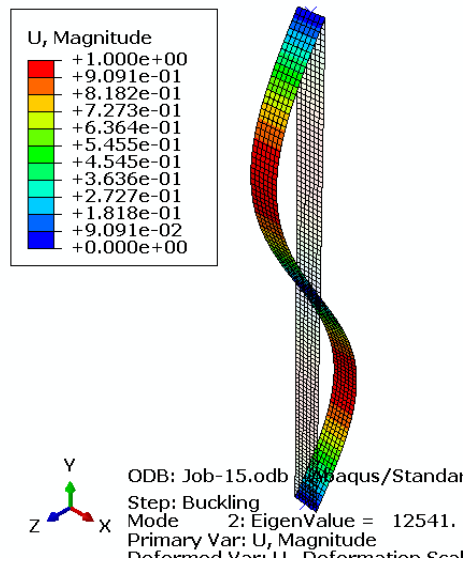


Figure 7.24 Second global buckling mode for specimen C6 by FE

The change in the load compression on the behaviour of the specimen C6 with $L = 540\text{mm}$ is plotted against the time of the test and is highlighted in Figure 7.25. The dotted circle line represents the critical global buckling load in which the specimen has been buckled globally, and is almost 3750N. The value of global buckling load which has been obtained by FE simulation is 3134.4N and in comparison with the Exp. value, the difference is 616N about 61kg with 16% of error. Consequently, the finite element simulations produce more accurate predictions in terms of load compressive response where is 3134N as shown in Figure 7.23 and this value is safer than Exp. value.

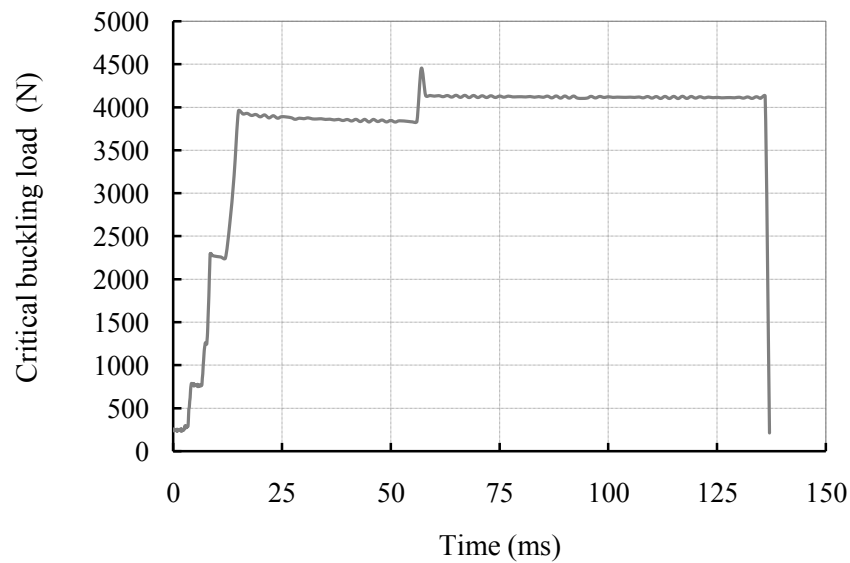


Figure 7.25 Critical buckling load response for specimen C6

7.6 CONCLUDING REMARKS

The purpose of this chapter was to experimentally examine and develop finite element solutions for different steel elements subjected to a compressive load. As mentioned early, the finite element simulation strategies as described in chapter 3 were used to follow the behaviour of the steel elements in terms of local and global buckling loads and compare the obtained results with the experimental tests as a validation. One boundary condition is used for the analyses in this study. This boundary condition is simply supported with restraints along two end edges of specimen except the displacement in the load direction. The following conclusions are drawn based on the results and observations presented herein.

- In the case of short length columns, the existence of global buckling in columns whose local buckling is higher can result unavailable.
- In case of long longer columns whose initial buckling is in the local buckling mode can result that the global buckling available.
- It can be concluded that the obtained experimental results have been shown good agreement with the finite element simulation solutions.

CHAPTER 8

8. CONCLUSIONS AND FUTURE WORK

8.1 SUMMARY

The purpose of this work was, basically to develop suitable finite element modelling strategies and solution procedures for the investigation of the local and global buckling failure behaviour of the structural elements which are subjected to uniaxial compression load. The work was carried out by adding the transverse stiffeners and longitudinal stiffeners in order to examine their influence and effect on the critical buckling loads. In the course of this work, the finite element simulation approaches were developed to be able to examine the buckling characteristics of the thin plates and to deal easily with different boundary conditions. In the initial stage, the thin plate structure under consideration is modeled as an individual plate element in order to validate the numerical simulation. The plate width-to-length ratio with different thicknesses was changed in order to monitor its influence on the critical buckling behaviour under classical boundary conditions as well as on the development of the elastic deformation. The width-to-thickness ratio of the thin plate with has been examined in order to observe its effect also on the critical buckling loads. The work has been developed to study the buckling behaviour of the beam-column structural with the simply supported in uniaxial compression load. The transverse and longitudinal stiffeners have been included in the beam-column in order to increase its critical buckling loads. A range of different distances between transverse stiffeners has been distributed through the beam-column with simply supported boundary conditions. The effect of changes in the distances between the stiffeners on the critical buckling loads of the stiffened beam-column has been studied for the different thicknesses of stiffeners considered. Moreover, the longitudinal stiffeners have been added as well to the beam-column with centrally located and equally one and two spaced between each other in order to investigate their role with transverse stiffeners on the critical buckling resistance.

The finite element techniques have also been carried out in order to examine the buckling behaviour and possible failure of the frame structural. Different dimensions and thickness of the frame are used during the numerical simulation analysis by using the same previous configurations.

8.2 CONCLUSIONS

This thesis has studied and presented the response of critical local and global buckling capacity of thin plates, beam-column and frame structural systems subjected to axial compression load. Finite element modelling strategies and solution procedures have been developed in order to investigate the local and global buckling behaviour for un-stiffened and stiffened structural systems. The investigation on the structural member's axial compression buckling behaviour, length to width and width to thickness response involved a large of finite element analyses of simply supported beam-column and frame structure. Furthermore, the study computationally investigated the effect of transverse and longitudinal stiffeners on the beam-column and frame structural systems to increase their local and global buckling resistance.

Some important points summarized from the presented work regarding the diagnostic analysis of the buckling behaviour of element structural in some detail as follows:

- The obtained results from this study throughout the development of the finite element modelling strategies and solution procedures employed in all cases, demonstrate that the effectiveness and uniqueness of using of the finite element method in being able to describe the critical buckling behaviour of thin plate, beam-column and frame structures subjected to uniaxial compression load.
- The used finite element approach that processed in the work has been shown to be able to efficiently and consistently capture all aspects of the critical local-global buckling loads of the thin plate, beam-column and frame structural systems analyzed. The distributed elastic analysis based on the shell elements is able to capture the development of buckling behaviour of the system under elastic buckling up to ultimate conditions.
- The finite element modelling technique which used for thin plate has been developed with regard to the uniaxial compressed load at different boundary conditions which has been termed as classical method or approach by previous

researchers. This simple method has been used to simplify the numerical procedures in the analysis of thin plate sections.

- In the case of the thin plate analysis, the obtained results have been shown that the highest value of critical buckling load P_{cr} occurred at short lengths of the plates which represented the highest critical buckling load where the plate may be fails.
- In the case of stiffened beam-column subjected to uniaxial compression load, three situations were investigated in the finite element analysis of simply supported beam-column. They are: 1) by using only transverse stiffeners, 2) by using transverse and two longitudinal stiffeners, 3) by using transverse and four longitudinal stiffeners. The beam-column examined without any stiffeners and with stiffeners with stiffeners positioned at specified locations as shown in chapter 5.
- Effects of transverse and longitudinal stiffeners were examined in this study. The results have been shown that the transverse stiffeners have a significant effect on the beam-column critical buckling load. The longitudinal stiffeners, on the other hand, do not have a significant effect on the beam-column critical buckling load.
- The critical buckling load versus length-to-width ratio curve of simply supported beam-column indicates that the maximum critical buckling is at the shorter distances between transverse stiffeners. The beam-column buckling drops dramatically between 0.5 to 1 meters where afterwards 1m there is no any noticeable change in critical buckling load.
- With regard to the local deformation shape of the beam-column condition, it has been shown from the figures that the local deformation crest occurs at the center of the beam-column.
- The analysis of frame structure with simply supported condition was also developed in the finite element analysis. Appropriate transverse and longitudinal stiffeners were included in the model for elastic buckling analysis. The two basic buckling modes (i.e. local and global buckling) as observed and investigated in the frame structure.
- The effect of both stiffeners in terms of distribution was also investigated in the finite element analysis. The buckling behaviour and results showed that the effect of the both stiffeners is significant. However, the transverse stiffeners have had a better effect in particular on the local buckling load than longitudinal stiffeners.

- The buckling behaviour shows that the expected position of critical local buckling load is unknown that means may be occurring on any beam on the frame.
- In a frame structure, the critical buckling loads were generally higher for short distances between transverse stiffeners than those of the long distance in both buckling modes. Namely, critical buckling loads decrease with increasing of the distance between the stiffeners.
- As a result, the finite element analyses that have been made of the frame structures show when one of the beams (members) in the frame fails in critical local and global buckling mode, the frame is not able to carry further loads.
- The finite element method is able to visualize the growth and the redistribution of stresses after local buckling, as well as the initiation of buckling throughout loading.
- The development of the von Mises stresses through the buckling behaviour can be monitored.
- the best improvement is obtained in the critical buckling load when transverse and longitudinal stiffeners are defined together.
- The main increase in the critical buckling load is obtained when the distance between the stiffeners is short.
- The study showed that the critical buckling loads are very sensitive to the location of stiffener.
- The compressive buckling behaviour of steel columns with simply supported conditions has been experimentally and numerically investigated in this study.
- Regarding the experimental results that have been obtained from the simply supported steel elements tests were used as solutions to validate with finite element simulation.

8.3 FUTURE WORK

The aim of the finite element modelling techniques and solution steps to diagnose the buckling behaviour of the structural element's behaviour in terms of local and global buckling has been successfully presented. In order to broaden the scope of the current research work, the author proposes some further opinions. Thus, the following recommendations are suggested for future work:

- The application of the finite element simulation techniques highlighted in the thesis can be further extended to study different thin plate structural configurations.
- The presented finite element for the beam-column can be utilized to extend the work of a stiffened beam-column by employing different stiffener's dimensions and shapes.
- Similarly the work of stiffened frame structural can be investigated further by changing the shapes of attached stiffeners.
- The work can be developed to study the behaviour of unstiffened and stiffened plate structures taking into account the geometrical imperfections and material nonlinearity.

REFERENCES

- [1] Rhodes, J. & Harvey, J.M., “*Plates in uniaxial compression with various support conditions at the unloaded boundaries*”, Int. J. Mech. Sci., Vol. 13 (1971) pp. 787-802.
- [2] Rhodes, J. & Harvey, J.M., “*Effects of eccentricity of load or compression on the buckling and post-buckling behaviour of flat plates*”, Int. J. Mech. Sci., Vol. 13(1971) pp. 867-879.
- [3] Kang, J.H. & Leissa, A.W., *Exact solutions for the buckling of rectangular plates having linearly varying in-plane loading on two opposite simply supported edges*, International Journal of Solids and Structures 42 (2005) 4220-4238.
- [4] Bakker, M.C.M., Rosmanit, M. & Hofmeyer, H., “*Approximate large-deflection analysis of simply supported rectangular plates under transverse loading using plate post-buckling solutions*”, Thin-Walled Structures 46 (2008) 1224-1235.
- [5] Eisenberger, M. & Alexandrov, A., “*Buckling loads of variable thickness thin isotropic plates*”, Thin-Walled Structures 41 (2003) 871-889.
- [6] Hancock, G.J., Davids, A.J., Key, P.W., Lau, S.C.W., Rasmussen, K.J.R., *Recent developments in the buckling and nonlinear analysis of thin-walled structural members*, Thin-Walled Structures, Vol. 9, No. 1-4, pp.309-338, 1990.
- [7] Hancock, G.J., & Rasmussen, K.J.R., “*Recent research on thin-walled beam columns*”, Thin-Walled Structures 32 (1998) 3-18.
- [8] Rhodes, J., “*Buckling of thin plates and members – and early work on rectangular tubes*”, Thin-Walled Structures 40 (2002) 87-108.
- [9] Rhodes, J., “*Some observations on the post-buckling behaviour of thin plates and thin-walled members*”, Thin-Walled Structures 41 (2003) 207-226.
- [10] Azhari, M., Shahidi, A.R., Saadatpour, M.M. & Bradford, M.A., “*Postbuckling behaviour of triangular plates*”, AIAA Journal, Vol. 43, No. 3 (2005), 690-696.
- [11] Tan, H.K.V., Bettess, P. & Bettess, J.A., “*Elastic buckling of isotropic triangular flat plates by finite elements*”, Appl. Math. Modelling, Vol. 7, (1983) 311-316.
- [12] Galambos T. V., *Structural Members and Frames*, Prentice-Hall, New Jersey, pp. 80-158, 1968.
- [13] Allen H. G., Bulson P. S., *Background to Buckling*, McGraw-Hill, Maidenhead, Berkshire, England, 1980.

- [14] Chen W. F., Goto Y., Richard Liew J. Y., *Stability Design of Semi-Rigid Frames*, John Wiley & Sons, Inc, 1996.
- [15] Bushnell D., *Computerized buckling analysis of shells*, 1985.
- [16] Calladine, C.R., *Theory of Shell Structures*, Cambridge University Press, Cambridge, 1983.
- [17] Bryan, G. K., “*On the stability of a plane plate under thrusts in its own plane with application on the ‘buckling’ of the sides of a ship*”, Proc. London Math. Soc., Vol. 22, pp. 54, 1891.
- [18] Timoshenko S., *Einige stabilitäts probleme der elasticitätstheorie*, *Zeitschrift für mathematic und physic*, 1910, 337; Sur la stabilité des systèmes élastiques, *Annales des pontset chaussées*, 1913, Fasc. III, IV and V. Russian, *Bull. Polytech. Inst. Kiev*, 1907.
- [19] Saint-Venant M., “*Discussion en Théorie de l’Elasticité des Corps Solides*”, by Clebsch, p.704, 1883.
- [20] Ugural A. C., *Stress in Plates and Shells*, McGraw-Hill, New York, 1999.
- [21] Timoshenko S.P., Gere J.M., “*Theory of Elastic Stability*”, 2nd edition, McGraw-Hill International Editions, 1963.
- [22] Lundquist, E. and Stowell, E. Z., “*Critical compressive stress for flat rectangular plates supported along all edges and elastically restrained against rotation along the unloaded edges.*”, NACA Report 733, 1942.
- [23] Kollbrunner C. F., Herrmann G., “*Elastische beulung von aufeinseitigen ungleichunbigen druckbeanspruchten platen.*” *Mitte der T.K.V.S.B.*, H. 1, p. 28, 1948.
- [24] Schuette E. H., McCulloch J. C., “*Charts for the minimum-weight design of multi-web wings in bending*”, NACA, Tech. Note No. 1323, 1947.
- [25] Walker A. C., *Thin-Walled Structures*, Chatto and Windus, Longdon, p. 208, 1968
- [26] Xiang Y., Wang C. M., Wang, C. Y., “*Buckling of rectangular plates with internal hinge*” *International Journal of Structural Stability and Dynamics*, Vol. 1, No. 2, 169-179, 2001.
- [27] S. F. Bassily, S. M. Dickinson, *On the use of beam functions for problems of plates involving free edges*, *Journal of Applied Mechanics*, Vol. 42, No. 4, 858–864, 1975.

-
- [28] Kielb R.E, Han L.S., *Vibration and Buckling of Rectangular Plates under In-Plane Hydrostatic Loading*, Journal of Sound and Vibration, Vol. 70, No. 4, 543-555, 1980.
- [29] Kaldas M.M., Dickinson S.M., *Vibration and Buckling Calculations for Rectangular Plates Subject to Complicated In-Plane Stress Distributions by Using Numerical Integration in a Rayleigh-Ritz Analysis*, Journal of Sound and Vibration, Vol.75,No. 2, 151-152, 1981.
- [30] Leissa, A.W., Kang J.H, *Exact solutions for vibration and buckling of an SS-C-SS-C rectangular plate loaded by linearly varying in-plane stresses*, International Journal of Mechanical Science Vol. 44, No. 9,1925-1945, 2002.
- [31] Sukajit P., Singhatanadgid P., *Identification of Buckling Load of Thin Plate Using the Vibration Correlation Technique*, Proceedings of the 21st Conference of Mechanical Engineering,10, pp520-525, 2007.
- [32] Von Kármán T., Sechler E.E., Donnell L.H. *The Strength of Thin Plates in Compression*, ASME, Vol. 54, No. 5, 53-57,1932.
- [33] Winter G., *Strength of Thin Steel Compression Flanges*, Transactions of the American Society of Civil Engineers, Vol. 112, No. 1, 527-554, 1947.
- [34] Harvey J.M., *Structural Strength of Thin-Walled Channel Sections*, Engineering, Vol. 175, No. 4545, 291-293, 1953.
- [35] Chilver A. H., *The Behavior of Thin-Walled Structural Members in Compression*, Engineering, Vol. 175, No. 4466, 281-282, 1951.
- [36] Kalyanaraman V., Peköz T., Winter G., *Unstiffened Compression Elements*, Journal of the Structural Division, ASCE, Vol. 103, No. ST9,1833-1848, 1977.
- [37] Desmond T.P., *The Behavior and Strength of Thin-Walled Compression Elements with Longitudinal Stiffeners*, doctoral thesis, Cornell University, 1977.
- [38] Dubas P., Gehri E., *Behaviour and Design of Steel Plated Structures*, Applied statics and steel structures, Swiss Federal Institute of Technology, Zurich, 1986.
- [39] Murray N. W., 1984. *Introduction to the theory of thin-walled structures*, Oxford Engineering Science Series, 1984.
- [40] Bonello M. A., Chryssanthopoulos M. K., Dowling P. J., *Ultimate strength design of stiffened plates under axial compression and bending*, Marine Structures, Vol. 6, No. 5-6, 533-552, 1993.

- [41] Cook, I. T., Rokey, K. C., *Shear buckling of clamped and simply-supported infinitely long plates reinforced by closed-section transverse stiffeners*, Aeronautical Quarterly, Vol. 13, pp. 212-222, 1962.
- [42] Nishino, F., Okumura, T., Experimental investigation of strength of plate girders in shear, Final Report, IABSE Congress, N.Y., pp. 451-463, 1968.
- [43] Komatsu, S., "Ultimate strength of stiffened plate girders subjected to shear", In: Proc. colloquium on design of plate and box girders for ultimate strength, IABSE, 1971, pp. 49-65.
- [44] Skaloud, M., "Ultimate load and failure mechanism of thin webs in shear", Report, IABSE Seminar, London, U.K., 1971, pp. 115-129.
- [45] Rokey, K. C., Skaloud, M., "Influence of flange stiffness upon the load carrying capacity of webs in shear", Final Report, IABSE Congress, New York, N.Y., 1968, pp. 429-439.
- [46] Plank, R. J., Williams, F. W., "Critical buckling of some stiffened panels in compression, shear and bending", Aeronautical Quarterly, 1974, pp. 165-179.
- [47] Wagner H. (1929). *Ebene blechträger mit sehr dünnem stegblech*, Zeitschrift für Flugtechnik und Motorluftschiffahrt, Vol. 20, 220, 1929.
- [48] Lee S.C., Yoo C.H., Yoon D.Y., *Behavior of intermediate transverse stiffeners attached on web panels*, Journal of Structural Engineering, Vol. 128, No. 3, 337-345, 2002.
- [49] Lee S.C., Yoo C.H., Yoon D.Y., *New design rule for intermediate transverse stiffeners attached on web panels*, Journal of Structural Engineering, Vol. 129, No. 12, 1607-1614, 2003.
- [50] Horne M.R., Grayson W.R., *Parametric finite element study of transverse stiffeners for webs in shear*, Instability and plastic collapse of steel structures, Proceedings of the Michael R. Horne Conference, L. J. Morris, Granada Publishing, London, 329-341, 1983.
- [51] Stanway G.S., Chapman J.C., Dowling P.J., *Behaviour of a web plate in shear with intermediate stiffener*, Proc. Inst. Civ. Eng. Struct. Build, Vol. 99, 327-344, 1993.
- [52] Rahal K.N., Harding J.E., *Transversely stiffened girder webs subjected to shear loading*, Part 1: Behaviour. Proc. Inst. Civ. Eng., Part 2, Res. Theory, Vol. 89, 47-65, 1990a.

-
- [53] Rahal K.N., Harding J.E., *Transversely stiffened girder webs subjected to shear loading*, Part 2: Stiffener Design, Proc. Inst. Civ. Eng., Part 2: Res. Theory, Vol. 89, 67-87, 1990b.
- [54] Kim Y.D., Jung S.K., White D., *Transverse stiffener requirements in straight and horizontally curved steel I-girders*, Journal of Bridge Engineering, ASCE, Vol. 12, No. 2, 174-183, 2007.
- [55] Fujikubo M., Yao T., *Elastic local buckling strength of stiffened plate considering plate/stiffener interaction and welding residual stress*, Marine Structures, Vol. 12, No. 9-10, 543-564, 1999.
- [56] Yao T., Fujikubo M., Yanagihara D., *Buckling/plastic collapse behaviour and strength of stiffened plates under thrust*. International Journal of Offshore and Polar Engineering, Vol. 7, No. 4, 285-292, 1997.
- [57] Dubas, C., *Contribution A` L' Etude Du Voilement Des To`les Raidies (A Contribution to the Buckling of Stiffened Plates)*, Publications de L'Institut De Statique Appliquee, No. 23, 1948.
- [58] Chwalla E., *Die Bemessung Der Waagrecht Ausgesteiften Stegbleche Vollwandiger Trager (The design of Longitudinally Stiffened Webs of Plate Girders)*", Preliminary Publications IABSE, 957, 1936b.
- [59] Kromm A., *Zur Frage der Mindeststeifigkeiten Von Plattenaussteifungen (On the Problem of Optimum Rigidity of Stiffened Plates)*" , Vol. 17, 81, 1944.
- [60] Kloppel K., Scheer J., *Das Praktische Aufstellen Von Beule Determinanten Für Rechteckplatten Mit Rand Parallelen Steifen Navierschen Randbedingungen (The Derivation of Buckling Determinants of Rectangular Plate Stiffeners, The Plate Being Simply Supported and the Stiffeners Parallel to the Edges)*, Vol. 25, 117, 1956.
- [61] Massonnet C. *La Stabilité De L`Ame Des Poutres Munies De Raidisseurs Horizontaux Et Sollicitees Par Flexion Pure (The Web stability of Longitudinally Stiffened Plate Girders Subjected to Pure Bending)*, 1940.
- [62] Van der Neut A., *Overall Buckling of Z-Stiffened Panels in Compression*, Delft University, 1983.
- [63] Hughes O.F., Ma M., *Elastic tripping analysis of asymmetrical stiffeners*, Computers and Structures, Vol. 60, No. 3, 369-389, 1996.

- [64] Thang D. D., Koo M.-S., Hameed A., Jeong Y.D., *Stiffness Requirement for Flat-Bar Longitudinal Stiffener of Box-Girder Compression Flanges*, Steel Structures, Vol. 9, No. 2, 115-122, 2009.
- [65] Nishino, F., Ueda, Y., Tall, L., *Experimental Investigation of the Buckling of Plates with Residual Stresses*, ASTM Special Technical Publication, No. 419, 12-30, 1967.
- [66] Dwight, J. B., Moxham, K.E., *Welded Steel Plates in Compression*, The Structural Engineer, Vol. 47, No. 2, 1969.
- [67] Courant R., *Variational methods for the solution of problems of equilibrium and vibrations*, Bull Am Math Soc, Vol. 49, 1–23, 1943.
- [68] Turner MJ., Clough RW., Martin HC., Topp LJ., *Stiffness and deflection analysis of complex structures*, J Aero Sci, Vol. 23, No. 9, 805–823, 1956.
- [69] Zienkiewicz OC., *The finite element method in engineering science*, McGraw-Hill, London, 1971.
- [70] Zienkiewicz OC., Taylor RL., *The finite element method*, Butterworth-Heinemann, Oxford, 2000.
- [71] Owen DJR., Hinton E., *An introduction to finite element computations*, Pineridge Press, Swansea, 1980.
- [72] Zienkiewicz OC., Cheung YK., *The finite element method in structural and continuum mechanics: numerical solution of problems in structural and continuum mechanics*, McGraw-Hill, London, 1967.
- [73] Crisfield MA., *Non-linear finite element analysis of solids and structures*, John Wiley & Sons, Inc, New York, 1997.
- [74] E. HNTON, *Introduction to Nonlinear Finite Element Analysis*, NAFEMS, Glasgow, 1992.
- [75] LUC WULLSCHLEGER, *Numerical Investigation of the Buckling Behaviour of Axially Compressed Circular Cylinders Having Parametric Initial Dimple Imperfections*, doctoral thesis, Zürich, 2006.
- [76] Campbell G., Ting W., Aghssa P., Hoff C. C., *Buckling and Geometric Nonlinear Analysis of a Tie Rod in MSC Nastran Version 68*, Worlds Users Conference, 1-15, Arlington, 1994.
- [77] Arlington. 1993 S. H. Lee., *Essential Considerations for Buckling Analysis*, Worldwide Aerospace Conference and Technology Showcase. Toulouse. 2001.

- [78] Cook R. D., Malkus D. S., Plesha M. E., Witt R. J., *Concepts and Applications of Finite Element Analysis*, John Wiley & Sons, 2002.
- [79] C. Felippa, *Introduction to Finite Element Methods*,
<http://www.colorado.edu/engineering/cas/courses.d/IFEM.d/>.
- [80] Bertollini A.F., *Review of Eigen solution Procedures for Linear Dynamic Finite Element Analysis*, Applied Mechanics Reviews, Vol. 51, No. 2, 155-172, 1998.
- [81] K. Bathe, *The Subspace Iteration Method Revisited*, Computers and Structures, Vol. 126, No.15, 177-183, 2013.
- [82] ABAQUS/Standard user's manual volumes I-III and ABAQUS CAE manual, Version 6.14-EF1, Dassault Systemes Corp., Providence, USA, 2010.
- [83] Cook R. D., Malkus D. S., Plesha M. E., Witt R. J., *Concepts and Applications of Finite Element Analysis*, John Wiley & Sons, 2002.
- [84] Rao, S., *The Finite Element Method in Engineering*, Butterworth-Heinemann, 2004.
- [85] El-Sawy K.M., Nazmy A.S., *Effect of aspect ratio on the elastic buckling of uniaxially loaded plates with eccentric holes*, Thin-Walled Structures, Vol. 39, No. 12, 983-998, 2001.
- [86] El-Sawy K.M., Nazmy A.S., Martini, M.I., *Elasto-plastic buckling of perforated plates under uniaxial compression*, Thin-walled structures, Vol. 42, No. 8, 1083-1101, 2004.
- [87] Kanchanalai, T., *The design and behaviour of beam-columns in unbraced steel frames*, AISI Project No. 189, Report No. 2, Civil Engineering/Structures Research Laboratory, University of Texas Austin, TX, USA, 1977.
- [88] Thurlimann, B., *Column buckling-historical and actual notes*, Journal of Constructional Steel Research, Vol. 17, No.1-2, 95-111, 1990.
- [89] White, D. W., *Material and geometric nonlinear analysis of local planar behaviour in steel frames using interactive computer graphics*, Cornell University, Ithaca, NY, USA, 1985.
- [90] Vogel, U., *Calibrating Frames*, Stahlbau, Vol. 54, 295-301, 1985.
- [91] Avery, P., *Advanced Analysis of steel Frame Structures Comprising Non-Compact Sections*, PhD thesis, School of Civil Engineering, Queensland University of Technology, 1998

- [92] Kim, S.E, Chen, W.F, Practical *Advanced Analysis for steel Frame Design*, PhD dissertation, School of Civil Engineering, Purdue University, West Lafayette, IN, USA, 1991.
- [93] Kim, S.E, Lee, D.H., *Second-order distributed plasticity analysis of space steel frames*, Engineering structures, Vol. 24, 735-744, 2002.
- [94] Clarke, M. J., Bridge, R. Q., Hancock, G. J., Tahair, N. S., *Advanced analysis of steel building frames*, Journal of Constructional Steel Research, Vol. 23, No. 1-3, 1-29, 1992.
- [95] T. Yao, M. Fujikubo, D. Yanagihara, *Buckling plastic collapse strength of stiffened plates under thrust*. Int. J. Offshore Polar Eng, Vol. 7, No. 4, 285–292, 1997.

Biography of the Author

Noureddine Toumi was born on 21st of February 1971 in Tripoli, Libyan nationality. At the end of 1989, Toumi finished his secondary education from Alanduls School, Tripoli-Libya. In spring 1995, he obtained his B.Sc. degree from Aeronautical Engineering Department, Tripoli University. In 2005, Toumi received his M.Sc. degree from the Faculty of Mechanical Engineering, University of Belgrade, Serbia. Since October 2013, he has been Ph.D. candidate at the University of Belgrade, Faculty of Mechanical Engineering. During the period between 1997 and 2008, he worked for the Research and Development Center (RDC) as an engineer in Tripoli-Libya. In 2007-2008, he worked as a part-time lecturer at Faculty of Economics, Tripoli University and Higher Institute of Civil Aviation in El-Spiaa-Libya. From 2009 up to 2012, Toumi worked as a full time lecturer at the Faculty of Engineering, Mechanical Department, University of Al-Gabal Al-Gharbi, Libya.

Прилог 1.

Изјава о ауторству

Потписани-а : НОУРЕДДИНЕ ТОУМИ

број индекса: Д4-2013

Изјављујем

да је докторска дисертација под насловом

**Нумеричка-експериментална дијагностика понашања
извијања структурних елемената**

**NUMERICAL AND EXPERIMENTAL DIAGNOSTICS OF
BUCKLING STRUCTURAL ELEMENT BEHAVIOR**

- резултат сопственог истраживачког рада,
- да предложена дисертација у целини ни у деловима није била предложена за добијање било које дипломе према студијским програмима других високошколских установа,
- да су резултати коректно наведени и
- да нисам кршио/ла ауторска права и користио интелектуалну својину других лица.

Потпис докторанда

У Београду, 17.10.2017 год.

Прилог 2.

**Изјава о истоветности штампане и електронске верзије
докторског рада**

Име и презиме аутора: НОУРЕДДИНЕ ТОУМИ

Број индекса: Д4-2013

Студијски програм: Докторска дисертација

Наслов рада Нумеричка-експериментална дијагностика понашања извијања
структурних елемената

NUMERICAL AND EXPERIMENTAL DIAGNOSTICS OF BUCKLING
STRUCTURAL ELEMENT BEHAVIOR

Ментор проф.др Ташко Манески

Потписани/а НОУРЕДДИНЕ ТОУМИ

Изјављујем да је штампана верзија мог докторског рада истоветна електронској верзији коју сам предао/ла за објављивање на порталу **Дигиталног репозиторијума Универзитета у Београду**.

Дозвољавам да се објаве моји лични подаци везани за добијање академског звања доктора наука, као што су име и презиме, година и место рођења и датум одбране рада.

Ови лични подаци могу се објавити на мрежним страницама дигиталне библиотеке, у електронском каталогу и у публикацијама Универзитета у Београду.

Потпис докторанда

У Београду, 17.10.2017 год.

Прилог 3.

Изјава о коришћењу

Овлашћујем Универзитетску библиотеку „Светозар Марковић“ да у Дигитални репозиторијум Универзитета у Београду унесе моју докторску дисертацију под насловом:

Нумеричка-експериментална дијагностика понашања извијања структурних елемената

NUMERICAL AND EXPERIMENTAL DIAGNOSTICS OF BUCKLING STRUCTURAL ELEMENT BEHAVIOR

која је моје ауторско дело.

Дисертацију са свим прилозима предао/ла сам у електронском формату погодном за трајно архивирање.

Моју докторску дисертацију похрањену у Дигитални репозиторијум Универзитета у Београду могу да користе сви који поштују одредбе садржане у одабраном типу лиценце Креативне заједнице (Creative Commons) за коју сам се одлучио/ла.

1. Ауторство

2. Ауторство - некомерцијално

3. Ауторство – некомерцијално – без прераде

4. Ауторство – некомерцијално – делити под истим условима

5. Ауторство – без прераде

6. Ауторство – делити под истим условима

(Молимо да заокружите само једну од шест понуђених лиценци, кратак опис лиценци дат је на полеђини листа).

Потпис докторанда

У Београду, 17.10.2017

1. Ауторство - Дозвољавање умножавање, дистрибуцију и јавно саопштавање дела, и прераде, ако се наведе име аутора на начин одређен од стране аутора или даваоца лиценце, чак и у комерцијалне сврхе. Ово је најслободнија од свих лиценци.
2. Ауторство – некомерцијално. Дозвољавање умножавање, дистрибуцију и јавно саопштавање дела, и прераде, ако се наведе име аутора на начин одређен од стране аутора или даваоца лиценце. Ова лиценца не дозвољава комерцијалну употребу дела.
3. Ауторство - некомерцијално – без прераде. Дозвољавање умножавање, дистрибуцију и јавно саопштавање дела, без промена, преобликовања или употребе дела у свом делу, ако се наведе име аутора на начин одређен од стране аутора или даваоца лиценце. Ова лиценца не дозвољава комерцијалну употребу дела. У односу на све остале лиценце, овом лиценцом се ограничава највећи обим права коришћења дела.
4. Ауторство - некомерцијално – делити под истим условима. Дозвољавање умножавање, дистрибуцију и јавно саопштавање дела, и прераде, ако се наведе име аутора на начин одређен од стране аутора или даваоца лиценце и ако се прерада дистрибуира под истом или сличном лиценцом. Ова лиценца не дозвољава комерцијалну употребу дела и прерада.
5. Ауторство – без прераде. Дозвољавање умножавање, дистрибуцију и јавно саопштавање дела, без промена, преобликовања или употребе дела у свом делу, ако се наведе име аутора на начин одређен од стране аутора или даваоца лиценце. Ова лиценца дозвољава комерцијалну употребу дела.
6. Ауторство - делити под истим условима. Дозвољавање умножавање, дистрибуцију и јавно саопштавање дела, и прераде, ако се наведе име аутора на начин одређен од стране аутора или даваоца лиценце и ако се прерада дистрибуира под истом или сличном лиценцом. Ова лиценца дозвољава комерцијалну употребу дела и прерада. Слична је софтверским лиценцама, односно лиценцама отвореног кода.